14th INTERNATIONAL INDUSTRIAL SIMULATION CONFERENCE

2016

ISC'2016

EDITED BY

Nicolae Vasiliu

and

Daniela Vasiliu

JUNE 6-8, 2016

BUCHAREST, ROMANIA

A Publication of EUROSIS-ETI

14th Industrial Simulation Conference 2016

BUCHAREST, ROMANIA

JUNE 6-8, 2016

Organised by

ETI - The European Technology Institute

Sponsored by

EUROSIS

University of Skövde

SIEMENS

Co-Sponsored by

Ghent University

Hosted by

University POLITEHNICA of Bucharest

Bucharest, Romania

EXECUTIVE EDITOR

PHILIPPE GERIL
(BELGIUM)

EDITORS

General Conference Chairs

Nicolae Vasiliu, University POLITEHNICA of Bucharest, Bucharest, Romania
Daniela Vasiliu, University POLITEHNICA of Bucharest, Bucharest, Romania

Past Conference Chairs

Carlos Enrique Palau Salvador, UPV, Valencia, Spain
Benjamin Molina, UPV, Valencia, Spain
Vicent Pla, Polytechnic University, Valencia, Spain

Publications Chairs

Peter Lawrence, Swinburne University, Australia
Yan Luo, NIST, Gaithersburg, USA

INTERNATIONAL PROGRAMME COMMITTEE

Discrete Simulation Methodology, Languages and Tools
Matthias Becker, University Hannover, Hannover, Germany
Helge Hagenauer, Universitaet Salzburg, Salzburg, Austria
Sophie Hennequin, ENIM, Metz Cedex, France
Bjorn Johansson, Chalmers University of Technology, Gothenburg, Sweden
Erik Lindskog, Chalmers University of Technology, Gothenburg, Sweden
Stefano Marrone, Seconda Universita di Napoli. Naples, Italy
Paulo Novais, Universidade do Minho, Braga, Portugal
Jiri Safarik, University of West Bohemia, Plzen, Czech Republic
Antonella Zanzi, Universita' degli Studi dell'Insubria, Varese, Italy

Ambient Intelligence and Simulation
Selwyn Piramuthu, University of Florida, Gainesville, USA

Cyber Physical Systems Simulation
Track Chair: Ioan Dumitrache, The Romanian Academy, Bucharest, Romania
Adina Magda Florea, University POLITEHNICA of Bucharest, Bucharest, Romania
Cornel Burileanu, University POLITEHNICA of Bucharest, Bucharest, Romania
Corneliu Bilan, University POLITEHNICA of Bucharest, Bucharest, Romania

Simulation in Manufacturing
Pascal Berruet, Universite Bretagne Sud, Lorient, France
Peter Byrne, Dublin City University, Dublin, Ireland
Ana Camacho, UNED, Madrid, Spain
Eduardo Castellano, IKERLAN Technol. Res. Centre, Mondragon-Arrasate, Spain
Remy Dupas, Universite Bordeaux 1, Bordeaux, France
Alexander Felfernig, University of Klagensfurt, Klagensfurt, Austria
Michel Gourgand, Universite Blaise Pascal, Clermont-Ferrand, France
Frank Heinze, (RIF) e.V., Dortmund, Germany
Pouria Homayonifar, Acona Flow Technology, Skien, Norway
Imed Kacem, Université Paul Verlaine Metz, Metz, France

INTERNATIONAL PROGRAMME COMMITTEE

Carlo Meloni, Politecnico di Bari - DEE, Bari, Italy
Pascal Meyer, Forschungszentrum Karlsruhe, Karlsruhe, Germany
José A V Oliveira, University of Minho, Braga, Portugal
Marina Valles, UPV, Valencia, Spain
Markus Vorderwinkler, PROFACTOR GmbH, Steyr, Austria
Roland Wischnewski, (RIF) e.V., Dortmund, Germany
Farouk Yalaoui, Universite de Technologie de Troyes, Troyes Cedex, France

Simulation in Steel Manufacturing
Brian Hollocks, Bournemouth University, Bournemouth, United Kingdom

Simulation in Automotive Systems
Naoufel Cheikhrouhou, EPFL, Lausanne, Switzerland
Julien Richert, Daimler AG, GR/PAA, Sindelfingen, Böblingen, Germany

Simulation in Robotics
A. Chatzinikolaou, Athens, Greece
Andrzej Dzielinski, Warsaw University of Technology, Warsaw, Poland
Markus Koch, Orga Systems GmbH, Paderborn, Germany
Martin Mellado, UPV, Valencia, Spain
Bogdan Raducanu, Computer Vision Centre, UAB, Barcelona, Spain
Sergiu-Dan Stan, Technical University of Cluj-Napoca, Cluj-Napoca, Romania

Simulation in Electronics, Computer and Telecommunications
Teresa Alvarez, University of Valladolid, Valladolid Spain
Christos Bouras, University of Patras, Patras, Greece
Adnane Latif, Cadi Ayyad University, Marrakech, Morocco
Silvia Mirri, University of Bologna, Bologna, Italy
Maurizio Palesi, Universita di Catania, Catania, Italy
Marco Roccetti, University of Bologna, Bologna, Italy
Fernando Boronat Segui, UPV, Valencia, Spain
Renate Sitte, Griffith University, Gold Coast, Australia

Simulation in Electronics Manufacturing
Theresa Roeder, San Francisco State University, USA
Gerald Weigert, Dresden University of Technology, Germany

Simulation of Complex Multiprocessor Systems
Orhan Gemikonakli, Middlesex University, London, United Kingdom

Simulation in Computer Science
Lipika Deka, Tezpur University and IIT Guwahati, India
Ernst Kesseler, NLR, Amsterdam, The Netherlands
Wolfgang Kreutzer, University of Canterbury, Christchurch, New Zealand

Simulation in Logistics, Transport and Harbour Simulation
Christian Almeder, European University Viadrina, Frankfurt (Oder), Germany
Maria Sameiro Carvalho, University of Minho, Guimaraes, Portugal
Isabel Garcia Guttierez, Univ. Carlos III de Madrid, Madrid, Spain .
Dmitry Ivanov, Chemnitz University of Technology, Chemnitz, Germany
Peter Lawrence, Swinburne University, Lilydale, Australia
Marie-Ange Manier, UTBM, Belfort, France
Roberto Montemanni, IDSIA, Manno-Lugano, Switzerland
Guilherme A B Pereira, University of Minho, Braga, Portugal
Roberto Razzoli, University of Genova, Genova, Italy
Rosaldo Rossetti, University of Porto, Porto, Portugal
Hans Veeke, TU Delft, Delft, The Netherlands
Pengjun Zheng, University of Southampton, Southampton, United Kingdom

INTERNATIONAL PROGRAMME COMMITTEE

Simulation in the aviation sector
Gabriel Lodewijks, Delft University of Technology, Delft, The Netherlands

Hospital Logistics Simulation
Track Chair: Giorgio Romanin-Jacur, University of Padova, Vicenza, Italy
Antonio Abelha, Universidade do Minho, Braga, Portugal
Jose Machado, University of Minho, Braga, Portugal
Peter Summons, University of Newcastle, Australia

Complex Systems Modelling
Track Chair: Igor N Litvine, Nelson Mandela Metropolitan University, Port Elizabeth, South Africa
Frantisek Capkovic, Slovak Academy of Sciences, Bratislava, Slovak Republic
Alexandre Nketsa, LAAS, Toulouse, France
Miguel Rocha, University do Minho, Braga, Portugal
Alfonso Urquia, UNED, Madrid, Spain

Apparel and Textile Simulation
Track Chair: Jocelyn Bellemare, University of Quebec in Montreal (UQAM), Montréal (Québec) Canada

Simulation in Aerospace
Reza Azadegan, Urmia University, Urmia, Iran
Wolfgang Kuehn, University of Wuppertal, Wuppertal, Germany
Martin Spieck, DLR, Goettingen, Germany

Marine Simulation
Sergeij Kalashnkikow, DANFOSS, Austria

Simulation in Industrial Design and Product Design
Chiara Catalano, IMATI-CNR, Genoa, Italy
Yan Luo, NIST, Gaithersburg, USA
Catarina Rizzi, University of Bergamo, Bergamo, Italy

Simulation in Engineering Processes
Chrissanti Angeli, Technological Institute of Piraeus, Athens, Greece
Alejandra Gomez Padilla, University of Guadalajara, Mexico
Jan Studzinski, Polish Academy of Sciences, Warsaw, Poland
Joao Tavares, University of Porto, Porto, Portugal
Henk Versteeg, Loughborough University, Loughborough, United Kingdom

Civil and Building Engineering
Alistair Borthwick, Oxford University, Oxford, United Kingdom
Graham Saunders, Loughborough University, Loughborough, United Kingdom

Simulation in Energy and Power Systems
Sergeij Kalashnkikow, DANFOSS, Austria
Janos-Sebestyen Janosy, KFKI Atomic Energy Research Institute, Budapest, Hungary

Simulation in Multibody Systems
Ignacio Garcia-Fernandez, University of Valencia, Valencia, Spain

Simulation in Chemical, Petroleum and Mining Engineering
Mohamad R. Riazi, Kuwait University, Kuwait

Simulation in Military and Defense
Roberto de Beauclair Seixas, IMPA, Rio de Janeiro, Brazil
Carlos Palau, UPV, Valencia, Spain
Matthias Reuter, CUTEC Gmbh, TU-Clausthal, Clausthal, Germany

INTERNATIONAL PROGRAMME COMMITTEE

Virtual Reality and Graphical Simulation in Industrial Simulation
Track Chair: Guodong Shao, NIST, Gaithersburg, USA
Emilio Camahort, Universidad Politecnica de Valencia, Valencia, Spain
Anders Hast, University of Gavle, Gavle, Sweden
Fabrizio Lamberti, Politecnico di Torino, Turin, Italy
Christoph Laroque, University of Paderborn, Paderborn, Germany
Sudhir Mudur, Concordia University, Montreal, Canada
Marta Pla-Castells, Universidad de Valencia, Valencia, Spain
Marcos A.Rodrigues, Sheffield Hallam University, Sheffield, United Kingdom

Simulation of Complex Multiprocessor Systems
Peter Kvasnica, Alexander Dubcek University of Trencin, Trencin, Slovakia

Verification, Validation and Accreditation
Roberto Revetria, University of Genoa, Genoa, Italy
Agustin Yague, Technical University of Madrid, Madrid, Spain

Simulation and Training
Manuel Alfonseca, Universidad Autonoma de Madrid, Madrid, Spain
Wenji Mao, Chinese Academy of Sciences, Beijing, P.R. China
Eshan Rajabally, Loughborough University, Loughborough, United Kingdom
Gerhard Schreck, Fraunhofer IPK, Berlin, Germany

Workshops

Simulation-based evaluation in Living Labs
Stefan Hellfeld, FZI - House of Living Labs, Karlsruhe, Germany
Benjamin Herd, King's College, London, United Kingdom

Workshop on Intelligent Transport Systems
Track Chair: Anna Syberfeldt, University of Skovde, Skovde, Sweden
Paul Davidsson, Blekinge Institute of Technology, Ronneby, Sweden
Petr Hanacek, Brno University of Technology, Brno, Czech Republic
Jairo Montoya Torres, Universidad de la Sabana, Chia, Columbia

NANOSIM
Clemens Heitzinger, Cambridge University, Cambridge, United Kingdom
Yong K. Kim, University of Massachusetts Dartmouth, Dartmouth, USA
Javier Marin, ETSI, University of Malaga, Malaga, Spain

Workshop Augmented Reality and Pervasive Systems in Simulation
Alessandro Genco, University of Palermo, Palermo, Italy

Workshop on Simulation in Lean Manufacturing
Track Chair: Leif Pehrsson, Volvo Car Corporation, Skovde, Sweden
El-Houssaine Aghezzaf, Ghent University, Ghent, Belgium
Hendrik Van Landeghem, Ghent University, Ghent, Belgium

Simulation-based Optimization in Industry
Amos H.C. Ng, University of Skovde, Skovde, Sweden
Anna Syberfeldt, University of Skovde, Skovde, Sweden

OPENSIM
Philippe Geril, ETI Bvba, Ostend, Belgium

HORIZON2020
Valerian Croitorescu, University of Bucharest, Bucharest, Romania

INDUSTRIAL SIMULATION 2016

All articles published in these Proceedings have been peer reviewed

EUROSIS-ETI Publications are ISI-Thomson, IET, SCOPUS and Elsevier Engineering Village referenced
Legal Repository: Koninklijke Bibliotheek van België, Keizerslaan 4, 1000 Brussels, Belgium
CIP 12.620 D/2011/12.620/1

Selected papers of this conference are published in scientific journals.

For permission to publish a complete paper write EUROSIS, c/o Philippe Geril, ETI Executive Director, Greenbridge NV, Ghent University - Ostend Campus, Wetenschapspark 1, Plassendale 1, B-8400 Ostend, Belgium.

EUROSIS is a Division of ETI Bvba, The European Technology Institute, Torhoutsesteenweg 162, Box 4, B-8400 Ostend, Belgium

Printed and bound in Belgium by Reproduct NV, Ghent, Belgium
Cover Design by Grafisch Bedrijf Lammaing, Ostend, Belgium

EUROSIS-ETI Publication
ISBN: 978-90-77381-93-9
EAN: **978-90-77381-93-9**

PREFACE

Dear participants,

On behalf of the Organizing Committee, we would like to welcome each and every one of you to the 14th Annual Industrial Simulation Conference (ISC 2016), hosted by the University POLITEHNICA of Bucharest, in co-operation with the Romanian Technical Science Academy, from June 6th to 8th, 2016.

During two and a half days, we offer a very high-level scientific program, covering a wide range of topics in simulation, from theory to applications, over a large spectrum of industrial and service domains.

The conference this year features five keynote speakers, coming from the Romanian Academy ITC Section, from Siemens PLM Software NV from Belgium, from National Instruments Corporation, from ENPC and INRIA from France who will share their professional expertise with the participants.

To encourage the exchange of techniques and ideas, which is the basic premise at the heart of the Industrial Simulation Conference, the timetable is organized to allow for ample opportunity to meet and discuss. We are convinced that this will permit you to elaborate on some issues and gain a collection of bright new ideas for your future research.

We are indebted to some people without the support of whom, the conference would not be possible. First of all, thanks go to all reviewers for critically evaluating the papers and keeping an eye on the scientific quality of the conference.

Moreover, we are grateful to the keynote and tutorial speakers for accepting our invitation and for presenting their latest contemplations on significant simulation themes.

We would like to express all our gratitude to Dr. Jan Leuridan, senior vice president in charge of simulation and test solutions for Siemens PLM Software, a business unit of the Siemens Digital Factory Division, and CEO for Siemens Industry Software NV. He awarded all the financial and logistic support to the Fluid Power Laboratory of the University POLITEHNICA of Bucharest in order to train a great number of master and PhD students for future research activities involving simulation with AMESim simulation software.

Many thanks are due to Dr. Cristinel Petru Irimia, manager of Siemens Industry Software SRL, for his permanent logistic help in organizing the conference.

Furthermore, we would like to express our thanks to Mr. Philippe Geril, General Secretary of EUROSIS, who has taken the responsibility for most of the organizational matters. The Industrial Simulation Conference is only possible thanks to his hard work and never-ending enthusiasm.

Finally, our warm thanks go to all of you for submitting your research results, attending sessions and actively participating and discussing. We wish you all a stimulating and productive meeting

General Conference Chair
Nicolae Vasiliu

CONTENTS

CONTENTS

SOLAR ENERGY SIMULATION

HYDROPOWER SIMULATION

CHEMICAL ENGINEERING SIMULATION

DATA ANALYSIS

CONTENTS

HARDWARE SIMULATION

LATE PAPERS

SCIENTIFIC PROGRAMME

KEYNOTES

Reactive Power Control for Photovoltaic Power Plants

M. Stremțan, R. Curatu, Prof. Dr. N Vasiliu

POLITEHNICA University of Bucharest
313, Splaiul Independentei, Sector 6, 060042 Bucharest, Romania

KEYWORDS
Photovoltaic, solar, reactive power, control, SCADA

ABSTRACT

This paper describes the practical implementation of a custom reactive power control strategy on a 9MW installed power photovoltaic plant, as an integrated component of a SCADA system, in the context of the instability generated by meteorological conditions and their impact on the quality of the energy delivered through power grid.

INTRODUCTION

Romania's energy production variety has recently evolved to include a large number of renewable sources with significant impact on the Romanian National Energy System. As seen in Fig. 7, renewable energy amounts to 43% of Romania's energy production, consisting of Hydropower (31.16%), Wind (10.14%), Solar (1.58%) and Biomass (0.84%). In terms of stability, renewable energy has a major impact on the national grid and its accelerated growth through the last years demands accurate control in order to minimize the impact on the grid's energy quality. Romania's National Energy Sector Regulation Authority (ANRE – Autoritatea Națională de Reglementare în Domeniul Energiei) has set into place rules and regulation for solar and wind plants control.

ANRE requires plants over 5MW installed capacity to have active power control depending on the grid frequency, and active and reactive power control and voltage based on dispatch orders, in the connection point. The reactive power control has to continuously ensure a power factor of maximum 0.9 capacitive and 0.9 inductive ($|\cos(\phi)| \in [0.9, 1]$). (Autoritatea Națională de Reglementare în Domeniul Energiei, 2013), (Autoritatea Națională de Reglementare în Domeniul Energiei, 2013).

THE NEED FOR REACTIVE POWER CONTROL

In order to comply with the previously described regulations, it is required to control the power factor in each inverter of the PV plant with regards to the feedback from the connection point to the grid. Although the output of the inverter can provide a power factor of 1, due to the influence of the transport and distribution networks, network components and consumers, the power factor can vary, and the PV plant will be required to compensate for these disturbances.

Loads can be:

- Inductive: consume reactive power to produce electromagnetic fields (such as motors)
- Capacitive: produce reactive power (such as high-voltage overhead transmission lines)

An important factor that influences the output of PV plants is weather, solar irradiance rapid variations having a significant impact and PV inverters must keep energy parameters within limits, no matter the energy output it gives.

Power factor ($\cos\varphi$) is an indicator of the quality and management of an electrical system and is a ratio of active power (P) and apparent power (S), as shown in Equation 1. Active power is the real power transmitted to loads such as motors, heaters, electronics, etc. The electrical active power is transformed into mechanical power, heat or light. Apparent power is the product of r.m.s. voltage and r.m.s. current (Equation 2) and is used for rating most electrical equipment.

$$\cos\varphi = \frac{P[W]}{S[VA]}$$

Equation 1

$$S[VA] = V_{rms}[V] \cdot I_{rms}[A]$$

Equation 2

Reactive power appears when the current I is lagging behind or leading the voltage V by an angle of φ and is defined as a relation of active and apparent power (Equation 3, Equation 1) or described by a power factor, $\cos\varphi$ (Equation 4). The essential difference between active and

reactive power is the fact that while active power is power transported from the generator to the load, reactive power is a measure of the energy stored in elements that act as coils and capacitors.

$$S^2 = P^2 + Q^2$$

Equation 3

A power factor (Equation 4) close to unity means that the apparent power is minimal, meaning that the electrical equipment rating is minimal for the transmission of a given active power to the load, while a low value indicates the opposite. Reactive power can also be calculated by using Equation 5, for a 3-phased circuit.

$$\cos\varphi = \frac{P}{S}$$

Equation 4

$$Q = \sqrt{3} \cdot U \cdot I \cdot \sin\varphi$$

Equation 5

If currents and voltages can be represented by sinusoidal signals, a vector diagram can be used for representation for the current (Fig. 1) and power (Fig. 2). Where the active component of current I_a is in phase with the voltage and the other, reactive component (I_r), lagging by $\pi/2$ (in quadrature). Current and the two components (active and reactive) can be used to define active, reactive and apparent power (Equation 6, Equation 7 and Equation 8).

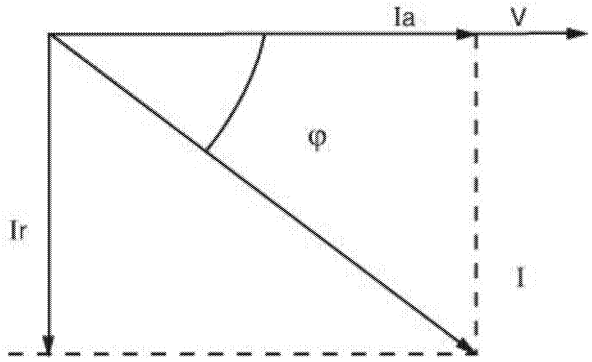

Fig. 1: Active and reactive current

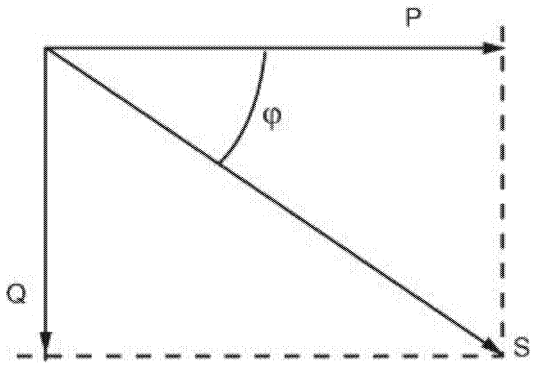

Fig. 2: Active, reactive and apparent power

$$S[VA] = V \cdot I$$

Equation 6

$$P[W] = V \cdot I_a$$

Equation 7

$$Q[var] = V \cdot I_r$$

Equation 8

Low power factors have negative consequences, both technical and economical, to the grid, such as increased costs (most European countries have tariffs that charge industrial consumers more when the power factor drops below 0.93), active power losses, the necessity to install thicker transmission cables (according to Table 1, (Schneider Electric, 2015)), and voltage drops (Micu, Pop, & Cuzumbil).

Table 1: Controlled system description

Cable cross-sectional area of the cable multiplying factor	1	1.25	1.67	2.5
$\cos\varphi$	1	0.8	0.6	0.4

The control strategy described in this paper is applied to a PV plant with a nameplate rating of 9 MVA that has 9 cabins with 3 inverters with a nameplate rating of 334 kVA and a low-voltage to medium-voltage transformer (6kW) each. Each inverter has 5 modules with a nameplate rating of 67 kVA, each having a DC input from 11 to 13 string connector boxes. Each string connector box is a junction of 22 strings and each string feeds power from 242 to 286 PV modules, each having a nominal power $P_{MPP}(Wp)$ of 255 W. This amounts to 27 inverters and approximately 35300 PV modules (panels).

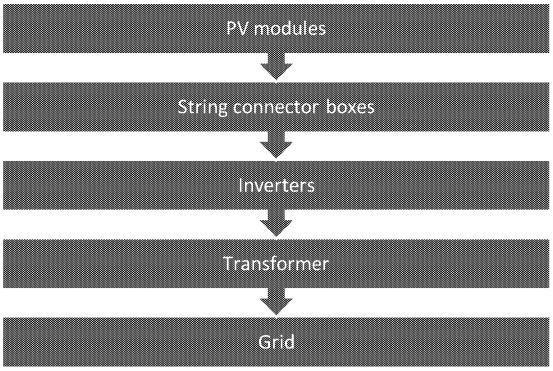

Fig. 3: Block architecture

Thus, the controlled PV plant has a maximum output of 9 MVA, at 6kV.

INVERTERS

The controlled inverters communicate on a proprietary variation of the Modbus protocol called "Aurora", over RS485 field buses. The following data is available by communicating with the inverters:

- Part number, Serial Number, Firmware Version
- General state of the inverter and its two DC inputs
- DC voltage and current
- AC voltage and current (on each phase)
- Active power, frequency and insulation resistance
- Inverter's temperature
- Daily energy counter
- Active power and power factor setpoint values in use

Active power and power factor commands are sent using the same communication channel.

CONTROL SYSTEM

The control system is an integral part of the Supervisory, Control and Data Acquisition (SCADA) system, giving it a separate functionality layer, by connecting HMI commands to required plant output.

Set-points are sent from the HMI, or if necessary, from a 3rd party dispatch center to the plant controller via Modbus. The dispatcher can send active and reactive power set-points and the controller will follow the setpoint, in a closed control loop, using feedback from the power quality meter, situated in the plant's substation. The plant controller (also noted as "Master PLC") sends commands to the inverters by sending commands to the PLCs that relay the information received by Modbus to the inverters on the Aurora protocol. The inverters accept active power (P) and power factor ($\cos\varphi$) commands, while the controller is programmed to use active power (P) and reactive power (Q) commands. The controller calculates and sends different commands to each PLC and the PLCs send the commands by broadcast to all inverters on the field busses connected (3 inverters for each cabin PLC).

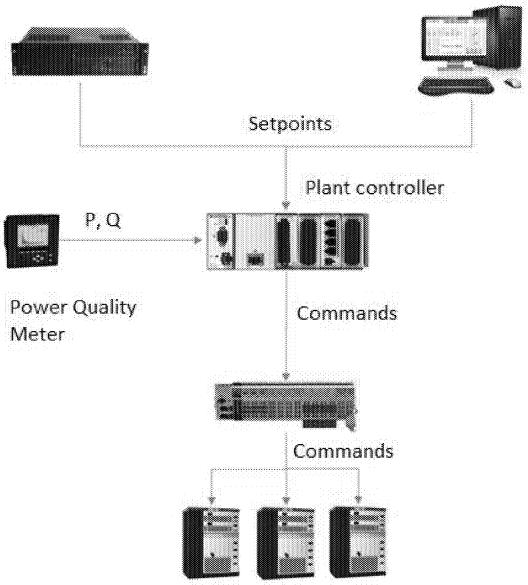

Fig. 4: Command and feedback data flow

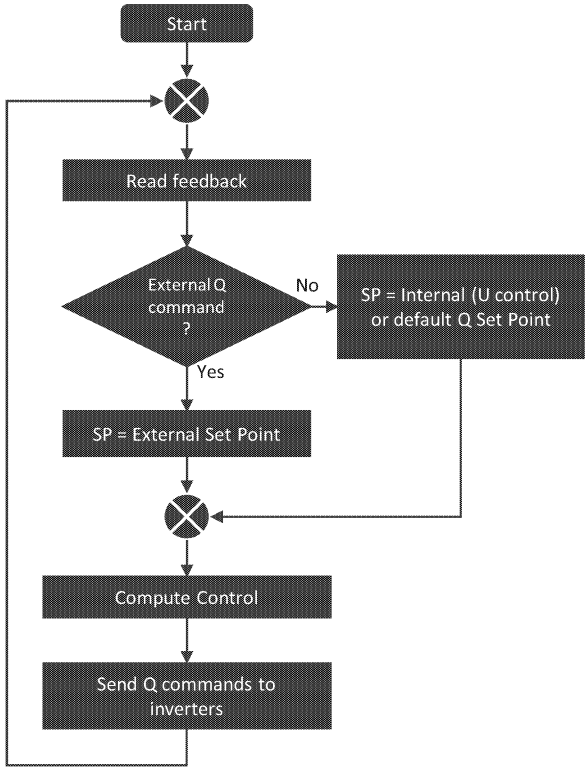

Fig. 5 – Reactive control state chart

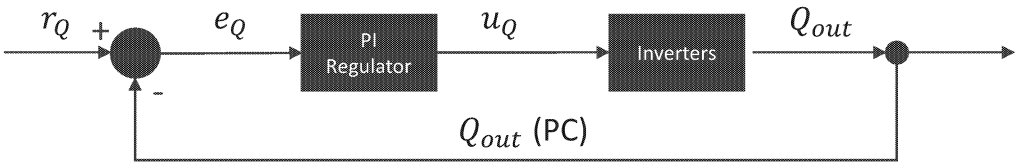

Fig. 6 – Reactive control diagram

The software implementation of the reactive power control is a PI with a few particularities:

- It can control both active and reactive power
- It is tuned to have a ramp of 1 Mvar/minute (and 1 MW/minute) during normal operation;
- It generates intermediary setpoints, in steps of 1Mvar or less (if the the error, $e_Q = Q_{set} - Q_{feedback}$);
- The output is always limited to a maximum step size, to mitigate any scenarios where the PID could have a large overcompensation command;
- The PID can be manually overridden and it follows the commands, in order to ensure a smooth transition when enabled back;
- It has a "soft-start" functionality, to decrease the shock to the system when it starts
- It calculates a reactive power setpoint every iteration and then it sends it to the PLCs. Before sending each command to the PLCs, it recalculates the value of the $\cos\varphi$ command;
- The PID gains change in value depending on the error, to compensate for large changes in reactive power.

The controller is programmed using National Instruments LabVIEW

FIELD RESULTS

The controller has been tuned and tested to ensure the plant follows the reactive power setpoint. Fig. 10 shows a reactive power test where the reactive power setpoint had the following values: 0 kvar, 2000 kvar, 4000 kvar, 2000 kvar, 0 kvar, -2000 kvar, -4000 kvar and 0 kvar.

Fig. 11 shows the reactive power control, having a setpoint of 0 kvar during a day with irregular solar irradiation. This sort of irregular irradiation usually generates large variations of reactive power, as shown by the behavior of another PV plant, also controlled, but with a different precision, shown in Fig.12.

CONCLUSIONS

As shown by Fig. 10 and Fig. 11, the system successfully controls the PV plant and complies with basic industrial control systems requirements, setpoint tracking and error rejection, as well as having more advanced control features and additional functionalities for data aggregation. The controller has proved itself a versatile automation tool that can achieve functionality of far more complicated and expensive COTS (Commercial Off The Shelve) devices.

REFERENCES

Autoritatea Națională de Reglementare în Domeniul Energiei. (2013). *Ordinul Nr. 30.* Bucharest.

Autoritatea Națională de Reglementare în Domeniul Energiei. (2013). *Ordinul nr. 74.* Bucharest.

Micu, D. D., Pop, A.-C., & Cuzumbil, L. (n.d.). *Scenarii de compensare al factorului de putere.*

Schneider Electric. (2015). *Installation guide according to IEC international standards*

Transelectrica. (2015, 05 25). *Productia, consumul si soldul SEN.* Retrieved from Transelectrica: http://transelectrica.ro/widget/web/tel/sen-grafic/

APPENDIX

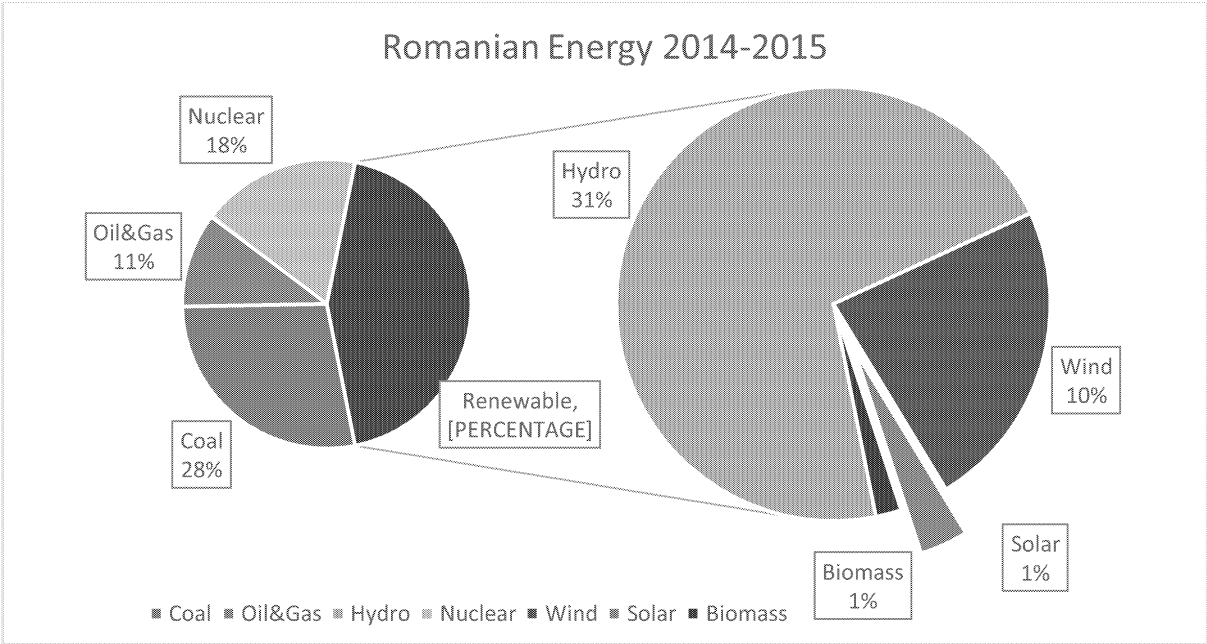

Fig. 7: Romanian Energy Production by source (Transelectrica, 2015)

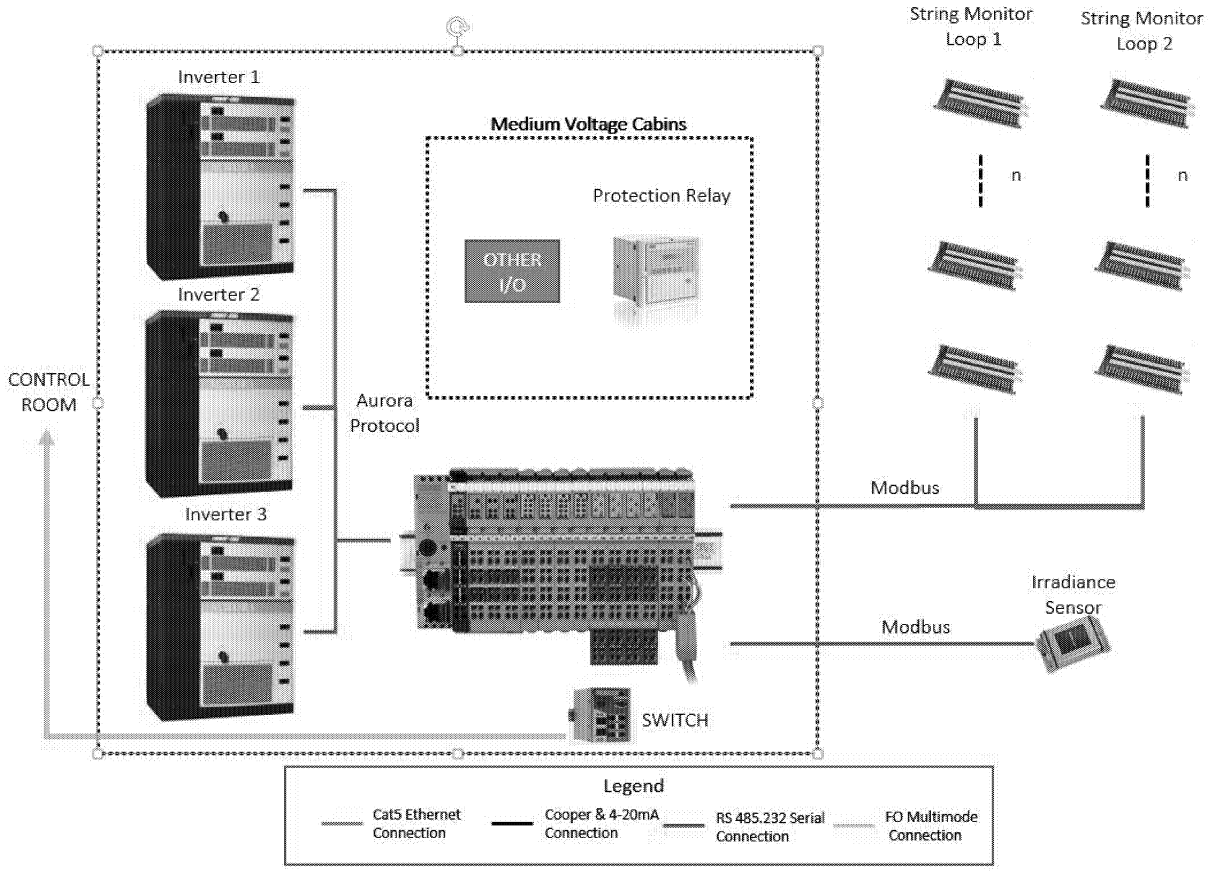

Fig. 8: Cabin architecture

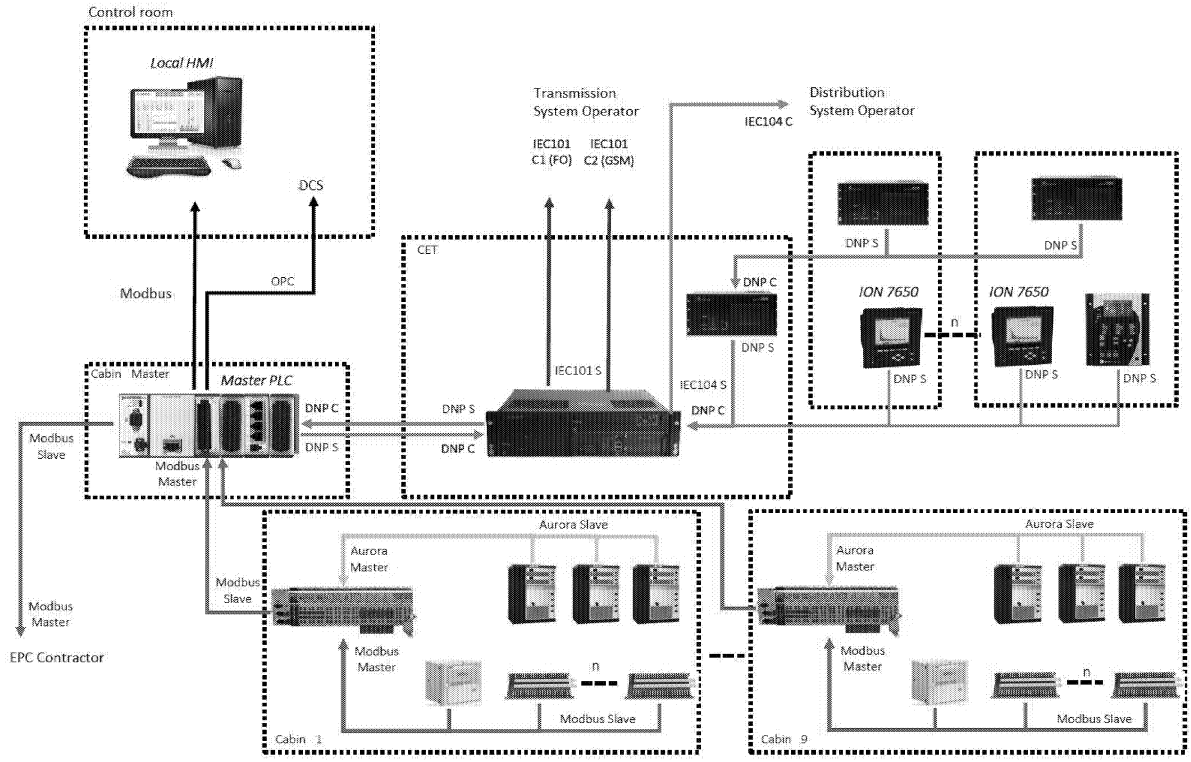

Fig. 9: Plant architecture overview

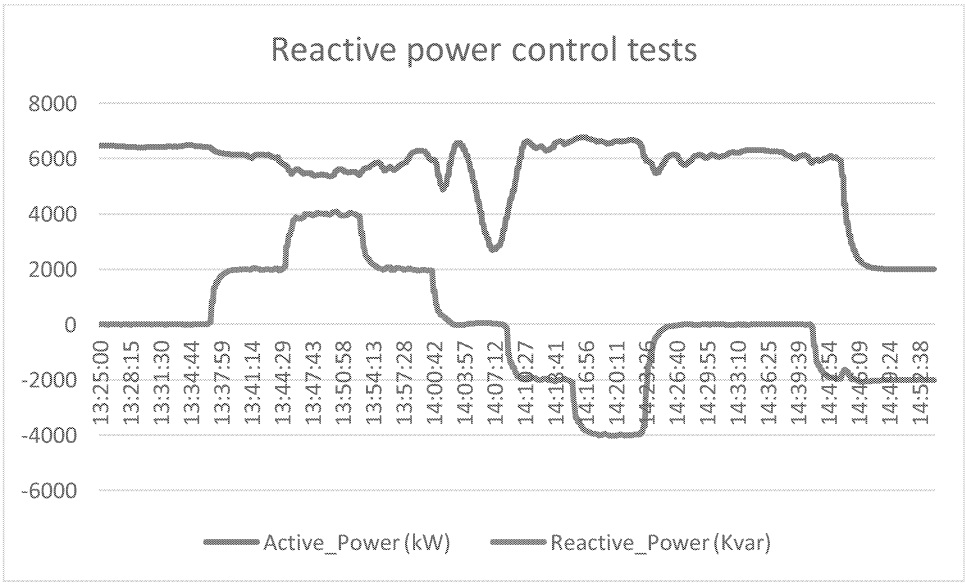

Fig. 10: Reactive power test

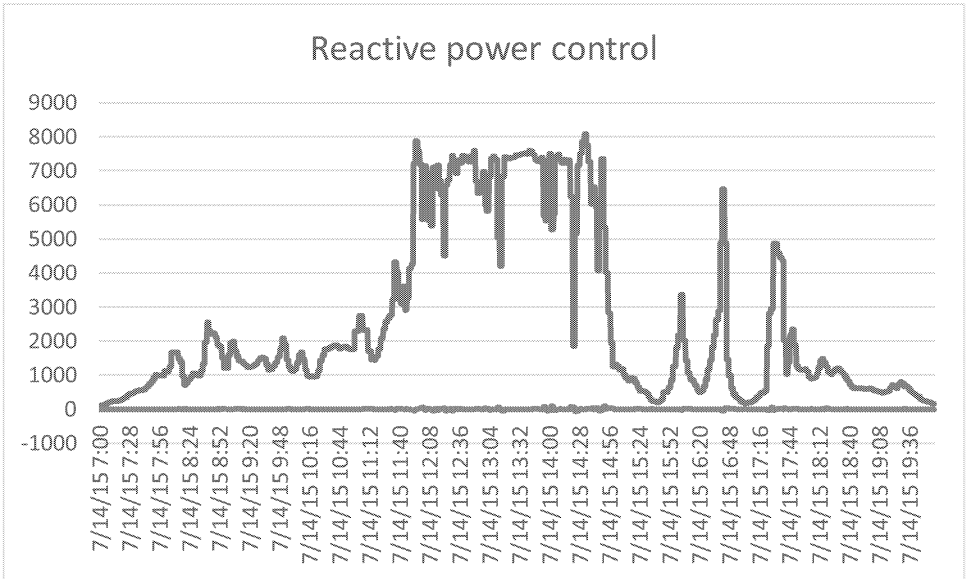

Fig. 11: 0 kvar setpoint during a day with irregular irradiation

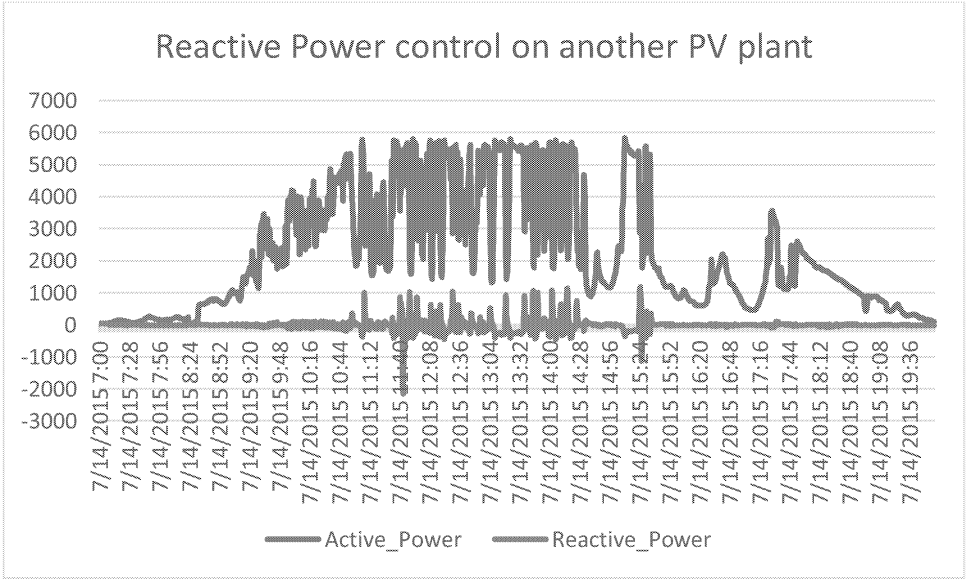

Fig. 12: 0 kvar setpoint during a day with irregular irradiation (another PV plant)

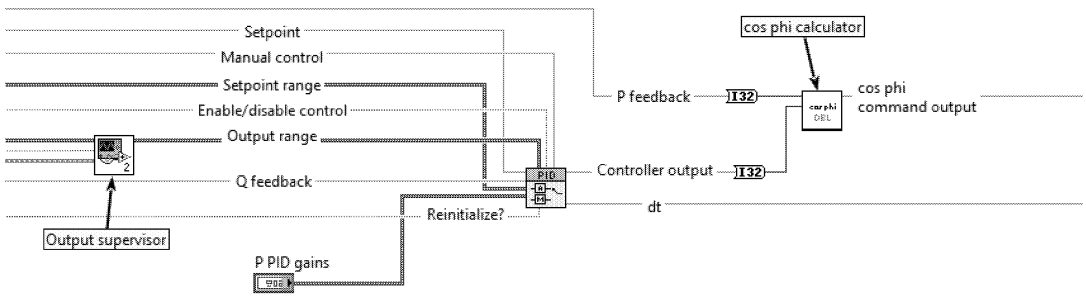

Fig. 9: Control software code snippet

AN OVERVIEW OF NSP/SCICOS
A SCIENTIFIC PACKAGE FOR MODELING AND SIMULATION

Jean-Philippe Chancelier
Cermics, ENPC,
6 et 8 avenue Blaise Pascal
77455, Marne la Vallée, Cedex, France
email: jpc@cermics.enpc.fr

Pierre Weis
INRIA,
2 rue Simone Iff, 75012 Paris, France
email: Pierre.Weis@inria.fr

KEYWORDS
Modeling, Simulation, Open-source software, Code Generation

ABSTRACT

We present the open-source scientific software package Nsp and its toolboxes, in particular the Scicos toolbox for modeling and simulation of hybrid dynamical systems.

INTRODUCTION

Nsp provides a matrix based Matlab-like language and contains a comprehensive set of scientific libraries and toolboxes. Nsp is freely distributed under the GPL open-source license.
Scicos, Campbell et al. (2010), is a modeling and simulation environment for dynamical systems. Based on a sound mathematical formalism as an extension of synchronous languages, Scicos can be used to model hybrid dynamical systems encountered in many areas of engineering.
The latest release of Nsp/Scicos introduces two major novelties: Simport, a comprehensive translator from Simulink models to Scicos models, and a code generator for Scicos, based on an original approach using partial evaluation.
The presentation, in addition to the Simport and code generation tools, will emphasize the new Nsp implementation of the Scicos toolbox. This implementation presents a number of improvements, such as a new GUI, new Coselica library for modeling cyber-physical systems based on Modelica, and new Modnum library for modeling and simulation of communication systems.

NSP

Nsp is a Matlab-like scientific software package distributed under the GPL license. Nsp is a high-level programming language; it can be used as a scripting language giving easy access to efficient numerical routines. Nsp is a full-fledged programming language. In addition, it provides an interactive computing environment.

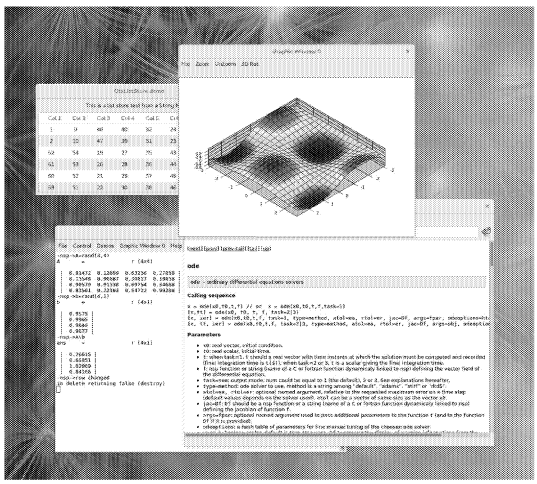

Figure 1: Nsp GUI

Nsp supports imperative programming, features automatic memory management, and obeys to a dynamic type system. Nsp contains a class system with simple inheritance and interface implementation.
When used as a programming environment, Nsp comes with online help and easy access to GUI and graphics programming (See Figure 1).
Nsp comes with a large set of external libraries, and it is easy to implement new ones. This requires writing wrapper codes, also called interfaces, to provide glue code between the external library and Nsp internal data. The interface mechanism can be either static or dynamic. Using dynamic functionalities, it is possible to build toolboxes.
Nsp shares many paradigms with other Matlab-like languages such as Matlab, Octave, Scilab and ScicosLab but also with scripting languages such as Python. Nsp syntax is quite similar to that of ScicosLab/Scilab.
Nsp includes a number of toolboxes, as for example

- Scicos: a block-diagram graphical editor for the construction and simulation of dynamical systems, which in turn includes Coselica, Reusch (2016), and Modnum, Layec (2005-2016), toolboxes and utilities for Simulink import and code generation.

- Maxplus: a library for performing (max, +) algebra operations.
- Sivp for image processing.
- Sedumi: Semi-definite programming.
- glpk, lp_solve: Linear programming.
- MPI: an interface to MPI a message-passing system to function on a wide variety of parallel computers for parallelism.
- Suitesparse: a suite of sparse matrix software.
- mexlib: implementation of the Matlab MEX Library API to facilitate the port to Nsp of Matlab toolboxes.
- Gtk2/Gtk2 language bindings for GUI construction.
- Premia: Nsp interface, Chancelier et al. (2012), to a software designed for option pricing, hedging and financial model calibration.

Nsp is developed and maintained by various academic research teams, in particular at INRIA (Institut National de Recherche en Informatique et en Automatique) and ENPC (École Nationale des Ponts et des Chaussées).

SCICOS

Scicos is a major Nsp toolbox. Scicos (see `www.scicos.org`) provides a block-diagram graphical editor for the construction and simulation of dynamical systems. Scicos is widely used at universities and engineering schools and has also gained ground in industrial environments. Nsp/Scicos is a free open-source alternative to commercial packages for dynamical system modeling and simulation, such as MATLAB/Simulink. Scicos is particularly useful for modeling systems where continuous-time and discrete-time components are interconnected. Such models can be programmed directly in Nsp, but these programs are complex and difficult to debug. Moreover, there is no simple systematic way of implementing these programs in a modular fashion.
Scicos provides a modular way to construct complex dynamical systems using a block diagram editor (See Figure 2). Scicos diagrams are compiled and simulated efficiently by a single click. Scicos handles, in particular, the interaction between continuous-time dynamics and system events including events associated with the timing of a discrete-time clock. Such events affect the way the numerical solver, which integrates the continuous-time dynamics, should be called. Handling efficiently such matters by hand for complex dynamical systems can be extremely difficult.

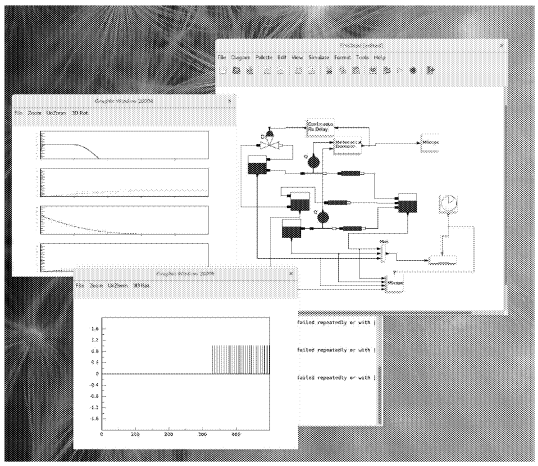

Figure 2: Scicos GUI

In Scicos, the user can construct a library of modules (blocks) that can be reused in different models in different projects. This is particularly useful when a large model is composed of blocks designed by different development teams. The Scicos formalism, which must be respected in designing blocks and sub-models, guarantees that blocks constructed separately and interconnected work harmoniously together.

A large number of blocks are already available in Scicos palettes. These blocks provide operations needed to construct models of many dynamical systems. Users seldom need to construct a new block from scratch.

Coselica toolbox

Scicos has another important feature: it supports "implicit" blocks. These blocks have no explicit inputs and outputs but rather have ports. Connecting these ports by links defines constraints. This allows the construction of systems using blocks modeling physical components in a natural way.

For example, we can define an electrical circuit with implicit blocks modeling resistors, capacitors, diodes, and other electrical components, and with links imposing Kirchhoff's laws of current and equality of voltages at the two connected ports. The possibility to mix implicit and normal blocks in the same diagram provides a powerful modeling environment.

Scicos contains an open-source Modelica compiler (`modelicac`), Najafi et al. (2005), which is used to construct implicit blocks modeling physical components. The Coselica toolbox, Reusch (2016), provides around 200 basic Modelica blocks for modeling and simulation of electrical (analog), mechanical (1D-translational, 1D-rotational, and 2D-planar) and thermodynamical (0/1D-heattransfer) systems. These blocks have been derived from the Modelica Standard Library 2.2.

Modnum toolbox

Modnum ("MODulations NUMériques"), Layec (2005-2016), contains an open source computational library for the modeling and simulation of communication systems. It includes Scicos blocks, diagrams and in-line functions of base-band PSK/QAM modulations for building communication chains. It also includes components to build spread-spectrum communication systems, such as Pseudo Noise sequence generators (Quasi-Chaotic, PN and Gold sequence generators).
Modnum provides miscellaneous scopes for Scicos such Eye Diagram scope, Scattered Diagram scope and Spectrum Analyzer scope. Modnum provides diagrams and blocks for integer and fractional frequency synthesizer components (Phase/Frequency Detector, VCO, Delta-Sigma modulators,...). Modnum handles the simulation of chaotic systems and includes simulation models for Chua's, Rössler's, Van Der Pol's and other systems.

SIMPORT TOOLBOX

Simport ("Simulink Import"), Weis (2015), is a comprehensive Simulink import assistant for Scicos. Using Simport, Scicos user can save a lot of time porting a Simulink model. Designed as a compiler (semantics passes + code generation), Simport is entirely written in OCaml and is easy to maintain and extend.
Simport translates Simulink models to Scicos models by preserving model hierarchy and diagram topology, respecting visual aspects of the original model and aiming at preserving semantics consistency. It supports both MDL and SLX file formats.
Each Simulink source block is translated either into a single equivalent Scicos block, or into a Super Block specialized according to the parameters of the source block, or into an empty Super Block for user completion, if the source block is unknown or not supported. Simport translation library covers a large subset of Simulink basic blocks.
Simulink model parameters are often defined in companion Matlab scripts. Simport allows users to associate one or more Matlab scripts (M-files) with each Simulink model to be translated. A simple translation scheme is used to translate these Matlab programs into Nsp code, which are included in the Scicos model. The extent of this translation is limited to generating legal Nsp syntax and should not be considered a Matlab import. Often the companion M-files contain simple parameter definitions and this translation is enough. If not, it provides a reasonable first draft that the user needs to edit. Matlab expressions used inside Simulink blocks are processed similarly.
The result of importing a Simulink model and its companion M-files is a Scicos model. The contents of the M-files are included in contexts of the Scicos diagrams. Unlike Simulink, Scicos models are self-contained: Scicos model contains the definition of all of its parameters.

CODE GENERATION TOOLBOX

Code generation is an important functionality in Scicos. In a typical application the diagram represents a controlled system. The controller part of the diagram, after validation of the control law through simulation, has to be implemented in an embedded system. To ease this process, Scicos supports C code generation for a part of the diagram designated by the user.
The built-in Scicos code generator uses block simulation routines as an external library. As such, the generated code cannot be inlined and is not efficient. The lack of efficiency is mainly due to the fact that the block routines are not always specialized, i.e., these routines contain switches depending on input types and dimensions. Even though the types and dimensions are known at compile time, these switches remain active throughout the simulation.
The new code generation toolbox aims at removing these drawbacks by generating efficient inlined code.
This code generation tool was developed during a three-year research project funded by the French FUI 2011 "P" Project (see `www.open-do.org/projects/p/`).
The basic idea of this approach is to express block behaviors as Nsp programs and automatically generate code from these programs, Chancelier and Nikoukhah (2015) and Chancelier and Nikoukhah (2014). The methodology is based on partial evaluation and takes advantage of the operator overloading facility available in Nsp.
The fundamental premise of this approach is that block semantics are frequently similar to Nsp primitive semantics. This makes it very convenient to express Scicos block behaviors in the Nsp language. In particular many blocks can be expressed in few lines of Nsp code that handles all data types and all data sizes. To handle type and size variability, the C simulation code for a block may include more than twenty routines.
In general, code generation for a piece of Nsp code is not possible or yields a very inefficient code. As for similar languages, the main culprit is dynamic typing: the types and sizes of the variables are only known at run time. It turns out that for the Nsp code associated with a Scicos diagram and its blocks, the type and size information can be determined in advance. This is done in particular by the Scicos compiler.
The code generator first creates an Nsp script based on the Scicos model. Then this script is executed after overloading all the basic functions and operators. This generates a pseudo code, which after optimization is pretty-printed into C. A pretty printer for Ada is also available.
There are many advantages in using this technique as opposed to developing an independent code generator: this code generator does not use a different parser for

the scripting language; the script is run using the tool itself. Similarly, the operator and functions used in the process of partial evaluation are that of the scripting language itself. Finally the operator overloading is being performed in the scripting language, so it can be customized easily for different targets.
Consider the following simple example: an Nsp function `f`, which converts its argument to a Boolean matrix.

```
function y=f(z);
  y=convert(z,"b");
endfunction;
```

To generate C code for a specialized version of function `f` applied to a 2 by 2 real matrix, type information arguments are given to the Nsp code that partially evaluates the body of `f`; after partial evaluation the following C code is emitted:

```
static void f(double *z,gboolean *tmp_17)
{
 gboolean tmp_1[4], tmp_3, tmp_5[4], tmp_7,
   tmp_9[4], tmp_11, tmp_13[4], tmp_15;
 double tmp_2, tmp_6, tmp_10, tmp_14;
    tmp_2=(z[0]);
    tmp_3=( tmp_2 != 0.0);
    memcpy(tmp_5,tmp_1,4*sizeof(gboolean));
    tmp_5[0]=tmp_3;
    tmp_6=(z[1]);
    tmp_7=( tmp_6 != 0.0);
    memcpy(tmp_9,tmp_5,4*sizeof(gboolean));
    tmp_9[1]=tmp_7;
    tmp_10=(z[2]);
    tmp_11=( tmp_10 != 0.0);
    memcpy(tmp_13,tmp_9,4*sizeof(gboolean));
    tmp_13[2]=tmp_11;
    tmp_14=(z[3]);
    tmp_15=( tmp_14 != 0.0);
    memcpy(tmp_17,tmp_13,4*sizeof(gboolean));
    tmp_17[3]=tmp_15;
};
```

Next, a code optimization phase simplifes the C code as follows:

```
static void f(double *z,gboolean *tmp_1)
{
   tmp_1[0]=( (z[0]) != 0.0);
   tmp_1[1]=( (z[1]) != 0.0);
   tmp_1[2]=( (z[2]) != 0.0);
   tmp_1[3]=( (z[3]) != 0.0);
};
```

In addition, the compiler also generated a C wrapper to export the new generated C function in Nsp.

```
static int int_f
  (Stack stack, int rhs, int opt, int lhs)
{
  NspMatrix *z;
  NspBMatrix *tmp_1;
  CheckStdRhs(1,1);
  CheckLhs(0,1);
  if ((z = GetMat (stack, 1))
       == NULLMAT) return RET_BUG;
  if ((tmp_1 = nsp_bmatrix_create(NVOID,2,2))
       == NULL) return RET_BUG;
  (void) f(z->R,tmp_1->B);
  if ( lhs >= 1 ) {;
  MoveObj(stack,1, NSP_OBJECT(tmp_1));}
  else { nsp_bmatrix_destroy(tmp_1);;}
  return Max(lhs,0);
}
```

CONCLUSION

Nsp/Scicos provides a powerful environment for modeling and simulation of large dynamical systems. A number of toolboxes facilitates the use of Nsp/Scicos in various application domains. After validation through simulation, Scicos code generation facility can generate efficient code for embedded applications. Finally, Simport is an import assistant tool for Nsp/Scicos: it helps the translation of existing Simulink models for reusing them in Nsp/Scicos.

REFERENCES

Campbell S.L.; Chancelier J.P.; and Nikoukhah R., 2010. *Modeling and Simulation in Scilab/Scicos with ScicosLab 4.4*. Springer.

Chancelier J.P.; Lelong J.; and Lapeyre B., 2012. *Using Premia and Nsp for Constructing a Risk Management Benchmark for Testing Parallel Architecture. Concurrency and Computation: Practice and Experience*, 26, no. 9, 1654–1665.

Chancelier J.P. and Nikoukhah R., 2014. *Code generation through partial evaluation for Scicos/Nsp.* In *Proceedings of Sim@SL, Cargèse, Oct. 19th-21st, 2014.*

Chancelier J.P. and Nikoukhah R., 2015. *A novel code generation methodology for block diagram modeler and simulators Scicos and VSS.* In *https://hal.archives-ouvertes.fr/hal-01213247*. HAL.

Layec A., 2005-2016. *Modnum toolbox, an open source computational library for the modelling and the simulation of communication systems.* In *www.scicos.org/ScicosModNum/modnum_web/web/eng.*

Najafi M.; Furic S.; and Nikoukhah R., 2005. *SCICOS: a general purpose modeling and simulation environment.* In *Proceedings of 4th International Modelica Conference, March 7-8, 2005.* The Modelica Association.

Reusch D., 2016. *Coselica toolbox, a library of Modelica blocks.* In *http://www.kybdr.de/software.*

Weis P., 2015. *A Simulink Model Importer for Scicos.* In *Proceedings of the 3rd Sim@SL, École Normale Supérieure de Cachan, October 14th-16th.*

AI BASED SIMULATION METHODOLOGY

SIMULATION AND ADAPTATION OF PATHFINDING ALGORITHMS UNDER REALISTIC PHYSICAL CONDITIONS IN 3D ENVIRONMENT

Erhan Bülbül
Measurement, Selection and Placement Center
Ankara, Turkey
erhan.bulbul@osym.gov.tr

Şahin Emrah Amrahov
Department of Computer Engineering
Ankara University
Ankara, Turkey
emrah@eng.ankara.edu.tr

KEYWORDS

Path Finding, Graphs, 3D Simulation, Dijkstra algorithm, A* algorithm, Shortest path.

ABSTRACT

In this paper we represent simulation of an object (mobile unit) moving under controllable physical conditions in a 3D heterogeneous environment. In our simulation, physical conditions depend on some parameters such as width of the path, gravity, fraction of surface, etc. The object has to find the shortest path from source to target. We use Dijkstra and A* algorithms, which we adapt for varying situations. The algorithms were compared with one another with respect to efficiency, time and cost of the preferred path.

INTRODUCTION

Commercial games generated a $22.41 billion industry in 2014 (ESA 2015) with a continuos annually growth rate. Developers strive toward greater gamer-satisfaction by improving the appeal of the visual stimuli. This is usually done via improving hardware which leads to more realistic graphics and lighting. However, gamer feedback often indicates that one of the most significant determinants of gamer experience and satisfaction is the AI quality.

Pathfinding is commonly used in multi agent applications, AI designs and games typically involving finding the shortest route.. The fact that in real life shortest route may not always coincide with the optimal path thus might impact the realistic perception of the application. Therefore, the unit should navigate the optimal path which is the most efficient one for the situation at hand which often involves maps, features of the moving unit and a time dimension. Therefore path planning may yield to differing outcomes depending upon environmental circumstances and features of the moving unit. This could be illustrated by real life situations. For instance, race car drivers try to attain optimal efficiency by choosing a path with the least number of turns and road-bumps. On the other hand, drivers of off-road vehicles may not be as concerned about bumps or turns since they will not cause significant loss in efficiency. Other features of vehicles such as their size may also pose limitations to efficiency. For example, navigating a narrow route may interfere with efficiency of a truck but not a car.

An optimal path involves planning a route with the least number of obstacles between a starting and a target point. Simulating this can be done in multiple ways.. A simple way could be to assume that each pixel of a computer screen is a vertex of a graph and the neighboring pixels are connected. Then path planning problem in a computer screen is transformed into the shortest path problem of the graph theory. Hence, the problem can be solved by either the Dijkstra (Dijkstra 1959) or A* (Hart et al. 1968) algorithms. The main downside of this approach is that we have too many vertices in the transformed graph. This is indeed the reason the problem cannot be solved in real life. Even if one chooses to look at pixels in a certain ellipse (Gasilov et al 2011) rather than looking at all the pixels he or she will still have a large count at hand. An efficient way is to use the Grid-Graph approach (Yap 2002). This method requires grouping of homogenous areas as tiles, forming in a grid, where all tiles are implemented as graph nodes. This approach is applicable to a variety of maps used in games (Sturtevant 2012).

As noted earlier environmental factors should be included as to create a realistic and dynamic appearance. One of the issues that make construction of a terrain more challenging and complex is the fact that all regions cannot be equivalent. Such map issues have been discussed extensively in previous studies. There have been studies on real-time path planning in heterogeneous environments (Jaklin et al 2013), indoor environments (Liu and Zlatanova 2013) and multi-layered environments (Toll et al 2011). Adding different physical factors makes path planning further intricate. In this paper we present simulation of path planning problem under realistic physical conditions in 3D environments and offer methods for adaptation to increase traveling efficiency.

METHOD

Graph Creation

We modeled a 3D space as a graph. We divided the planes with size 40x40 into 5x5 sized micro planes. These micro planes were considered as a vertex (node) of the graph. Therefore, the graph consists of 64 vertices. We assigned the center point of micro planes as the coordinate of the related vertex.

Connections between vertices of the graph are made by the undirected edges. We utilized different connection models for the used implementation of edges of the graph. In the first model, each vertex has 4 degree, namely from vertices inside there are four directions which are up, down, left and right. For this model we have a graph with 64 vertices and 112 edges. In the second model, for each vertex we used 8-way connections which include extra 4 ways by diagonal. In this connection model an 8x8 graph requires 210 edges (see figure 1). The third model includes optional circular connections that link to diagonal vertices and therefore could be used as an alternative to direct diagonal connections. With the addition of these circular connections the edge number rose to 308 (see Figure 5).

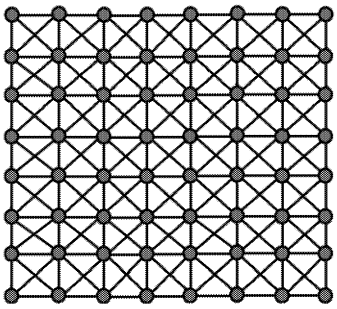

Figure 1: Vertices and connections of 8x8 graphs (Second Model)

High planes are also designed as vertices. Connections between high planes and lower planes are made by ramps. Ramps involve micro planes with an angle value that helps to determine its length and a direction value showing available connections. Ramps are designed to have only 2 connections on one direction.

Angle value shows the angle between the normal of the ground and the ramp. Therefore if the ramp's maximum height is known then its length can be calculated. Length of a ramp is calculated as:

$$L=H/\sin\alpha$$

where L is length of the ramp's surface, H is height of the ramp and α is the angle between the normal of the ground and normal of the ramp.

Design of the Map

As mentioned above, the map is designed as a plane that consists of 64 micro planes. The map which we used in the simulation should involve testing of all factors and allow observing of the changes depending on these parameters. The map also should include different available paths between start and target points. Final design of the map is illustrated below.

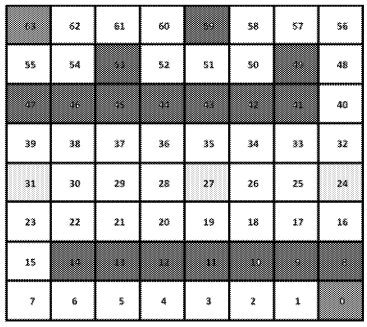

Figure 2: Map used in the simulation. Green vertices are starting and target vertices, white vertices are regular vertices, red vertices are those with high cost (fraction), yellow vertices are ramps connecting 2 different levels.

Calculating the Weight of Edges

Without inclusion of the physical factors, weight of edges is calculated according only to distance between the adjacent vertices that edge connects. As noted above, a 5x5 unit sized micro-plane represents a vertex of the graph and center point of this micro-plane is considered as vertex's coordinates. As a result of this dependency vertical and horizontal edge lengths are 5, while diagonal edges' weight is 7 which has an approximate value of $5\sqrt{2}$. In this model all edges are symmetric. In other words, weight of edges are the same in both directions.

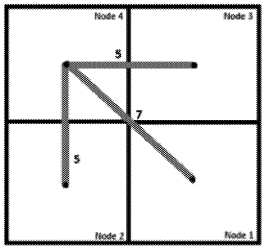

Figure 3: Weight of edges without physical factors involved

Design of the Mobile Unit

A mobile unit is needed to navigate the path determined by the algorithm. Considering that the unit will have to move on micro planes; which in this case vertices, size of the unit must be less than the size of each micro plane so as to allow the unit to get on micro planes (on the vertex). The size of the unit size is set as (4.0x,2.0y,2.0z); the size of a micro-plane is set as (5.0x,5.0y,5.0z) and the size of the whole graph plane is (40.0x,10.0y,40.0z).

Heuristic Analysis

While utilizing A* pathfinding algorithm the heuristic value used is the calculated distance from the center of the vertex being processed to the center point of the target vertex. A coefficient value is applied to change the effect of heuristic value and it is used to observe different behaviors depending on the inaccurate heuristic analysis. Default coefficient value

is 1, which gives the exact distance between the points as the heuristic value.

Adding Physical Factors

Physical factors affect efficiency in different ways. Some factors may increase the time needed to navigate the path while some factors increase the power needed to move the unit from one point to another.

Gravity

Adding gravity factor to the calculations could be done with minor weight differences. Gravity affects power needed for climbing ramps, and creates fraction on the vertices.

Gravity pulls the unit on $-y$. This has no effect on flat surface. On the other hand, when the unit is climbing a ramp, gravity creates a force that pulls the unit backward. This force's magnitude is calculated as follows:

$$F=mg\sin\alpha$$

where m is mass of the unit, g is the gravity value which equals to 9.8 m/s^2, α is the angle between the ground and the ramp and F is the force that pulls the unit backward. As highlighted above, while α increases, gravity pulls the unit backward with a greater force. On the other hand, while the unit is climbing downward, this force accelerates the unit.

Texture/Fraction

In real life the material of the ground varies and this may affect movement of objects on these planes in many ways. Thus, some vertices are given different weights and the corresponding planes are textured accordingly to discriminate them from others.

Size of the Unit

Point units are commonly used in theoretical studies but it has no correspondence in practice. We live in 3D space which necessitates taking the size and volumes of moving objects into account. Therefore, the size of the mobile unit needs to be determined

As stated above, the size of the area that corresponds to a vertex of the graph is 5×5 units. To navigate easily between these vertices, the mobile unit needs to be smaller than a graph area. Considering realistic width/length ratios of cars; the measures of the unit are set to $4 \times 2 \times 2$, which is also the size of the unit's model.

Having a width causes the unit to travel along a plane rather than a line. This plane may include surfaces t of different vertices. Therefore, if the size of the unit is implemented, calculation of edges needs to be revised.

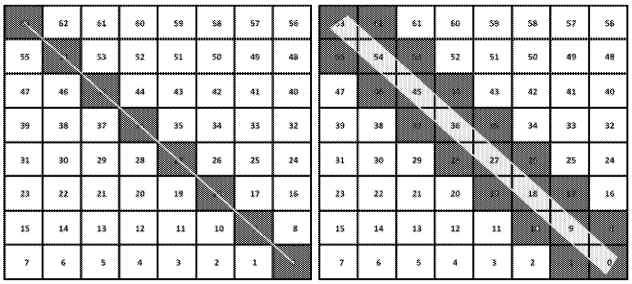

Figure 4: The surfaces interacting with the unit change depending on the size of the unit. Point unit (left) and non-point unit (right) interactions are as shown

Movement Type (Linear/Circular)

Most vehicles are capable of making oval turns. This movement may be advantageous in some circumstances. With circular movement enabled, the degree of the graph is 16.

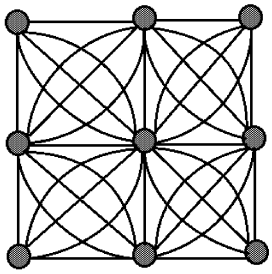

Figure 5: Connection model with both linear and circular edges

Circular edges make the unit move in a circular route ending at a diagonally adjacent vertex. Avoiding high weight vertex makes this movement less costly.

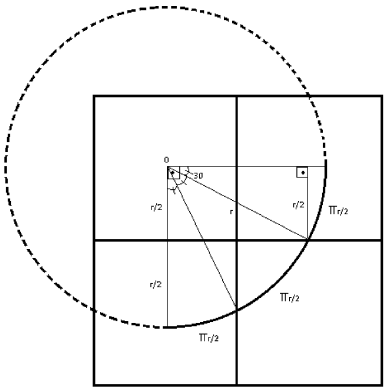

Figure 6: Calculation of the weight of circular edges

Acceleration

Vehicles are easier to control while driving on a straight road than taking turns. Therefore, most drivers raise their speed when they are on a straight road to reach their destination in a shorter time. Using this strategy is essential for time efficiency.

The mobile unit is considered to have a line of sight with a range of 5 units. Using this information the unit can check the direction and type of the next edge. If the sequential edges on the path are on the same direction, the unit gains 1 speed per edge unless edges are circular or the corresponding vertices are ramps. If the sequential edge's direction or type is different, the unit (vehicle) slows down. Starting speed is 4 units/second which is also the slowest speed of the vehicle. Maximum speed is determined as 12 units/second. A speed coefficient is used to determine the advantage of speed and acceleration which is calculated as:

$$\text{Speed Coefficient} = \text{MinS}/\text{CurS} \qquad (1)$$

where MinS is the minimum speed possible and CurS is the speed of the unit at the beginning of the edge. The lower Speed Coefficient value gives lower costs for edges. The pseudo-code for calculating Speed Coefficient is given below:

```
Calculation of speed coefficient for edge E<N,X>
  Set Acceleration to 0
  Set Coefficient to 1
  If current movement direction=direction of E<N,X>
    If N is not ramp and X is not ramp and E is not circular
        If speed<MAXspeed then
            Set Acceleration to 1
        Else Set Acceleration to 0
    Else Set Speed to MinSpeed
  Speed+=Acceleration
  Coefficient=MinSpeed/Speed
```

The effect of the Speed Coefficient is enabled via "Acceleration" parameter. This parameter does not control the ability to accelerate; it determines whether or not acceleration will be used to reduce the traveling time. The unit gets accelerated when it is traveling on same direction regardless of the acceleration parameter.

SIMULATION RESULTS

The appearance of the terrain and the mobile unit is seen as in Figures 7 and 8.

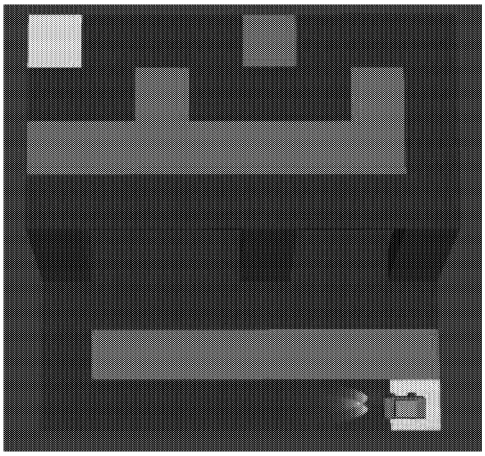

Figure 7: A screenshot of the simulation showing the terrain and the mobile unit (top-down view)

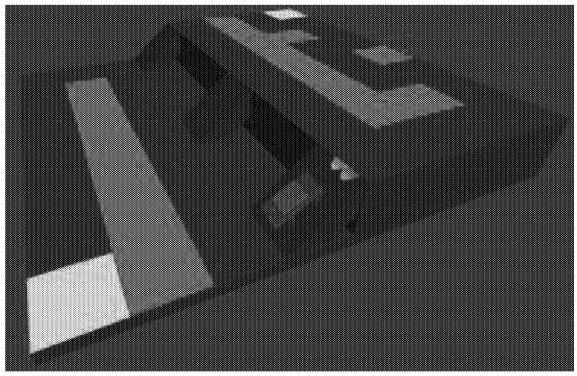

Figure 8: A screenshot of the simulation illustrating the map and the mobile unit (side view)

We conducted several tests to determine the shortest path by taking the physical conditions (Table 1) into account. "Heuristic" parameter controls if the heuristic approach is used. "Acceleration" parameter determines whether or not acceleration will be used to reduce the traveling time. "Circular" parameter enables or disables the circular edges. "Volume" parameter-if set true-defines the unit as non-point unit and "Gravity" parameter turns the gravity feature on or off. Test results show the effects and connections of parameters. Efficiency of tests is measured with two parameters; one is the total cost of the navigated path from start to finish; the other is the total time elapsed in navigating the path.

In first 6 tests, we measured separate effects of parameters on the algorithms' performance. Heuristic approach and acceleration calculations, have significantly shortened the time to reach the goal. On the other hand, the other factors do not have a significant effect on required time. The expected change of the total cost depending on the volume parameter stated above is illustrated by comparing Test1 and Test 5 (see Figure 9).

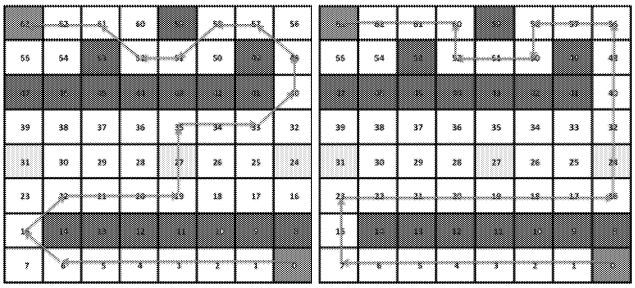

Figure 9: Tests 1 (left) and 5 (right). If the unit is considered as a point, it uses diagonal edges, if not, it avoids them

If volume is correct, circular edges provide a lower-cost-path than diagonal edges in some cases. Therefore, the unit prefers to track these circular edges to lessen the cost. Results of this choice are shown in comparison of Tests 4 and 10 where both the needed time and the total cost were optimized with the help of circular edges. (see Figure 10)

Table 1: Test Conditions and Results

Test No	Heuristic	Acceleration	Circular	Volume	Gravity	Total Cost	Time(sec)
1	False	False	False	False	False	137	63,85
2	True	False	False	False	False	140	54,68
3	False	True	False	False	False	140	54,31
4	False	False	True	False	False	137	63,86
5	False	False	False	True	False	155	63,96
6	False	False	False	False	True	137	64,03
7	False	True	True	False	False	140	53,73
8	False	True	False	True	False	155	64,47
9	False	True	False	False	True	140	53,76
10	False	False	True	True	False	142	58,34
11	False	False	True	False	True	137	63,82
12	False	False	False	True	True	155	63,89
13	False	True	True	True	False	148,56	55,59
14	False	True	True	False	True	140	54,14
15	False	True	False	True	True	155	64,12
16	False	False	True	True	True	142,12	58,47
17	False	True	True	True	True	148,56	55,19
18	True	True	False	False	False	140	54,58
19	True	False	True	False	False	140,85	52,16
20	True	False	False	True	False	155	63,98
21	True	False	False	False	True	140	54,47
22	True	True	True	False	False	140,85	52,18
23	True	True	False	True	False	155	63,82
24	True	True	False	False	True	140	54,10
25	True	False	True	True	False	144,269	50,59
26	True	False	True	False	True	140,85	51,83
27	True	False	False	True	True	155	63,62
28	True	True	True	True	False	144,26	50,84
29	True	True	True	False	True	140	51,76
30	True	True	False	True	True	155	62,96
31	True	False	True	True	True	144,26	50,73
32	True	True	True	True	True	144,26	50,41

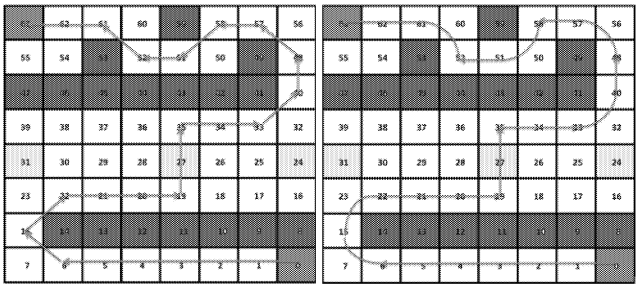

Figure 10: Tests 4 (left) and 10 (right) If volume is correct and circular edges are allowed, unit uses circular edges to avoid penalty vertices

If the benefits of acceleration are taken into account by algorithm, with enough speed; the unit refuses to use diagonal or circular edges and prefers to turn with a square-like move to maintain its speed for one more vertex. This rises the total cost but decreases the time needed to reach the goal. Results of Test 10 and Test 13 are presented below (see Figure 11).

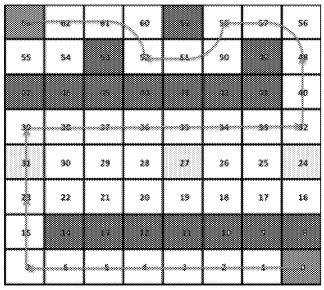

Figure 11: Test 13. If benefits of acceleration are calculated, the unit refuses to turn at first chance to maintain its speed and benefit from its speed at maximum level

When the unit is considered as a point, best test results are achieved at Test 29. On the other hand, if volume parameter is correct, Test 32 provides the best results. In both tests heuristic approach is used, acceleration benefits are calculated, circular movement is allowed and gravity is on. The only difference between the two tests is that Test 29 is the movement of a point unit while Test 32 is the movement of a unit that has a size and a volume. Therefore, it would be accurate to conclude that these modifications adapt the

algorithm to some physical conditions and yield more efficient results.

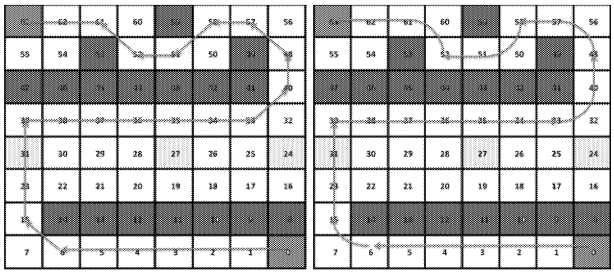

Figure 12: Tests 29(left) and 32(right)

Trade-Offs of Parameters

Tests show that value of the physical and other parameters influence efficiency. Tests run on a 4x4 graph with 16 vertices were not efficient because a small map does not allow the unit to gain speed. Thus, it is safe to say that the algorithm takes the advantage of high speed as the map gets bigger. Correspondingly, maximum and minimum speed limits are quite relevant to efficiency. Minimum speed is used to determine speed coefficient value as seen in equation 1. Higher minimum speed would decrease the effect of acceleration parameter on the choices of algorithms while lower minimum speed would increase it.

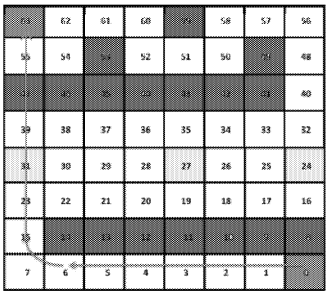

Figure 13: Test 32 with (2*Speed-Coefficient) setting

As seen in Figure 13 when speed-coefficient is doubled, the advantage of acceleration seems more desirable and the algorithm rejects making a turn at the 39th vertex to maintain the speed of the unit.

CONCLUSION

In this paper we simulated effects of some real time factors on Dijkstra algorithm and observed results in terms of time and cost. Simulation has been done in 3D environment that consists of a graph with 64 nodes and 308 connections. Effects of gravity, the size of unit, acceleration, fraction, movement and turning abilities were tested. In addition to Dijkstra algorithm, advantages of using a variation of Dijkstra with heuristic approach (A*) were also examined.. Tests were run with different parameter settings to determine the degree to which the cost of the chosen path and time needed were affected. Results of the tests showed that each factor has a varying impact on the path. Combination of these effects might dramatically compromise efficiency.

Given results of the current study show that effects of parameters depend on the map that simulation is running on, future work should focus on customization of the maps in order to attain maximum levels of efficiency.

Further tests on different maps and circumstances could be tested in terms of their benefits and downsides which in turn lead to creating optimal setting presets for varying circumstances and goals.

REFERENCES

Dijkstra.E. W. 1959. "A note on two problems in connexion with graphs", *Numerische Mathematik*, *Vol. 1*, 269-271.

Entertainment Software Association(ESA). 2015. *Essential Facts About Computer and Video Game Industry*.

Gasilov N.; Dogan M. and Arıcı V. 2011. "Two-stage shortest path algorithm for solving optimal obstacle avoidance problem", *IETE Journal of Research, Vol. 57*, 278-285.

Hart P. E.; Nilsson N. J. and Raphael B. 1968. "A formal basis for the heuristic determination of minimum cost paths", *IEEE Transactions on Systems Science and Cybernetics Vol. 4*, 100–107.

Jaklin N.; Cook IV A. and Geraerts R. 2013. "Real-time path planning in heterogeneous environments", *Computer Animation and Virtual Worlds, vol. 24,* 285-295.

Liu L. and Zlatanova S. 2013. "A two-level path-finding strategy for indoor navigation", *Intelligent Systems for Crisis Management, Lecture Notes in Geoinformation and Cartography*, 31-42.

Sturtevant N. R. 2012."Benchmarks for grid-based pathfinding", *Transactions on Computational Intelligence and AI in Games*, *Vol. 4,* 144-148.

Toll W., Cook IV A. and Geraerts R 2011. "Navigation meshes for realistic multi-layered environments", *IEEE/RSJ International Conference on Intelligent Robots and Systems*, pp. 3526-3532, September 25-30. San Francisco, CA, USA.

Yap. P. 2002. "Grid-gased path-finding." *Lecture Notes in Computer Science, Vol. 2338*, 44-55.

BIOGRAPHIES

ERHAN BÜLBÜL received the degrees of B.Sc. in Computer Engineering in 2010 from Karadeniz Technical University and M.Sc. in the Department of Computer Engineering at Ankara University. He is currently a PhD candidate studying at Gazi University, Ankara in the field aforementioned. His research interests are computer graphics, artificial intelligence and algorithms. Address for correspondence: OSYM Baskanligi 06800 Bilkent/Ankara, Turkey. Email: erhan.bulbul@osym.gov.tr

ŞAHİN EMRAH AMRAHOV is an Associate Professor at Computer Engineering department, Ankara University, Ankara, Turkey. He received B.Sc. and Ph.D. degrees in applied mathematics in 1984 and 1989, respectively, from Lomonosov Moscow State University, Russia. His research interests include the areas of mathematical modeling, algorithms, artificial intelligence, fuzzy sets and systems, optimal control, theory of stability and numerical methods in differential equations. Email: emrah@eng.ankara.edu.tr

A COMPARATIVE APPROACH TO MODEL TRAFFIC LIGHT CONTROLLER BASED ON ARTIFICIAL NEURAL NETWORKS

Jinan Aboutaam
Arab Open University
Lebanon
jha009@aou.edu.lb

Nouhad Amaneddine
Arab Open University
Lebanon
namaneddine@aou.edu.lb

Marwan Al-Akaidi
Arab Open University
Kuwait
m.al-akaidi@arabou.edu.kw

KEYWORDS
ANN, TLC, Adaptive system, Modelling TLC.

ABSTRACT

We propose in this paper a new approach to model traffic light controller (TLC) relying exclusively on Artificial Neural Networks (ANN) technology; we present as well a comparative approach of ANN architectures applied to solve the underlying traffic problem. Traditional controllers have limitations and cannot adapt to changing traffic demands, where adaptive controlling requires mathematical modelling and optimisation where traditional methods is insufficient for modelling and controlling the system due to non-linearity and non-deterministic nature of traffic control model. Artificial intelligence techniques were highly utilised to deal with problems of similar category, and proves superiority in TLC applications. In this work, we explore the generalisation capability of various ANN models in solving the TLC problem. The performances of different models are compared by analysing the training and testing results of each network.

INTRODUCTION

Traffic congestion is becoming a constant fact in the majority of modern cities, this is leading to an increasing global traffic management problem and thus, it needs an intelligent automation of the traffic controllers while the interference of adaptive controllers is becoming highly required. Advanced technologies have to be utilised to enhance traffic management systems (Singh 2014), our work aimed to tackle the problem with Artificial Neural Network while providing a comparative approaches of variants ANN architectures for an exclusively NN-based traffic light controller.
Research in transportation domain provides various attempts in order to optimise traffic flow to relieve traffic congestion which is becoming constant. Given the increasing number of road users (vehicles) and the limited resources provided by traffic infrastructures, road users experience increased travel time resulting negative environmental and economical impacts (Dabahde and Kshirsagar 2015). One of the cost-efficient and effective way to deal with traffic management is by using intelligent controlling of traffic lights (Yang 2004, Kamal et al. 2014). Although some governments and local authorities particularly in north America tend to replace traffic light by modern roundabout aiming at reducing pollution and fatalities, this choice is not deployed in the majority of the countries due to the restrictions imposed by the required space, particularly in city centers, business areas and regions crowded with modern buildings.
Traffic light control problem has been addressed by many research works that utilise various artificial intelligence (AI) techniques such as fuzzy logic, expert systems, reinforcement learning, evolutionary algorithm and artificial neural networks (Liu 2007). Exclusive use of Artificial neural network was successful to solve problems in various transportation domains, this includes but not limited to traffic forecasting, traffic incidents and traffic flow modelling (Sommer et al. 2013, Zhang et al. 1997, Srinivasan et al. 2004). In TLC, ANN has been widely used but mostly combined with other AI techniques. Our work aims at modelling TLC by relying exclusively on ANN and, assessing the performance of variants ANN based models.
The remaining sections of this paper are organised as follows: section two discusses the TLC problem, including the limitations of current traditional controllers and the challenges of adaptive controlling as well as the rational behind choosing NN, and thus how ANN tackles the problem. In section three we present some recent approach from the literature. Section four presents the proposed model and summarises the observation processes used to explore the performance of different network architectures. We present the experimental findings and the related analysis in section five. We finish the paper by providing the best ANN settings to model the traffic light controller aiming at contributing in solving the traffic congestion problem and presenting a potential future horizon.

TRAFFIC LIGHT CONTROLLER (TLC)

We are concerned with traffic light controller as an integral part of the traffic control system, the main role of such system is to optimise the traffic flow. The prob-

lems encountered by using traditional controllers have to be addressed. This includes heavy traffic jam, which varies with respect to time slots and leads to increased traveling time, unreasonable latency time of stoppage in case of no traffic this occurs while waiting the green light, and deficiency in adapting to dynamic changes of traffic demand. To deal with different traffic conditions (fluctuation in traffic), we propose an adaptive controller where the main challenges to consider is modelling and optimisation (Liu 2007).

Traffic jam might be dealt by using controllers in which different setting delays are assigned to different junctions (i.e larger for junctions of higher traffic volume). Cases of waiting while no traffic may be dealt with by other types of controllers in which timing of signals is set according to detected traffic flow on each road, and where traffic signals in adjacent junctions are synchronised. For managing different traffic conditions, an appropriate solution is to utilise the learning capabilities of artificial neural networks that mimic human intelligent behaviour. Hence we propose a model for intelligent adaptive controller for traffic lights based on traffic-volume that is an alternative to traditional time-division based controllers, and which mainly aims at reducing the waiting time at intersections. This requires an optimisation of model equations which appropriately solved by artificial intelligence techniques.

An adaptive controller is defined as a methodology that includes a mathematical model representing traffic behaviour, in addition to that it uses an adaptive algorithm (i.e model optimisation algorithm) which searches for the optimal signal settings for traffic signal at intersection (Lam 2013). It is affirmed that no amount of math can perfectly model traffic situations (Berman 2014), and that some control-related variables are almost inaccessible unless estimation techniques are applied (Varga et al. 2006), therefore we consider that it is a natural choice to utilise the capabilities of ANN to approximate vehicle behaviour at intersection as it has widely been used to approximate complex system behaviour, and also for optimisation of model equations which are best dealt with by artificial intelligence techniques (Rass and Kyamakya 2007), it is realised that ANN is highly used to enhance optimisation problems.

ANN application is considered appropriate for the traffic domain and traffic light control problem due to the non-linearity and not deterministic nature of the problem, and also due to its ability to mimic human intelligence in solving problems and its capability of evolution and learning. ANN is distinguished from conventional computing and traditional AI approaches by its properties of parallel information processing, extremely fault tolerance due to Knowledge distribution throughout the system; and in addition to that ANN is considered to be an adaptive model. ANN tackle the problem using a network that takes a set of inputs and the corresponding desired outputs, as training set, and then, the system learns from those training examples by automatically inferring the rules for TLC settings when exposed to new situation with a variety of input sets.

STATE OF THE ART

TLC problem has been addressed by considerable research work that utilised various artificial intelligence techniques. As for ANN, its application in the traffic light control has been mainly tackled using three different methodologies: first, solely and directly addressing the control problem, second, combined with other technique, and finally utilising its generalisation capability based on other method (Liu 2007). The literature includes ANN variants as well as non ANN-based approaches. So far, it has been realised that ANN is mostly utilised in combination with other techniques and methods. This has been justified by the modest performance of ANN depending on the underneath model (Singh 2014). This problem is inviting to further investigate this performance impact on our proposed model.

Exclusive ANN-based Approach:

Nahatsuji and Kaku (Nakatsuji and Kaku 1991) have an attempt to use ANN to exclusively and directly alter traffic control parameters by developing a self-organised control system, where a NN is directly trained to suggest the optimum green splits for single intersection. The model inputs split length of signal phases and outputs measures of effectiveness as queue lengths and performance indexes. A multilayer feedforward neural network is trained using backpropagation method and optimisation is carried out by hybrid method combining Cauchy machine with a feedback method to minimise the squared sum of queue lengths. The approach deals with split optimisation, based on simplification assumptions that consider a common fixed cycle length and eliminate offsets between intersections. Also, the approach is tested using simulation-based experiments which measure traffic after three cycles only, where longer simulation time should have been considered. However, at the time of the work, ANN technique was in early stage and accumulative developments have been undertaken which advanced the technique.

Combined with Other AI Techniques:

Ranganathan and Patel (Ranganathan and Patel 2001) presented an intelligent decision-making system for urban traffic control (IDUTC) which integrates a back-propagation-based ANN and a fuzzy expert system (FES) for decision-making. The neural network was used to predict the traffic parameters for the next time frame and to compute the cycle time adjustment values which are processed by the fuzzy expert system rules. Simulations were conducted to evaluate the per-

formance of the systems against NN-based model and FES model. However, the adopted simulation model has some limitations where a more realistic simulation would be achieved by a model with two-way roads, and by representing vehicles turning situation. The IDUTC system was then adopted by (Singh 2014) to present a novel approach that uses image mosaicking techniques to deal with traffic light control problem.

Using ANN To Enhance Traditional Methods:

Oliveira and Neto (de Oliveira and de Almeida Neto 2014) presented a neural networks based traffic controller. An approach that uses the Environment Observation Method (EOM) based on multiple neural networks. The authors adopt the EOM which is a mathematical method for determining traffic lights timing, EOM improvements has been achieved by using ANN to estimate EOM parameters which derive time adjustments. The research explores the benefits of using multiple neural network MNN over single ANN, and supports its choice of MNN by analysing training results demonstrating that MNN speeds up learning process and enhances the network robustness. The approach is concerned with EOM enhancement, and simulation-based experiments were conducted to evaluate and compare the performance of the proposed controller against variants of fixed-time control techniques. However, in the literature, adaptive controlling have been extensively addressed, and some traffic authorities are already using adaptive controlling systems, thus, adaptive controllers should have been considered when comparing the performance of the proposed system.

Advancement of ANN in Other Transportation Domains:

Sommer (Sommer et al. 2013) proposed an approach to enhance organic traffic control system with ANN-based short-term forecasting component. Using Elman recurrent neural network and a hybrid training strategy with Resilient Propagation algorithm, and the classic Levebgerg-Marquardt. The network uses current traffic data of an intersection to predict traffic flows for the next five minutes. Experiments were conducted to demonstrate variations in performance between Multi-task learning (MTL) and single-task learning (STL) for three variants of ANN topologies (Feedforward/Elman/Jordan). Prediction outputs have been compared with best results, and the prediction accuracy was compared with results of recent research work. While its affirmed that the performance of the proposed network architecture varies depending on the number of traffic participants, it is desirable to validate the findings over a more complex system.

THE MODEL: ANN-BASED TLC

We have considered a basic intersection with four roads each is a two-way road with two lanes for each way. The outgoing traffic from each road could be either left or straight/Right flow. To hold the number of traffic phases to a minimum, which generally improves operations (Mahmoud et al. 2013); a four-phases sequence has been proposed. The order of this sequence depends on the controller decision. Hence, an intersection will have eight traffic lights and the state of intersection's traffic lights will be represented as a vector of 0's and 1's (0 and 1 represents the red and green states respectively). The model inputs queue length of all outgoing lanes at intersection and outputs the state of intersection's traffic lights.

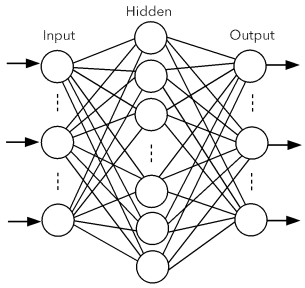

Figure 1: ANN Model

An observation process has been followed to explore the performance of different network architectures to model the solution. First, to assess the sufficient size of training set required for effective training, various networks were created and trained using Levenberg-Marquardt algorithm, each with different training set size. Second, the training set with the best result has been used to train two sets of networks, Feedforward neural networks (FFNNs) and Elman recurrent neural networks (ERNNs); where FFNNs were created and trained each with different training algorithm, based on the best achieved performance. Another set of FFNNs with different neural framework were created and trained. A set of ERNN were also created and trained to assess the most outperforming training algorithm and best neural framework according to the underlying problem.
As for the neural framework, we have adopted a single hidden layer model, the choice is based on theoretical works which proved that single layer is sufficient for approximating any complex problem (Heaton 2008). However, there is no theoretical basis for choosing the number of neurones in hidden layer, our choice is based on the common followed way which is trial and error approach starting by some rule-of-thumb methods (Heaton 2008).
Training sets were obtained using a script which we have developed, it generates random traffic volume data with

the corresponding intersection's TL state based on the highest traffic volume.
To assess the validity of the results and the generalisation capability of the trained networks, a simulation of networks performances is conducted using a data set which was not encountered during the training.

EXPERIMENTAL RESULTS

Different Training Set Size

In order to study the size of the training set that is required to train the network, experiment process was conducted to evaluate the performance of the model with different training set sizes. We tackle the network using many training sets with different sizes, as examples, training sets of sizes 16, 100 and 3000 respectively have been used. The variation in the training set sizes presented in Table 1 has been chosen each to represent a bunch of variants that have been tested. We have chosen to present 16 for the tenth size, 100 for the hundreds sizes and 3000 for the thousands ones. And we have chosen a network with 8-10-8 neural framework, the number of hidden neurones was chosen based on a rule of thumb which recommends that the hidden layer size should be 2/3 the size of the input layer plus the size of the output layer (Heaton 2008).
Table 1 shows the performance evaluated using the mean square error (MSE) and the regression (Reg) results of three FFNN networks with 8-10-8 neural framework. These networks are trained using Levenberg-Marquardt algorithm. The result shows that the accuracy has potentially increased when the training set was increased to 3000 instances. MSE is the mean squared error calculated by the evaluation of the difference between the network outputs and the desired one. The regression result is used to validate the network by showing the relationship between network outputs and targets (i.e Reg value 1 implies perfect training). Although the training regression values were close when using training sets of 100 and 3000 instances, regression results for validation and testing show distinguished variations between the network outputs and the targets using training set of size 100.

Table 1: Training Networks with Different Set Sizes

Training set Size	MSE	Reg	Train Reg	Val Reg	Test Reg
16	0.6622	-0.12424	-0.17151	-0.42581	0.47598
100	0.0885	0.73724	0.87528	0.54635	0.33343
3000	0.0730	0.78132	0.78726	0.77179	0.76429

Performance plots in Figure 2 shows relatively big variations in performance during training, validation and testing when the network was trained using data sets of 16 instances. Figure 2 (a) indicates that the data set was not sufficient for the network to learn. Figure 2 (b) indicates a problem with the training, where the validation and the test curves are not similar.

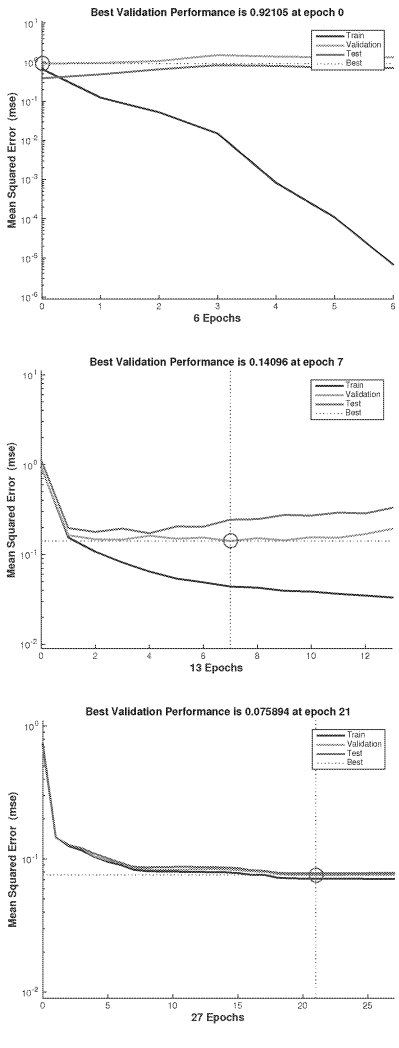

Figure 2: Training, Validation and Testing Performances (Data Set of Size 16 (a) 100 (b) 3000 (c))

Feedforward Neural Networks

FFNN Trained with Different Training Algorithms:
Table 2 shows the results of training a variant model using different training algorithms. Feedforward networks with a neural framework of 8-10-8 was trained using a data set of 3000 instances. The table presents for the algorithms used to train the network, the Epoch that indicates the number of iterations after which the training was stopped, the time taken for training, the MSE and the best validation performance reached (i.e minimum MSE reached during validation). Based on the resulting performance, in which lower MSE indicates better performance, Levenberg-Marquardt algorithm has achieved best results. While using these same algorithms on new data sets, we have found that the best performance has been achieved by Levemberg-Marquardt algorithm.

Table 2: Feedforward Networks Performance with Different Training Algorithms

Algorithm	Epoch	Time	MSE	Best Per.
Levenberg-Marquardt	28	0:00:08	**0.0699**	0.079811
BFGS Quasi-Newton	108	0:00:02	0.0745	0.073718
Conjugate Gradient with Powell/Beale Restarts	75	0:00:01	0.0735	0.076866
Fletcher-Powell Conjugate Gradient	85	0:00:01	0.105	0.10401
Polak-Ribire Conjugate Gradient	67	0:00:01	0.0863	0.085119
Variable Learning Rate Backpropagation	214	0:00:01	0.0996	0.10639
One Step Secant	156	0:00:02	0.0743	0.076719
Resilient Backpropagation	271	0:00:01	0.0757	0.077479
Scaled Conjugate Gradient	117	0:00:01	0.0723	0.077569

FFNNs with Different Neural Framework (Number of Neurones in Hidden Layer):

While the network performance is highly depending on its neural framework, the number of neurones in the hidden layer depends on the network application. We have explored the performance of the model by using variants of FFNNs with different number of neurones in the hidden layer.
In Table 3 we present the results when the networks was trained using Levenberg-Marquardt algorithm. It shows the size of the hidden layer, regression values for training, validation and testing, performance and regression values when the network is simulated with data not encountered during training (per NT and Reg NT). The most optimal result is reached when the network has 20 neurones in its hidden layer. Although a lower MSE is reached with 200 neurones, the best validation performance was better in other variants (best when network's hidden layer size was 20), and validation and test regressions were better with 20 neurones. Also, the simulation of network performance when the network is tested with data not encountered during training shows that performance and regression results were comparable approximately to one with 20 neurones. However, increased number of neurone could be considered as increased network complexity which also leads to extended training time.

Table 3: Feedforward Networks Performance with Different Number of Neurone in Hidden Layer

Hidden	Tr Reg	Val Reg	Test Reg	Reg (all)	Per NT	Reg NT
5	0.65575	0.65966	0.64538	0.65477	0.0628	0.8264
6	0.68712	0.65968	0.64393	0.67634	0.0717	0.78967
7	0.74028	0.75383	0.71308	0.73822	0.0394	0.90062
8	0.74358	0.72959	0.73034	0.73944	0.0455	0.87297
9	0.78516	0.75942	0.7644	0.77818	0.0304	0.91892
10	0.74549	0.73008	0.73548	0.74168	0.0343	0.91376
11	0.79042	0.75578	0.78045	0.78376	0.0387	0.89341
15	0.79559	0.76834	0.78291	0.78954	0.0294	0.91822
16	0.7978	0.78167	0.75422	0.78877	0.0482	0.87098
18	0.80374	0.76748	0.76824	0.79296	0.0400	0.88734
20	0.80423	**0.79371**	0.787	0.80001	**0.0273**	**0.92652**
30	0.82955	0.79191	0.80032	0.81953	0.0485	0.86836
40	0.82699	0.78391	0.79077	0.81512	0.0464	0.8806
50	0.86309	0.77329	0.78888	0.83799	0.0483	0.90137
100	0.87338	0.77323	0.7839	0.84524	0.0355	0.91469
200	0.90143	0.74953	0.74837	0.85625	0.0282	**0.9315**

Elman Recurrent Neural Networks

ERNNs Trained with Different Training Algorithms:
As in FFNN experiment, we assess the performance of different training algorithm by using Elman Recurrent Neural Networks (ERNN). The results returned by the train function when given a training set of 3000 instances shows a comparable mean square error for the various algorithms, as well as the regression results. However, Table 4 presents performances and regressions results when simulating networks performance with data set not encountered during training.
While the performance and regression result returned by the train function are approximately comparable, Table 4 shows that Levenberg-Marquardt training provides the best results.

Table 4: Elman Recurrent Networks Performance and Regression with Different Training Algorithms using New Sata Set

Algorithm	performance	Reg
Levenberg-Marquardt	**0.0303**	**0.91861**
BFGS Quasi-Newton	0.0327	0.91236
Conjugate Gradient with Powell/Beale Restarts	0.0354	0.90206
Fletcher-Powell Conjugate Gradient	0.0332	0.9102
Polak-Ribire Conjugate Gradient	0.0342	0.90588
Variable Learning Rate Backpropagation	0.0370	0.89713
One Step Secant	0.0330	0.9103
Resilient Backpropagation	0.0404	0.88639
Scaled Conjugate Gradient	0.0345	0.90531

ERNNs with Different Neural Framework (Number of Neurones in Hidden Layer):
FFNNs' Experiment was re-conducted to explore the performance of the model using variants of ERNNs with different number of neurones in the hidden layer. Table 5 presents the results where the most appropriate result is reached when the network has 18 neurones in its hidden layer. Although a lower MSE is reached when the network has 30 neurones in its hidden layer, however this is not the case when the network performance is simulated with dataset is not encountered during the training. Also network training experienced a relatively high training time.

Table 5: Elman Recurrent Networks Performance with Different Number of Neurone in Hidden Layer

Hidden	Epoch	Time	MSE	Best Per.	Tr Reg	perf NT	RegNT
5	40	0:00:03	0.104	0.10438	0.6658	0.0398	0.88939
6	69	0:00:06	0.0937	0.093736	0.70716	0.0423	0.89078
7	46	0:00:05	0.0845	0.084524	0.74108	0.0443	0.87622
8	192	0:00:26	0.0810	0.081021	0.75358	0.0360	0.90484
9	1000	0:02:50	0.0719	0.071868	0.78531	0.0354	0.90057
10	1000	0:03:30	0.0712	0.071175	0.78765	0.0398	0.88791
11	1000	0:04:56	0.0700	0.069951	0.79179	0.0317	0.91422
15	1000	0:07:01	0.0679	0.067926	0.79858	0.0356	0.90015
16	1000	0:09:38	0.0669	0.06691	0.80196	0.0387	0.89629
18	1000	0:13:54	**0.0645**	**0.064483**	**0.81**	**0.0317**	**0.91168**
20	1000	0:18:24	0.0647	0.0647	0.80928	0.0343	0.90417
30	1000	0:56:17	0.0580	0.057982	0.83112	0.0399	0.90806

CONCLUSION

In this paper we perform a comparison between variants of neural network models applied to solve the traffic light

control problem. The performance of both feedforward and Elman recurrent neural networks were analysed, where the networks were trained using different training algorithms and different neural frameworks. Even though both models (FFNN and ERNN) provided satisfactory results, we could pointout that the most appropriate network architecture is a FFNN with neural framework of 8-20-8 trained with Levenberg-Marquardt algorithm, where acceptable performance is achieved within acceptable training time. The average performance reached for all experiments was 0.0733 during training and 0.0399 when the network simulated with data not encountered during training. The chosen architecture yields performances of 0.0659 and 0.0273 during training and when simulated with untrained data respectively. A 10% enhanced performance than the average performance of all experiments was reached. And a 31% enhanced performance than the average performance reached when all networks were simulated with data not encountered during training.

It is also noticed that using Levenberg-Marquardt algorithm, ERRNs experiences longer training time than FFNNs. However, using all the other explored algorithms ERNN shows better result for training times.

As for the neural framework, less that eight neurones in the hidden layer will not yield acceptable result for both topologies.

It is noticed that even enormous variation in network architecture yield almost nominal enhancement in performance. However, more studies are to be conducted in further research to explore the effect of using emergent techniques as combining multiple neural networks (MNN) and utilising Multi Task learning technique (MTL); and to study to what extent variants model are influenced by the application of generalisation improvement techniques; in order to establish a clear distinction of performance between variant neural networks models. Moreover, in this study we have covered the two major types of neural networks, further research may include other NN types.

REFERENCES

Berman B., 2014. *How AI Turns Traffic Lights Into Intelligent Agents. readwrite Internet publication.*

Dabahde V. and Kshirsagar R., 2015. *FPGA-Based Intelligent Traffic Light Controller System Design. IJISET - International Journal of Innovative Science, Engineering and Technology*, 2, no. 4, 1268 – 1271.

de Oliveira M.B.W. and de Almeida Neto A., 2014. *Optimization of Traffic Lights Timing based on Multiple Neural networks. IEEE 17th International Conference on Intelligent Transportation Systems (ITSC).*

Heaton J., 2008. *Introduction to Neural Networks with Java.* Heaton Research, Inc, second edition ed.

Kamal M.A.S.; Imura J.i.; Hayakawa T.; Ohata A.; and Aihara K., 2014. *A vehicle-intersection coordination scheme for smooth flows of traffic without using traffic lights. IEEE Intelligent Transportation Systems Conference.*

Lam J.K., 2013. *Challenges and benefits of adaptive signal control. ITS International.*

Liu Z., 2007. *A Survey of Intelligence Methods in Urban Traffic Signal Control. IJCSNS International Journal of Computer Science and Network Security*, 7, no. 7, 105–112.

Mahmoud M.S.; Al-Nasser F.A.; and Al-Sunni F.M., 2013. *Network-based strategies for signalised traffic intersections. Int J Systems, Control and Communications*, 5, no. 1.

Nakatsuji T. and Kaku T., 1991. *DEVELOPMENT OF A SELF-ORGANIZING TRAFFIC CONTROL SYSTEM USING NEURAL NETWORK MODELS. Transportation Research Record*, , no. 1324, 137–145.

Ranganathan N. and Patel M., 2001. *IDUTC: an intelligent decision-making system for urban traffic control applications. IEEE Transactions on Vehicular Technology*, 816–829.

Rass S. and Kyamakya K., 2007. *Artificial Intelligence Techniques in Traffic Control. ÖGAI Journal*, 25, no. 3.

Singh Y., 2014. *A Novel Approach for Automatic Control of Road Traffic Congestion using Image Mosaicking Technique. International Journal of Emerging Technology and Advanced Engineering*, 4, no. 1, 382–389.

Sommer M.; Tomforde S.; and Hahner J., 2013. *Using a Neural Network for Forecasting in an Organic Traffic Control Management System. Workshop on Embedded Self-Organizing Systems.*

Srinivasan D.; Jin X.; and Cheub R.L., 2004. *Adaptive neural network models for automatic incident detection on freeways. Trends in Neurocomputing: 12th European Symposium on Artificial Neural Networks*, 64, 473–496.

Varga I.; Kulcsár B.; and Tamás P., 2006. *Design of an Intelligent Traffic-Control System. ERCIM News*, , no. 65, 38–39.

Yang J.S., 2004. *TRAFFIC SIGNAL TIMING CONTROL FOR A SMALL-SCALE ROAD NETWORK. Control and Applications*, 441, 48–49.

Zhang H.; Ritchie S.G.; and Lo Z.P., 1997. *Macroscopic Modeling of Freeway Traffic Using an Artificial Neural Network. Transportation research record*, , no. 1588.

DATA MINING FOR CORRELATION AND PROFIT

William Conley
Austin Cofrin School of Business
480 Wood Hall
University of Wisconsin-Green Bay
Green Bay, Wisconsin, U.S.A.
Conleyw@uwgb.edu

KEYWORDS
Statistical correlation, complex systems, multi stage Monte Carlo optimization

ABSTRACT

Multi Stage Monte Carlo optimization (MSMCO) is a general purpose statistical simulation optimization technique. It has been useful in solving large scale shortest route problems (the so called "traveling salesman problem") for delivering products or services or routing materials and workers in factories efficiently saving distance, time and money.

However, it is possible to use the MSMCO simulation technology to find shortest routes through spreadsheets of data in order to prove statistically whether the data was generated by variables that were correlated or not. After some two dimensional illustrations are presented here, ten dimensional examples are featured and tested for correlation.

INTRODUCTION

Figure 1 shows the graph of two sets of n=64 (x, y) points with shortest routes for each data set illustrated with the two closed loop routes. Note that the total length of the outside route is shorter than the total length of the shortest route for the points inside the boundary. That is because the points on the border came from x and y variables that are correlated (following a pattern). However, the n=64 points in the middle do not appear to follow a pattern (they are fairly random). Therefore, those x and y variables that produced that data are uncorrelated and its longer shortest route confirms that. It turns out that using the multi stage Monte Carlo optimization (MSMCO) shortest route approach generalized to spread sheets of data in k dimensional space (using a k dimensional version of the Pythagorean Theorem) for k variables one can prove (statistically) whether the k variables are correlated or not.

Two ten variable spreadsheet of data (with n=59 points and another for n=7-0 points) are tested for correlation in this presentation. The author has run many tests on this in two through twelve dimensions and shortest routes in higher dimensions also indicate correlation even though they are harder to picture than in two dimensional space.

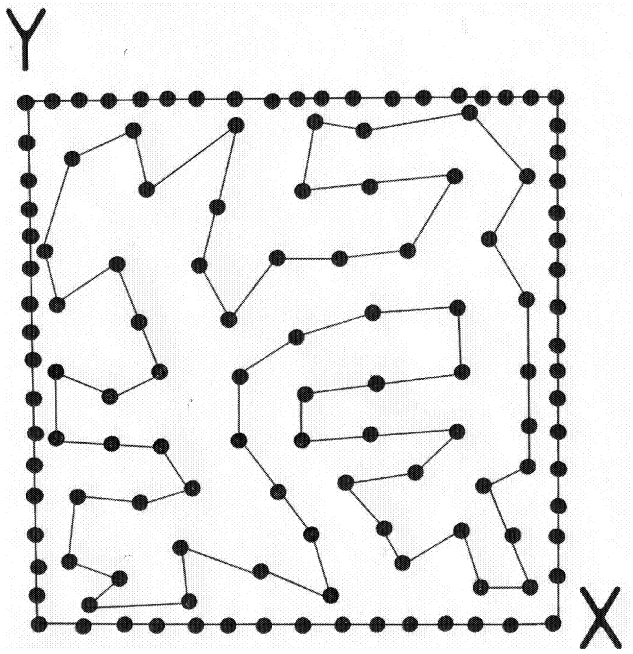

Figure 1. Border points represent correlated variables. Inside points do not have correlated variables.

A TEN BY SEVENTY POINTS EXAMPLE

The logistics department in a firm thinks that the data in Table 1 may have come from ten variables (represented by the columns) that are correlated in some fashion (linear or nonlinear, etc.)

Therefore, they use the MSMCO shortest route simulation optimization approach to find a shortest route connecting the n=70 ten dimensional points in a closed loop total distance (using the generalization of the Pythagorean Theorem distance measure) of d=4029.903

24	66	50	27	69	36	8	34	1	14
51	20	23	15	68	2	64	29	4	21

70	16	17	30	54	43	47	5	63	38
9	58	19	40	56	25	67	44	55	35
28	13	57	31	53	42	32	3	45	12
7	18	41	6	33	60	61	10	37	26
22	39	46	52	49	62	48	59	65	11

The route (read left to right and top to bottom) goes through ten dimensional space from point 24 to point 66 to point 50 to . . . point 59 to point 65 to point 11 and back to point 24. Then the logistics department uses a random number generator to create four sets of random data of 70 rows and 10 columns in the same 0 to 100 range as our "real" data.

Table 1. Data Set One

	X_1	X_2	X_3	X_4	X_5	X_6	X_7	X_8	X_9	X_{10}
1	60	27	61	21	59	69	89	17	62	77
2	52	26	97	34	29	27	5	100	49	41
3	19	30	45	18	14	87	74	83	77	46
4	47	26	17	17	58	74	22	100	50	17
5	45	64	46	84	47	12	68	85	74	76
6	54	50	94	44	36	100	65	14	46	60
7	19	69	6	75	1	69	92	31	69	54
8	78	31	57	17	87	95	100	60	85	44
9	54	39	79	34	44	81	87	100	92	58
10	32	9	15	3	30	32	32	2	20	35
11	29	8	70	9	15	17	69	50	62	78
12	21	53	0	48	9	96	69	73	70	31
13	79	19	81	17	100	45	96	64	84	58
14	70	4	68	1	69	14	93	7	61	72
15	45	39	86	47	11	39	31	42	35	76
16	73	53	43	58	96	62	30	45	35	43
17	81	43	82	37	91	91	39	46	41	39
18	25	53	20	54	20	76	65	17	47	59
19	55	76	83	87	52	51	51	55	52	73
20	57	5	17	13	65	0	46	68	54	52
21	56	66	14	68	61	83	51	80	61	41
22	10	31	16	21	9	85	9	20	13	0
23	49	14	59	21	42	15	31	46	36	70
24	55	14	70	18	53	20	65	100	78	66
25	73	67	17	82	37	33	69	13	48	74
26	16	22	19	17	1	55	3	54	21	15
27	46	59	20	55	60	100	80	66	74	44
28	68	24	100	27	64	40	88	60	77	82
29	45	30	35	20	55	85	19	83	42	25
30	91	78	91	84	90	70	32	81	50	32
31	76	22	88	17	78	56	57	46	52	66
32	27	29	63	12	1	100	72	35	58	51
33	51	32	100	31	40	62	8	18	11	38
34	54	24	44	7	47	87	100	35	75	62
35	52	48	90	54	36	54	100	32	74	93
36	72	24	12	11	100	77	89	52	75	32
37	4	28	6	38	2	25	29	47	35	37
38	34	43	74	48	24	52	94	92	93	74
39	38	34	32	23	25	92	5	46	20	17
40	70	85	81	94	69	59	41	34	38	56
41	42	39	36	29	39	100	55	27	44	49
42	28	24	55	11	20	77	67	25	51	63
43	47	87	32	100	61	45	32	100	57	31
44	31	39	18	55	36	14	78	24	58	81
45	10	29	21	12	5	100	49	94	65	10
46	27	45	45	44	1	75	12	31	19	35
47	50	81	51	93	34	45	64	85	71	70
48	35	69	62	68	10	96	67	57	63	60
49	25	87	64	88	14	94	18	96	46	11
50	48	45	12	51	71	52	93	86	90	54
51	46	2	6	3	77	4	66	39	56	44
52	24	85	19	89	18	82	8	45	21	8
53	45	20	66	8	50	66	53	34	46	65
54	59	77	56	89	61	44	31	100	58	47
55	43	44	87	66	28	2	74	3	47	91
56	55	79	33	83	58	78	53	33	45	55
57	78	33	80	32	78	62	85	55	73	75
58	51	70	94	81	35	47	68	88	75	74
59	24	48	49	55	19	52	39	79	53	63
60	92	24	100	37	99	12	20	14	17	34
61	59	29	52	32	75	45	17	11	14	41
62	40	67	64	64	39	100	46	100	66	35
63	32	70	50	88	26	21	100	94	97	68
64	50	21	56	21	51	43	10	95	41	37
65	31	28	59	29	1	48	65	64	64	79
66	48	35	35	48	40	22	84	96	88	75
67	13	80	23	100	2	14	60	22	45	56
68	46	22	96	18	10	54	26	86	48	52
69	63	58	6	57	96	89	88	43	71	34
70	69	64	28	61	97	99	39	75	52	16

They then use MSMCO to find shortest routes through these comparable random data sets of total distances d_2=5871.142, d_3=5478.140, d_4=5826.141 and d_5=5483.470. Therefore, the real data must have come from variables that are correlated because its shortest route d=4029.903 is much shorter.

However, to bring some precision to their conclusion they use the new CTSP statistic (short for Correlation with the Traveling Salesman Problem approach) which is defined as the shortest route distance from the real data divided by the median of the shortest routes from the random data sets.

The median is (5483.470+5826.141)/2=5654.806. Therefore, CTSP = 4029.903/5654.806=.713. Now looking at the 12 quotients pairs from the random data sets

5871.142/5478.140=1.072
5871.142/5826.141=1.008
5871.142/5483.470=1.071
5478.140/5871.142=.933
5826.141/5871.142=.992
5483.470/5871.142=.934
5478.140/5826.141=.940
5478.140/5483.470=.999
5826.141/5478.140=1.064
5483.470/5478.140=1.001
5826.141/5483.470=1.063
5483.470/5826.141=.941

we can see that the range is from .933 to 1.072 where the vast majority of the sampling distribution of CTSP should be if Ho of no correlation is true.

Therefore, formally the test of the null hypothesis is

Ho: no correlation between the variables

H_A: the ten variables are correlated

Now CTSP=.713 which leads the company to conclude that the variables are correlated. Note CTSP is a one-sided test as CTSP values significantly less than one indicate correlation because the shortest route is smaller than for the random data set's shorter routes.

It turns out that that the nonlinear equation

$$x_{10} = 11(.004(50000 - \sum_{i=1}^{9}(x_i - c_i)^2) - 10) \text{ for } c_1=80$$

$c_2=57$, $c_3=71$, $c_4=45$, $c_5=16$, $c_6=11$, $c_7=95$, $c_8=36$, $c_9=64$ or multiplied out

$$x_{10} = .00444 - \sum_{i=1}^{9} x_1^2 + .0044\,(160x_1+114x_2+142x_3+90x_4$$

$$+32x_5+22x_6+190x_7+72x_8+128x_9)-28.6$$

fits the data quite well with x_{10} being a function of the company's profit. Let us look at a second example.

A TEN BY FIFTY-NINE POINTS EXAMPLE

Researchers at another organization want to analyze the data in Table 2 to see if the ten variables represented in the columns are correlated or not using the CTSP statistic approach. Therefore, they find a shortest route through their Table 2 data with the MSMCO shortest route algorithm adjusted for n=59 lines of data (observations).

Table 2. Data Set Two

	X_1	X_2	X_3	X_4	X_5	X_6	X_7	X_8	X_9	X_{10}
1	90	8	57	72	5	46	41	13	8	13
2	32	18	47	92	100	45	77	28	42	48
3	100	19	51	23	23	54	55	77	93	100
4	76	33	59	58	9	45	42	63	96	100
5	5	7	35	100	14	12	17	96	8	37
6	20	50	42	43	29	74	73	86	71	89
7	67	78	78	77	100	95	100	85	44	66
8	21	48	40	38	55	42	59	49	72	80
9	90	100	83	40	7	15	17	0	5	4
10	30	26	30	24	92	85	100	43	96	99
11	78	26	54	49	96	26	61	56	52	65
12	11	23	15	2	20	64	62	100	79	100
13	63	84	69	42	93	61	87	87	35	59
14	62	52	62	59	78	78	95	1	1	1
15	100	69	91	97	52	80	87	85	84	100
16	51	77	68	62	91	37	68	100	54	78
17	46	3	45	89	82	3	37	84	19	44
18	89	47	63	40	76	8	39	83	52	72
19	91	77	68	15	19	90	81	34	45	53
20	66	93	63	7	38	13	29	70	87	99
21	100	45	71	56	2	33	29	38	92	94
22	99	81	93	88	7	54	48	6	32	32
23	31	0	36	80	67	58	76	41	31	43
24	26	88	74	100	35	89	87	58	4	23
25	26	12	33	58	37	69	73	54	44	58
26	91	42	53	10	41	98	96	74	9	32
27	15	10	27	53	42	46	57	21	0	9
28	20	6	26	51	55	76	85	43	53	62
29	31	23	21	0	92	36	67	90	66	86
30	6	75	57	83	25	97	89	8	94	86
31	65	69	58	22	100	5	45	70	27	47
32	55	88	59	13	52	55	68	3	61	55
33	21	2	20	35	46	96	97	16	84	80
34	45	40	59	88	4	89	73	47	55	65
35	8	79	45	35	54	88	94	70	76	90
36	31	27	50	90	100	35	70	38	16	29
37	70	58	49	3	53	84	90	39	89	92
38	74	62	80	96	75	41	65	94	23	50
39	30	76	71	100	98	55	85	95	48	72
40	69	84	81	77	55	96	100	24	72	73
41	0	86	62	98	62	56	72	25	97	94
42	37	84	56	27	62	61	76	78	0	25
43	28	61	48	41	57	10	33	13	82	78
44	58	26	35	8	94	50	79	50	70	79
45	77	37	72	100	13	40	40	29	63	67
46	8	6	11	16	100	38	72	54	39	53
47	57	100	61	3	24	18	27	0	68	59
48	90	32	47	6	77	100	100	64	72	85
49	63	43	55	48	89	59	84	36	49	57
50	68	73	76	76	21	68	65	31	65	69
51	100	41	81	100	7	100	83	38	60	67
52	12	58	55	93	90	91	100	4	97	87
53	16	64	58	87	72	92	100	74	30	51
54	40	70	56	42	4	86	71	73	59	76
55	7	34	20	10	47	71	78	3	100	89
56	67	100	77	44	6	54	47	73	17	39
57	79	2	58	96	17	96	85	57	69	80
58	3	26	36	80	86	88	100	27	88	87
59	70	44	56	42	78	44	69	9	18	21

It yields a shortest route of d=3871.503.

46	29	44	48	37	10	58	52	41	30
40	50	34	57	51	15	7	13	16	38
39	53	24	14	59	49	11	18	31	42
26	19	32	47	20	3	4	21	45	1
22	9	56	54	35	6	12	8	43	55
33	28	25	23	2	36	17	5	27	46

The route goes from points 46 to 29 to 44 . . . to 5 to 27 and back to point 46 in a complete closed loop tour through ten dimensional space. Then four sets of comparable random data are created and their shortest routes with MSMCO are found to be d_2 = 4682.677, d_3 = 4926.012, d_4 = 4972.896, and d_5 = 4880.797.

Now formally the researchers test Ho: no correlation between the variables versus HA: the variables are correlated. The median is (4880.797+4926.012/2 = 4903.405 so CTSP = d/median = 3871.503/4903.405 = .78906 which easily leads to a rejection of Ho because the 12 quotients of the pairs of random data set's shortest route

4682.677/4926.012=.951

<4682.677/4972.896=.942

4682.677/4880.797=.959
4926.012/4682.677=1.052
<4972.896/4682.677=1.06
4880.797/4682.677=1.042
4926.012/4972.896=.991
4962.012/4880.797=1.009
4972.896/4926.012=1.001
4880.797/4926.012=.991
4972.896/4880.797=1.019
4880.797/4972.896=.981

yield a quotient range of .942 to 1.06. Therefore, with CTSP=.7896 much below that region Ho must be rejected. The conclusion is that the variables are correlated. It turns out nonlinear equations

$$x_3 = .49x_1^{.93} + .51x_2^{.94} + 47x_4^{.90}$$

$$x_7 = .74x_5^{.87} = x_6^{.95} \text{ and}$$

$$x_{10} = .81x_8^{.79} + x_9^{.97}$$

fit the data very well.

MULTI STAGE MONTE CARLO OPTIMIZATION

Multi Stage Monte Carlo Optimization (MSMCO) is like the regular Monte Carlo random search for an optimal solution except that is only considered to be stage one of the simulation. Then in stage two centered about this best answer so far from stage one a new "random" sample of thousands more feasible solutions is looked at and its best solution is stored. Then centered about the stage two best answer a stage three Monte Carlo "random" search takes place in a slightly reduced region. The process is repeated for as many stages as necessary until the optimal solution or a useful approximation solution is found. Figure 2 presents a partial geometric and statistical representation of this MSMCO simulation approach.

CONCLUSION

The two multivariate correlation examples presented here are hypothetical but the fact remains that shorter shortest routes in k dimensional space (than for comparable random data) indicate variables that are correlated is very real. This can be used on a wide variety of correlation analysis studies. The examples featured here with ten variables and 59 and 70 observations (the spreadsheet analyses) showed correlations that turned out to be nonlinear. The CTSP approach will also work to identify correlations that are linear. Also, (Hayter 2002), (Anderson 2003), (Black 2014) and (McClave, et al 2001) present the standard linear correlation coefficient r and its multivariate generalization to Big R, while (Klibanoff, et al 2006) present case studies. CTSP will not only work to identify linear or nonlinear correlation. (Conley 2006) presents an example that finds a correlation that is not

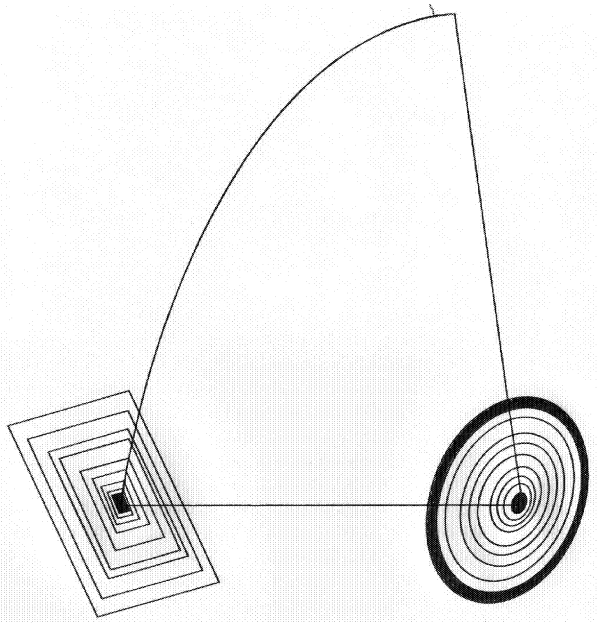

Figure 2. Multi Stage Monte Pursuing Optimal Solutions

represented by a function (but a relation equation). Please again see Figure 1 (the border points).

(Conley 1989) used the n=100 two variable test data from (Eilon, Watson-Gandy and Christofides 1971) reported to have a shortest route ever found (connecting the points in a closed loop) of 640.9 units in (Lawler, Lenstra, Rinnooy Kan, and Shmoys 1985) and found shorter shortest routes with the multi stage Monte Carlo optimization (MSMCO) shortest route algorithm.

(Lawler, Lenstra, Rinnooy Kan and Shmoys 1985) then put a chart in their book containing the test problem's numbers 30, 31, 32 and 33 (of sizes n=150 and n=200 points) (in the mathematics literature) with their shortest routes ever found using all other methods. (Conley 1991a), (Conley 1991b) and (Conley 1993) then found literally hundreds of shorter shortest routes than the best ever found on these well-known test problems using the MSMCO simulation shortest route algorithm adapted for two dimensions.

(Wong 1996), (Szarkowicz 1995), (Conley 2008), and (Conley and Wichowski 1988) among others also feature the multi stage Monte Carlo optimization (MSMCO) simulation technique on a wide variety of optimization problems from mathematics, engineering, environmental work, biology and medicine. (Kristensen 1997) reports earnings of 1.5 million U.S. dollars per year for his company's fleet of 600 trucks using the MSMCO shortest route algorithm. (Conley 2007) presents the CTSP idea and mentions illustrative examples in two dimensions only.

The advances in computer speeds (and decreasing costs) along with simulation techniques are making possible the solution of large scale two and three dimensional shortest route problems for shipping (trucks, rail, barge, air freight, etc.). However, do not stop there. Take the shortest routes through higher dimensions (four, five . . . ten, etc.) to the frontiers of optimization (Conley 2000) and statistical analysis.

REFERENCES

Anderson, T. W. 2003. Multivariate Statistical Analysis, 3rd edition, Wiley and Sons, New York.

Black, K. 2014. *Business Statistics for Contemporary Decision Making*, 8th edition. John Wiley and Sons, New York.

Conley, W. C. and Wichowski, H. C. 1988. Simulation and Model Optimization of Three Biomedical Systems, *Journal of the Japan Society for Simulation Technology,* Vol. 7, No. 4, Tokyo, pp. 47-57.

Conley, W. A 1989. Shipping Route Minimization Technique with Thirty and One Hundred Point Examples. *Journal of the Japan Society for Simulation Technology*, Vol. 8, No. 3, Tokyo, pp. 40-44.

Conley, W. C. 1991a. "Programming an Automated Punch or Drill." *International Journal of Systems Science*, Vol. 22, No. 11, pp. 2039-2056.

Conley, W. C. 1991b. Multi Stage Monte Carlo Optimization Applied to a Two Hundred Point Traveling Salesman Problem. *Proceedings of the Summer Computer Simulation Conference SCSC 1991, Baltimore, SCS* San Diego, pp. 145-151.

Conley, W. C. 1993. Multi Stage Monte Carlo Optimization Applied to a Three Hundred Point Traveling Salesman Problem. *Mathematical Modeling and Scientific Computing,* Principia Scientia, St. Louis, Madison, pp. 398-403.

Conley, W. C. 2000. Statistical Simulation and A Six Dimensional Shortest Route Problem. *Proceedings of the 2000 Japanese Society of Simulation Technology, JSST* 2000, Tokyo, Japan, pp. 90-93.

Conley, W. 2006. Discovering Relationships that are Not Functions. In *Proceedings of 4th International Industrial Simulation Conference, ISC* 2006 (Palermo, Italy, June 5-7), EUROSIS-ETI, Ghent, Belgium, 163-167.

Conley, W.C. 2007. Simulation Optimization and Correlation with Multi Stage Monte Carlo Optimization. *International Journal of Systems Science,* Vol. 38, N. 12, pp. 1013-1019.

Conley, W.C. 2008. Ecological Optimization of Pollution Control Equipment and Planning from a Simulation Perspective. *International Journal of Systems Science,* Vol. 39, N. 1, pp. 1-7.

Eilon, S. Watson-Gandy, C. D.T. and Christofides, N. 1971. *Distribution Management, Mathematical Modeling and Practical Analysis*, Griffin Ltd. London, 240 pages.

Hayter, A. 2002. *Probability and Statistics for Engineers and Scientists*, 2nd Edition, Duxbury Press, Pacific Grove, CA.

Klibanoff, P., Sandroni, A., Moselle, B., Saraniti, B. 2006. *Managerial Statistics: A Case-Based Approach.* Thomson Southwestern, Mason, Ohio.

Kristensen, S.E. 1997. Personal Communication.

Lawler, E., Lenstra, J, Rinnooy Kan, A., and Shmoys, D. 1985. *The Traveling Salesman Problem,* John Wiley and Sons, New York, 465 pages.

McClave, J. T., Benson, P. G., Sincich, T. 2001. *Statistics for Business and Economics*, 8th edition. Prentice Hall, Inc., Upper Saddle River, New Jersey.

Sarkowicz, D. S. 1995. Investigating the Brachistochrone with a multi stage Monte Carlo Method, *International Journal of Systems Science*, Vol. 26, No. 2, pp. 223-243.

Wong, J. Y. 1996. A Note on Optimization in Integers. *International Journal of Mathematical Education In Science and Technology*, Vol. 27, pp. 865- 874.

BIOGRAPHY

WILLIAM CONLEY received a B.A. in mathematics (with honors) from Albion College in 1970, an M.A. in mathematics from Western Michigan University in 1971, an M.Sc. in statistics in 1973 and a Ph.D. in mathematics - computer statistics from the University of Windsor in 1976. He has taught mathematics, statistics, and computer programming in universities for over 30 years. He is currently a professor emeritus of Business Administration and Statistics at the University of Wisconsin at Green Bay. The developer of multi stage Monte Carlo optimization and the CTSP multivariate correlation statistics, he is the author of five books and more than 200 publications world- wide. He is a member of the American Chemical Society, a fellow in the Institution of Electronic and Telecommunication Engineers and a senior member of the Society for Computer Simulation. Career highlights include presentation of two papers at National Aeronautics and Space Administration (NASA) conferences in Houston, Texas and Washington, D.C.

VIRTUAL SIMULATION

THE VIRTUAL SENSOR TESTBED
THE EROBOTICS APPROACH
TO THE DEVELOPMENT OF SENSOR-ENABLED APPLICATIONS

Jürgen Rossmann, Michael Schluse, Markus Emde, Thomas Steil
Institute for Man-Machine Interaction, RWTH Aachen University, Ahornstrasse 55, D-52074 Aachen, Germany
E-mail: {rossmann, schluse, emde, steil}@mmi.rwth-aachen.de

KEYWORDS
eRobotics; 3D Simulation; Virtual Testbed; Sensors; Mobile, Space and Industrial Robotics

ABSTRACT

Today, Digital Prototyping and simulation technologies are widely used in the development of new technical systems in research and industry. They allow cost- and time-efficient tests in all stages of development and support decision making. The eRobotics methodology addresses this by providing platforms where engineers can exchange ideas and collaborate with experts from other disciplines for developing complex technical systems and automated solutions. Sensor simulation is an important aspect in many simulation scenarios, not only in robotic applications. In this contribution, we describe how various sensor simulation aspects are integrated into Virtual Sensor Testbeds in order to enable the full spectrum of the eRobotics methodology for engineers developing sensor-enabled applications

INTRODUCTION

Developing new complex technical systems is a cost-intensive and time-critical process. In the development process of new components, testing and verification are important tasks. With Digital Prototyping (DP), development time can be shortened, while the quality of products can be improved, as newly developed tools and algorithms are tested simultaneously. This paper focuses on the new concept of the Virtual Sensor Testbed providing various means for a close-to-reality test, validation, characterization and optimization of sensor-enabled applications in their operation environments using sophisticated Virtual Testbeds (Rossmann 2011a). Providing simulated sensor data close to the equivalent physical components, sensor simulation supports decision making already in the early design and development phase. Furthermore, development and testing of algorithms based thereon can be carried out in an early stage.

VTBs are the central method in eRobotics, where complex technical systems and their interaction with prospective working environments are first designed, programmed, controlled and optimized in 3D simulation, before commissioning the real system. Figure 1 shows various Virtual Sensor Testbeds. Using Virtual Sensor Testbeds, 3D simulations including comprehensive sensor simulations are used right from the beginning of the development process to test first system design studies in the concept phase. During system development, fully functioning interactive virtual prototypes allow for an efficient and goal directed development, test and verification both on component, as well on system level – at any point of time. Besides, 3D simulation technology not only allows to visualize, simulate, test and experience the virtual prototype using VTBs, but can also be used as a development framework to implement both control and supervisor algorithms (like motor controllers, robot programs, image processing algorithms) using concepts of "Simulation-based Control" (Rossmann et al. 2012a).

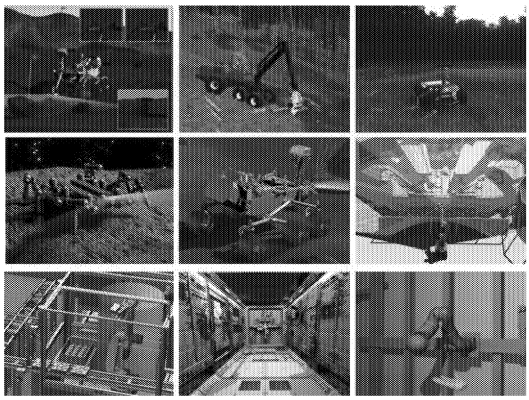

Figure 1: Typical Virtual Sensor Testbeds

The contribution is organized as followed. We start with a short overview over the state of the art in sensor simulation. The following chapter introduces the key concepts of the eRobotics approach and the Virtual Testbed methodology. The concepts lead to a new approach to 3D simulation for sensor simulation, which is the basis for the Virtual Sensor Testbed concept presented in this paper. The contribution closes with an overview of selected applications and a conclusion summarizing the current status as well as future work.

STATE OF THE ART

Taking a look at the state of the art of simulation technology reveals various approaches to simulation technology. Discrete event simulation systems (Banks 2010), block oriented simulation approaches like the Matlab/Simulink framework (www.mathworks.de/products/simulink/) or the Modelica modeling language (Fritzson 2003) as well as various FEM-based simulation tools (e.g. www.comsol.com) are probably the most well-known ones. But even if focusing on simulation systems providing sensor simulation components, various approaches can be found. An example for a research and development testbed focusing on camera sensor systems for mobile

robots is described in (Franti et al. 2005). Most of these approaches focus on mobile robot prototyping like the ROAMS simulation environment (Huntsberger et al. 2008a), the 3DROV simulation and verification tool (Huntsberger et al. 2008b), Microsoft Robotics Developer Studio (Almeida 2007) or the Player/Stage/Gazebo project (Gerkey 2003) or combinations of adapted and integrated off-the-shelf software tools like Matlab/Simulink and SIMPACK as described in (Schäfer 2008). Simulation systems designed to meet the needs of mobile robotics test environments like EyeSim or USARSim (Balaguer 2008) are designed for certain robot platforms and are limited in their functionality.

Besides these simulation-based approaches, there exist several approaches using physical mockups. One of them is the testbed for rendezvous and capture (INVERITAS) described in (Paul et al. 2014) which allows for the testing of sensor prototypes for the optical navigation during the approach to satellites in a Hardware-in-the-Loop environment.

The drawback of nearly all these systems is the loss of flexibility, as they are developed for a very specific field of applications only. Often, the configuration is complex and error-prone. Moreover, the systems hardly run in real-time. Most of these simulation systems do not use the GPU to accelerate or improve the simulation results.

EROBOTICS AND VIRTUAL TESTBEDS

eRobotics (Rossmann 2015) combines the use of electronic media, state of the art simulation technologies and concepts from robotics. Its usage evolved from pure robotic applications to general mechatronics as well as various other fields such as environment modeling and simulation (e.g. forests and cities) and industrial automation. The eRobotics methodology makes extensive use of 3D simulation technologies. A central method in eRobotics are so called Virtual Testbeds, which themselves provide the necessary basis for developing new "Simulation-based X" concepts (Rossmann 2015).

Virtual Testbeds greatly enhance the scope of the conventional approach to simulation. While typical simulation applications examine only specific aspects of an application (e.g. working principle of a laser scanner), a Virtual Testbed enables engineers to examine the entire technical system in its environment (e.g. a harvester for forestry is equipped with laser scanners within forest environmental model). In order to replicate the entire technical system, the Virtual Testbed also contains the necessary algorithms for data processing and control (e.g. localization of the harvester based on laser scans). Finally, we take these algorithms back to the real word to control the real system (Simulation-based Control) or use them to set up versatile user interfaces.

A systematic view on Virtual Testbeds is given in Figure 2: A Virtual Testbed combines a data processing system (DPS) with a simulated environment. The simulated environment comprises the simulated technical system represented by its internal system vector $\underline{s}_{sys}^{sim}(t)$ (e.g., harvester), its simulated sensors $\underline{s}_{sense}^{sim}(t)$ (e.g., laser scanners) and actuators $\underline{s}_{act}^{sim}(t)$ (e.g., harvester drive and crane) and a simulated environment $\underline{s}_{env}^{sim}(t)$ (e.g., virtual forest model). The DPS processes sensor data or commands a system's movements and is represented by $\underline{s}_{impl}^{dps}(t)$ (e.g., localization algorithm), sensor input $\underline{s}_{sense}^{dps}(t)$, actuator output $\underline{s}_{act}^{dps}(t)$ and its "perceived" environment $\underline{s}_{env}^{dps}(t)$ (e.g., scanned trees). The simulated environment has to adequately mimic the corresponding real environment $\underline{s}_{sense}^{real}(t)$, $\underline{s}_{sys}^{real}(t)$, $\underline{s}_{act}^{real}(t)$, $\underline{s}_{env}^{real}(t)$. By turning the switches T_{sense} and T_{act}, the DPS can either be used with the simulated or the real environment – a key idea of the Virtual Testbed concept. This enables development, evaluation, optimization, and productive operation in the very same hard- and software environment.

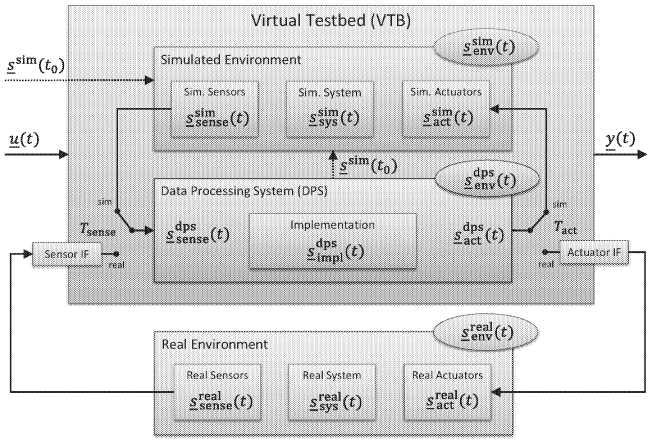

Figure 2: Systematic view on Virtual Testbeds (Rossmann 2015)

THE 3D SIMULATION INFRASTRUCTURE FOR THE VIRTUAL SENSOR TESTBED

The Virtual Sensor Testbed concept presented in this paper requires a new holistic and encompassing approach to simulation technology allowing for the synergetic use of different data sources in combination with various simulation methods (not only sensor simulation but also kinematics, rigid body dynamics etc.) on a single database. This is crucial to sensor simulation to overcome the limitations of most approaches focusing only single application areas. This presents an interdisciplinary use of various data sources, various sensor types in various application areas and their integration for new applications.

For realizing such a concept, the major prerequisite is the use of one single but comprehensive and integrated 3D simulation framework which is able to implement all the methods and support all the processes outlined above. The advantage of such an integrated framework is to minimize conversion tasks and the ability to simulate, at the same time, all simulated components within one single but comprehensive "Virtual Sensor Testbed". This leads to various requirements of the underlying 3D simulation framework (Rossmann 2013) concerning overall flexibility, performance, freely configurable databases, distributed and parallel simulation, realism using calibrated simulation algorithms, flexible and standardized interfaces, integration of data processing algorithms, the seamless transition between simulation and reality as well as cross platform support.

The key idea of our approach to 3D simulation technology is to introduce an on-line database, the "Versatile Simulation Database" (VSD). This database is highly configurable, integrates all data necessary for an application using their original data formats as well as all simulation and data processing algorithms for the visualization, interaction and simulation part of the applications as well as their interfaces to the real world. The VSD acts as the micro kernel of the entire simulation system (see Figure 3). It is an object-oriented real-time database managing the simulation model. It provides the infrastructure for data management, meta information, communication, persistence, and user interaction. Furthermore, VSD is an *active* database not only containing data, but also the algorithms and interfaces for its manipulation.

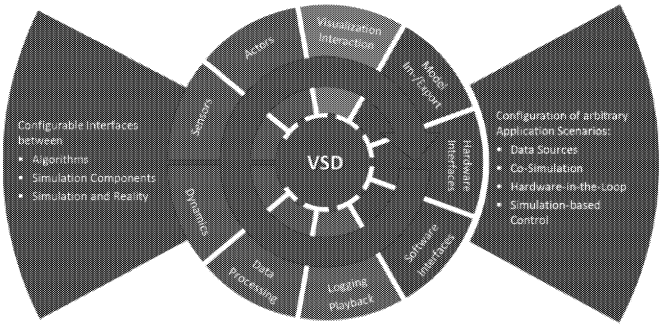

Figure 3: The micro kernel architecture (Rossmann 2015)

This flexibility of VSD makes it an ideal basis for (simulation) models from various sources and data formats from fields like environment (CityGML, ForestGML, SEDRIS, IFC, …) or industry (AutomationML, X3D, VRML, STEP, IGES, …). To make such data available within VSD, a three-tiered database synchronization approach has been introduced (Hoppen 2012). It can be used to synchronize VSD with an external database containing the considered data (e.g., a city model, a forest model, a building model, an industrial assembly station model, …). Ideally, the external database is a "real" database with a database management system (DBMS). However, the approach can also be applied to file-based formats that bring their schema description (e.g., XML files plus corresponding XSD file or STEP/IFC file with corresponding EXPRESS file). After data synchronization, the simulation system can access all the data from the external database. However, when using third party schemata like those mentioned above, it often cannot understand or interpret it. For that purpose a semantics translation is performed (Hoppen 2014).

THE VIRTUAL SENSOR TESTBED CONCEPT

Virtual Sensor Testbeds are important tools to develop and verify hardware components and implementations of algorithms in sensor-enabled applications. The benefits of such Virtual Sensor Testbeds can be improved if processes and tasks are executed not only in a predefined, but in an interactive and flexible way, taking into account all interacting components of the entire system to be develop and therefore integrating information of different data sources. In physical testbeds, sensors are used to measure the internal and external states, providing detailed information of the current status. In Virtual Sensor Testbeds, sensors are modeled appropriately to simulate their behavior accordingly. Providing consistent interfaces to connect to these sensors and use the information in a standardized way allows for the easy setup of different Virtual Sensor Testbeds and for a uniform data transmission as input for algorithms and applications. Therefore, the central component of a Virtual Sensor Testbed is a modular sensor framework allowing for the parallel integration of real and simulated sensors and providing a smooth transition between simulation and real world setups. It allows for easy setups of Virtual Sensor Testbeds using a generic communication concept for the interaction of all components. In addition to the aforementioned real and simulated sensors, playback and virtual sensors have been introduced.

The sensor framework provides methods for the modeling, simulation and visualization of a wide range of sensors. It offers a consistent data interchange within the simulation environment, as well as between real sensors and simulation algorithms in hardware-in-the-loop scenarios. Logging and playback mechanisms allow for an efficient offline development for real sensors, while the introduction of various error models enable the detailed analysis of sensor data processing algorithms under different boundary conditions.

General Concept

Figure 4 gives an overview of the sensor framework architecture as a diagram with its different layers. The architecture consists of three different layers. The first one realizes a generic communication concept for the interaction of all components. It offers a focused view on every component of the system to analyze and optimize its behavior. The generic communication concept is based on an IO-board metaphor (see Figure 5) and allows for a standardized input and output of sensor data. This provides connectivity to different system plugins like the sensor- and the render-plugin used to support sensor simulation tasks. As all data types representing sensor data output or input inherit from this generic data type, communication between different components of the framework is possible in an unconfined way.

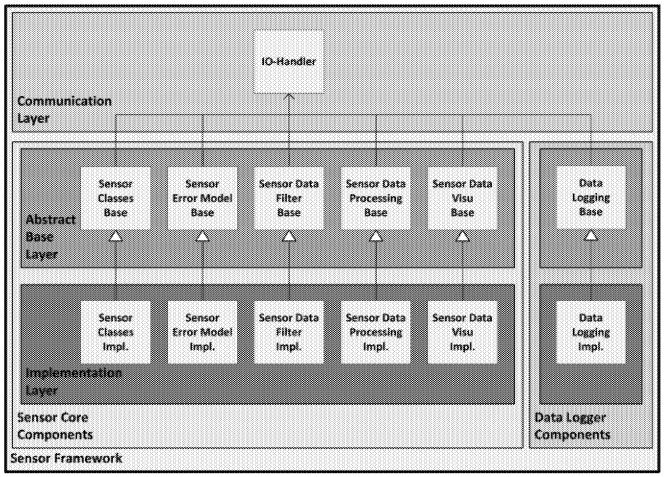

Figure 4: Architecture of the sensor framework with three layers: communication layer, abstract base layer and implementation layer

Abstract sensors, error models, sensor data filters, sensor data processing components, data logging components, as well as the visualization components inherit from the first layer and constitute the second layer of the sensor framework. Basic inputs and outputs required for all inherited components are placed in this layer. For instance, if a group of real sensor components has a power switch, the equivalent simulated sensors are modeled to have available a switch to enable them as well (as shown in Figure 5, "enabled"-input of the sensor).

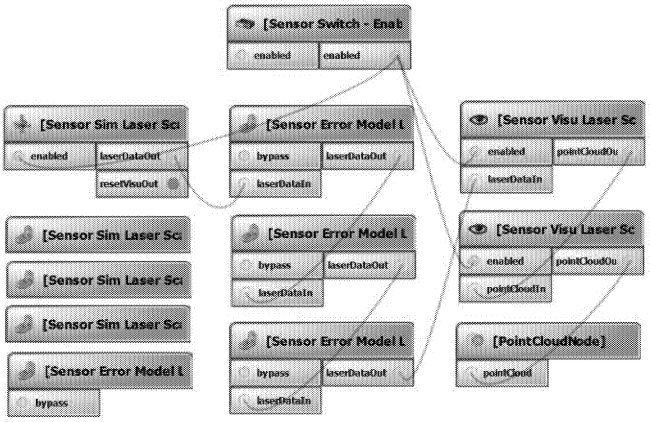

Figure 5: Example of an IO-network with connected virtual sensor components

The interface to this functionality is defined in the corresponding base class. The third layer inherits the abstract realization and efficiently implements the sensors, error models, visualization options and data logging mechanism. In detail, the third layer differentiates among four kinds of sensors (see Figure 6). They are classified as an implementation of real hardware application programming interface (API), simulated sensors, 'playpack' sensors as well as virtual sensors.

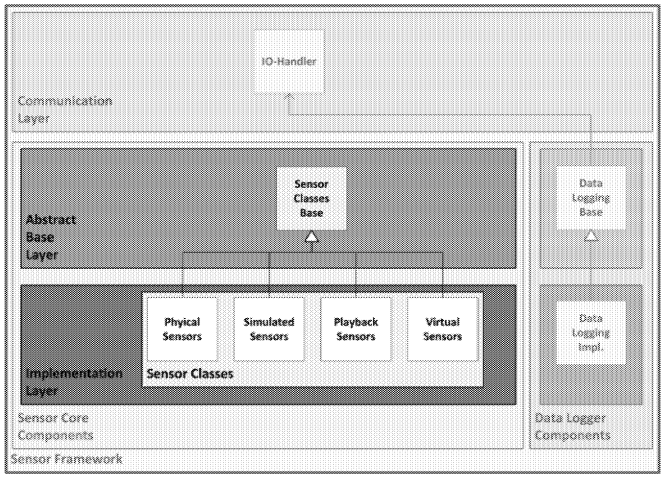

Figure 6: Differentiation between 4 types of sensors in the sensor framework

Physical Sensor Components: In physical testbeds, different physical sensor components are used to measure internal as well as external states. Using the example of an exploration rover, the battery level is queried as well as characteristics of the environment are measured. In both cases, accessing the sensor components, querying actual states and, if necessary, altering of parameters at run-time is essential. To fulfill these tasks sensors must offer an appropriate API to access and alter states and parameters. The sensor framework integrates all these capabilities of the real components APIs and integrates them into the Virtual Sensor Testbed to provide sensor independent interfaces to realize the aforementioned tasks. For example, laser scanner APIs of different scanner manufacturers (SICK, Riegl, Zoller + Fröhlich) have been integrated. Connecting, parametrizing at run-time and access to scanning results is possible.

Simulated Sensor Components: Simulated sensors are the second class of sensors. Carrying out necessary test series without real physical hardware available can be performed using simulated sensors in an appropriate Virtual Sensor Testbed using the very same sensor independent interface used for physical sensors. Instances of simulated sensors can be added to a testbed in the same way as real ones. Simulated sensors in the sensor framework are modeled so that they behave like their real counterparts in terms of their control or sensor data output. In some cases, sensor component parameters must be specified in addition to meet real hardware components behavior like maximum and minimum limits of the distance measured by distance measuring equipment. Differences emerge as simulated sensors are modeled to deliver or work on ideal data resulting in ideal sensor data. Specific filters or error models need to be applied to grant close-to-reality simulations required for Virtual Sensor Testbed scenarios.

'Playback' Sensors: 'Playback' sensors are the third class of sensors in our framework. They are used to induct algorithmic recorded data into the network of connected components. Like virtual sensors they use error models especially designed to represent different error scenarios of a sensor or specialized sensor data visualization for different use cases. Mechanisms to playback sensor data resemble the mechanisms of virtual sensors. Thus, we are able to run as many virtual tests as possible and as few physical tests as necessary.

Virtual Sensors: Analogous to the reproduction of real or simulated sensor data in playback sensors, results of complex calculations can be considered as the output of a so called virtual sensor. For example, the results of a camera-based localization approach such as 'visual odometry', can be connected in parallel with a wheel odometer to the system, which greatly simplifies the comparison of the two components as the algorithmic results can be seen as the output of a 'visual odometry-sensor'. They are communicating via the very same interfaces than physical or simulated sensors, so that the combination of real, simulated and virtual sensors is easy and the results in hybrid testbeds (Sondermann 2013) are ideal for validating the simulated components against the correspondent real components. One of the biggest advantages of the virtual sensor concept is, that they are "normal" sensors. This way, any algorithmic output data can be used as input data for further algorithms. Thus defining new interfaces for every new algorithm is not necessary.

Calibration

In order to achieve trustable results, the sensor simulation modules of the Virtual Sensor Testbed have to be calibrated by physical reference data (see Figure 7). Therefore, a physical mockup is used, e. g. as described in (Rossmann 2012c and

Steil et al. 2014). To achieve trustable result the simulation is calibrated in an iterative process with available hardware. Once the simulation reaches the desired level of accuracy the scenarios and sensor parameters can be varied in this validated virtual model.

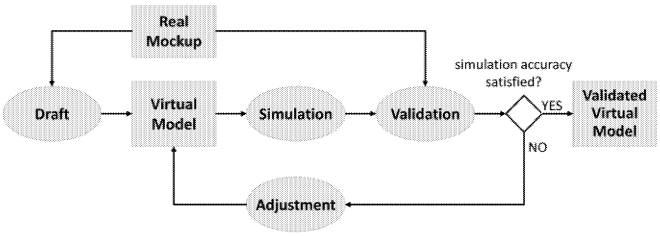

Figure 7: Iterative process for model validation

Currently Supported Sensors

There are various sensors of different types which are currently supported by the Virtual Sensor Testbed. In the following, the most important simulated sensor types as well as the most important interfaces to physical sensors are listed:

Simulated Sensors:

- Altimeter
- (Stereo) camera
- Compass
- GPS receiver
- IMU
- Inclinometer
- Laserscanner (1D/2D/3D)
- Light barrier
- PMD sensor
- Ultrasonic sensor
- Radar sensor
- RFID sensor
- 6 DOF force torque sensor
- Contact force sensor

Physical sensors:

- (Stereo) cameras
  - Nikon, Canon
  - UVC, GigE, IP
  - Point Grey Bumblebee
- Compass
  - PNI TCM 2.6
  - KVH C100
- GPS receiver
  - NMEA 0183
- IMU & Inclinometer
  - SBG IG500A
- Sensors of mobile platforms
- RFID sensors
- Laserscanner
  - Riegl LMS Q120i
  - SICK LDLRS2100, …
  - von Hörner & Sulger
  - Z+F Imager 5006
  - Hokuyo UTM-30LX
- PMD sensors
  - MESA SR4000
  - Microsoft Kinect

Camera Simulation

One of the most important sensors are camera sensors. One the one hand camera sensors are widely used in sensor-enabled applications, but on the other hand choosing the right camera, integrating this camera into the overall process and programming the image processing algorithms is error-prone. But the realistic visualization of optical effects is still a difficult task for modern computer graphics (Hullin et al. 2011, Kriss 2015) and even more if a realistic simulation of the used camera is needed (Farrell et al. 2012). To provide close-to-reality sensor simulation results and to – at the same time – achieve real-time simulation, we utilize rasterization techniques for the Virtual Sensor Testbed that can be implemented in modern shader-driven GPUs for hardware accelerated real-time rendering. Modern rasterization-based graphics hardware is fully programmable with significant arithmetic capabilities and high floating-point operation performance in comparison to current CPUs as described in (Rossmann et al. 2012b) Therefore a realistic simulation of various optical and electronic effects of digital cameras is possible in real-time. Effects with the biggest influence on the image are described in the following section.

In a first step the camera parameters are measured according to (Hartley 2003) or obtained by the documentation of the manufacturer. These parameters are used for a close-to-reality rendering using various effects (see Figure 8). Therefore the geometric scene information is passed to the graphics card which adds image based effects in a post-processing step.

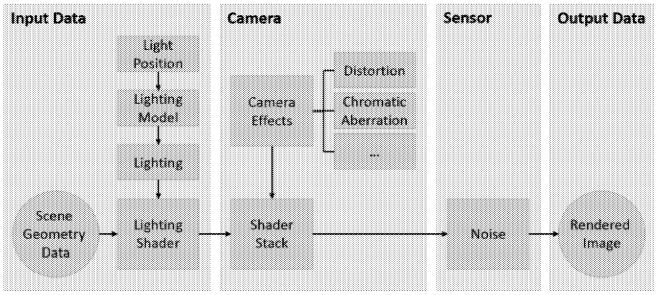

Figure 8: Concept of rendering the scene with various effects

Depending on the scenario some effects have greater impact on the artificial images. If the scenario simulates optical components very close to the observed object depth of field is an important effect, that substantially influences computer vision algorithms. Therefore the correct simulation of depth of field effects is an important part of the Virtual Sensor Testbed as shown in Figure 9.

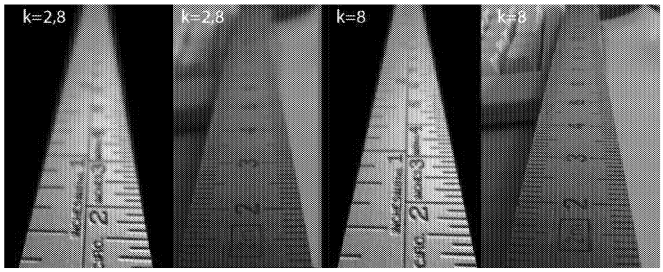

Figure 9: Depth of field: real and virtual images

The optical sensor is, depending on quality and manufacturer, susceptible to a wide range of effects like noise and saturation effects. These saturation effects appear if the sensor is exposed to bright light and the number of photons exceed the intake capacity as shown in Figure 10.

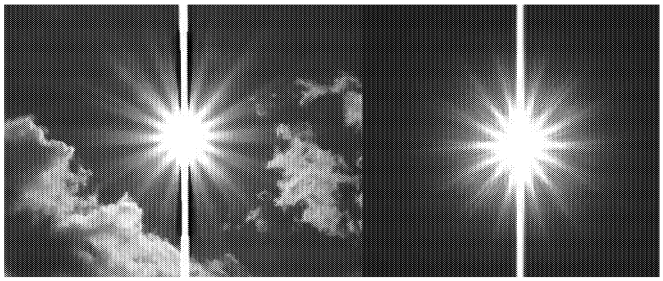

Figure 10: Real and simulated smear effect

In addition to the two effects illustrated above, the camera simulation component of the Virtual Sensor Testbed integrates other effects like

- blooming,
- smear,
- noise,
- distortion,
- chromatic aberration,
- depth of field and
- flares.

Laser Scanner Simulation

Simulation of laser scanners has been studied in different domains since their physical counterparts are available. Examples for laser scanner simulations are airborne laser scanning (Baltsavias 1999), space exploration (Yu et al. 2011) or LiDAR simulations for forest measurements (Kukko 2007). (Blume 2007) describes a laser scanner simulation for a probabilistic object tracking application. (Laue 2006) introduces a laser scanner simulation in the context of a general robot simulator which is for example simulating mobile robots playing soccer. (Wang et al. 2012) describe the use of simulated sensors like laser scanners in the domain of autonomous car testing. Other well-known examples are USARSim (Belaguer 2008) and Player/Stage/Gazebo (Koenig 2004) featuring sensor simulation components including LiDAR. Simulation and modelling of 2d and 3d laser scanners is described in (Peinecke 2008), (Bedkowski 2008) and (Koceski 2009).

Most of these approaches focus on dedicated hardware, do not allow flexible pattern generation, and are not real-time capable. In addition to this, to provide realistic and close-to-reality sensor data, a laser scanner simulation requires error modeling, filter algorithms and specific modules to adapt characteristics of selected systems. Taking into account all these aspects, different laser scanner simulation modules have been implemented for the Virtual Sensor Testbed as described in (Emde 2011), (Emde 2013) and (Emde 2015).

SELECTED APPLICATIONS

The Virtual Sensor Testbed introduced above has been used to realize a large variety of different sensor-enabled applications so far. Currently, these applications mainly focus on three application areas, environment (e.g. forest inventory or forest machines), industry (e.g. industrial automation) and space (e.g. space robots), for which the Virtual Sensor Testbed provides a common development approach. In this chapter we shortly outline the results of four applications, one for each application area.

Localization of Forest Machines: In this application, the Virtual Sensor Testbed has been used to enhance the rigid body simulation of a forest harvester operating in a close-to-reality forest environment with laser scanners and stereo cameras to develop an intelligent sensor measuring the surrounding forest for localization and forest inventory purposes (Rossmann 2011b). In addition to this, the same simulation has been used to design and implement the data processing algorithms themselves. The simulation database, able to store and update the world model, and simulation components like collision detection or input/output networks, were used to implement the algorithms and to interface them to virtual or real sensors or onboard computer hardware. Following this approach, after approx. two years of development it took about two days before the real system was fully operational. Figure 11 shows on the left hand side the Virtual Sensor Testbed. On the right hand side, the user interface is displayed

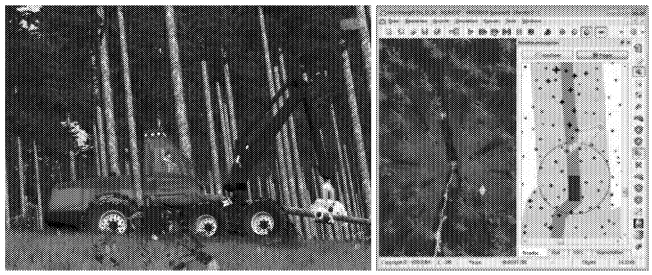

Figure 11: A Virtual Sensor Testbed to develop localization and navigation methods for forest machines and the resulting user interface (Rossmann et al. 2011b)

Driver Assistance Systems: In the automotive sector, Virtual Sensor Testbeds can be used to simulate cars driving in close-to-reality environments (see Figure 12) while being equipped with various optical sensors (cameras, laser scanners, radar and ultrasonic sensors). These sensors are the basis for driver assistance systems (ADAS) like automated parking, lane keeping or cruise control.

Figure 12: Virtual Sensor Testbed to simulate various sensors used for the development of driver assistance systems

Space Robotics: eRobotics has its roots in space robotics, be it mobile robots, landers for planetary exploration (see Figure 13), robot manipulators on satellites or the International Space Station (see Figure 14). Here, the eRobotics framework is used to its full extend, starting with design studies over virtual testing environments for prototype testing and validation at systems level and ending with the development of intuitive and interactive user interfaces.

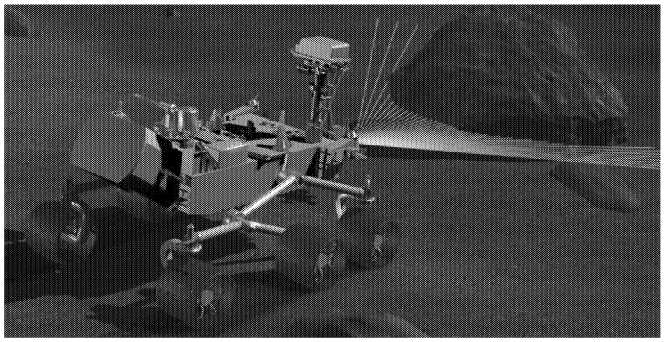

Figure 13: VST with mobile robot equipped with sensors operating in a planetary environment.

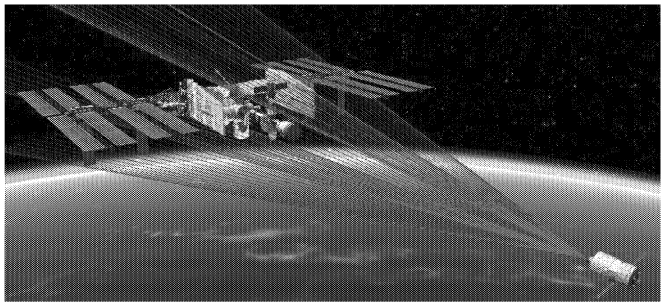

Figure 14: ATV approching the ISS in VT while scanning. Red lines indicate the sensor data of the last simulation step. Color coded dots represent hit points on the target (ISS)

Integrating high quality environment models with semantic information and simulated sensors providing close to reality sensor data and allow for the develepment of new algorithms, for example for autonomous orbital rendezvous and docking scenarios or self-localization and mapping on planetary surfaces.

Following the ESA terminology for system modelling and simulation in space engineering (Space Engineering 2010), Virtual Sensor Testbeds aim at covering and integrating the functionality of various "Functional Verification and Mission Operations (FV & MO)" systems, namely:

- "System Concept Simulators" (used in phase 0 to define a baseline mission scenario which is consolidated in phase A, providing the basis for the system functional analysis and leading towards the functional specification),
- "Mission Performance Simulators" (used to analyze mission and payload performance during all development phases),
- "Functional Engineering Simulators (FES)" (used for requirements consolidation and to system design definition, justification, and verification),
- "Functional Validation Testbenches (FVT)" (providing a complete system simulation to support the test of critical subsystem designs in system context),
- "Software Validation Facilities (SVF)" (targeting the validation of on-board software under varying boundary conditions) and
- "Spacecraft AIV Simulators (AIV Simulator, Spacecraft V&V)" (assembly, integration, and verification (AIV) simulation for validation and verification (V & V) on spacecraft level).

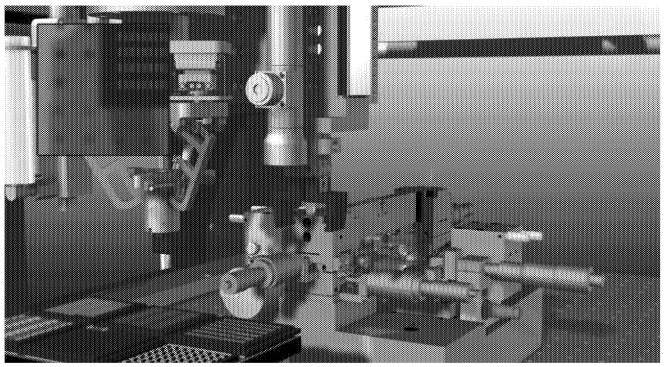

Figure 15: Simulated assembly process of laser lenses with a virtual camera (top left)

Industrial Automation: The close-to-reality simulation of optical sensors and lenses is important for various industrial processes. One example is the assembly of laser lenses. Using a Virtual Sensor Testbed, a simulation of the used optical components in early development stages can be used to plan and simulate the assembly process and the trajectories of the used robots. Figure 15 illustrates this process. The Virtual Sensor Testbed simulates the depth of field of a fixed focal lens and allows the test of computer vision algorithms responsible for identifying the position of remaining workpieces and is described in (Schlette et al. 2015).

CONCLUSION

The applications outlined above clearly show that the Virtual Sensor Testbed approach presented in this paper is feasible and promising. Even complex scenarios consisting of close-to-reality environment models, dynamic plant models (e. g. robots, cars, production lines etc.) and all sensors needed to set up powerful and reliable sensor-enabled applications can be modeled. Virtual Sensor Testbeds have the potential to greatly simplify the development process decreasing development costs and times while increasing quality and reliability of the developed components.

While developing future sensor-enabled applications, providing simulation models and using simulation for development, characterization, verification, validation, and optimization should become as natural as developing the hardware and/or software itself. This holds great promises concerning efficient development, quality, performance, reuse, and technology transfer for new components. The continuous and integrated use of simulation technology in a Simulation-based Engineering process leads to a cost-efficient development process, better designs, and more reliable systems.

Today, we can provide a reference implementation which is ready to be used in a variety of application areas (see applications above). But there are still tasks to do e. g. adding new sensor simulation algorithms (e. g. GPU ray-traced single ray laser scanner simulation), calibrating existing simulations in other application areas (e. g. on-orbit servicing) or setting up a library of sensors and materials to ease the development of new testbeds.

ACKNOWLEDGEMENTS

Parts of the presented work was funded by the German Aerospace Center (DLR) with funds provided by the Federal Ministry of Economics and Technology (BMWi) under grant numbers 50RA0913 (Virtual Crater), 50RA0911 (SELOK), 50RA1306 (INVIRTES) and 50RA1304 (ViTOS).

REFERENCES

Almeida, O., Helander, J., Nielsen, H., and Khantal, N. 2007. "Connecting Sensors and Robots through the internet by integrating Microsoft Robotics Studio and embedded web services", IADIS International Conference WWW/Internet, IADIS, Vila Real, Portugal

Banks, J. 2010. "Discrete-Event System Simulation", Prentice-Hall

Balaguer, B., Balakirsky, S., Carpin, S., Lewis, M., and Scrapper, C.. "USARSim 2008: a validated simulator for research in robotics

and automation", IEEE Workshop on Robot Simulators: Available Software, Scientific Applications and Future Trends, IEEE/RSJ

Baltsavias, E. 1999. "Airborne laser scanning: basic relations and formulas", ISPRS Journal of Photogrammetry and Remote Sensing, vol. 54, no. 2-3, pp. 199–214

Bedkowski, J., Kretkiewicz, M., and Masowski, A. 2008. "3d laser range finder simulation based on rotated lms sick 200", Proceedings of the EURON/IARP International Workshop on Robotics for Risky Interventions and Surveillance of the Environment, Benicassim, Spain

Blume, H. and Heimann, B. 2007. "A laser range scanner simulation for probabilistic object tracking", isr.uc.pt

Emde, M., Rossmann, J., Sondermann, B., and Hempe, N. 2011. "Advanced Sensor Simulation In Virtual Testbeds: A Cost-Efficient Way To Develop And Verify Space Applications.", AIAA SPACE, Long Beach, California

Emde, M. and Rossmann, J. 2013. "Validating a simulation of a single ray based laser scanner used in mobile robot applications". In IEEE International Symposium on Robotic and Sensors Environments, ROSE, pages 55–60

Emde, M. and Rossmann, J. 2015. "Modelling and Simulation of a Laser Scanner with Adjustable Pattern as Virtual Prototype for Future Space Missions", IEEE Third International Conference on Artificial Intelligence, Modelling and Simulation (AIMS), to be published

Farrell, J. E., Catrysse, P. B., and Wandell, B. A. 2012. "Digital camera simulation." Applied Optics 51.4

Franti, E. et al. 2005. "Virtual Experiments Environment For Mobile Robots Design And Testing", Proceedings of the 4th WSEAS/IASME Int. Conf. on System Science and Simulation in Engineering, Tenerife, Spain

Fritzson, P. 2003. "Principles of object-oriented modeling and simulation with modelica 2.1", Wiley

Gerkey, B., Vaughan, R. T., and Howard, A. 2003. "The Player/Stage Project: Tools for Multi-Robot and Distributed Sensor Systems", Proceedings of the 11th International Conference on Advanced Robotics (ICAR 2003), Coimbra, Portugal, pp. 317-323

Hartley, R., and Zisserman, A. 2003. "Multiple view geometry in computer vision", Cambridge university press

Hoppen, M., Schluse, M., Rossmann, J., and Weitzig, B. 2012. "Database-Driven Distributed 3D Simulation", in Proceedings of the 2012 Winter Simulation Conference

Hoppen, M., and Rossmann, J. 2014. "A Database Synchronization Approach for 3D Simulation Systems", In: The 6th International Conference on Advances in Databases, Knowledge, and Data Applications (DBKDA 2014)

Hullin, M., et al. 2011. "Physically-based real-time lens flare rendering", ACM Transactions on Graphics (TOG). Vol. 30. No. 4. ACM

Huntsberger, T., et al. 2008a. "Characterization of the ROAMS Simulation Environment for Testing Rover Mobility on Sloped Terrain", Proceedings of i-SAIRAS, USA

Huntsberger, T., et al. 2008b. "3DROV: A Planetary Robot Design, Visualization and Verification Tool", Proceedings of i-SAIRAS, USA

Koceski, S., Koceska, N., Beomonte Zobel, P., and Durante, F. 2009. "Characterization and modeling of a 3D scanner for mobile robot navigation", Proceedings of the 17th Mediterranean Conference on Control & Automation, Makedonia Palace, Thessaloniki, Greece, June 24 - 26

Koenig, N., and Howard, A. 2004. "Design and use paradigms for gazebo, an open-source multi-robot simulator", in Proc. of IEEERSJ International Conference on Intelligent Robots and Systems IROS, vol. 3, pp. 2149–2154

Kriss, Michael 2015. "Handbook of digital imaging" Wiley

Kukko, A., and Hyyppä, J. 2007. "Laser scanner simulator for system analysis and algorithm development: A case with forest measurements", ISPRS Workshop on Laser Scanning 2007 and SilviLaser 2007, pp. 234–240

Laue, T., Spiess, K., and Röfer, T. 2006. "SimRobot - A General Physical Robot Simulator and Its Application in RoboCup", RoboCup 2005: Robot Soccer World Cup IX, pp. 173–183

Paul, J., et al. 2014. "Robotics rendezvous and capture test facility "inveritas"", Proceedings of 12th International Symposium on Artificial Intelligence, Robotics and Automation in Space (i-SAIRAS 2014), Montreal, Canada

Peinecke, N., Lueken, T., and Korn, B. R. 2008. "Lidar Simulation Using Graphics Hardware Acceleration", Proc. of the 27th DASC, USA

Rossmann, J., and Schluse, M. 2011a. "Virtual Robotic Testbeds: A foundation for e-Robotics in Space, in Industry – and in the woods", DeSE, Dubai

Rossmann, J., Schlette, C., Emde, M., and Sondermann, B. 2011b. "Advanced Self-Localization and Navigation for Mobile Robots in Extraterrestrial Environments.", Computer Technology and Application, Vol. 2, Number 5

Rossmann, J., Schluse, M., Schlette, C., and Waspe, R. 2012a. "Control by 3D Simulation – A New eRobotics Approach to Control Design in Automation". ICIRA, Montreal, Canada

Rossmann, J., Hempe, N., Emde, M., and Steil, T. 2012b. "A real-time optical sensor simulation framework for development and testing of industrial and mobile robot applications." Proc. of 7th German Conference on ROBOTIK 2012

Rossmann, J., Steil, T., and Springer, M., 2012c. "Validating the Camera and Light Simulation of a Virtual Space Robotics Testbed by Means of Physical Mockup Data", i-SAIRAS, Turin, Italy

Rossmann, J., Schluse, M., Schlette, C., and Waspe, R. 2013. „A New Approach to 3D Simulation Technology as Enabling Technology for eROBOTICS", In 1st International Simulation Tools Conference & EXPO 2013 (SIMEX 2013)

Rossmann, J., Schluse, M., Rast, M., and Atorf, L. 2015. "eRobotics Combining Electronic Media and Simulation Technology to Develop (Not Only) Robotics Applications", in E-Systems for the 21st Century: Concept, Developments, and Applications, S. Kadry and A. El Hami, Eds. Apple Academic Press, 2015. (to be published)

Schäfer, B., Rebele, B., and Gibbesch, A. 2008. „Verification and Validation Process on 3D Dynamics Simulation in Support of Planetary Rover Development", Proc. of the 10th ESA Workshop on Advanced Space Technologies for Robotics and Automation, The Nederlands

Schlette, C., et al. "Virtual commissioning of automated micro-optical assembly." SPIE LASE. International Society for Optics and Photonics, 2015

Sondermann, B., Emde, M., Rast, and M., and Rossmann, J. 2013. "Simulation-based Engineering with Hybrid Testbeds" , In Proceedings of the UKSim-AMSS 7th European Modelling Symposium on Computer Modelling and Simulation (EMS 2013)

Steil, T., and Rossmann J. 2014. "Validating the Camera and Light Simulation of a Virtual Reality Testbed by Means of Physical Mockup Data", Artificial Intelligence, 2nd International Conference on Modelling and Simulation (AIMS)

Wang, S., Heinrich, S., Wang, M., and Rojas, R. 2012. "Shader-based sensor simulation for autonomous car testing", 15th International IEEE Conference on Intelligent Transportation Systems (ITSC), Anchorage, AK

Yu, A., Harding, D., Krainak, M., Abshire, J., Sun, X., Cavanaugh, J., Valett, S., and Ramos-Izquierdo, L. 2011. "Development of an airborne lidar surface topography simulator", in Conference on Lasers and Electro-Optics (CLEO)

WEB REFERENCES

Space Engineering – System modelling and simulation, ESA ESTEC, Available at: http://www.ecss.nl/forums/ecss/dispatch.cgi/publictions/showFile/100141/d20100416115956/No/ECSS-E-TM-10-21A(16April2010).pdf

SYSTEMATIC ANALYSIS OF COLLABORATIVE HUMAN-MACHINE SCENARIOS: TASK EXECUTION ON MOVED OBJECTS

Titanilla Komenda
Doctoral Programme in Engineering Sciences
Technical University of Vienna
Wiedner Hauptstraße 8-10, 1040 Vienna, Austria
E-mail: e1227880@student.tuwien.ac.at

KEYWORDS
Collaboration, cobots, human-robot interaction, video analysis.

ABSTRACT

Human-machine collaboration is affected by parameters that may conflict cycle time or productivity. The optimal set of parameters may be specified by simulation models aiming a minimal ratio between target variables. In this paper, operational factors influencing task execution on moved objects are presented as a basis for modelling and optimizing collaborative human-machine scenarios. For that, a test series of 20 different collaborative tasks conducted at 4 different velocities by 3 different subjects were analysed. The results of the video analysis showed, that especially the velocity of moved objects influence the correctness of task execution whereas the position of motion paths is neglectable.

INTRODUCTION

Collaboration is defined as a state in which purposely designed machines work in direct cooperation with humans in a defined workspace, i.e. a human is asked to operate on objects moved by the machine. This interaction is affected by parameters resulting from operational objectives, mechanical and human factors as well as the performed collaborative task. The challenge in successfully implementing human-machine collaborations lies in defining an optimal set of those parameters without sacrificing too much of productivity. Usually, machines are programmed meeting the needs for short cycle time and high product quality. When collaborating with humans, additional factors need to be taken into account, such as safety, ergonomics, anthropometry as well as physical limitations. Especially physical limitations or psychophysiological impacts are essential when it comes to validation – e.g. in some cases, task execution by the human may not be completed on a moved object as the machine was moving the object too fast.

ANALYSING COLLABORATIVE OPERATIONS

User studies of human-robot interactions already show a great number of possible collaborative operations (Bauer et al. 2008; Goodrich and Schultz 2007). The matter of interest in these studies is often an applicable and safe interaction (Cherubini et al. 2016; Kim et al. 2015) or an psychological analysis (Giuliani et al. 2015). Therefore, data representing ergonomics and physical limitations may be discarded from further analysis. However, this data may bear potentially valuable insights and ideas for improving the implementation of human-machine collaboration. Collaborative work includes tasks such as removing, inserting, examining, mounting, machining or screwing (Bélanger-Barrette 2015; Tan et al. 2010). A collaborative operation *CO* can be defined as a function of following parameters (regardless of the operation type and the correctness of the task execution): collaboration space *CS*, object pose including position and orientation *p*, distance between human and machine *d*, velocity *v*, acceleration *a*, ergonomic specifications *e* and physical limitations *l*. More specifically, these parameters are a function of an individual human *H* executing the collaborative task (Stadler et al. 2013). This means, there may exists a set of collaborative parameters for each human H_n that meets the objective function of minimal cycle time and maximal productivity (1).

$$t_{min}\ [\mathbf{CO_H}(CS_n, p_n, d_n, v_n, a_n, e_n, l_n)] \qquad (1)$$

The collaborative space, the pose or rather the motion path of the object as well as the velocity and acceleration can be defined by the robot programmer dependent on the human worker (Puls 2015; Thiemermann 2005). Ergonomic guidelines for collaborative applications can be adopted from guidelines specifying ergonomic working environments for human workers, such as ergonomic working heights or free space regulations around human workers. Physical limitations, however, need to be identified by conducting research experiments and might as well influence productivity.

In this sense, 20 different collaborative tasks executed on objects moved by an industrial robot were performed and analysed. Tasks executed by the human subjects were based on tasks defined within the Methods-Time Measurement system (MTM) and within ema. MTM is a predetermined motion time system that is used to analyse manual tasks as a result of standardised times for individual tasks. ema is a world leading simulation tool for planning human work and is itself based on MTM, i.e. individual manual tasks modelled have predetermined times corresponding to the standardised times of MTM. However, as humans are able to adapt to velocities of moved objects, dynamic tasks in the sense of tasks executed on moved objects cannot be simulated yet. Furthermore, physical limitations of human task execution need to be considered in the dynamic model of task execution on moved objects.

METHODOLOGY

In this section, the applied methodology for analysing collaborative work on moved objects is presented. Firstly, the objects of investigation were defined. Secondly, specific collaborative tasks were selected and circumstantiated. Thirdly, the human-machine collaborations were executed with a set of subjects, from which video data was collected. Finally, the video data was analysed resulting in a derived set of information for executing reliable human-robot collaboration.

Hypotheses

Based on the analysis of collaborative operations in the context of human-machine interactions, following hypotheses for the experiments can be derived:

- H1 – Operations on moved objects are constrained by minimal and maximal velocities, where operators are either subchallenged or overstrained.
- H2 – The error rate of operations on moved objects increases with an increase of velocity.
- H3 – There is an optimal speed of movement resulting in a minimal ratio between excessive demand and error rate.

Experimental Design

The experiments for analysing collaborative operations during human-robot interactions were carried out with an ABB robot IRB 120, four HD cameras mounted in different positions and angles and three subjects. The subjects were of different height h_H resulting in different human workspaces (WH). The robot with a reach of 580 mm (WR) and a maximum payload of 3 kg was allowed to move within a pre-defined collaborative space *CS* of 400x200x350 mm. The robot was mounted on a platform of 770 mm height h_T, resulting in an ergonomic, collaborative working height of 920-1,270 mm (Figure 1). In total, 20 tasks including examining, mounting, pressing, picking and placing objects, using tools such as electric screwdrivers or walking to moved objects from different distances and angles were analysed. Influencing factors included velocity, motion path, distance between human and machine and human anthrompometry. The position of the subjects relative to the robot was freely selectable. Nevertheless, the subjects chose to work in front of the robot. The anthropometric data of the subjects executing the collaborative tasks is given in Table 1. The corresponding anthropometric percentiles are given in parenthesis in each case.

Experimental Procedure

The collaborative tasks were executed after one day of practice (in order to minimize any influence of learning) at different velocities and motion paths. The velocities of the robot ranged from 50 – 200 mm/s in 50 mm/s steps. Motion paths included horizontal, vertical and diagonal movements within the collaborative workspace at constant orientation. Additionally, three different heights, distances and offsets were specified, resulting in overall six different horizontal, six

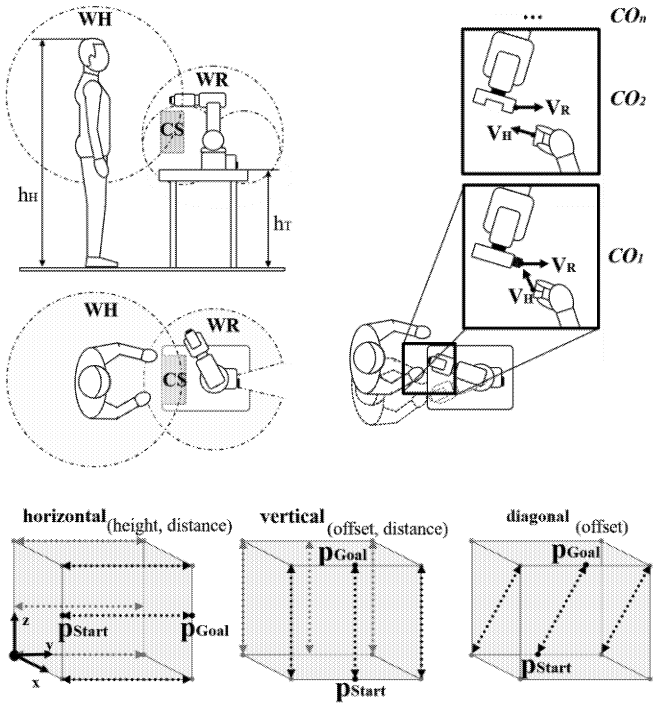

Figure 1: Experimental Design (left), Set of Collaborative Tasks (right) and Motion Paths (below)

vertical and three diagonal motion paths. Thus, experiments conducted by 3 different subjects, at 4 different velocities and 15 different motion paths resulted in a test series of 180 data sets for one collaborative task, while each motion path at a specific velocity was completed 10 times in a row. The cameras were used to film the collaborative operations from four different angles in order to detect unexpected human behavior. Furthermore, the video data was used to measure the time for executing the collaborative task as well as to identify the number of error situations.

Table 1: Subject Characteristics

	Subject 1	Subject 2	Subject 3
Gender	male	male	female
Age	26	21	26
Height [cm]	179 (73 %)	178 (68 %)	158 (21 %)

RESULTS

As an example, the results for the collaborative task screwing by hand are shown. In this task, the subjects were asked to manually screw a hexagon nut on an object moved by the robot (Figure 2).

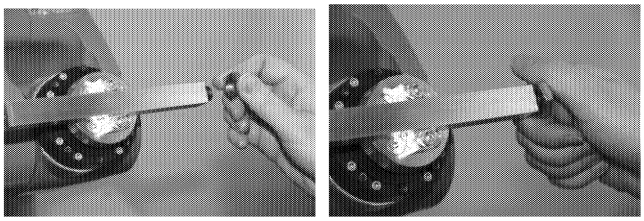

Figure 2: Screenshot of the Collaborative Task Screwing

Table 2 shows a statistical analysis of measured cycle times for conducting the collaborative operation in one vertical direction with regard to the robot's velocity for each subject. Table 3 shows the number of missed parts (out of ten) in vertical motion for each subject dependent on the robot's velocity. The standard deviation is given in parenthesis in each case.

Table 2: Mean Cycle Time in Seconds of Executed Task in One Vertical Motion for each Subject dependent on Velocity

	Subject 1	Subject 2	Subject 3
50 mm/s	2.33 (0.432)	4.04 (1.466)	3.70 (0.832)
100 mm/s	3.08 (0.378)	3.05 (1.045)	4.33 (0.591)
150 mm/s	2.37 (0.296)	3.77 (1.975)	4.15 (1.190)
200 mm/s	3.33 (0.467)	4.51 (2.902)	6.97 (6.356)

Table 3: Mean Number of Missed Parts in Vertical Motion for each Subject dependent on Velocity

	Subject 1	Subject 2	Subject 3
50 mm/s	0.00 (0.000)	0.00 (0.000)	0.00 (0.000)
100 mm/s	1.00 (0.894)	2.33 (1.633)	3.67 (1.211)
150 mm/s	4.33 (1.033)	5.00 (1.673)	5.50 (0.837)
200 mm/s	7.83 (0.753)	6.67 (1.366)	7.17 (0.408)

DISCUSSION

The analysis of parameters influencing collaborative human-robot tasks on moved objects shows six main results:

- The number of errors increases with an increase of the robot's velocity.
- The distance between human and robot decreases with an increase of velocity.
- The relative movement between human and robot decreases with an increase of velocity.
- The optimal velocity for task execution on moved objects is between 50 – 100 mm/s.
- The position of the object or the motion path within the collaboration space does not influence task execution.
- The type of motion does not influence task execution.

CONCLUSION

The analysis in this work showed that there are parameters of collaborative work that result in a conflict of physical limitation and cycle time or rather productivity. The findings presented do have implications for the design and implementation of human-robot collaboration tasks and should be considered in the design of dynamic models for collaborative tasks.

Referring to the given hypotheses following conclusions can be drawn:

- Operations on moved objects are constrained by a minimal and maximal velocity.
- The error rate of operations on moved objects increases with an increase of velocity.
- There is an optimal velocity for executing tasks on moved objects resulting in a minimal ratio between excessive demand and error rate.

In future work, analysis is being conducted with a different set of machines, i.e. conveyor belts, mobile robots and industrial robots of different size (resulting in different sizes of collaborative workspaces) as well as a more comprehensive test group.

REFERENCES

Bauer, A.; Wollherr, D. and Buss, M. 2008. "Human-Robot Collaboration: A Survey". In *International Journal of Humanoid Robotics*. World Scientific Publishing Company.

Bélanger-Barrette, M. 2015. *Collaborative Robot Ebook*. Robotiq, Lévis, Canada (Oct.).

Cherubini, A.; Passama, R.; Crosnier, A.; Lasnier, A. and Fraisse, P. 2016. "Collaborative manufacturing with physical human-robot interaction". In *Robotics and Computer-Integrated Manufacturing*. Elsevier, Amsterdam, Netherlands, 1-13.

Giuliani, M.: Mirnig, N.; Sollnberger, G.; Stadler, S.; Buchner, R. and Tscheligi, M. 2015. "Systematic analysis of video data from different human-robot interaction studies: a categorization of social signals during error situations". In *Frontiers in Psychology 6:931. doi: 10.3389/fpsyg.2015.00931.* Lausanne, Switzerland.

Goodrich, M.A. and Schultz, A.C. 2007. "Human-Robot Interaction: A Survey". In *Foundations and Trends in Human-Computer Interaction*. Now Publishers Inc., Hanover, MA, USA, 203-275.

Kim, J.; You, S.; Kamat, V.; Sanghyun Lee, S. and Robert, L.P. 2015. "Evaluation of Human Robot Collaboration in Masonry Work Using Immersive Virtual Environments". In *Proceedings of the 15th International Conference on Construction Applications of Virtual Reality* (Banff, Alberta, Canada, Oct. 5-7). Organizing Committee of the 15th International Conference on Construction Applications of Virtual Reality, 132-141.

Puls, S. 2015. *Situationsverstehen für die Risikobeurteilung bei der Mensch-Roboter-Kooperation.* PhD thesis, Fakultät für Informatik des Karlsruher Instituts für Technologie.

Stadler, S.; Weiss, A.; Mirnig, N. and Tscheligi, M. 2013. "Anthropomorphism in the factory – a paradigm change?". In *Proceedings of the 8th ACM/IEEE International Conference on Human-Robot Interaction* (Tokyo, Japan, Mar. 3-6). IEEE Press, Piscataway, NJ, USA, 231-232.

Tan, J.T.C.; Duan, F.; Kato, R. and Arai, T. 2010. "Collaboration Planning by Task Analysis in Human-Robot Collaborative Manufacturing System". In *Advances in Robotic Manipulators,* Hall, E. (Ed.). InTech, Rijeka, Croatia, 113-132.

Thiemermann, S. 2005. *Direkte Mensch-Roboter-Kooperation in der Kleinteilmontage mit einem SCARA-Roboter.* PhD thesis, Fakultät für Maschinenbau der Universität Stuttgart.

AUTHOR BIOGRAPHY

TITANILLA KOMENDA was born in Vienna, Austria and went to the University of Applied Sciences Technikum Wien, where she studied Mechatronics/Robotics and obtained her Master's degree in 2011. She worked as a lecturer and research assistant for the above mentioned university for a couple of years before moving to ProAutomation in 2013 and to Centauro in 2014, where she has been working in the field of simulating automation systems ever since. In September 2014 she additionally started working on her doctoral thesis in the field of simulating human-machine collaboration.

Simulation based customized garment design for the physically disabled people of scoliosis type

Yan Hong
ENSAIT
2 allée Louise et Victor Champier, 59056
Roubaix Cedex 1, France
E-mail: yannichonghk@gmail.com

Pascal Bruniaux
ENSAIT
2 allée Louise et Victor Champier, 59056
Roubaix Cedex 1, France
E-mail: pascal.bruniaux@ensait.fr

Xianyi Zeng
ENSAIT
2 allée Louise et Victor Champier, 59056
Roubaix Cedex 1, France
E-mail: xianyi.zeng@ensait.fr

Antonela Curteza
Technical University of Iasi, Dimitrie Mangeron
Bd., 53, Iasi -700050, Romania
Email: acurteza@gmail.com

KEYWORDS
Computer Aided Design (CAD), Health sciences, Interactive programs

ABSTRACT
This paper introduces a visualization-based method for simulation customized 3D garment and generation corresponding 2D block patterns for physically disabled people of scoliosis type. The proposed design process and method follows that of traditional garment prototyping and draping in reality. First, a simulation process is first performed on a scanned 3D human body for creating a digitalized human body model. Second, feature points of the human body for the garment simulation are discussed and classified with wearing ease for desired fit of the garment based on the parameterized model. A basic garment wireframe aligned with body features is then established based on the defined feature points of the human body. Based on the deformed wireframe, a 3D expandable garment block is simulated. In this process, Customized 2D and 3D virtual garment prototyping tools are ensured to create customized products based on the concept of from reality to simulation and visualization, which can be further applied to the design automation to create fit-ensured mass-customized apparel products (the top body type) for the disabled people with scoliosis. The experimental results show that the proposed method is easier to be implemented and can generate patterns with satisfactory fit.

INTRODUCTION
Scoliosis is a three-dimensional deformation of all or part of the spine (cervical, thoracic or lumbar) causing twisting of one or more vertebras and causing a distortion of the thorax, abdomen and paravertebral areas (close to the vertebrae) (Elliott and Knight 1997; Subramanyam, et al. 2015). The figures of the disabled people are not fit into the standard sizes that are available in the stores(Iezzoni, et al. 2014). These people constitute an important part of the population, represents a consumer market with special requirements of customized products(Komeili, et al. 2015). But because of the deformation of the body figure, there are several technical limits for the customized design(Stjepanovic 1995). Also,

the technical limits lead to the unaffordable price for the customized service(De la Garza-Ramos, et al. 2016).

For normal people, the location of the key feature points, such as neck points, on the virtual body model with a standard posture, can be performed using a standard body measurement procedure(Goldstein, et al. 2009). The symmetric of the body ensures an easy identification of the key features points(Wang, et al. 2007). However, for disabled people of scoliosis type, locating these key feature points is very difficult because of the atypical body shapes. Many key positions (neck points, scapular points etc.,) are hidden inside the body surface because their standard postures cannot be obtained. The anthropometric landmarks of atypical body shapes cannot be detected automatically and a lot of manual adjustments are needed for obtaining a complete 3D body shape(Kwong 2004). The traditional pattern making method, which is based on the accurate measurements of body shape, is not applicable(Thomassey and Bruniaux 2013).

In the real customized garment design and pattern generation process, the fabric draping process using 3D customized physical mannequin permits to the generation of the pattern pieces(Jeong, et al. 2006). The garment shape will be firstly moulded by designers with the operation of moulding, cutting and pinning fabric to a mannequin or individual(Liu, et al. 2010). The draping process is frequently used by designers for quickly generating the form of a garment and corresponding 2D garment patterns(Whife 2005). In this process, style lines and constructions details of the drape are carefully marked and removed step by step take the corresponding lines and points of the human body or mannequin(Zhong and Xu 2006). Fabric pieces with the construction and style details are generated. Darts will be generated in the same time at the same time(Hutchinson and Munden 1977). The fabric pieces are then laid to be flat and traced over a pattern paper. The pattern is finalized by adding directional marks such as grain lines, notches, buttonholes, correct seam and hem allowances and facings(Kim 2015).

In this context, a new visualization-based 3D-to-2D CAD method is proposed for designing customized garments that can be accessible to find technical solution, permitting the industrial production and fitting the deformation of human body(Wang, et al. 2009). To overcome the technical limitations presented previously, it is proposed in this paper the implementation of a new virtual reality-based design method for an adapted 3D garment (sleeveless hip-length shirt with from-fitting bodice) and its corresponding 2D block patterns. The proposed method can be applied to create fit-ensured mass-customized apparel products for the disabled people with scoliosis (Wang, et al. 2014).

SIMULATION OF THE CUSTOMIZE GARMENT DESIGN

The simulation process and method, following that of traditional garment prototyping and draping in reality, which can effectively ensure the ideal garment shape fit performance of the desired garment, is introduced.

Simulation of the human body model

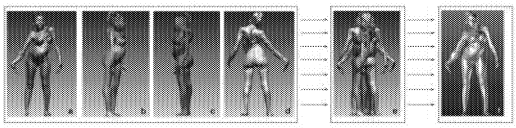

Figure 1: From the scanning results to the digitalized human body model

At this step, data on a body shape are acquired using a 3D scanner and the software *ScanWorX* of the Human Solutions Company. This method first takes various scanning pictures in different views for the same consumer with the same posture (Figure 1-a, b, c, d) during the 3D scanning procedure. Each of these pictures, taken with the same reference axis of the 3D scanner from different views, can be regarded as 1/4 of the full scan result. Then, the data from the

scanned body shape are imported to another software, called *RapidForm*, permitting to edit and correct the defects of the 3D meshed object. Using the *RapidForm* software, these four pictures (Figure 1-e) are combined, rotated and merged in order to generate one complete 3D virtual human body model (Figure 1-f).

By using this reference axis, the corresponding positions of different images or different views in order to generate the unique virtual human body model can be easily found. The proposed method will permit to automatically generate the digitalized 3D human body model. The mesh of the 3D shape is then re-triangulated using *RapidForm* software.(Wang, et al. 2005) The holes that are invariably made as a result of scanning are filled. Irregular forms generated as a result of filling holes, like near the hands and feet, are removed. A plane is used to cut the feet to make it parallel to the X-axis. The body form is smoothened using a smoothening tool. It is ensured that all holes (near hair and armpit area) are filled. Normally the holes will be in the hair and armpit and in small size. Plain planes are created to repair the holes. As the sizes of these holes are small and the wearing allowance will be designed in future operation, plain planes will be created to fill the holes. A special function of *RapidForm* is applied to mesh the surface of the body model with 600-700 facets. With this procedure, the body made of point clouds will be transferred into small facets. These facets can be regarded as the sub surface of the body, which can be modified. The number of the facets will determine the quality of the virtual body surface. If the precision of the virtual body is not high enough, more facets can be added to meet the desired precision. The 3D body model modified by *RapidForm* is then imported into the Design Concept. The result obtained in the *DesignConcept* is the final digitalized human body model, from which a 3D garment can be created. Using the *DesignConcept* software, the 3D surface of the body shape can be modelled and simulated.

The operation of 3D scanning permits to directly obtain the 3D body shape, on which 3D draping of a virtual garment can be realized. The detailed body measurements will not be necessary. Different from the traditional pattern making method, which is based on the accurate measurements of body shape, the proposed method using the simulated human body model, serving as the individual mannequin, ensures the 3D customized garment design.

Establishing reference planes

At this step, following the design process of the traditional garment design method, several reference planes, related to the feature points of the desired garment, will be established. These reference planes will permit to the location of the feature curves and feature points of the human body, in order to simulate the body shape information. But, different from that of normal people, the quantity and orientation of the reference planes are different because of the deformation (Figure 2)(De la Garza-Ramos, et al. 2016). In this context, the definition of these reference planes should follow the following principles: (1) following the traditional 3D real draping method, (2) satisfying the requirements of the disability, (3) meeting the requirement of better observing the human body.

Based on these principles, different XY planes are oriented in the 3D space in the design process to help to cut the body and create the morphological curves (the morphological curves are curves in Figure 3-a). By adjusting the inclinations of the XY planes, the morphological curves can then be adjusted visually. The yellow axis between the feet is perpendicular to the ground. The red axis between the feet is parallel to the ground. All the subsequent red axes made on the body are parallel to the ground (Figure 3-b). Since the legs of the woman are more or less

similar to those of normal people, all the axes between the legs are parallel to the floor.

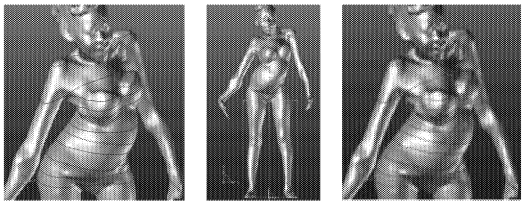

Figure 2: The morphological curves of the customer and the subsequent red axes for establishing the morphological curves

A set of special planes is defined following the shape of spine in the position of waist, hip and breast, which are important positions for garment design. Considering the irregular shape of the body and hyperbolic-curvature of the spine, more planes close to those defined initially are defined in order to ensure the reference planes can fully simulate the shape of the human body(Hsiao and Chen 2013). As shown in Figure 6, three such planes are made in the waist region, one being on the waist, one above and another below it; three planes are made in the chest area, one running through the bust points, one below and another above it; other three planes are made on the hip region. These planes are defined in the *DesignConcept* software taking the reference of on the ground floor. The distance between the plane and the ground floor can be adjusted and tested until the numbers of the planes and distances are qualified enough to modeling the shape of the human body(Fontana, et al. 2005).

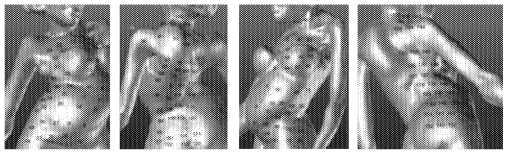

Figure 3: Names of the fit points and fashion points

Feature points definition, ease distribution and wireframe formation

Using the defined reference planes, the feature curves of the human body can be easily obtained to simulate the body shape information of the customer. Based on these feature curves, the feature points of human body can be determined. The design knowledge and 2D pattern making knowledge are both applied in this process for determining feature points of human body, using an interactive design process. The designer first locates these points by his/her professional experience. Several modification operations are performed repeatedly until the final positions of these points on the curves are acceptable for both designers and customers. Same as the identification of the reference planes, more points are added than what the designers will do for normal people in order to make the result more accurate.

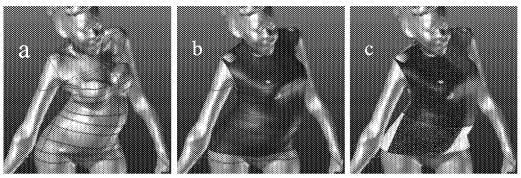

Figure 4: The wireframe of the garment surface and the meshed garment surfaces

Referring to the relationship between the feature points of the human body and those of the garment in the research carried out in another study, the fit points of the human body should be distinguished from the non-fit points. The fit point refers to the points on the garment surface that exists no wearing ease between the garment and the human body, while that of the non-fit point exists wearing ease(Thomassey and Bruniaux 2013). The non-fit feature points on the garment surface will be determined by the non-fit points of the human body by adding some values of wearing ease, in order to show desired fashion and comfort effects. A wearing ease represents the distance between the body and the garment. Figure 7 shows the defined fit points and non-fit points. The points marked

with white color are the fit points while those with black color are the non-fit points.

In our study, a technical method is developed for generating values of wearing ease. The Normal lines of the non-fit points on the human body will be applied to the corresponding feature points of the garment surface. Their lengths of these Normal lines take values from the desired wearing ease given at different positions. The lengths, representing the value of wearing ease, can be adjusted by the designers in the 3D environment, according to the wearing purpose desired both by the wearer and designer. Design knowledge and 2D pattern making knowledge of the designer will be used for the determination of the wearing ease value. Besides, the directions of the normal lines can also be adjusted based on the simulation result in the following process (the green lines in Figure 7). Using this method, the consumer's requirements are fully considered not only at functional level but also at aesthetic level, which ensures the wearer and the designer to set up a compromise between desired fashion requirements and comfort feeling for different wearing purposes(Luo and Yuen 2005).

Table. 1 shows a number of representative wearing ease defined by designers and pattern makers with their design knowledge and 2D pattern making knowledge for different wearing purposes.

Purpose	Fit points label					
	22	26	46	71	115	135
Basic fitting (mm)	30	8	30	10	32	30
Sports (mm)	40	16	40	18	44	40
Home (mm)	35	13	35	15	37	35
Dinner (mm)	32	10	32	12	34	32

Table 1: Wearing ease distribution for different wearing purposes

After this step, all the feature points of the desired garment block are determined. For determination of the feature curves defining the structure of the garment, the feature points of the garment are linked together in horizontal and vertical directions, in order to guarantee that garment patterns follow in the both horizontal and vertical directions correctly. In this process, the 2D pattern making knowledge will provide inspiration and reference. These curves are neck and armhole curves, princess lines and so on. Finally a wireframe of the garment block surface can be obtained (Figure 8-a)(Meng, et al. 2010).

Developing 3D garments and 2D Block Patterns

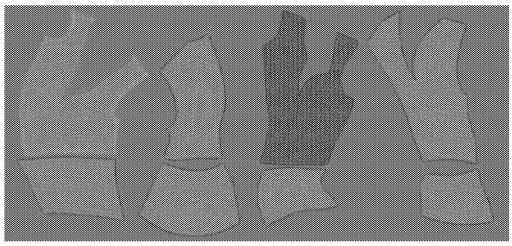

Figure 5: 2D patterns generated from the 3D garment block

The wireframe of the garment block is then modeled by triangulating and assembling different parts bounded by the deformed wireframe (Figure 8-b and Figure 8-c). The technical method is the same as the creation of a digitalized human body model using the *RapidForm* software. The number and size of the mesh is determined by the designers using several experimental adjustments until the final result is acceptable for the flattening operation. As the fabric information will be given in the virtual try-on section, there will be no specific requirement for the number and size of the mesh. The meshed garment block surface can then be applied to generate with the flattening operation to obtain the corresponding 2D pattern. The generation of flattened 2D pattern also strictly follows the principle of the classical 2D pattern design knowledge. Darts, folds, opening, fabric direction (Warp and Weft direction) and other important 2D pattern design elements should be fully considered(Meng, et al. 2012). Then the

meshed virtual garment surface is divided into 4 parts: right front, left front, right back and left back (Figure 9). Eight different surfaces are generated: 4 in the front and 4 in the back. Then the 2D patterns can be flattened automatically and easily(Volino, et al. 2005).

To make sure that the final result can be applicable for industry, the flattened 2D pattern is then input into the *Modaris* software for adjustment in order to satisfy the desired practical properties used in apparel industry. Then a customized garment block and corresponding 2D patterns with the proposed method can be generated and applied for industrial use(Wang, et al. 2003).

ACKNOWLEDGEMENT

Special thanks to LECTRA Computer for software support.

CONCLUSION

In this study, a visualization-based method is proposed for simulation customized 3D garment and generation corresponding 2D block patterns for physically disabled people of scoliosis type. The simulation process and method for the garment design follows that of traditional garment prototyping and draping in reality. A simulation process is performed from a scanned 3D human body for creating a digitalized human body model to ensure the identification of the feature points on the human body surface. Then the feature points on the body surface are discussed and classified with wearing ease for desired fit of the garment based on the parameterized model. A basic garment wireframe aligned with body features is then established based on the defined feature points of the human body. Based on the deformed wireframe, a 3D expandable garment block is simulated. In this process, Customized 2D and 3D virtual garment prototyping tools are ensured to create customized products based on the concept of from reality to simulation and visualization, which can be further applied to the design automation to create fit-ensured mass-customized apparel products (the top body type) for the disabled people with scoliosis. The experimental results show that the proposed method is easier to be implemented and can generate patterns with satisfactory fit.

REFERENCES

De la Garza-Ramos, R., et al.
2016 Visual loss after corrective surgery for pediatric scoliosis: incidence and risk factors from a nationwide database. Spine J.

Elliott, Julia, and Anne Knight
1997 The Oxford paperback dictionary & thesaurus: Oxford University Press.

Fontana, Marzia, Caterina Rizzi, and Umberto Cugini
2005 3D virtual apparel design for industrial applications. Computer-Aided Design 37(6):609-622.

Goldstein, Yaron, et al.
2009 Virtual prototyping: from concept to 3D design and prototyping in hours. *In* Transforming Clothing Production into a Demand-Driven, Knowledge-Based, High-Tech Industry. Pp. 95-139: Springer.

Hsiao, Shih-Wen, and Rong-Qi Chen
2013 A study of surface reconstruction for 3D mannequins based on feature curves. Computer-Aided Design 45(11):1426-1441.

Hutchinson, Richard, and DL Munden
1977 The geometrical requirements of patterns for women's garments to achieve satisfactory fit, University of Leeds.

Iezzoni, L. I., et al.
2014 General health, health conditions, and current pregnancy among U.S. women with and without

chronic physical disabilities. Disabil Health J 7(2):181-8.

Jeong, Yeonhee, Kyunghi Hong, and See-Jo Kim

2006 3D pattern construction and its application to tight-fitting garments for comfortable pressure sensation. Fibers and polymers 7(2):195-202.

Kim, Ryang-Hee

2015 Development and Emotional Evaluation of Scented Clothing using Microcapsules. Procedia Manufacturing 3:558-565.

Komeili, A., et al.

2015 Monitoring for idiopathic scoliosis curve progression using surface topography asymmetry analysis of the torso in adolescents. Spine J 15(4):743-51.

Kwong, M. y

2004 Garment design for individual fit. *In* Clothing Appearance and Fit. W. Yu and L. Hunter, eds. Pp. 196-233: Woodhead Publishing.

Liu, Yong-Jin, Dong-Liang Zhang, and Matthew Ming-Fai Yuen

2010 A survey on CAD methods in 3D garment design. Computers in Industry 61(6):576-593.

Luo, Ze Gang, and M. M. F. Yuen

2005 Reactive 2D/3D garment pattern design modification. Computer-Aided Design 37(6):623-630.

Meng, Yuwei, P. Y. Mok, and Xiaogang Jin

2010 Interactive virtual try-on clothing design systems. Computer-Aided Design 42(4):310-321.

Stjepanovic, Zoran

1995 Computer-aided processes in garment production: features of CAD/CAM hardware. International Journal of Clothing Science and Technology 7(2/3):81-88.

Subramanyam, R., et al.

2015 Systematic review of risk factors for surgical site infection in pediatric scoliosis surgery. Spine J 15(6):1422-31.

Thomassey, S., and P. Bruniaux

2013 A template of ease allowance for garments based on a 3D reverse methodology. International Journal of Industrial Ergonomics 43(5):406-416.

Volino, Pascal, Frederic Cordier, and Nadia Magnenat-Thalmann

2005 From early virtual garment simulation to interactive fashion design. Computer-Aided Design 37(6):593-608.

Wang, Charlie C. L., Yu Wang, and Matthew M. F. Yuen

2003 Feature based 3D garment design through 2D sketches. Computer-Aided Design 35(7):659-672.

Wang, Jin, et al.

2007 Pattern design on 3D triangular garment surfaces. Journal of Zhejiang University SCIENCE A 8(10):1642-1649.

Wang, Jin, et al.

2009 Interactive 3D garment design with constrained contour curves and style curves. Computer-Aided Design 41(9):614-625.

Wang, Y., et al.

2014 Evaluation on an ergonomic design of functional clothing for wheelchair users. Applied Ergonomics 45(3):550-5.

Whife, Archibald Allon

2005 Designing and Cutting Ladies Garments: Tailor and cutter.

Zhong, Yueqi, and Bugao Xu

2006 A physically based method for triangulated surface flattening. Computer-Aided Design 38(10):1062-1073.

AUTOMOTIVE SIMULATION

The Role of the Numerical Simulation in Optimization of the Automotive Systems

Alexandru DOBRE, Nicolae VASILIU and Cristian Nicolae ANDREESCU
University POLITEHNICA of Bucharest
313, Splaiul Independentei, 6th County
RO 060042 Bucharest, Romania
E-mail: alexandru.c.dobre@gmail.com; nicolae.vasiliu@upb.com; cristian.andreeescu@upb.com

KEYWORDS

Simulation, automotive systems, suspension, brake, comfort, AMESim

ABSTRACT
Comfort is the main parameter that characterizes the quality of a car suspension system. The isolation of the forces transmitted by external excitations represents the main task for any automotive system design. Determination of the constructive parameters of an automotive system involves the solving of a set of differential equations, which describes the automotive dynamic behavior. Generally, the real behavior of an automotive system differs from the theoretical one, lengthy and costly iterations being necessary, which include the mathematical modelling, constructive design, implementation, and test. It is possible to reduce considerably these chained steps by using numerical simulation. This way, the design and the operational parameters of the automotive system are changed until the overall performances become satisfactory. The main objective of this paper consists in optimizing the constructive and functional parameters of some automotive systems using numerical simulation with the AMESim modelling and simulation program. Two automotive systems - suspension and brake one are studied.

INTRODUCTION

In recent years, a group of teachers skilled in hydro pneumatic control systems (Lebrun and Richards 1997) developed a new language of modeling and numerical simulation of the technical systems, called *AMESim*. It was quickly implemented both in industrial and in academic environment. The language allows the assembly of the mathematical models of the studied processes from fair models of technical components stored in libraries written in C programming language. From the user's point of view, the language presents a graphical interface, which shows the progress of the whole simulation process system during different stages. The motto of the creators of this engineering instrument is "To create Good Models without Writing a Single Line of Code". Like any language of modeling and simulation, the AMESim program accepts equations systems, which define the dynamic behavior of the engineering systems implemented in the form of numeric codes, called "system models". A model is built from equations and from numerical descriptions of the all system components. These are considered sub-models and are defined in a large number from the libraries language.
In the automotive industry there are three categories of modern suspensions: adaptive, semi-active and active. The semi-active suspension (which controls the dissipated energy) is preferred for automotive manufacturers since they can achieve a desirable performance than passive suspension and there are no external power source requirements (other than for control valve actuation) and much more simple in comparison with fully active suspension (El-Demardash 2002; Alessandro et al. 2004; Tao 2005). Similar researches were presented in the papers (Dixon 2007; Choi, Han 2015; Gołdasz and Sapiński 2015; Alexandridis 2000).
The complete brake system can be divided into the service brakes, which slow and stop the moving vehicle, and the parking brakes, which hold the vehicle stationary.
On most late-model vehicles, the antilock brake system (ABS) is a third major subsystem; and many cars now also include traction control as part of the brake system functions (Owen 2011).
The maximum performance of brake system is, therefore, conditioned by many factors outside the system itself: while the recognition of the latter is the job of drivers, who are in charge of limiting vehicle speed and controlling the distance between close vehicles, vertical loads cannot be easy understood. These are determined by different factors, such as payload and its distribution in the vehicle, road slope, longitudinal acceleration, in particular, the same braking acceleration (Genta and Morello 2009).

THE MODELING AND SIMULATION OF THE AUTOMOTIVE SYSTEMS

For example, it will simulate a complete vehicle brake system, presented in Figure 1. The vehicle brake system simulated is formed of a pneumatic vacuum booster, a master cylinder, pipelines and calipers.
Disc brakes are a type of axial braking system, meaning that the clamping force of the caliper acts in an axial direction. This force is applied by hydraulic cylinders to the brake pads, which are pressed against the planar frictional surfaces of the brake discs (Heibing and Metin 2011).
Due to the mathematical equations already inserted in models, the software AMESim offers the main advantage of working time reduction. The software's interface is very accessible for any kind of engineering user (LMS 2013).

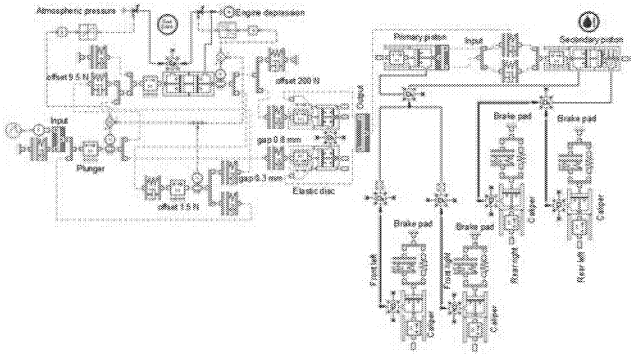

Figure 1. The brake system model

The pedal turns the brake stroke input the driver into an input on the booster that can be either a displacement or a force.
The pneumatic vacuum booster amplifies the pedal force value. The vacuum booster model is presented in figure 2. The default model must be defined by different options thanks to scalar amplification ratio and saturation force. One can also choose to use a data table by selecting the corresponding option.

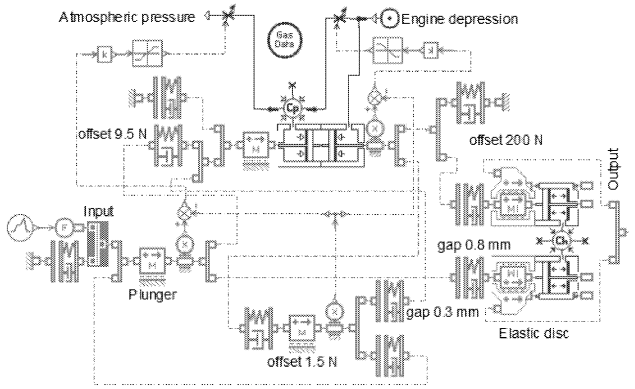

Figure 2. The pneumatic vacuum booster model

The major problem of such an element is the way of consideration of the internal movements of the rubber part called “the reaction disc” (or elastic disc). The static behavior and consequently the pneumatic amplification of the booster derives from the properties and the model of this rubber part.
The master cylinder converts the force from the booster into a pressure that feeds the electronic braking systems; the simulation model is presented in figure 3. The main function simulated for the master cylinder is the piston effect within its two chambers. The return parts needed to avoid cavitation in the chambers are not considered in the above master cylinder model (Vasiliu N. and Vasiliu D. 2005). The master cylinder model takes into account the restrictions on the output of the front chamber only; the rear chamber has restrictions but they have big holes diameters. The friction force function of the pressure is also not taken into account. The calipers model is presented in the figure 4.

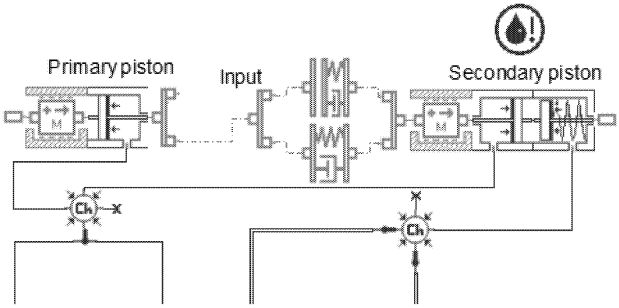

Figure 3. The master cylinder model

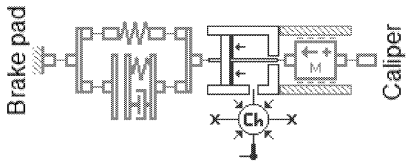

Figure 4. The caliper model

The common purpose of a braking system is to slow down and stop the vehicle by applying friction torques on wheels when the brake pedal is pushed. A part of results of the simulations are presented in figures 5, 6, 7 and 8.

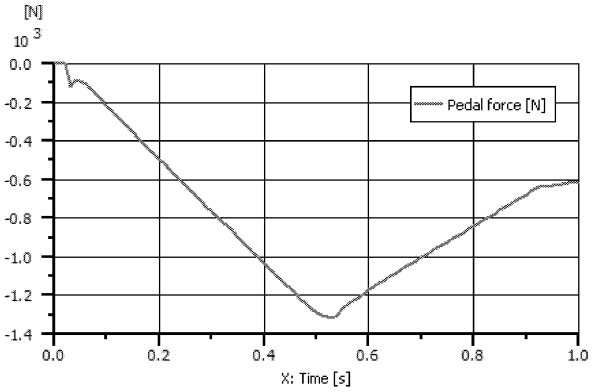

Figure 5. Variation of the pedal force amplified by the pneumatic vacuum booster depending

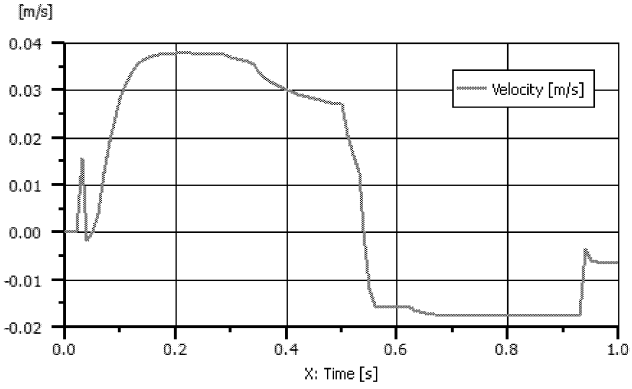

Figure 6. The velocity resulted at the exit from pneumatic vacuum booster depending on time

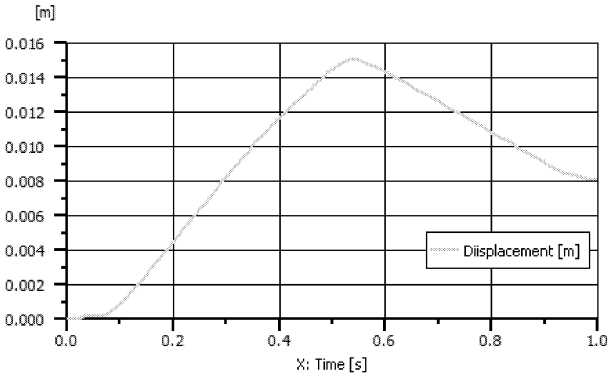

Figure 7. The displacement resulted at the exit from pneumatic vacuum booster depending on time

At the end of the simulation of the brake system the forces applied on the brake pads don't remain at the zero value. This aspect it is due to the fact that the stick-slip friction of the seals is considered constant (normally - a function of the pressure) and the neutral position pressure relief valves inside the master cylinder aren't considered. The maximum force applied on the brake pad front left is about 5800 N, while the maximum applied on the brake pad rear left is 2.3 times smaller (figure 8).

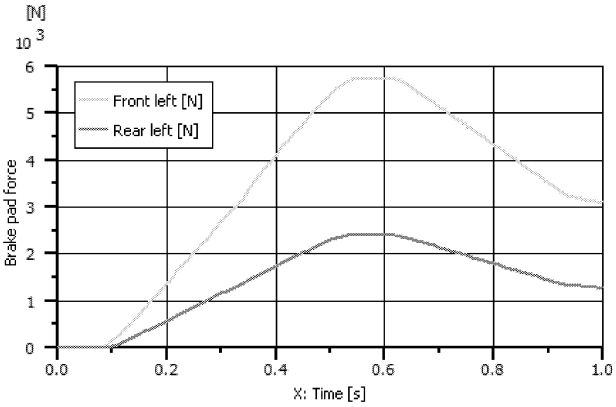

Figure 8. The brake pads force depending on time

In the second part of the paper it will presented the simulation of a typical car's suspension system. The calculus is performed for the damper, modeled by the network from figure 10. The theoretical characteristics of this classical device, supplied by modeling and simulation are shown in figures 11 and 12.

The damper simulation model was validated by experimental test. Some results obtained for a classical damper are presented in the figures 13 and 14. The curves have been obtained by the test bench presented in figure 9. The maximum force sites in the range (-1000 N ... +1000 N) for a velocity of the piston sited in the range (-160 mm/s…+160 mm/s). The input signal was a sine wave with a frequency of 3 Hz.

The test bench was also used for testing a modern magneto-rheological damper (figure 15).

Figure 9. Test bench for testing classical dampers

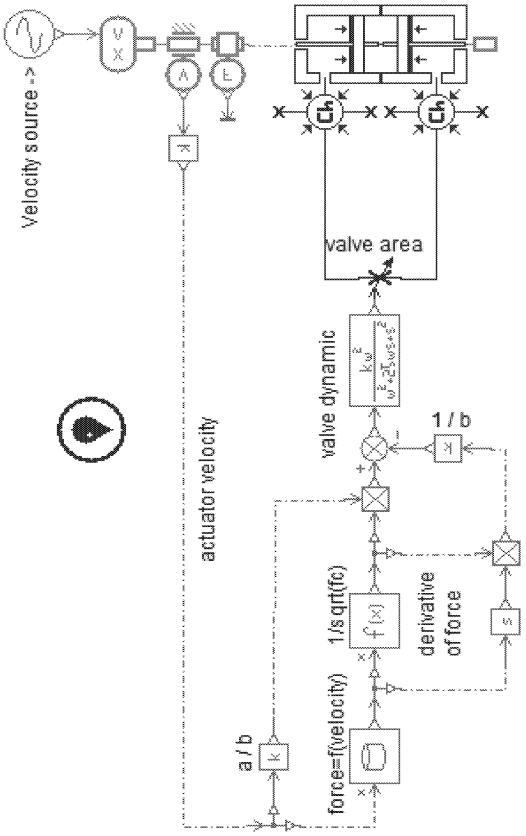

Figure 10. The shock absorber model

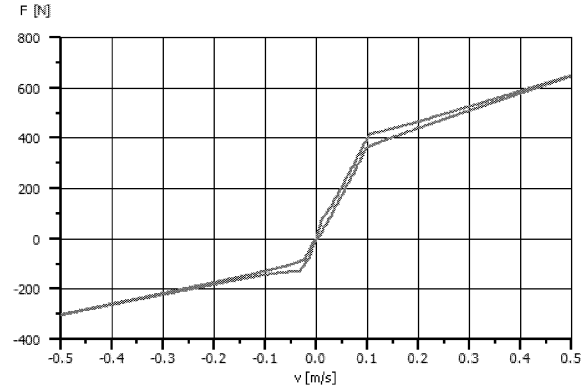

Figure 11. The damping force versus the velocity, for a classical damper (simulation)

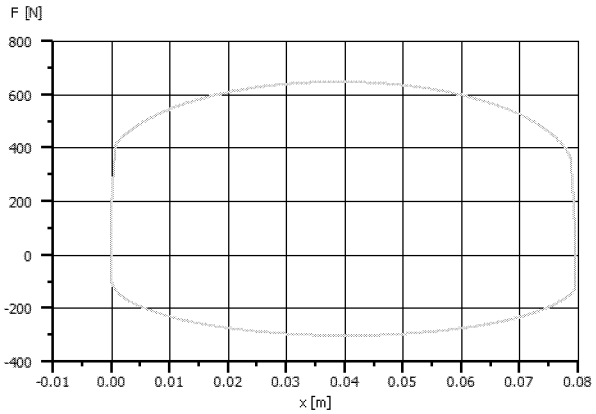

Figure 12. The damping force depending on the rod displacement for a classical damper (simulation)

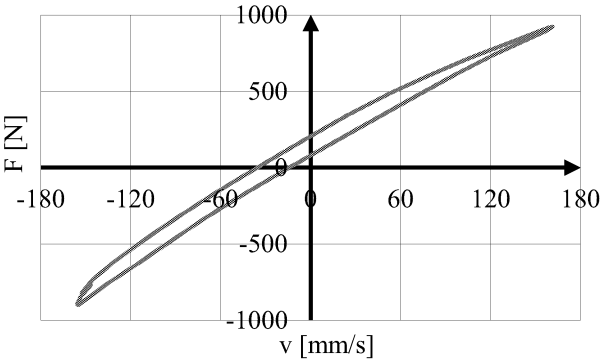

Figure 13. The real damping force depending on the velocity, for a classical damper

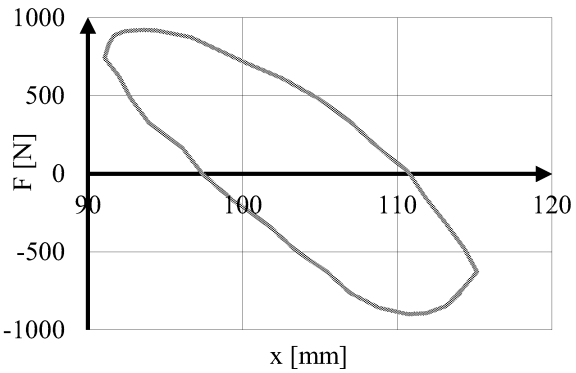

Figure 14. The real damping force depending on the displacement, for a classical damper

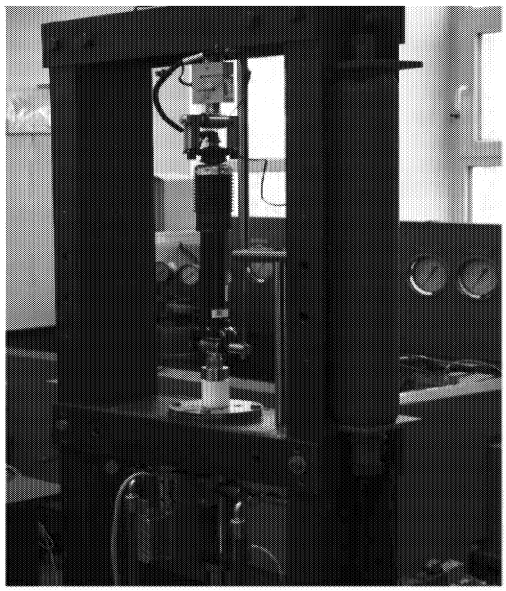

Figure 15. Test bench for testing magneto-rheological dampers (Fluid Power Laboratory of U.P.B)

The graphics from figures 16 and 17 show that the maximum force developed by the magneto-rheological shock absorber for a law current intensity is 1.4 times higher than that of the classical one.

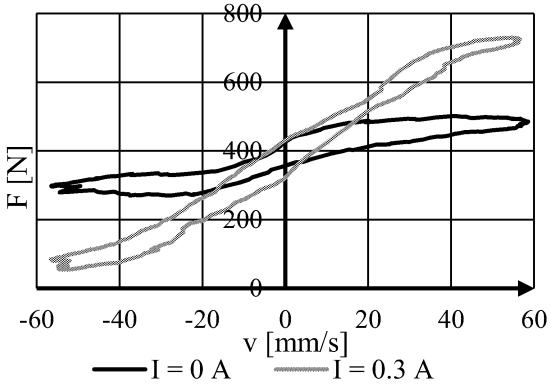

Figure 16. The damping force versus the rod velocity for a magneto-rheological damper

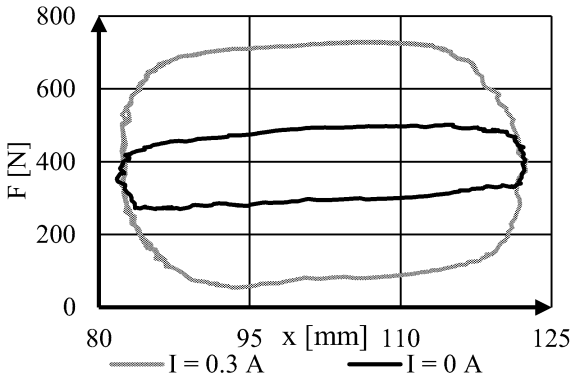

Figure 17. The damping force versus the rod displacement for a magneto-rheological damper

When the control strategy is designed for low frequencies only, the magneto-rheological solution is cheap, involving a velocity transducer speed only. Figure 18 presents the response of such a shock absorber for a linear input signal of 0.3 Hz and a current intensity of 0.5 A.

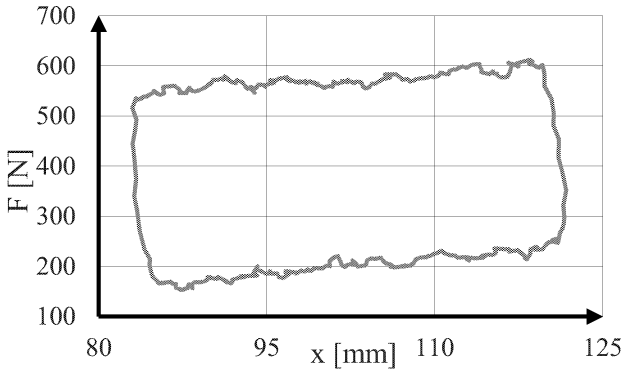

Figure 18. The damping force versus the displacement for a typical magneto-rheological damper

ACKNOWLEDGEMENTS

The authors are grateful for all the technical support received from the LMS COMPANY (now - a member of SIEMENS Group of Companies) in different manners: free licenses, free technical training for the research team members, and many other facilities.

CONCLUSIONS

The modeling and numerical simulation with the AMESim program allow a fast optimization of the constructive and functional parameters of the automotive systems for obtaining the maximum performances. The models simulated with AMESim program can be easily adapted for any type of automotive system due to language many facilities. The modelling and simulation with AMESim became in the last decade the first class instrument of study for engineers, which design, and test the automotive systems.

REFERENCES

Alessandro G., Mauro M., Carla S. and Giampaolo U. 2004. "Design of Predictive Semi-Active Suspension System," Journal of Vehicle System Dynamics, Vol. 41, No. 4, pp. 277-300. doi: 10.1080/00423110412331315169.

Alexandridis A. A. 2000. „MagneRide: Magnetorheological fluid-based semi-active suspension system", in European Conference on Vehicle Electronic Systems. Vehicle Electronic Systems 2000, Stratford-upon-Avon, England.

Choi S-B. and Han Y-M. 2015. „Magnetorheological Fluid Technology - Applications in Vehicle Systems", publishing house CRC Press, ISBN 978-1-4398-5673-4.

Dixon J. C. 2007. „The Shock Absorber Handbook", 2nd edition, John Wiley & Sons Ltd, London, ISBN 978-0-470-51020-9.

El-Demardash S. M. 2002. "Improvement of Trucks Ride Dynamics Using a Hydraulic Semi-Active Suspension System", SAE Paper No 2002-01-3039, SP-1728.

Genta G. and Morello L. 2009." The Automotive Chassis", vol. 1: Components Design, Springer Publishing House. ISBN: 978-1-4020-8674-8.

Gołdasz J. and Sapiński B., 2015 „Insight into Magnetorheological Shock Absorbers", Springer, Publishing House, Swiss, ISBN 978-3-319-13232-7.

Heibing B., Metin E. 2011." Chassis Handbook – Fundamentals, Driving Dynamics, Components, Mechatronics, Perspectives", Vieweg+Teubner, Germany, ISBN: 978-3-8348-0994-0.

Lebrun, M. and Richard, Cl. „How to create Good Models without Writing a Single Line of Code". The Fifth Scandinavian International Conference on Fluid Power at Linköping, Sweden, 1997.

Owen E. Clifton. 2011." Automotive Brake Systems", Fifth Edition, ISBN-13: 978-1-4354-8657-7, Delmar Cengage Learning, Inc., United States.

Tao S., Zhenyu H. and Dayue C. 2005. "Signal Frequency-Based Semi-Active Fuzzy Control for Two-Stage Vibration Isolation System", Journal of Sound and Vibration, Vol. 280, No. 3-5, pp. 965-981.

Vasiliu N. and Vasiliu D. 2005." Fluid Power Systems", Technical Press House, Bucharest.

***LMS. 2013. "Advanced Modeling and Simulation Environment", Release 13 User Manual, Leuven.

BIOGRAPHIES

Alexandru DOBRE graduated in Automotive Engineering from University POLITEHNICA of Bucharest in 2010. He became a Ph.D. in Mechanical Engineering. He is currently assistant in the AUTOMOTIVE ENGINEERING DEPARTMENT from the University POLITEHNICA of Bucharest. He works in the field of modeling, simulation, and experimental identification of the automotive suspensions and transmissions.

Nicolae VASILIU graduated in Hydropower Engineering from University POLITEHNICA of Bucharest in 1969. He became a Ph.D. in Fluid Mechanics after a research stages in Ghent State University and Von Karman Institute from Bruxelles. He became state professor in 1994, leading the ENERGY & ENVIRONMENT RESEARCH CENTRE from the University POLITEHNICA of Bucharest. He managed five years the Innovation Romanian Agency. He worked always for the industry, as project manager or scientific advisor, promoting the numerical simulation as an engineering tool. He is correspondent member of the ACADEMY of TECHNICAL SCIENCES of ROMANIA

Cristian Nicolae ANDREESCU graduated in Automotive Engineering from University POLITEHNICA of Bucharest in 1972. He became a Ph.D. in Internal Combustion Engines. He became professor in 1997, leading the AUTOMOTIVE ENGINEERING DEPARTMENT from the University POLITEHNICA of Bucharest between 2000-2016. He is correspondent member of the ACADEMY of TECHNICAL SCIENCES of ROMANIA.

Driving Simulator Development
Phase III – Defining Basic Vehicle Dynamics by Driving Simulation

Valerian CROITORESCU[1], Cristian ANDREESCU[1]

[1]Scientific Research and Continuous Training Center for Sustainable Automotive Technologies
University POLITEHNICA of Bucharest, 313 Splaiul Independentei st., 6th Sector, 060042, Room JC004, Bucharest, ROMANIA

E-mail: valerian.croitorescu@upb.ro

KEYWORDS
Vehicle dynamics, motion control, driving simulator, hexapod

ABSTRACT

Vehicle dynamics represent a well debated subject with a high level of interest for all vehicle manufacturers. Vehicle dynamics represent the key for the autonomous driving technologies in order to develop the control algorithms for the advance driving assistance systems. Defining vehicle dynamics may be considered a truism, but the necessity for its definition is more than mandatory to be completed by researchers regarding the new approaches in terms of autonomous driving. The driving scenarios and the vehicle behavior can be investigated and defined using a driving simulator, based on a 6 Degrees Of Freedom hexapod.
This paper aims to highlight several studied approaches for defining vehicle dynamics through driving simulation using different scenarios, mechanical modeling as well as the mathematical description and analysis of vehicle motion and virtual reality technologies.

INTRODUCTION

Currently the vehicles are not only a mode of transport, they represent part of the mobility and can be considered a connection hub between humans and different networks. The big challenge for both automotive manufacturers and users is to harmonize the vehicle behavior with the stringent requests, while the connected cars are in the central role. But the connected car is able to operate only if its` dynamic behavior is well set and defined.
The automotive research domains include the driving simulation as an important research phase for investigating human factors on driving as close as possible to reality. Based on these investigations, the driving assistance systems can be defined and developed.
The vehicles dynamics represents one of the main domains for the automotive engineers, for both mechanical and software development that are used on controlling and design.
The vehicle dynamics can be described not only through mathematical models that are able to compute the reality, but also using driving simulators for vehicle motions.
Driving simulators are important in developing experiments because they allow understanding the human response for and during different conditions. The driving simulator is used to investigate how the drivers respond to the continuously upgraded vehicle systems. For example, speaking about the steering advanced assistance system, the approach how the vehicles will achieve the solutions for the lane keeping task is defined using the driving simulator. The same situation is met to define other vehicles` safety systems that works together with vehicle dynamics, using the driving simulator.
The vehicle`s behavior is defined long before production using the driving simulator by implementing the scenarios which are impossible to test on real roads.
This paper aims to highlight the approach on how vehicle dynamics can be defined using the driving simulator and based on that, the approach on how the driving assistance systems are defined.

AIMS AND OBJECTIVES

The driving experience inside a driving simulator is defined as close as possible to reality, taking into account the vehicle`s vertical, lateral and longitudinal dynamics. All these motions are based on accurate human perceptions in order to be able to compare different maneuvers between the driving simulator and the real vehicle.
The virtual reality experienced by driving simulation is able to provide the discrepancies perceived by human controlled systems, demonstrated by the correct perception for the acceleration and speed, distances and drivers` actions.
The driver is able to control the vehicle`s trajectory through the steering wheel, giving different torque values to the steering-wheel that defines the interaction between the vehicle and the road. The steering-wheel torque feedback ensures the vehicle behavior under the drivers` actions, depending on the vehicle speed, road quality and slope.
The aim is to define the vehicle dynamics starting from the vehicle`s motion to the driving simulator`s motion, using a high-fidelity simulator. A high fidelity driving simulator has six degrees of freedom (6 DOF) and it is a motion based driving simulator.
The simulator design consists of an upper platform that is linked to the bottom platform by linear cylinders acting as actuators. The hexapod ground fixed platform is linked by six identical kinematic links to the upper mobile platform. The kinematic links consist of six spherical joints and six universal joints. The joints are located in the ends of the actuators that consist of a screw ball and a rod, working inside a shell (Croitorescu et al, 2015). Three different pairs of joints are linking another pair of two neighboring actuators to the upper platform. The bottom platform integrates other three pairs of different joints, each one for a different pairs of actuators.
The actuators are using defined control corresponding to all the vehicles motions. All the forces and torques acting on the vehicle are being reproduced via the driving simulator actuators. Therefore, the hexapod motions are directly related with the vehicle motion and behavior.
The purpose of the approaches is to perform a parametric definition for all the basic vehicle motions, taking into account the necessities of assisting the driving and optimizing the simulator control systems.
The objectives include the definitions for all the basic vehicle motions made from the driving simulator operation`s perspective.
To obtain an optimal definition of the vehicle dynamics by the driving simulator, significant causes are still being debated while representing major challenges for the dedicated control of the actuators which ensure the upper platform motion. The ability to obtain very close to reality definitions is demonstrated by human

perceptions and by the differences between real and virtual conditions.
Since a dedicated control is needed to operate the driving simulator, the vehicle motions mathematical models are defined using mechanics laws, mathematical equations and physics.

PROBLEM DESCRIPTION AND THE NEED FOR A DRIVING SIMULATION SOLUTION

Driver – Vehicle and Vehicle – Simulator Sensing

Vehicle dynamics performances are provided through user-specific driving behavior as well as through the road and other environment properties. The vehicles performances are in close relationship with the driving behavior, especially when harmful emissions, fuel economy and autonomy are subjects for investigations. All vehicle manufacturers are using the user-specific driving behavior and based on it, through which detailed data can be collected. Even if it is not clear how the user-specific driving behavior defines the performances, the sensing human capabilities allows comparing the results coming from real and virtual vehicle behavior.

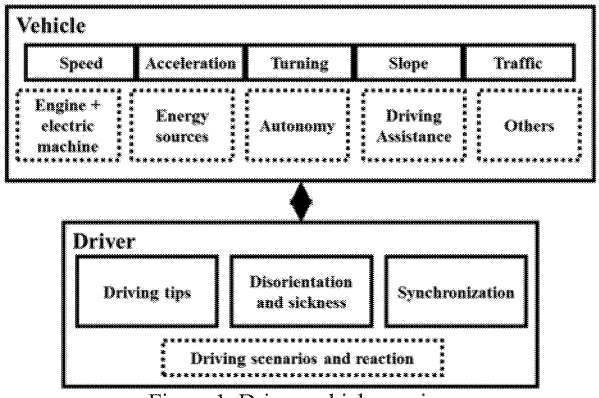

Figure 1: Driver-vehicle sensing

The vehicles dynamics performances correspond to user-specific driving behavior. Based on each driver driving topology, the vehicles dynamics depend on the speed, acceleration, road conditions and environmental properties (figure 1).
The driver may often be disorientated and may show sickness due to that. But, the driver will be able to synchronize his human behavior with the vehicle behavior, while the vehicle behavior may be supported also by the driving assistance systems. The powertrain plays an important role to the entire human reaction, as far as the propulsion system achieves the dynamic performances the driver is requesting. The propulsion system can be conventional, including only the internal combustion engine, or can be hybrid, including beside the internal combustion engine also an electric machine and batteries. The driver reactions may differ according to the vehicle mode of operation during hard acceleration, turning or braking.
Including the traffic influences, the driver will react differently corresponding to the driving scenarios.
The accurate characterization between user-specific driving conditions and vehicle dynamics impacts can be well described by using sensors and dedicated instrumentation: three-axis gyroscope and three axis accelerometer for the roll, pitch and yaw motions (figure 2) defining the raw, pitch and yaw angles (RPY).
To simplify the vehicle dynamics simulation, a single point in space can be used, defined as the center of gravity, having a given mass and a moment of inertia.

Through simulation, the vehicles are illustrated using the parameters that define the motions: angles, distances, speeds, accelerations, forces and torques, all of these being reported to the vehicles components, usually to the wheels and to the vehicle center of gravity.

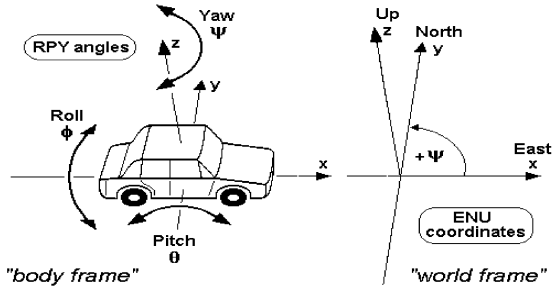

Figure 2: The three axis vehicle motions [***]

The vehicle center of gravity is able to move across three different dimensions in space. The vehicle is moving along all three axis while also rotating around them (figure 2). The rolling is the rotation around the X-axis, being determined by the rotation angle. The pitch is the rotation around the Y-axis. The yaw is the rotation around the Z-axis.

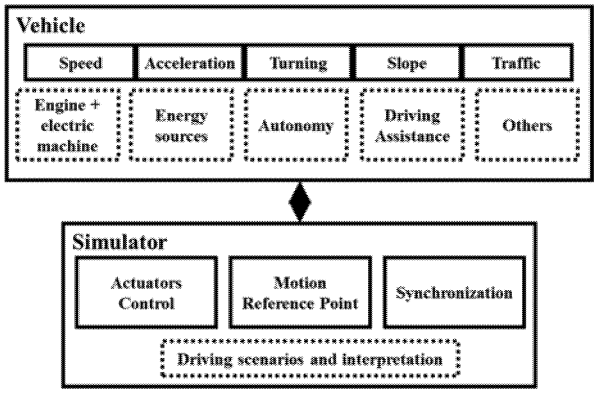

Figure 3: Vehicle-simulator sensing

The vehicle is able to replicate its behavior through simulations, using different scenarios inside a driving simulator or into a virtual reality. The driving simulator motion system is designed to artificially recreate the dynamic cues of both longitudinal (brake and ride) and lateral (cornering and stability) vehicle accelerations. (Tuca et al, 2015-3).
The vehicle-simulator sensing is defined by how the simulator takes action after the vehicle commands. The vehicle behavior is given by the driver, while the simulator itself is controlled by the control algorithm that uses all the drivers' requests. The control algorithm takes into account the actuators operation limits, in terms of response speed, maximum track, and also the spherical joints maximum operation angles.
All the forces, torques and moments of inertia are concentrated inside the vehicle center of gravity. From it, the forces, torques, moment of inertia split to the center of the wheels and from these points to the wheels locations points (WLP = the wheels location points are defined as the intersection of the wheels with the road).
The driving simulator has its own center of gravity, but all the forces, torques etc. are acting in the motion reference point (MRP).
The motion reference point (MRP) denotes the point in space at which the platform translations and rotations are centered (Nahon and Reid, 1990). For the hexapod system, although the location of

the MRP can vary, it is usually located with respect to the geometry of the motion platform. Most commonly, it is defined as the centroid of the two triangles formed at the upper joint rotation points (figure 4).

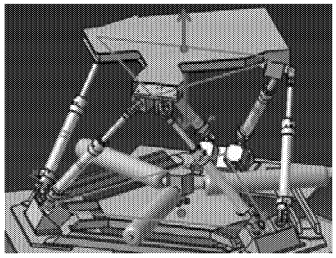

Figure 4: The motion reference point (Tuca et al, 2015-1)

From the MRP, the forces, torques etc. are split to the joints and from them to the actuators.
Installing the vehicle on the upper platform, which is mobile due to the links between the joints and actuators, all the forces, torques etc. that act on the WLPs will act on the MRP, from the MRP to the joints, and from the joints to the actuators rod, making possible the roll, pitch and yaw motions by the longitudinal displacement of the rod. The obtained motion for the entire system is very complex. The motion platform is emulating angular motions also: roll, pitch and yaw.

Basic architecture for driving assistance

All vehicle manufacturers implemented at least one assistance driving system nowadays. The trend they followed is perceived sometimes as a trap for researchers. Even if all the needed sensors are used for offering a safe journey, the intelligent networking of mechatronic systems between vehicles is currently missing on large scale to cover all traffic. The basic architecture for implementing the driving assistance procedures using the driving simulator is presented in figure 5.

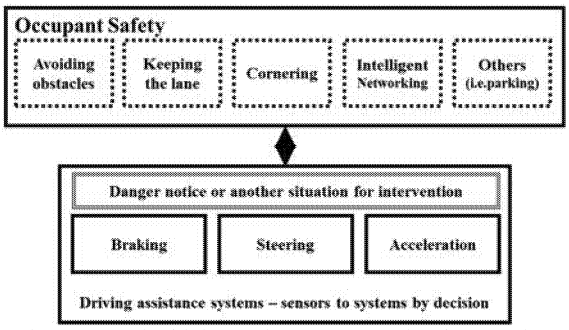

Figure 5: Basic driving assistance system implementation

The vehicle responds to dynamics, defining linear and angular positions, velocities and accelerations.
The control structure can be designed as a parallel structure. It consists of the driving controllers that are designed to calculate the yaw, roll and pitch torques based on the angular position, velocities and accelerations, and the controllers that calculate the wheels slipping. The controllers' outputs are used as input data for the simulator actuators in order to replicate the vehicle behavior (figure 6) being able to introduce the longitudinal motion of the actuators, while the rotation and the lateral motion are realized using also the joints from the upper and from the bottom platforms.

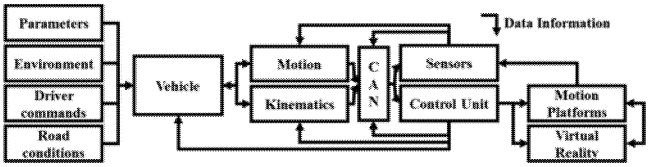

Figure 6: Driving simulator control loops

The simulator is set to achieve the safety that the vehicle has to offer in real driving. While following a defined driving scenario, including obstacles, traffic jams, tight curves etc., the driving assistance systems are intervening using the data received from the sensors. In this case, the sensors are programmed to follow the virtual driving scenarios. The motion platform is running basically on the information received from the control unit and from the virtual reality operation. The closed loop consists of a continuous control setting of the refined behavior of the vehicle.
Removing the vehicle, but keeping all the information from it as necessary input data, makes the motion platform the principal unit for providing accelerations, velocities and position at high fidelity in order to allow the driver to have the perception close to reality. But without the driver, these human factors are read by sensors and the motion platform responses using driving patterns. The motion platform has limited workspace and the accelerations are coordinated smoothly.

BASIC VEHICLE DYNAMICS DEFINITION

Inertia is naturally maintained, in rest or in motion, according to the vehicle states. In order to modify the state, a force has to be applied to the vehicle. The applied forces, including the turning forces, act on the entire vehicle (figure 7). The forces that act along the longitudinal axis are the motive, the aerodynamic drag and the rolling force. The forces that act laterally on the vehicle are the steering force, the centrifugal force when cornering or crosswinds and the tire forces which act laterally. The tires are receiving the longitudinal and lateral forces either downwards or sideways, being transmitted to the road through the chassis, the steering, the engine and transmission, and the braking system.

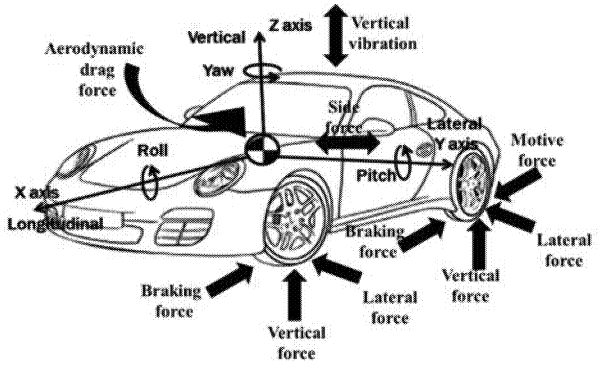

Figure 7: Vehicle`s applied forces according to ISO 8855:2011

Vehicle motion

The vehicle is moving using the Newton and Euler equations of motion, related to the coordination system.
The vehicle fixed coordination system has its origin in the vehicle`s center of gravity being related to the Earth fixed coordination system through the Euler angles. The Euler angles are defined by the sequence of three angular rotations: the yaw rotation around the

Z axis, the pitch rotation around the Y axis, the roll motion around the X axis (figure 7, figure 8).
For better interpretation of vehicle dynamics, the equilibrium conditions should be taken into account for both translational and rotation systems:

$$\sum F_x = m \times a_x \quad (1)$$
$$\sum F_y = m \times a_y \quad (2)$$
$$\sum T_z = I_{zz} \times a_z \quad (3)$$

The Newton equations for motion are expressed for reaching the equilibrium along the X axis and also along the Y axis, and also to rotation around the Z axis (figure 8).

$$F_{x1} \cdot \cos(\delta_{w1}) - F_{y1} \cdot \sin(\delta_{w1}) + F_{x2} \cdot \cos(\delta_{w2}) - F_{y2} \cdot \sin(\delta_{w2}) + F_{x3} \cdot \cos(\delta_{w3}) - F_{y3} \cdot \sin(\delta_{w3}) + F_{x4} \cdot \cos(\delta_{w4}) - F_{y4} \cdot \sin(\delta_{w4}) - F_{drag} - F_{rolling} - F_{slope} = m \cdot a_x \quad (4)$$

$$F_{drag} = \frac{1}{2} \cdot \rho_{air} \cdot c_x \cdot A \cdot v_x^2 \cdot sign(v_x) \quad (5)$$

$$F_{rolling} = f_r \cdot m \cdot g \cdot cos(\varphi_{slope}) \quad (6)$$

$$F_{slope} = m \cdot g \cdot sin(\varphi_{slope}) \quad (7)$$

$$F_{x1} \cdot \sin(\delta_{w1}) + F_{y1} \cdot \cos(\delta_{w1}) + F_{x2} \cdot \sin(\delta_{w2}) + F_{y2} \cdot \cos(\delta_{w2}) + F_{x3} \cdot \sin(\delta_{w3}) + F_{y3} \cdot \cos(\delta_{w3}) + F_{x4} \cdot \sin(\delta_{w4}) + F_{y4} \cdot \cos(\delta_{w4}) + F_{bank} = m \cdot a_y \quad (8)$$

$$F_{bank} = -m \cdot g \cdot \sin(\theta_{road}) \quad (9)$$

$$a_x = \dot{v_x} - v_y \cdot \dot{\psi} \quad (10)$$

$$a_y = \dot{v_y} + v_x \cdot \dot{\psi} \quad (11)$$

$$\left[F_{x1} \cdot \sin(\delta_{w1}) + F_{y1} \cdot \cos(\delta_{w1})\right] \cdot L_1 + \left[F_{x2} \cdot \sin(\delta_{w2}) + F_{y2} \cdot \cos(\delta_{w2})\right] \cdot L_1 - \left[F_{x3} \cdot \sin(\delta_{w3}) + F_{y3} \cdot \cos(\delta_{w3})\right] \cdot L_2 - \left[F_{x4} \cdot \sin(\delta_{w4}) + F_{y4} \cdot \cos(\delta_{w4})\right] \cdot L_2 - \left[F_{x1} \cdot \cos(\delta_{w1}) - F_{y1} \cdot \sin(\delta_{w1})\right] \cdot \frac{t_f}{2} + \left[F_{x2} \cdot \cos(\delta_{w2}) - F_{y2} \cdot \sin(\delta_{w2})\right] \cdot \frac{t_f}{2} - \left[F_{x3} \cdot \cos(\delta_{w3}) - F_{y3} \cdot \sin(\delta_{w3})\right] \cdot \frac{t_r}{2} + \left[F_{x4} \cdot \cos(\delta_{w4}) - F_{y4} \cdot \sin(\delta_{w4})\right] \cdot \frac{t_r}{2} + \sum_1^4 M_{z_i} = I_z \cdot \ddot{\psi} \quad (12)$$

$$\ddot{\psi} = \frac{d\dot{\psi}}{dt} \quad (13)$$

$$\dot{\psi} = \frac{d\psi}{dt} \quad (14)$$

$$F_{ext,x} = \sum_1^4 F_{xi} \quad (15)$$

$$F_{ext,y} = \sum_1^4 F_{yi} \quad (16)$$

where F_{xi} and F_{yi} represent the longitudinal and lateral forces for each of the `i` wheels acting in the tires` centers, $F_{ext,x}$ and $F_{ext,y}$ represent the sum of the forces acting in each WLP on the X-axis and on the Y-axis, translated both to the MRP, δ_{w_i} are the angles between the longitudinal axis and the axis corresponding to each wheel motion direction, the F_{drag} is the aerodynamic drag force, $F_{rolling}$ is the force generated by the tire rolling resistance while moving along longitudinal axis, F_{slope} is the force due to gravity when a road slope is present, F_{bank} is the lateral force due to gravity when a road bank is present, f_r is the rolling resistance coefficient, m is the vehicle mass, g is the gravitational acceleration, ρ_{air} is air density, c_x is the aerodynamic coefficient, A is the transversal vehicle`s area, φ_{slope} is the road slope angle, θ_{road} is the road bank angle, v_x is the longitudinal absolute velocity, v_y is the lateral absolute velocity, $\dot{v_x}$ is the longitudinal absolute acceleration, $\dot{v_y}$ is the lateral absolute acceleration, a_x is the vehicle longitudinal acceleration, a_y is the vehicle`s lateral acceleration, $\ddot{\psi}$ is the yaw acceleration, $\dot{\psi}$ is the yaw rate, $\psi$ is the yaw angle, $M_{zi}$ represents the torque generated by the kingpin offset corresponding to the `i` tire, $I_z$ is the vehicle`s moment of inertia with respect to the Z-axis, $t_{r/f}$ is the rear/front vehicle`s track, $L_{1/2}$ is the distance from the CoG to the front/rear axle, on longitudinal direction.

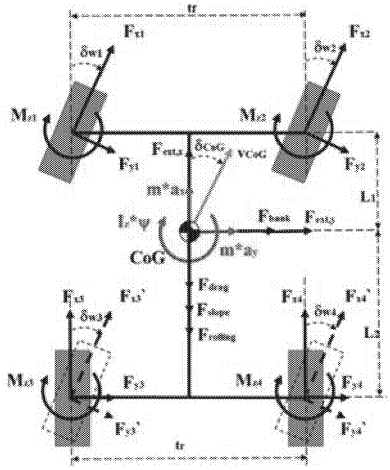

Figure 8: Forces acting on vehicle with respect to the two axis coordination system

The vehicle position is calculated in relation with the Earth fixed coordinate system. The vehicle dynamics include the vehicle representation in terms of spatial integration.

Driving Simulator motion

The driving simulator motion is achieved by the actuators longitudinal motion.
The driving simulator is able to sense the artificial ride and to perform the handling quality. Three different motions are considered: the longitudinal motion, the lateral motion and the vertical motion (figure 9).
The simulator fixed coordination system has the origin in the simulator`s motion reference point, the MRP, being related to the Earth fixed coordination system. All forces and torques coming and going to the vehicle act in the MRP.
The usual motion platform consists of the upper platform and the vehicle on top of it. The currently applied approach is not taking into account either the suspension system or the tires. It takes into account that the upper platform holds the vehicle directly to the

chassis. The approach considers that the wheels are always in contact with the ground, the wheels elastic behavior is not taken into account, the wheels can move neither in vertical direction, since their suspension and the suspension geometry are neglected. When the car is driven up to its limits it has nonlinear behavior, otherwise the car is validated in linear conditions.
The upper platform has three different pairs of spherical joints, each pair has two different joints. The spherical joints has axial rotation, their maximum rotation being constrained by their own design. The ground platform has another three different pairs of spherical joints, each pair has two different joints. Each one by one joint from the upper platform is connected with another one by one joint from the ground platform (figure 9). Each joint has its own center of gravity, J_{CoG}, where the forces and torques that act to the vehicle`s CoG , respectively to the simulator`s MRP, are translated.

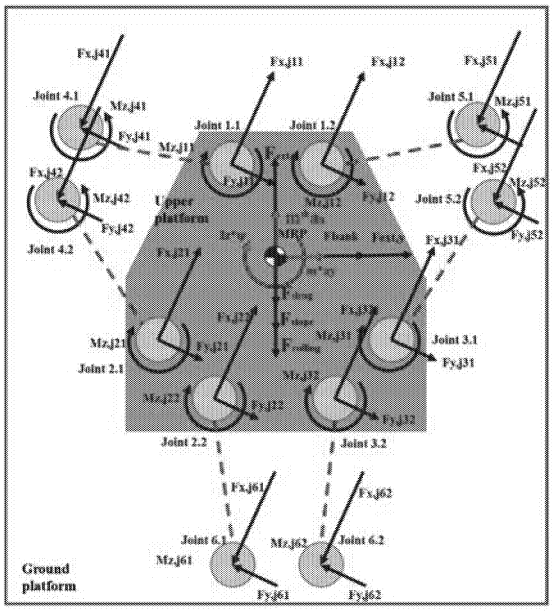

Figure 9: Forces acting on simulator with respect to the two axis coordination system

All the forces that act on the MRP and JCoG are directly computed by the virtual vehicle model while the vehicle is driven following a defined driving cycle. The vehicle virtual model data is used for controlling the simulator, which uses the longitudinal absolute velocity v_x, the lateral absolute velocity v_y, the vehicle longitudinal acceleration a_x, the vehicle lateral acceleration a_y, the yaw rate $\dot{\psi}$. The vehicle dynamics simulation comes from the defined model. The driver role is to control all the vehicle motions and to obtain from the vehicle all the wanted states and the requested behavior, with respect to the requirements and legal issues. The driver is used as a transfer function between the vehicle and the requested behavior, basically including also control and actuating functions coming from the simulator.
Replicating the vehicle motion consists of the simulation technology that uses the classic motion algorithm (Tuca et al, 2015-1). The simulator is replicating the high frequencies corresponding to the translational motions and rotational motions. The motion platform allows operations for all six degrees-of-freedom of the Cartesian inertial frame.
All the motions are related to the rods displacements inside the cylinders that make the actuating operations possible (figure 11).
The simulator motions for all the six degrees of freedom are limited by the joints and actuators design. The maximum permitted joint angles together with the maximum displacement of the rods are able to provide and define the maximum upper platform tilt related to the three axis. But the tilt motion cannot be used for defining the heave motion.

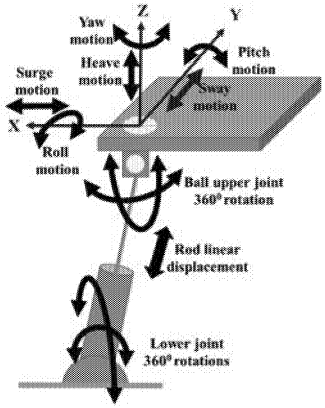

Figure 10: Simplified actuator operation related to the upper platform joint motions

The surge motion consists of the forward and backward translations along the X-axis. The sway motion consists of the sideways translation along the Y-axis. The heave motion consists of the vertical translation along the Z-axis. The pitch motion consists of the tilting rotation around the Y-axis. The roll motion consists of the tilting rotation around the X-axis. The yaw motion consists of the horizontal rotation around the Z-axis.
As no elastic behavior is taking into account and as the suspension system behavior is not taken into account also, the vertical forces that acts on the upper platform joints are neglected (figure 11).

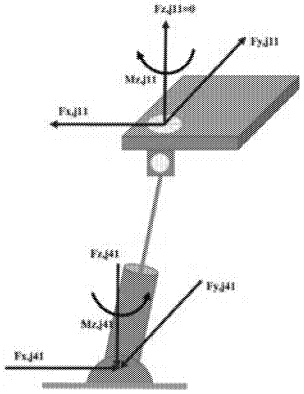

Figure 11: The forces acting on one upper and lower platform joints with respect to the two axis coordination system

The rod available linear displacement is defined by the maximum rotation angle of the spherical joints. The length varies as the upper platform changes the equilibrium position. The force feedback that comes from each actuators depends on the load capacity, being different distributed to each actuator. Therefore, the driving simulator uses a complex function in order to reproduce the vehicle behavior:

$$f_{motion} = f_{motion}(l_j, \tau_j, G_j) \qquad (17)$$

where l_j is the maximum available linear displacement for the `j` actuator, τ_j is the angle that can be obtained between the rod axle and the upper platform geometrical plan, G_j is the load for the `j` actuator.

DISCUSSIONS

Electric actuators are used to enhance vehicles dynamics performances. As a result of the fast response the actuators are able to give under several requests from the driver, the vehicle is following strategies for secure and safe operation between two different destinations while successfully negotiate the traffic and obstacles.

A great impact on vehicles dynamics is the potential of using electric and hybrid electric powertrain. The possibility for moving between two destinations with a reduced environmental footprint represents one of the most fundamental advantages for powertrains. The propulsion system type and its influence on vehicle dynamics are not discussed in this paper, but they represent a further research objective.

Another great impact on vehicle dynamics are the noise, the vibrations and the harshness, being also a major goal for further research.

The vehicle dynamics may suffer from possible driving events and strategies taken by the drivers. The already existing systems that are assisting the human drivers for controlling the vehicle emphasize the vehicle dynamics control as an enforcement for rapid control. The human factors used for motion investigation should be taken from different drivers on both the same tracks and different tracks.

One example regarding this approach consists of the longitudinal motion for a vehicle that is following another vehicle, similar to vehicle platooning. The control closed loop is taking into account the distance between the two consecutive vehicles and is sending the information to the driving assistance systems on the vehicle. The distance should be kept constant and the rolling force should be kept inside quite small range, affecting the longitudinal motion of the vehicle.

The vehicle`s behavior is assimilated in the upper driving simulator platform. Originating from the driver making control inputs from the vehicle cab, each sub-system plays a vital role in forming the perception of the virtual driving environment. While the vehicle accelerates, the upper platform will change its position (front side will go higher, while the back side will go down) and the actuators from the front will be decompressed while the actuators from behind will be compressed.

CONCLUSIONS

Even the most experienced human driver will meet difficulties in negotiating with real driving scenarios, therefore the driving simulator robotics may not achieve the operating perfection, but the viable solutions that are able to offer represent the performances in terms of computing, avoiding obstacles, reaching high intelligence levels.

In order to define the vehicle dynamics from a new perspective, without using any vehicle, the driving simulator's behavior is offering to understand and to learn how all the key sub-systems of the driving simulators are working and the importance of each of them, the static limits for the motion platform, the actuating cylinder and joints operation boundaries, how to simulate different moving scenarios starting from a sketch.

The understanding of the vehicle dynamics using only the driving simulator is very useful from small to large scales laboratory work and teaching,. The advantages consist also of learning how to set up and how to implement the instrumentation, how to understand the mathematical modeling and where the reference sensors positions for better investigation are chosen, being also needed for testing.

In addition, based on how to define vehicle dynamics and on the basic understanding of the driving simulator's behavior, the dedicated control algorithms and the motion platform kinematics can be optimized.

REFERENCES

Chang, A., (2015), *Basic Dynamics of Ground Vehicles*, National Instruments White Paper, December 2015

Croitorescu, V., Tudorache, Gh., Stamin, Ş., Jiga, G. (2015), Screw Ball Actuator Stress Behavior, *Applied Mechanics and Materials* Vols. 809-810 (2015) pp 616-621, Trans Tech Publications, Switzerland, DOI:10.4028/www.scientific.net/AMM.809-810.616, Proceedings of Innovative Manufacturing Engineering International Conference – IManE 2015, Iaşi, Romania

Gietelink O., Ploeg J., De Schutter B., Verhaegen M., (2006), Development of advanced driver assistance systems with vehicle hardware-in-the-loop simulations, *Vehicle System Dynamics*, vol. 44, no. 7, pp. 569–590

Gómez Fernández, J., (2012), A Vehicle Dynamics Model for Driving Simulators, Master's Thesis 2012:26, ISSN 1652-8557 Department of Applied Mechanics, Division of Vehicle Engineering and Autonomous Systems, Vehicle Dynamics, Chalmers University of Technology, SE-412 96, Göteborg Sweden

Mohajer N., Abdi H., Nelson K., Nahavandi S., (2015) Vehicle motion simulators, a key step towards road vehicle dynamics improvement, *Vehicle System Dynamics: International Journal of Vehicle Mechanics and Mobility*, 53:8, 1204-1226, DOI: 10.1080/00423114.2015.1039551

Nahon, M. A., Reid, L. D. (1990), Simulator Motion-Drive Algorithms: A designer's perspective, *AIAA Journal of Guidance, Control and Dynamics*, 13(2), pp. 356-362, 1990

Nordmark, S., Lidström, M., (1984) Moving base driving simulator with wide angle visual system, S*AE Technical Paper Series 845100", Society of Automotive Engineers*, Warrendale, PA, USA, 1984

Obialero, E., (2013), A Refined Vehicle Dynamic Model for Driving, Master's Thesis 2013:10, ISSN 1652-8557, Department of Applied Mechanics, Division of Vehicle Engineering and Autonomous Systems, Vehicle Dynamics, Chalmers University of Technology, SE-412 96 Göteborg, Sweden

Reif, K., (2014), Brakes, Brake Control and Driver Assistance Systems Function, Regulation and Components, Bosch Professional Automotive Information VIII, Ed. Springer, ISBN 978-3-658-03977-6

Reymond, G., Heidet, A., Canry, M., KEmeny, A., (2000) *Validation of Renault`s dynamic simulator for Adaptive Cruise Control experiments*, Proceedings of the Driving Simulation Conference DSC'2000, pages 181–192, Paris, France, September 6–8, 2000

Tucă, A., Croitorescu, V., Brandmeier, T., (2015) *Driving Simulator Development: Phase I – From State of Art to State of Work*, Proceedings of Industrial Simulation Conference, Universidad Politecnica de Valencia, Spain

Tucă, A., Croitorescu, V., Brandmeier, T., (2015), *Driving Simulator Development Phase II – Building and Controlling Scenarios through the Motion Algorithm*, Proceeding of European Simulation and Modelling Conference, UK

Tucă, A., Croitorescu, V., Oprean, M., Brandmeier, T., (2015) *Driving Simulators for Human Vehicle Interaction Design*, Proceedings of the IETEC-BRCEBE Conference, Sibiu, Romania

***, ISO 8855:2011, "*Road vehicles -- Vehicle dynamics and road-holding ability*"

BIOGRAPHY

VALERIAN CROITORESCU received his Doctoral degree in Automotive Engineering in 2012 at University POLITEHNICA of Bucharest, concerning Hybrid Electric Vehicles Development. A part of his Ph.D. thesis has been accomplished during international research stages at LMS International. He earned his Automotive Engineer Degree in 2007, as valedictorian. He prepared the diploma project in France, inside Ecole Nationale D`Ingenieurs De Tarbes. He also attended two master of sciences programs, at University POLITEHNICA of Bucharest: `Efficiency and Security in Automotive Engineering` and `Environmental Management`. His main fields of interest are powertrain and alternative powertrain (hybrid, electric) design and development, vehicle dynamics, modeling and simulation of engineering systems, real-time simulation, automotive driving behavior and driving simulation. His strong involvement in international cooperation activities and his academic records include numerous awards and certifications. From September 2007 Valerian joined the academic stuff of Automotive Engineering Department. From 2013, he is Founder and Executive Director of the Scientific Research and Continuous Training Center for Sustainable Automotive Technologies (SRCTCSAT), organized in 2013 inside University POLITEHNICA of Bucharest

ENGINEERING SIMULATION

A DIRECT METHOD FOR THE RE-ENGINEERING BY SIMULATION OF RADIAL OR MIXED FLOW IMPELLERS

Sanda Budea
Adrian Ciocanea
Ionuț Șișman
Department of Hydraulics, Hydraulic Machines and Environmental Engineering
Power Engineering Faculty, University "Politehnica" of Bucharest,
313 Spl. Independentei, 060042, Bucharest, Romania
Email: sanda.budea@upb.ro, adrian.ciocanea@upb.ro

KEYWORDS
Re-engineering, pump impeller, simulation, NPSHr, hydraulic efficiency.

ABSTRACT

The paper presents a direct method for the re-engineering of radial or mixed flow impellers of centrifugal pumps. Starting from an existing radial impeller, a rapid simulation algorithm is performed. The existing and new data were compared and geometry modification was observed according to blade inlet angle. The most appropriate value for inlet blade angle was selected, by considering simultaneous the efficiency and Net Positive Suction Head required ($NPSH_r$) criteria. In order to validate the simulations a rapid prototyping technology was used for impeller manufacturing and tests were performed for the most appropriate impeller. A good agreement between simulated and experimental data has been achieved. By using the proposed method one obtain either an impeller with good hydraulic efficiency, or with a low $NPSH_r$, designed by a rapid and practical procedure.

INTRODUCTION

In pump simulation, the key issues are the turbulence prediction and cavitation initiation which in practical terms is referring to hydraulic efficiency and required $NPSH_r$. Some studies based on turbulent flow and cavitation models throughout the pump/impeller are known, either theoretically based, by using simulation tools followed by experimental validation (Miyauchi et al. 2006; Li et al. 2013; Visser et al. 2000; Sedlá et al. 2015; Luo et al. 2008) or experimentally based and used for calibration of the theoretical models (Ladouani and Nemdili 2009; Liu et al. 2014; Misiewicz and Skrzypacz 2011; Luo et al. 2008; Mittag 2015).

Even CFD tools are based on relatively accurate models for turbulent flow (e.g. standard k-ε and RNG are the widely adopted) and cavitation (e.g. Rayleigh-Plesset equation applied to describe the vapor phase change) still results deviate from experiment mostly due to the difficulty to select empirical coefficients.
The paper presents a rapid iterative algorithm for the re-engineering of radial or mixed flow impellers. Using dedicated software, simulations are performed in order to optimize performance of $NPSH_r$ and the hydraulic efficiency of a centrifugal pump impeller starting from an existing one. The simulation software provides 3D cylindrical coordinates (R,θ,Z) for the impeller geometry and estimates the impeller performance of $NPSH_r$ and global efficiency.

In the first stage, semi empirical Pfleiderer method has been applied to define the blade shape with double curvature. Also $NPSH_r$ and hydraulic efficiency of the impeller were computed. In the second stage, the most appropriate blade inlet angle was selected and influence on the $NPSH_r$ and hydraulic losses have been evaluated. A new impeller was manufactured and tested obtaining a good approximation between theoretical and experimental data. By using the proposed method, one obtain either an impeller with good hydraulic efficiency, or with a low $NPSH_r$ (see case study), designed by a rapid and practical procedure.

IMPELLER MODEL AND SIMULATION

The algorithm used for deriving the simulation software is consisting both of basic formulas and original contributions reported in literature. Therefore, in order to establish the main dimensions of the radial impeller there were used some equations (Stepanoff 1993; Stepanoff 1963; Pfleiderer 1932; Karassik et al. 2001; Rutter 1965) processed by the authors:

$$\begin{gathered} D_1 = f(n_s, D_h, D_2) \\ D_2 = 2\left(\frac{n_s}{2.463} + 192.89\right)^2 \frac{\sqrt{H}}{n} \\ \Delta z = (D_{2B} - D_0)\left(\frac{n_s}{74}\right)^{1.07} + \frac{b_2}{2\cos\gamma} \\ b_1 = \Delta z_{max} - f(r_0) \end{gathered} \quad (1)$$

$$b_2 = \frac{\tau_2 Q}{c_{m2}\pi D_2}$$

where: H – discharge head (m); Q – fluid flow (m^3/h); n – impeller rotational velocity; n_s – specific speed; β_1 – blade inlet/suction angle; β_2 – blade outlet/discharge angle; b_1 – inlet width of impeller; b_2 – outlet width of impeller; D_0 – inlet impeller diameter; D_1 – inlet blade diameter; D_2 – outlet impeller diameter (these diameters have indices A, B or C for medium streamline, front disc and back disc streamline); D_h – hub impeller diameter; z – number of the blades; Δz - blade width in meridian plane (maximal value is Δz_{max}); η – overall efficiency of the impeller; η_h – hydraulic efficiency; η_m – mechanical efficiency; η_v – volumetric efficiency; γ - angle between the back disc and horizontal plane, r_c – radius of curvature for the back disc. In figure 1 is presented the impeller geometry in meridian plane.

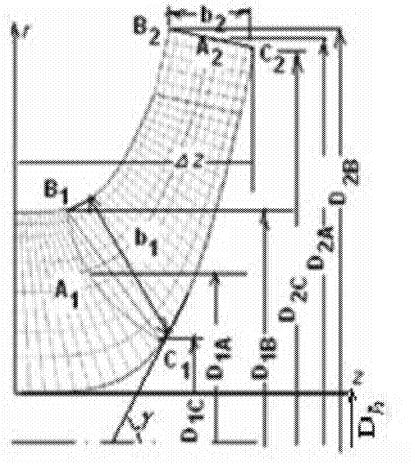

Figure 1: Geometry and streamlines of the impeller (Budea and Varzaru 2012)

By using the semi empirical relation provided by Pfleiderer (Pfleiderer 1932) and introducing the corrective coefficients C_p, the streamlines were derived, based the hypothesis of the constant hydraulic torque:

$$\psi = (0.55 \div 0.68) + 0.6 sin\beta_2$$
$$C_p = 2\frac{\psi}{z}\frac{1}{1-\left(\frac{D_1}{D_2}\right)^2} \quad (2)$$

where: ψ - pressure coefficient.

The simulation software provides 3D cylindrical coordinates for meridian plane and also for parallel plane. Details regarding this application are presented in Budea and Varzaru 2012.

In order to predict the pump efficiency an original relation is proposed (Budea 2006, Budea and Ciocanea 2008, Budea and Varzaru 2012) - similar with the formulas provided by Anderson (Anderson 1980) and Stepanoff (Stepanoff 1993, Stepanoff 1963), which has been experimentally validated by a rumanian pump manufacturer – "Aversa S.A":

$$\eta = f(n_s, Q), \quad \eta = \eta_h \eta_v \eta_m$$
$$\eta = \left[\left(1 + \frac{10.87}{n_s^{\frac{5}{3}}}\right)^{-1} - \frac{1}{1.81 Q^{0.25}}\right]^{1.1} \quad (3)$$

In order to compute the hydraulic efficiency of the impeller, the losses through the impeller passages (L_{imp}) were considered (Karassik et al. 2001):

$$\eta_h = 1 - \frac{L_{imp}}{H}$$
$$L_{imp} = k\frac{w_1^2}{2} + f\frac{\overline{w}^2}{2}\frac{l}{D_h}$$
$$D_{hy} = \frac{2 b_a t}{t + b_a} \quad (4)$$

where: D_{hy} – passage hydraulic diameter; l – passage length; f – pipe type friction factor; k – incidence loss coefficient; $\overline{w}^2$ - the average square of the relative velocity; w_1 – inlet relative velocity; b_a - the average width of the blade; t - step between blades. The method is validated using data provided by Stepanoff (Stepanoff 1993) - figure 2:

$$n_s = \frac{n\sqrt{Q}}{H^{0.75}}, \quad n_{sf} = 3.65 n_s.$$

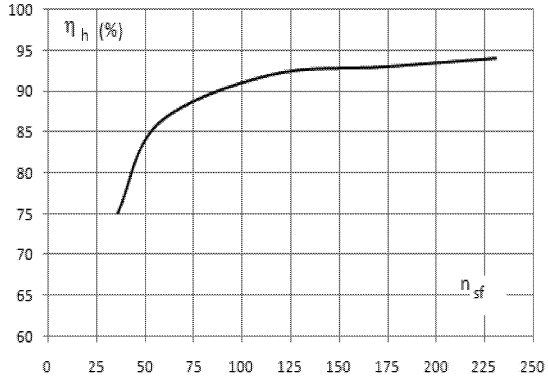

Figure 2: Hydraulic efficiency depending on the fluid specific speed

$NPSH_r$ was computed by using formulas where inlet angle β_1 and suction specific speed n_{ss}, are related:

$$n_{ss} = \frac{n\sqrt{Q}}{NPSH^{0.75}}$$
$$NPSH = \left(\frac{n\sqrt{Q}}{4520} tg(\beta_1)\right)^{\frac{4}{3}} \quad (5)$$

By applying a numerical iterative algorithm considering the flow continuity equation and the hypothesis of constant hydraulic torque, blade shape with double curvature was obtained. Also, using the proposed relations it have been computed both hydraulic efficiency and $NPSH_r$ for considered impellers, if inlet angles β_1 with various values are adopted.

Simulations were performed, considering an existing impeller in order to obtaining appropriate performance for hydraulic efficiency and $NPSH_r$. The parameters for the centrifugal pump were: flow rate Q = 75 m^3/h, total head H = 52 m and rotational velocity n = 2960 rpm. The dimensions of the existing closed impeller type were: impeller diameter D_2 = 200 mm; blade width at exit b_2 = 12

mm; blade angle at inlet β_1 = 15°; blade angle at outlet β_2 = 30°; hub diameter D_h = 60 mm; number of blades z =8; blade width s = 3 mm; the curve radius for the back disc r_c = 25 mm.

RESULTS

Considering the performances of the existing pump (e.g. for best efficiency point –BEP, η = 0.62 and $NPSH_r$ = 5.5 m, as presented in figure 4) simulations were performed in order to assess the influence of the inlet angle on the overall efficiency and $NPSH_r$. The results are presented in Table 1.

Table 1: Simulation results

β_1 (^{0})	Z (-)	η_h (-)	NPSHr (m)	η (-)	$\Delta NPSH$ (-)
10	5	0.686	1.50	0.574	0.85
13	5	0.780	2.15	0.653	0.79
14	6	0.795	2.35	0.665	0.77
15	6	0.800	2.58	0.677	0.75
16	**6**	**0.821**	**2.87**	**0.687**	**0.72**
17	**7**	**0.861**	**3.05**	**0.720**	**0.70**
18	7	0.863	3.49	0.722	0.66
19	7	0.866	3.72	0.724	0.63
20	8	0.871	3.93	0.726	0.61
22	8	0.877	4.52	0.734	0.56

The pump efficiency was computed for a mechanical efficiency η_m = 0.94 and a volumetric efficiency η_v = 0.89 respectively.

According to the simulation results when the same number of blades z =8 is selected, the new impeller has the overall efficiency η =0.73 at BEP and $NPSH_r$ = 3.93 m. Still, these values are not the most appropriate ones if both efficiency and $NPSH_r$ are considered in the same time. For such a comparison a constant value was defined in order to take into account the atmospheric pressure:

$$\Delta NPSH = \frac{10.33 - NPSHr}{10.33} \quad (6)$$

In figure 3 is presented both variation of η (β_1) and Δ $NPSH_r$ (β_1), resulting the most appropriate inlet angle between $\beta_1 = 16^0$-17^0.

This result is in line with the data in Table 1 where for β_1 =17^0 the efficiency η = 0.72 (0.6% lower comparing with the case where β_1 =20^0) and $NPSH_r$ = 3.05 m (about 0.9 m lower comparing with the same case). The new impeller has z = 7 blades which explain the better performances, see figure 4. An interesting result is related to the sudden efficiency increasing (3.3%), from β_1 =16^0 to β_1 =17^0 followed by lower gradient values for higher inlet angles (0.2%). Figure 4 shows the efficiency and $NPSH_r$ performance for the old impeller compared with the proposed impeller, new geometry with β_1 =17^0.

In figure 5 is presented the modification of the leading edge of the impeller. It can be observed that for the lower inlet angle the leding edge is more vertical (line3) oriented hence

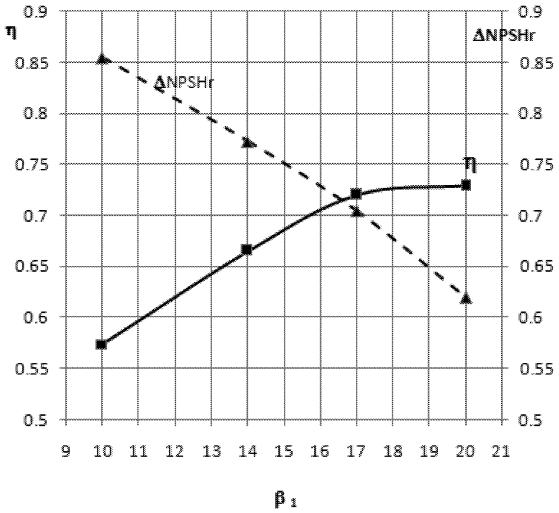

Figure 3: Appropriate inlet angles for BEP and low *NPSHr*

better cavitation performances will be obtained for the pump – based on conclusions reported in literature (Luo et al. 2008; Anton 1985; Schöneberger 1966). This result is confirmed by lower *NPSHr* values obtained during simulation at smaller inlet angles.

The better performance for $NPSH_r$ and the improved efficiency as a result of re-engineering the impeller were experimental validated for the case β_1 =17^0. An impeller was manufactured by using a rapid prototyping technology (using 3D printer), see figure 6, and tested (figure 4).

The values obtained for the overall efficiency in BEP was η = 0.71 and accordingly $NPSH_r$ = 4.2 m. The reduced gap between simulation and experimental results allow positive conclusions concerning the accuracy of the theoretical model used for re-engineering radial and mixed flow impellers.

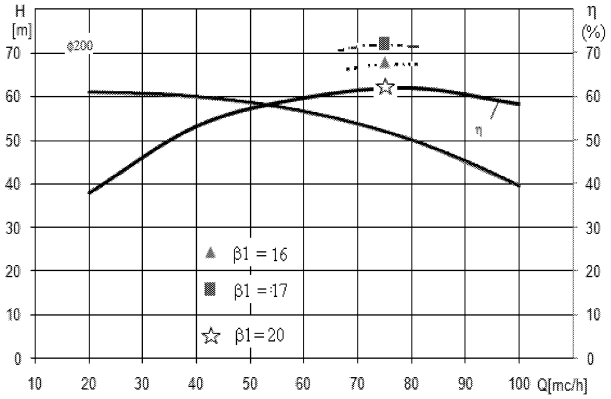

(a)

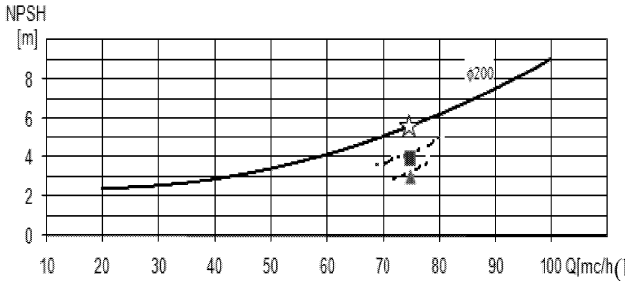

(b)

Figure 4: The efficiency of the impeller at BEP (a) and *NPSHr* (b) for the old impeller (β_1 =20^0 and η = 0.62) and proposed impeller (β_1 =17^0, η = 0.72 and *NPSHr* = 3.05m)

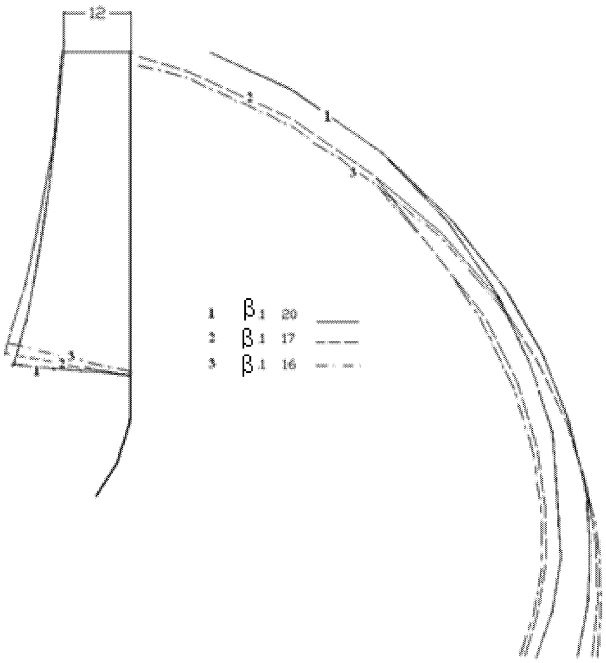

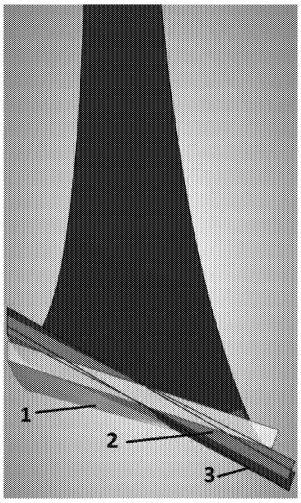

Figure 5: The leading edge of the new impeller for $\beta_1 = 20^0$ - 1 ; $\beta_1 = 17^0$ - 2; $\beta_1 = 16^0$ -3

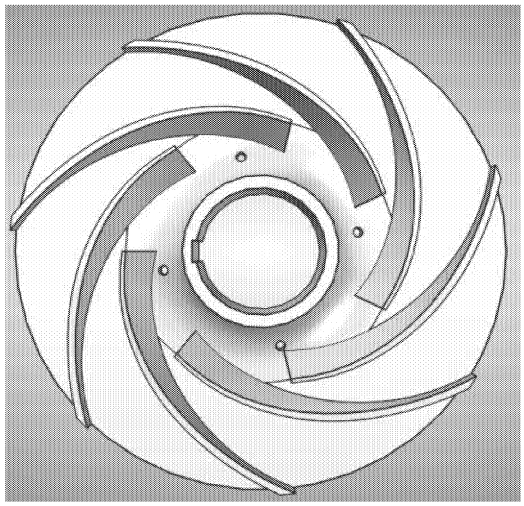

a) new design of the impeller

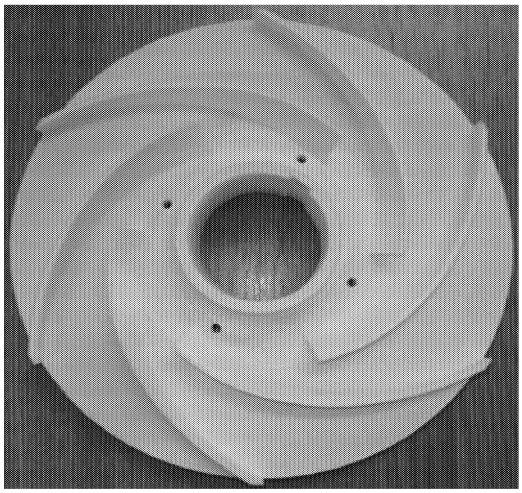

b) 3D printed impeller

Figure 6: The impeller without the shroud disc, with the new geometry

CONCLUSIONS

A simulation software was proposed, for the re-engineering of radial and mixed flow impellers. As a case study, an existing impeller was considered and simulated providing a new geometry as the result of modifying the inlet blade angle. The new impeller has better efficiency and $NPSH_r$ for the same number of blades. In order to identify the most appropriate impeller, considering both efficiency and $NPSH_r$ as simultaneous criteria, a constant $\Delta NPSH_r$ was defined. A geometrical method was used in order to obtaining the optimum value for the inlet angle. The optimum value obtained was $\beta_1 = 17°$ for the inlet angle. For the new geometry it has been observed that, a more vertical direction of the leading edge corresponds for a low $NPSH_r$, which is confirmed by some studies. Hence, the simulation results could be considered in good agreement with experimental research. The performances for the new impeller were experimentally validated.

A rapid prototyping technology was used for impeller manufacturing. Values for BEP and $NPSH_r$ were close to simulated values. By using the proposed method one obtain either an impeller with good hydraulic efficiency, or with a low $NPSH_r$, designed by a rapid and practical procedure.

ACKNOWLEDGEMENT

This research was supported under UEFISCDI contract no.75/2014 – "IPOIDEN" - Hybrid installation for water purification by reverse osmosis.

REFERENCES

Anderson, H., 1980, "Prediction of head, quantity and efficiency in Pumps - The area Ratio Principle, Performance Prediction of Centrifugal Pumps and Compressors", *ASME Symp., New York*, vol. I00127, 201-211.

Anton, I, "Cavitatia", 1985, vol. II, Ed. Academiei.

Budea, S., 2006, "Guide for centrifugal pumps design", Ed. Printech, Bucuresti,.

Budea, S. and A. Ciocanea, 2008, "The influence of the suction vortex over the NPSH available of centrifugal pumps", 5-th National Conference of the Romanian Hydropower Engineers, Univ. Politehnica of Bucharest *Scientific Bulletin*, Series D: Mechanical Engineering no. 4/2008 vol. 70, 157-166.

Budea, S. and D. Varzaru, 2012, " The influence of the inlet angle over the impeller geometry. Approach with ANSYS", *JESR vol 18, no. 4, JESR201204V18S01A0004 [0003709], 32-39.*

Karassik, I.J.; J.P. Messina; P. Cooper; C.C. Heald, 2001, "Pumps Handbook", Third Edition, MC Graw – Hill, Ney York, 2.15-2.48.

Ladouani, A. and A. Nemdili, 2009, "Influence of Reynolds number on net positive suction head of centrifugal pumps in relation to disc friction losses", *Forsch Ingenieurwes No.73: 173–182.*

Li ,P. ; Y. F. Huang; J. Li, 2013, "Cavitation simulation and NPSH prediction of a double suction centrifugal pump", *IOP Conference Series-Earth and Environmental Science*, Volume: 15, Article Number: 062025.

Liu, H.; J. Wang; Y. Wang; H. Zhang; H. Huang, 2014, "Influence of the empirical coefficients of cavitation model on predicting cavitating flow in the centrifugal pump", *Int. J. Nav. Archit. Ocean Eng.* (2014) 6:119~131 http://dx.doi.org/10.2478/IJNAOE-2013-0167 pISSN: 2092-6782, eISSN: 2092-6790.

Luo, X; Y. Zhang; J. Peng; H. Xu; W. Yu, 2008, "Impeller inlet geometry effect on performance improvement for centrifugal pumps", *Journal of Mechanical Science and Technology* No. 22, 1971~1976.

Luo, X.; S. Liu; Y. Zhang; H. Xu, 2008, "Cavitation in semi-open centrifugal impellers for a miniature Pump", *Front. Energy Power Eng. China* No. 2(1): 31–35, DOI 10.1007/s11708-008-0011-8.

Misiewicz, A. and J. Skrzypacz, 2011, "Cavitation behaviours of low specyfic speed pump impellers designed according to the „tight inlet" rule", in *Cent. Eur. J. Eng.* 1(2), 195-201, DOI: 10.2478/s13531-011-0019-4.

Mittag, S. and M. Gabi, 2015, "Experimental and Numerical Investigation of Centrifugal Pumps with Asymmetric Inflow Conditions", *Journal of Thermal Science* Vol.24, No.6 516-525.

Miyauchi, S; N. Kasai; J. Fukutomi, 2006, "Optimization of meridional shape design of pump impeller" In: *23rd IAHR symposium on hydraulic machinery and systems,* Yokohama, Japan. Paper F310.

Pfleiderer, C., 1932, "Die kreiselpumpen", Spriger, Berlin.

Rutter, D.K., 1965, "Pompy wirowe", Warszawa, p.122-164.

Schöneberger, W, 1966, "Untersuchungen über Kavitation an radialen Kreiselpumpenrädern", Diss. Dr. Ing. Tech. Hoch. Darmstadt,.

Sedlá, M; J. Šoukal; T. Krátký; M. Vyroubal, 2015, "Numerical Prediction of Impacts of Cavitation in Pumps for Power Generation", ISSN 0040_6015, *Thermal Engineering*, 2015, Vol. 62, No. 6, 408–413. © Pleiades Publishing, Inc.

Stepanoff, A.J., 1993, "Centrifugal and axial flow pumps. Theory, Design and Application", Krieger Publishing Company Malabar, Florida.

Stepanoff, A.J., 1963, "Centrifugal pump performance as a function of specific speed", *Trans. ASME, New York, vol.65.*

Visser, F.C.; R.J.C Dijkers; J.G.H Woerd, 2000, "Numerical flow-field analysis and design optimization of a high-energy first-stage centrifugal pump impeller", *Comput Visual Sci* No. 3, 103–108.

BIOGRAPHIES

SANDA BUDEA graduated in mechanical engineering from University POLITEHNICA of Bucharest in 1984. In 1999 she became Ph.D. in the field of the Hydraulics and Fluids Mechanics. She is currently lecturer at Hydraulics, Hydraulic Machines and Environmental Engineering Department from University POLITEHNICA of Bucharest. She works in the fields of hydraulic machines and renewable sources of energies - design, modeling, simulation and experimental research and also in renewable energy.

ADRIAN CIOCĂNEA is a professor at University Politehnica of Bucharest. He attended the University POLITEHNICA of Bucharest where he studied mechanical engineering, obtaining his bachelor degree in 1985. He obtained his PhD in 1998 in the field of applied fluid mechanics (fluid-structure interaction). His main fields of interest are related to numerical integration of Navier-Stokes equations, turbomachinery, hydro-aerodynamics and renewable sources of energy.

Simulation of the Overlap Influence on the Flow Control Valves Performances

Ina COSTIN, Constantin CALINOIU, Daniela VASILIU, Nicolae VASILIU
University POLITEHNICA of Bucharest
313, Splaiul Independentei, Sector 6
RO 060042 Bucharest, Romania
E-mail: vasiliu@fluid-power.pub.ro

KEYWORDS
Numerical simulation, hydraulic flow control valves, hydraulic overlap, steady state and dynamic performances

ABSTRACT
The paper presents the results of the theoretical reseach carried out on the overlap influence on the steady-state and dynamic performances of the electrohydraulic flow control valves. The valve behavior around the nul point has a esential influence on the accuracy, and stability of the electrohydraulic servo systems. A lot of peculiarities of the operation conditions have to be taken in account, like the environmental temperature variation, the power lost by internal leakages etc. The modern mechatronics systems development needs a large amount of numerical simulations in order to find out the best structure for specified performances. AMESIM language, called now LMS Imagine.Lab™Amesim, includes a realistic hydraulic components library which can be used to point out with high accuracy the influence of different kind of parameters on the electrohydraulic components and systems performances. The results of the simulation are validated by the author's experiments carried out on different type of servovalves tested in standard conditions.

INTRODUCTION

The modern electrohydraulic servo valves are hybrid equipments used for controlling the flow sent by the pressure supply systems to the hydraulic motors included in position (angle) or force (torque) servo systems. The industrial requirements of the CIM led to the replace of the classical two stages flapper-nozzle servovalves by direct drive servovalves (DDV). This ones keep the flow control valve geometry, but the spool is directly actuated by a linear electromechanical convertor which uses one of the following three principle: moving coil (fig. 1), a solenoids (fig. 2), and a linear force motor (fig.3). The accuracy of the flow control strongly depends on the resolution of the position transducer attached by the spool. Another important feature concerning the dynamic performance is the maximum force supplied by the electromechanical actuator. The mobile equipment, the position trnsducer, the electromechanical actuator and the controller are in fact the components of a position loop.The controller of this loop supply the input signl for the internal position loop according the needs of the governed process. The overal static and dynamic performances of a servovalve depend on the performances of all the components. The main feature of these electrohydraulic converters is the behavior around the null point. This one strongly depends on the „hydraulic overlap". The relation between the valve spool displacement, x, and the flow sent to the hydraulic motor,

$$Q=f(x, d_s, \Delta p, \delta, j) \qquad (1)$$

includes the spool diameter d_s , hydraulic overlap δ, the pressure drop on the valve Δp, and j - average radial clearance between the spool and the sleeve (bushing).

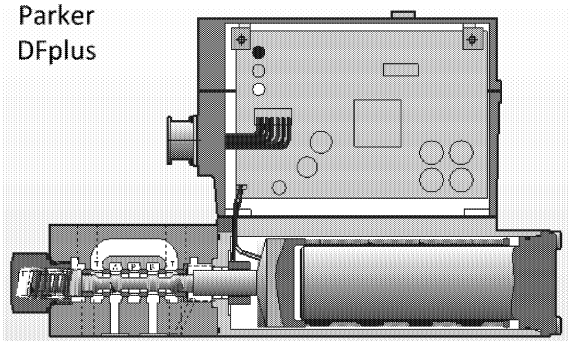

Figure 1. High speed industrial moving coil servo valve

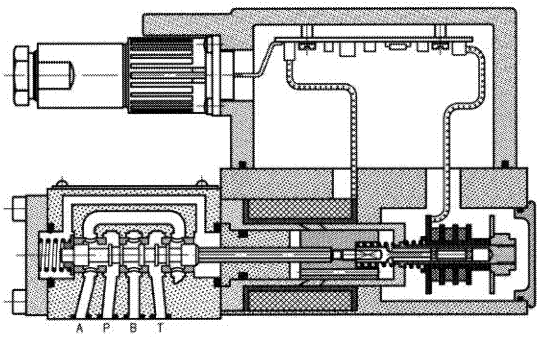

Figure 2. High speed industrial solenoid servo valve (BOSCH 4WRPEH 6)

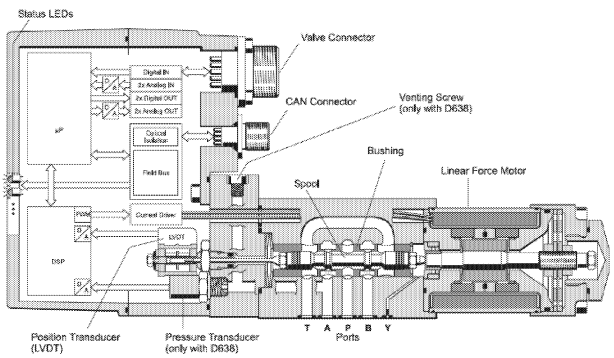

Figure 3. Digital DDV with CAN BUS (MOOG S638)

The static and dynamic performances of the servo valves are supplied by the manufacturers as average complex diagrams as presented in the figures 4,5 and 6. Numerical simulation offers the possibility to refine and explain the aspect of these curves.

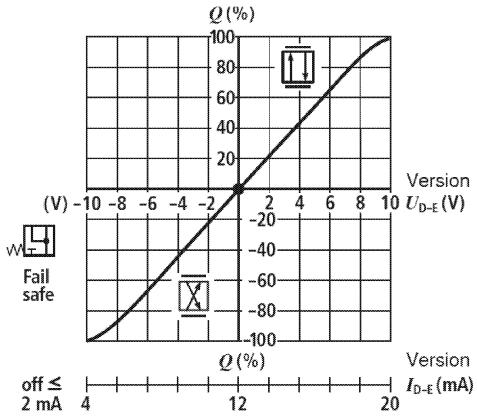

Figure 4. Typical steady-state flow characteristics of a high speed industrial servo valve (PARKER)

.

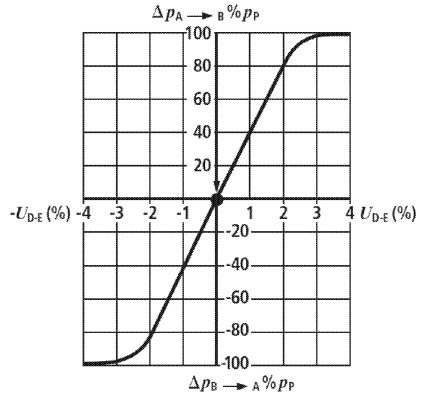

Figure 5. Typical pressure sensitivity of a high speed industrial servo valve (BOSCH)

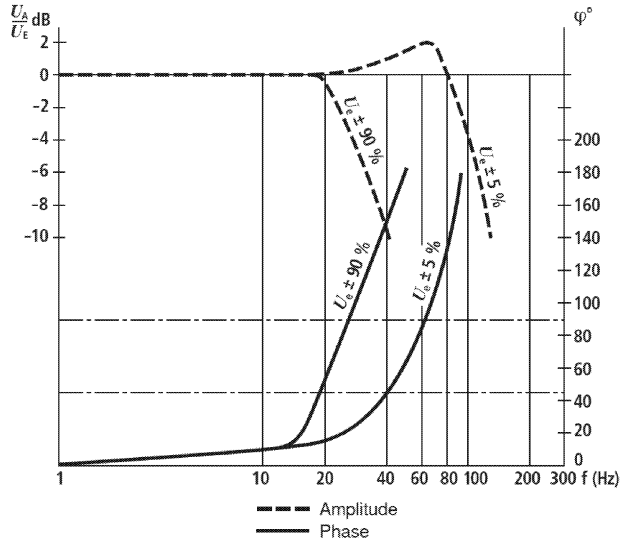

Figure 6. Typical dynamic performance of a high speed industrial servo valve (BOSCH)

NUMERICAL SIMULATION BY AMESIM

AMESIM software (Lebrun et al., 2009), produced by LMS Company, now - a member of SIEMENS Group, was selected as a current simulation tool (LMS 2013). This complex software offers numerous advantages: rich library of hydraulic symbols and components, which allow the authors to use existing, proven models for well-known components (valves, cylinders); ability to simulate different part of the system at different levels of complexity, which allows the authors to model different parts of the system at different levels of detail, as required. AMESIM models are fully compatible with LabVIEW for real time and Hardware-in-the-Loop simulations, can be imported in LabVIEW and connected to a real-time or HIL simulation system. A realistic image of the behavior of a servo valves can be created *before* the prototype manufacturing by numerical simulation, avoiding the "cut-and-try" time and money consuming procedure. A realistic AMESIM simulation model of a direct drive servo valve with moving coil is presented in the figure 7. This model gives the steady-state flow characteristics for different kind of valve overlap.

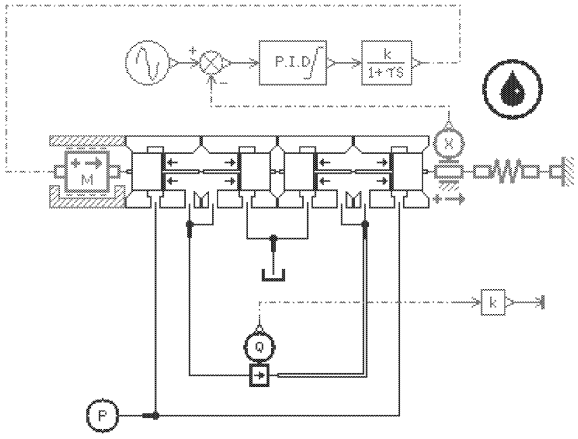

Figure 7. AMESIM model used for finding the steady-state flow characteristics

A low frequency sine input (1Hz) is used in order to pass through all the position of the spool, with very small steps (Imagine 2001). All the three cases encountered in the servo valve practice were investigated (figs. 8, 9 and 10).

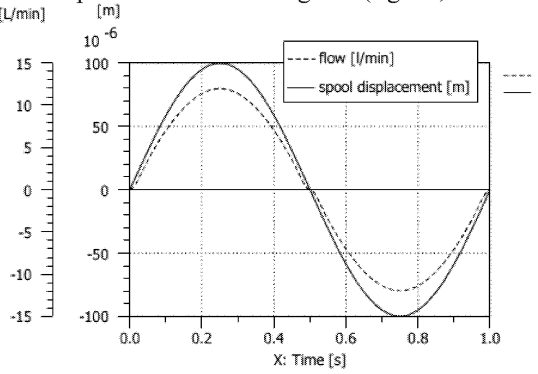

Figure 8. Low frequency sine input response of a critical overlap flow control valve.

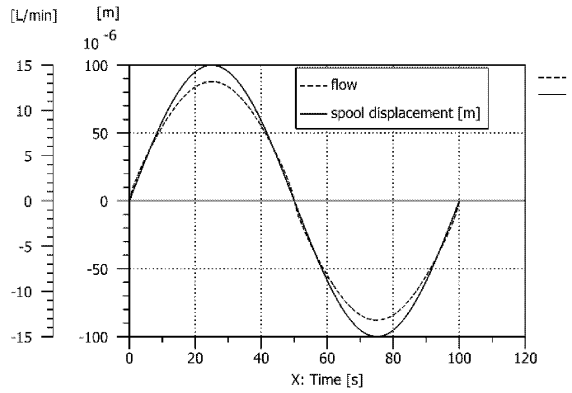

Figure 9. Low frequency sine input response of a negative lap flow control valve.

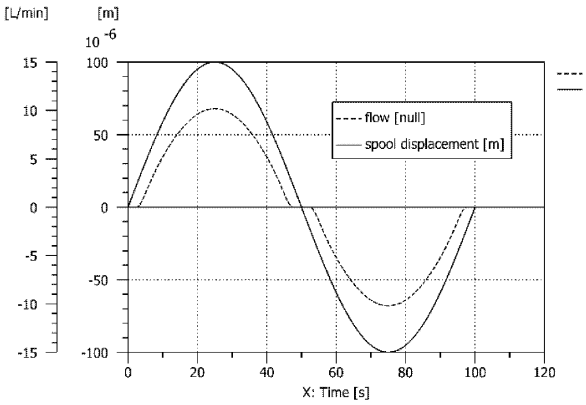

Figure 10. Low frequency sine input response of a positive lap flow control valve.

The results of these simulations are presented in the figures 11, 12 and 13. They are in very good agreement with the experimental results published by the most important researchers in the field (Merritt 1967; Viersma 1980; Guillon 1992; Mare 2016). The very small slope of the flow characteristics around the null point, shown by the figure 13 pointed out the small laminar leakages through the radial clearances, which cannot be ignored in the synthesis of the high accuracy position servo systems.

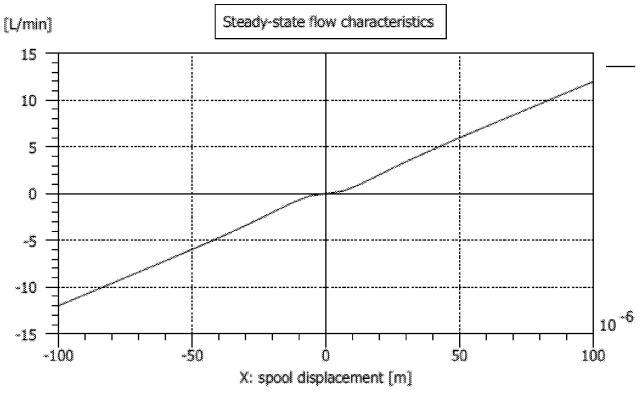

Figure 11. Steady-state flow characteristics of a critical lap flow control valve

The high slope of the flow characteristics around the null point of the negative overlap valves (figure 12) is used in all the applications where the load random variations have to be quickly rejected. A typical case is encountered in the automotive steering systems, and in other similar applications, which involve the automatic recovery of a variable reference position (Guillon 1992; Rösth 2007). Usually, these systems are supplied by a constant flow system, in order to keep the response time at the same value for any load variation (Vasiliu C. 2002; Rösth 2007).

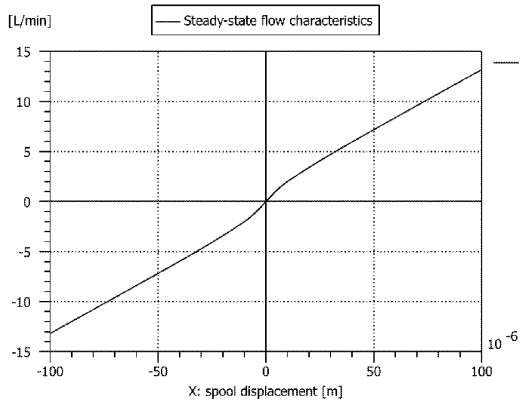

Figure 12. Steady-state flow characteristics of a negative lap flow control valve (-10µm)

A wide dead band of the flow characteristics (figure 13) is useful for increasing the stability of the hydraulic servomechanisms, but it reduces the absolute accuracy. However, it strongly reduces the leakages, which can be important in the overall system power consumption.

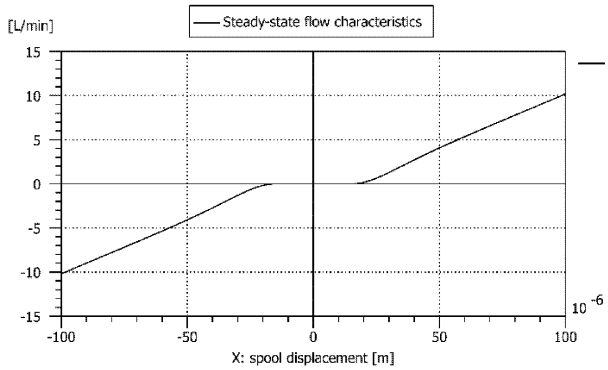

Figure 13. Steady-state flow characteristics of a positive lap flow control valve (+10µm)

All the above conclusions have technological consequences, leading to specific domains of applications (Vasiliu et al. 2007; Mare 2016). The second series of numerical simulation was devoted to the correlation between the overlap and the valve pressure sensitivity. The simulation model from the figure 14 was used in the same cases studied above. The results are presented in the figures 15, 16 and 17. As expected from the geometrical peculiarities of the valves, the highest-pressure sensitivity is supplied by the critical case, which is used in the most performant applications (MOOG 2008).

The negative overlap is always giving a smooth pressure sensitivity curve, used in constant flow supply applications. The positive overlap is giving a "relay" pressure behavior, which can be useful in slow position control process. The reduction of the geometrical gain by notches of different shapes leads to a continuous variation of the pressure difference between the hydraulic motor ports. This is the case of the proportional industrial servo valves actuated by proportional force solenoids (BOSCH 1999).

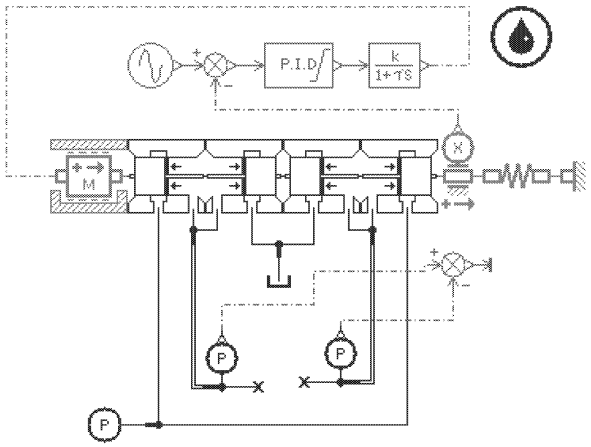

Figure 14. AMESIM model used for finding the pressure sensitivity of a flow control valve

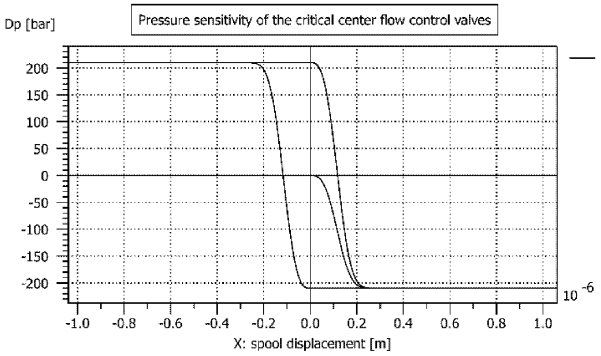

Figure 15. Pressure sensitivity of a critical lap flow control valve

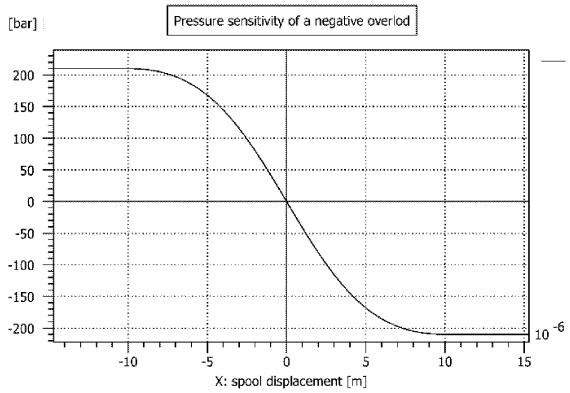

Figure 16. Pressure sensitivity of a negative lap flow control valve (-10 μm)

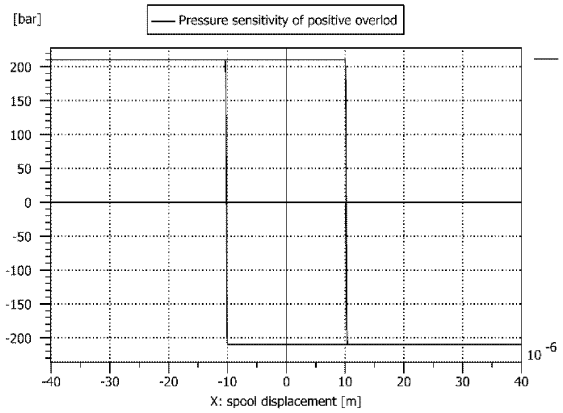

Figure 17. Pressure sensitivity of a positive lap flow control valve (10 μm)

The final series of simulations is devoted to the overlap influence on the frequency response of the servo valve. The control library of AMESIM includes a Frequency Response Analyzer block called SIGDYNFRA01, which is running as a real device, which generates a constant magnitude input with a variable frequency. For a moving coil actuator of the spool, a first order transfer function with a few milliseconds constant time is a fair dynamic representation. The simulation model is presented in the figure 18, and the input signal – in the figure 19.

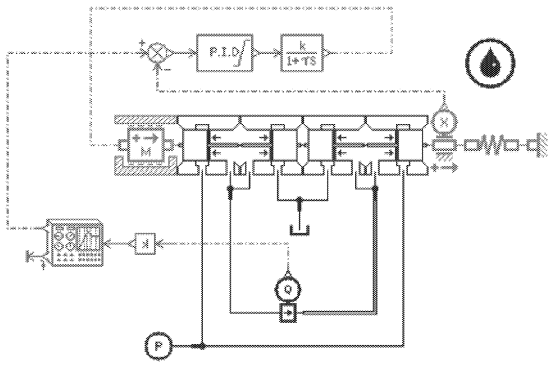

Figure 18. Frequency response AMESIM model for a flow control valve.

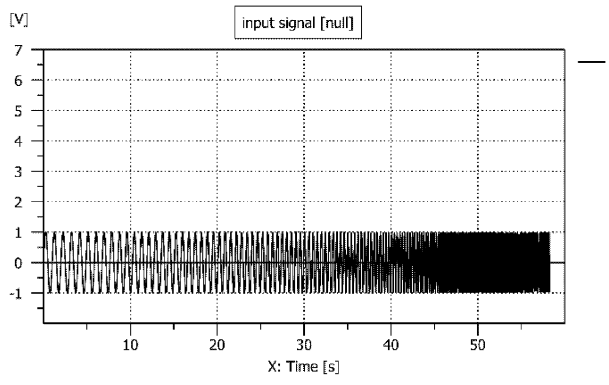

Figure 19. The sine input applied to the electro mechanic actuator for obtaining the frequency response.

The force developed by the actuator strongly increase with the input voltage frequency (fig. 20). The flow passing through the servo valve (fig. 21) is overpassing 100 Hz for the critical overlap (fig. 22), increase a little in the case of a negative lap (fig. 23), and decrease for a positive overlap (fig. 24).

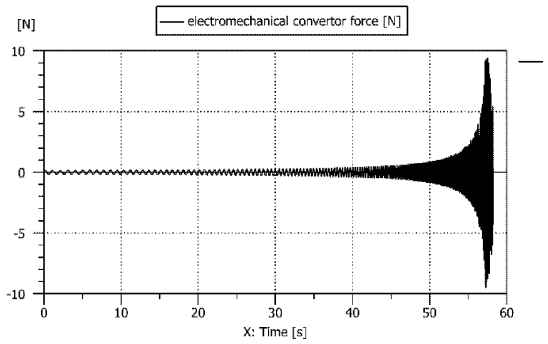

Figure 20. Force applied to the spool by the electro mechanical actuator

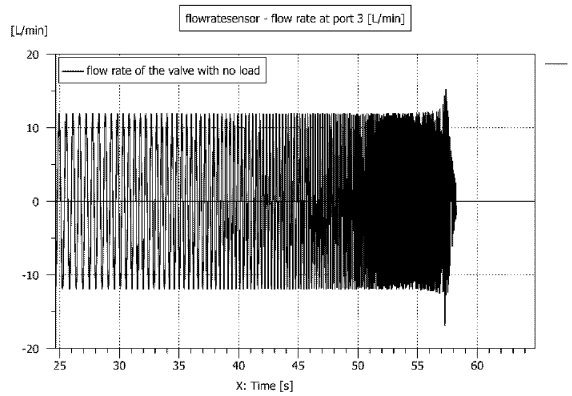

Figure 21. The flow passing by the valve without load.

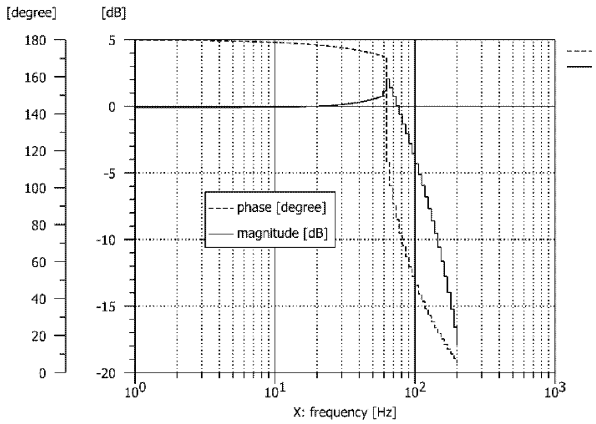

Figure 22. Frequency response of a critical lap flow valve for a sine input of ±10%.

The realistic choice of the servo valve parameters leads to normal results for this kind of device.

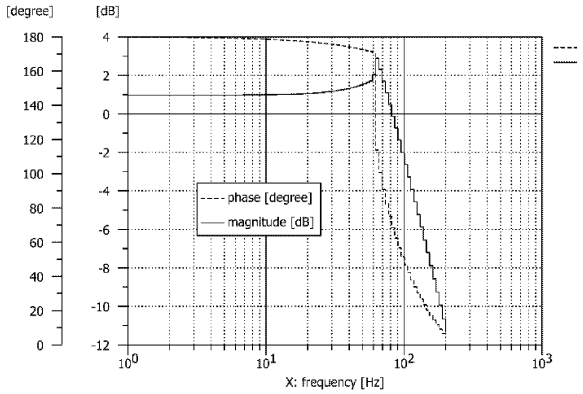

Figure 23. Frequency response of a negative lap flow valve for a sine input of ±10%.

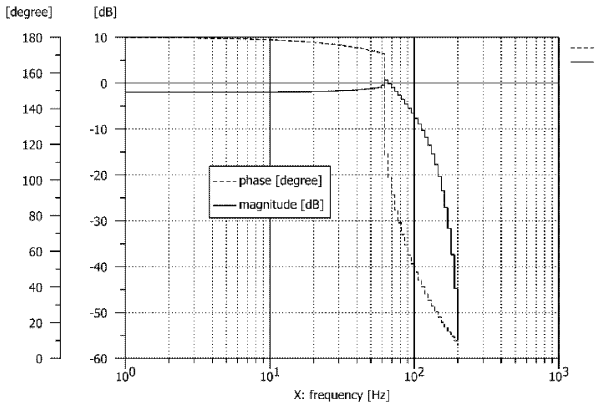

Figure 24. Frequency response of a positive lap flow valve for a sine input of ±10%.

EXPERIMENTAL VALIDATION OF THE DESIGN

The authors performed the validation of the simulation results in the fluid power laboratory of the University POLITEHNICA of Bucharest, in the section devoted to the electrohydraulic servo valves. The test bench designed for this kind of flow control valves (figs. 25, 26) allows all types of standard tests.

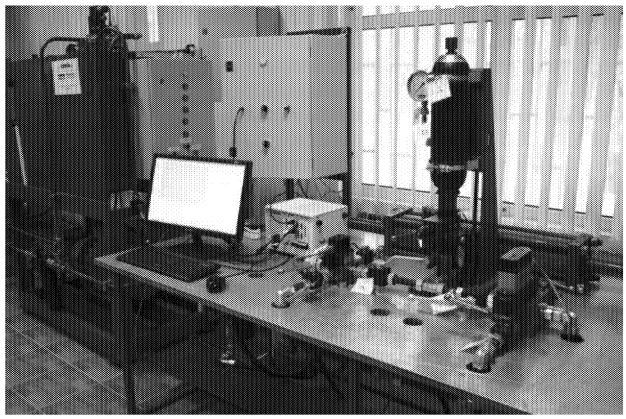

Figure 25. Overall view of the servo valve static test bench from the certification laboratory of the University POLITEHNICA of Bucharest

The steady state and the frequency response found experimentally in the lab for a direct drive valve with moving coil type DFPlus (Parker) are found close to the simulated ones with AMESIM software (figs. 27 and 28). It is important to mention the very small real clearance of the spool, which introduces a good viscous dumping.

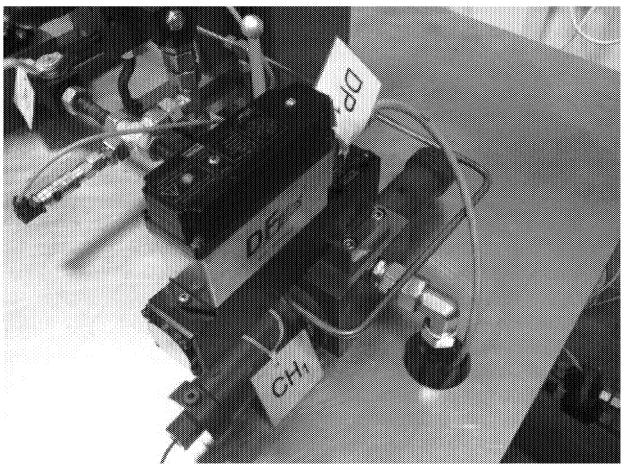

Figure 26. View of the dynamic test bench for electrohydraulic single stage servo valves

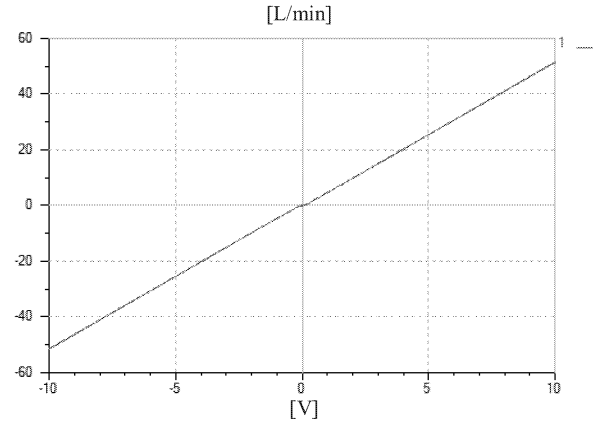

Figure 27. Experimental steady state characteristics for a DFPlus industrial high speed servo valve (p_s=100 bar, U_i = ±10V)

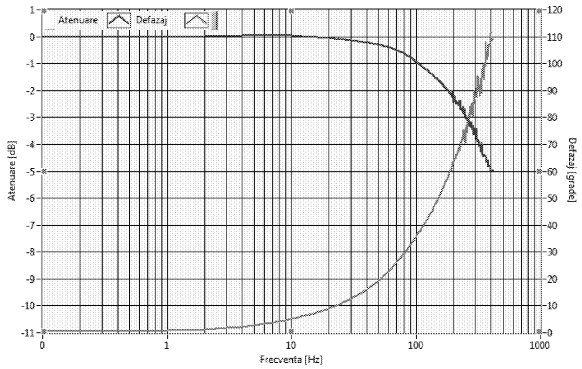

Figure 28. Experimental frequency response for DFPlus industrial high speed servo valve (p_s=100 bar, U_i = 10%)

CONCLUSIONS

All the design, test, and identification stages of the commercial servo valve performed by the authors pointed out that AMESim provided a strong solver and numerical core for steady state and transient simulation. As modeling a complex multi-physics system is not the main objective of engineers, it is important to have tools and interfaces, which accelerate and optimize the design. From this point of view, AMESim is a complete software perfectly adapted for model creation and deployment. The users working both in the high-level corporation and in strong research universities continuously extend the wide field of applications (Dardac et al. 2014; Negoita 2011; Popescu 2011; Vasiliu C. 2007).

ACKNOWLEDGEMENTS

The authors are grateful for all the technical support received from the LMS COMPANY (now - a SIEMENS business) in different manners: free licenses, free technical training for the research team members, and many other facilities.

REFERENCES

Dardac L.T., Vasiliu N., Călinoiu, C. 2016. "Electrohydraulic VVT System fo High Power Diesel Engines". Romanian Patent no. RO126878.

Guillon, M. and Thoraval, B. 1992. "Commande et asservissement hydrauliques et electrohydrauliques". Technique et documentation – Lavoisier, Paris.

Lebrun M., Vasiliu D., Vasiliu N. 2009. "Numerical simulation of the Fluid Control Systems by AMESim". *Studies in Informatics and Control with Emphasis on Useful Applications of Advanced Technology*, Volume 18, Issue 2, p.111-118.

Mare J.Ch. 2016. Les actioneurs aeronautiques 1. ISTE Editions.

Negoita, G.C. 2011. "Researches on the Dynamics of the Hydrostatic Transmission". Ph.D. Thesis, University POLITEHNICA of Bucharest.

Popescu, T.C. et al. 2011. "Numerical Simulation - a Design Tool for Electro Hydraulic Servo Systems", in *"Numerical Simulations, Applications, Examples and Theory"*, INTECH PRESS, Zieglergasse 14, 1070 Vienna, Austria.

Rösth M.R. 2007. Hydraulic Power Steering System Design in Road Vehicles. Ph.D. Thesis, Linköping University.

Vasiliu C. 2011. RTS of the Electric Powertrains. Ph.D. Thesis, University POLITEHNICA of Bucharest.

Vasiliu N., Călinoiu C., Vasiliu D. 2007. "Modeling, Simulation and Identification of the Electrohydraulic Speed Governors for Kaplan Turbines by AMESim". Symposium on Power Transmission and Motion Control - PTMC 2007, Bath, United King., ISBN 978-0-86197-140-4.

Viersma, T.J. 1980. "Analysis. Synthesis and Design of Hydraulic Servosystems and Pipelines". Elsevier Scientific Publishing Company, Amsterdam.

***BOSCH - Automation Technology. 1999. "Servo Solenoid Valves. Technical Specification 13/2". Stuttgart.

***Imagine. 2001. Numerical Challanges posed by Modeling Hydraulic Systems. Technical Bulletin 114.

***LMS, 2013. "Advanced Modeling and Simulation Environment", Release 13 User Manual, Leuven.

***MOOG. 2008. D680 Series Mini Direct Drive Valve Piloted

Servo-Proportional Control Valves with Integrated Electronics ISO 4401 Size 05 to 08.

WEB REFERENCES

http://www.duplomatic.com/
http://www.boschrexroth.com/
http://www.eaton.com/
http://www.sauer-danfoss.com/
http://www.moog.com/
http://www.hydac.com/
http://www.parker.com
http://www.siemens.com/
http://www.mathworks.com/products/simulink/
http://www.dspace.com/
http://www.adwin.de/
http://www.fluidpower.net/

BIOGRAPHIES

Ina COSTIN graduated in mechanical engineering in 1984 and is preparing a Ph.D. thesis in the field of the dynamics of the fluid power systems in the frame of the Fluid Power Laboratory of the University POLITEHNICA of Bucharest. She is currently R&D Manager in DUPLOMATIC OLEODINAMICA SpA from Italy. She works in the field of design, modeling, simulation, and experimental identification of the electro hydraulic control systems. Member of FPNI, ASME etc.

Constantin CALINOIU graduated in Hydropower Engineering from University POLITEHNICA of Bucharest in 1975. In 1980, he became a member of the Hydraulic Laboratory from the Romanian Aerospace Institute. In 1998, he became Ph.D. and associated professor in the Fluid Power Laboratory from U.P.B. He is working mainly in modeling, simulation, and identification of the hydraulic and electro hydraulic control systems.

Daniela VASILIU graduated in mechanical engineering in 1981 and prepared the Ph.D. thesis in the field of the dynamics of the hydrostatic transmissions. She is currently professor in the Department of Hydraulics, Hydraulic Machines and Environmental Engineering, head of Fluid Power Laboratory of the University POLITEHNICA of Bucharest. She works in the field of modeling, simulation, and experimental identification of the electro hydraulic control systems; member of EUROSIS, FPNI, SIA, FLUIDAS etc.

Nicolae VASILIU graduated in Hydropower Engineering from University POLITEHNICA of Bucharest in 1969. He became a Ph.D. in Fluid Mechanics after a research stages in Ghent State University and Von Karman Institute from Bruxelles. He became state professor in 1994, leading the ENERGY & ENVIRONMENT RESEARCH CENTRE from the University POLITEHNICA of Bucharest. He managed five years the Innovation Romanian Agency. He worked always for the industry, as project manager or scientific advisor, promoting the numerical simulation as an engineering tool.

MODELING SIMULATION AND TEST OF THE HIGH PRESSURE RELIEF VALVES

Cătalin DUMITRESCU, Teodor Costinel POPESCU, Liliana DUMITRESCU
Hydraulics &Pneumatics Research Institute INOE 2000 – IHP
040558, Bucharest, Romania
E-mail: dumitrescu.ihp@fluidas.ro

Daniela VASILIU
University POLITEHNICA Bucharest,
313 Splaiul Independentei, 6th County
E-mail: vasiliu1946@gmail.com

Dragos Daniel ION GUTĂ
INCAS Bucharest, Romania
E-mail: guta.dragos@incas.ro

KEYWORDS
High pressure relief valves, simulation, test, AMESIM

ABSTRACT

Pressure is a main parameter of hydraulics, in evolving. The increasing trend of working pressures is evident both in the industrial hydraulics, as well as in the mobile one. If in our country the equipment of high pressure (over 350 bar) are not in the manufacturers' production programs, testing and repair can be done successfully, being determined by the availability of adequate means test. Mathematical modeling and numerical simulations are an important support for the concept and exploit the means test. In this context, experts from the Research Institute for Hydraulics and Pneumatics, in collaboration with specialists in modeling / simulation and hydraulics from Polytechnic University of Bucharest and the Incas, developed a stand to verify performance of equipment working at high pressure (max. 630 bar). The first steps in achievement the stand was modeling / simulation of hydraulic components, followed by experimental validation. The article presents the results on the testing pressure valve, a key element of the stand.

INTRODUCTION

Increasing work pressure is strongly supported by favorable results in materials science and the emergence of working fluids with superior properties. The evolution of the operating pressure in the last 50 years, in mobile hydraulics, is shown in the chart below.

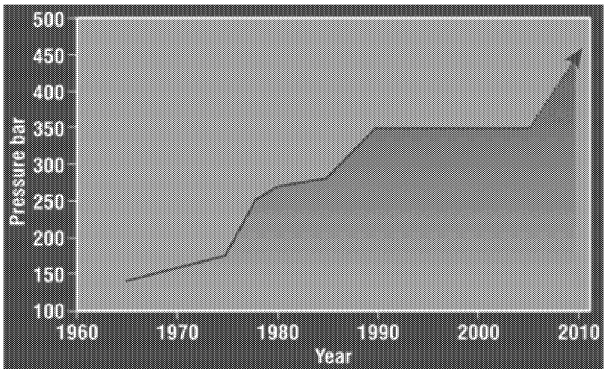

Figure 1: Evolution of Working Pressures in Mobile Hydraulics

A pressure level of 450 bar in hydraulics is estimated by most experts in the field, including in our country, for years to come, with the possibility to increase up to 550-750 bar in a time horizon of 10 ... 15 years, mainly in mobile hydraulics, but also for the industrial one (Vasiliu et. Al. 2012; Avram 2005). The trend of increasing pressure is also present in other areas such as military and civil aviation. One of the latest achievements in the field, where it is visible this trend, is the AIRBUS A 380 plane, whose weight fully charged exceeds 500 tons (551 tons). To take off with this load without increasing the weight and size of hydraulic actuators, AIRBUS company increased working pressure from 3000 PSI (210 bar), the standard for commercial aviation, to 5000 PSI (approx. 350 bar). This enables relatively small hydraulic cylinders to generate large forces needed to withdraw the landing gear and drive the steering and aircraft flaps. Our country is connected to trends and technical level of European and international hydraulics; for these reasons, increasing pressures is visible from imported equipment which is working here, and which should be kept in running at optimal parameters.

Testing and repair must be able to perform in the country, this having economic, technical and financial positive aspects. In this context, design and implementation for the first time in Romania a stand for testing hydraulics high pressure (max. 630 bar), based on modern solutions and equipment, in a national research – development institute (INOE 2000-IHP Bucharest), followed by its introduction in the circuit for research, both for industrial activities, is positive and desirable.

The article presents results of modeling / simulation and experimentation for a pressure valve which belongs to the stand. Authors' objectives were, on the one hand, testing valve quality and, on the other hand, validation after experimentation of the proposed models.

PRESENTATION OF THE RELIEF VALVE

Based on previous work in the field of hydraulic drive in general and hydraulic equipment operating at high pressures, on the experience resulted from the designing, implementation and testing equipment in the hydraulic domain, and taking into account the current level of development, it has developed a powerful stand for

testing hydraulic pressure equipment at max. 630 bar. [3].
The stand has as essential element a high-pressure flow generator (radial piston hydraulic pump), which can sustain in circuit pressures up to 1000 bar. Besides that, hydraulic equipment allows working at pressures up to 630 bar. High pressure valve DBDS type is produced by BOSCH REXROTH, and it is a direct acting valve, having the role to limit the pressure in a hydraulic circuit. The main components are the body (1), the spring (2), the conical washer with shock absorber (3) for pressures up to 400 bar, or ball (4) for maximum pressure up to 630 bar, and the adjustment knob (5). Spring (2) press the conical washer (3) or ball (4) on their seat. P port is connected to the system and the pressure present in the system is applied to the surface of the ball or washer, where applicable.

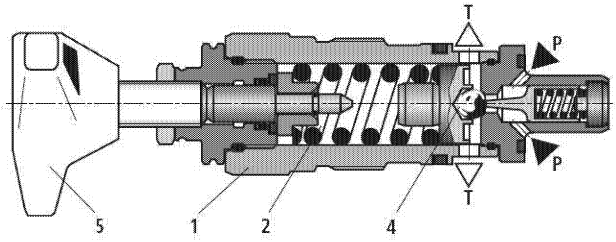

Figure 2: Relief valve type DBDS, with Ball, for pressure up to 630 bar (BOSCH)

Considering the use for the first time in the institute of apparatus with such high performance level in terms of operating pressure, they were considered useful the modeling and simulation in various conditions of some apparatus belonging of the stand. [4]

MODELING THE VALVE DYNAMICS

The valve has two constructive peculiarities looking to other valve designs, features deriving from its destination, namely the high pressures domain (up to 630 bar, in this case):
- the closing element is a ball mounted in the central portion of a plate;
- the cushioning system is provided with a spring shock absorber.

A direct acting pressure valve (Fig. 3), limits the upper pump discharge pressure because it drains the flow at high pressure to the tank through the annular gap between the shutter and body. Axial movement of the slide to enlarge the slot is determined by the resultant pressure forces acting on the surface.

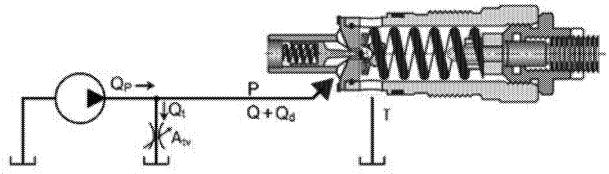

Figure 3: The system used for analyzing a normally closed valve

The studied system consists of: oil tank, volumetric pump, throttle valve and normally closed pressure valve. Delivered under pressure oil is sent to the tank through the throttle that simulates a load and through the valve (excess flow). The valve has a spherical shutter, a conical seat surface for the shutter, a washer for the hydrodynamic force compensation, a small piston for damping of oscillations, the elastic springs (mainspring that presses the shutter and a spring that forces the small piston of the damper to "follow" the spherical shutter) and tensioner element of the main spring.
For this model it was neglected the dynamic behavior of oil in the pipe between pump and valve. The system behavior is described by the following equations:

1. *Flow area and the area on which pressure is acting, for the valve-seat subsystem*

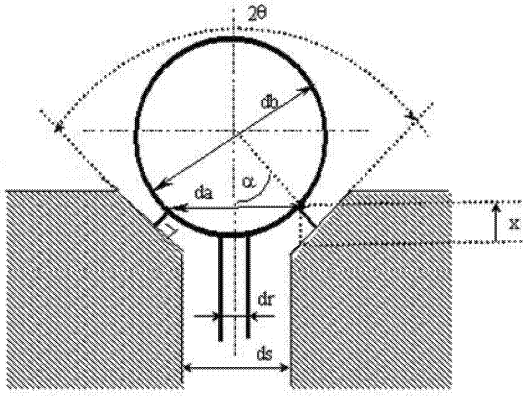

Figure 4: Valve – seat subsystem

$$\alpha = \left(\frac{\pi}{2}\right) - \theta \quad (1)$$

$$da = db \sin(\alpha) \quad (2)$$

$$\beta = acos\left(\frac{da}{db}\right) \quad (3)$$

$$A_t = \pi x\,[db + x\cos(\alpha)]\sin(\alpha)\cos(\alpha) \quad (4)$$

$$A_p = \frac{\pi}{4}d_a^2 = \frac{\pi}{4}d_b^2\ sin^2\left(\frac{1}{2}\pi - \theta\right) \quad (5)$$

2. *The equation of motion of the closing valve*

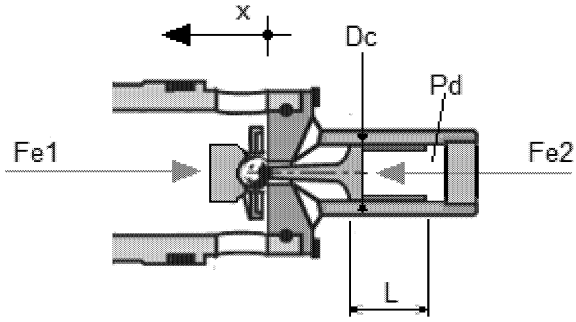

Figure 5: Valve closing and damping effect

$$P_d A_d + F_{SR} - P(A_d - A_p) - F_h + F_c = m\frac{d^2x}{dt^2} + f\frac{dx}{dt} + F_{e1} - F_{e2} \quad (6)$$

$$F_{e1} = k_{rv1}(x_0 + x) \quad (7)$$

$$F_{e2} = k_{rv2}(x_1 + x) \quad (8)$$

$$F_h = C_d A_t (P - P_T)\cos(\beta) \quad (9)$$

$$Fc = \rho\, Q\, C_{vs} \sqrt{2\frac{P}{\rho}}\cos(\delta) \quad (10)$$

3. Reaction forces between valve and seat

$$F_{SR} = \begin{cases} 0; & x > 0 \\ k_s|x| - R_s\frac{dx}{dt}; & x < 0 \end{cases} \quad (11)$$

4. Oil flow transfused through the radial clearance in the damper chamber

$$Q_d = \frac{\pi D_d c^3}{12\mu L}(P - P_d) \quad (12)$$

5. Oil flow transfused through the flow area of the valve

$$Q = C_d A_t \sqrt{2\frac{P}{\rho}} \quad (13)$$

6. Continuity equation applied to the damper chamber

$$Q_d - A_d\frac{dx}{dt} = \frac{V_0 + A_d x}{B}\frac{dP_d}{dt} \quad (14)$$

7. Flow delivered by the pump

$$Q_p = Q_{th} - \frac{P}{R_L} \quad (15)$$

8. Flow transfused through the throttle

$$Q_t = C_d A_{tv} \sqrt{2\frac{P}{\rho}} \quad (16)$$

9. Continuity equation applied to the junction between the pump, load (throttle) and valve

$$Q_P - Q - Q_d - Q_t = \frac{V_p}{B}\frac{dP}{dt} \quad (17)$$

In the above equations, the following symbols and notations were used:
db = ball diameter (m)
2θ = taper angle of the seat (rad)
ds = seat diameter (m)
dr = damping piston rod diameter (m)
β = flow angle (rad)
δ = deflector angle (rad)
A_d = damper piston area (m^2)
A_p = valve area subjected to pressure (m^2)
A_t = flow area between the valve and seat (m^2)
A_{tv} = flow area through the throttle (m^2)
B = Bulk module of the oil compressibility (Pa)
c = radial clearance of the damper (m)
c_d = flow coefficient
c_{vs} = speed coefficient of the valve aperture
D_d = damper piston diameter (m)
f = the coefficient of viscous friction of the piston (Ns/m)
FSR = seat reaction force (N)
F_h = hydrodynamic force (N)
F_c = compensation force due to the washer (N)
F_{e1} = elastic force generated by the spring acting on the valve (N)
F_{e2} = elastic force generated by the spring acting on the damper (N)
k_{rv1} = stiffness of the spring acting on the valve (N/m)
k_{rv2} = stiffness of the spring acting on the damper (N/m)
k_s = stiffness of the seat (N/m)
L = damper piston length (m)
m = equivalent mass of the moving elements (kg)
P = pressure upstream of the valve (Pa)
P_d = pressure in the damper chamber (Pa)
P_T = pressure in the tank (Pa)
Q = oil flow passing through the valve (m^3/s)
Q_d= oil flow passing through the damper radial clearance (m^3/s)
Q_P = flow supplied by the pump (m^3/s)
Q_t = flow passing through the area between the valve and the seat (m^3/s)
Q_{th} = theoretical flow pump (m^3/s)
R_L = coefficient of the internal leakage of the pump ($Pa\cdot s/m^3$)
R_S = seat damping coefficient (Ns/m)
V_0 = initial volume of oil in the damper chamber (m^3)
x = ball stroke (m)
x_0 = preload of the spring acting on the valve (m)
x_1 = preload of the spring acting on the damper (m)
μ = dynamic viscosity ($Pa\cdot s$)
ρ = oil density (kg / m^3)

NUMERICAL SIMULATION OF NORMALLY CLOSED VALVE

In order to build a realistic model of the valve, numerical simulations were performed using AMESIM R13. Numerical simulation were performed for the following parameters:
m = 0.04 kg, db = 0.008 m, dr = 0.0025 m, D_d = 0.010 m, ds = 0.004 m, c = 0.06 mm, θ = 30^0, L = 0.015 m, ρ = 850 kg/m^3, δ = π, c_d = 0.7, B = $12\cdot10^8$ Pa, k_{rv1} = 74,000 N/m, k_{rv2} = 20,000 N/m.

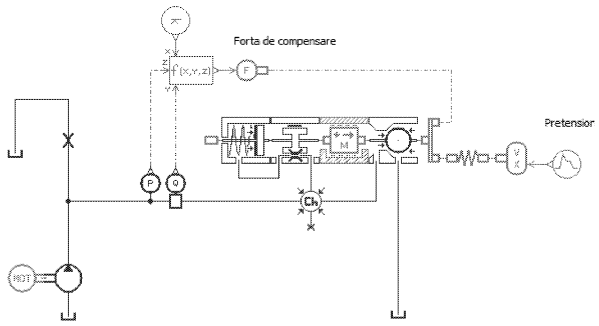

Figure 6: System network simulation (AMESIM)

Simulations were performed in order to analyze the behavior of the valve for various flow rates input steps between 4.2 and 20 l / min, finding mainly the time when the pressure is stabilized at the desired value.

The simulation results for a maximum pressures of 630 bar are shown in the figures 7 and 8. These theoretical results, we determined the delay time td, rise time tr and stabilization time ts; these results will be compared with those obtained experimentally. Thus, for the graph in Figure 7, we have the following values obtained from simulation:

td = 0.178 s, tr = 0.297 s, ts = 0.381 s,

For the testing at 20 l/min, the significant time values are:

td = 0.039 s, tr = 0.044 s, ts = 0.072 s

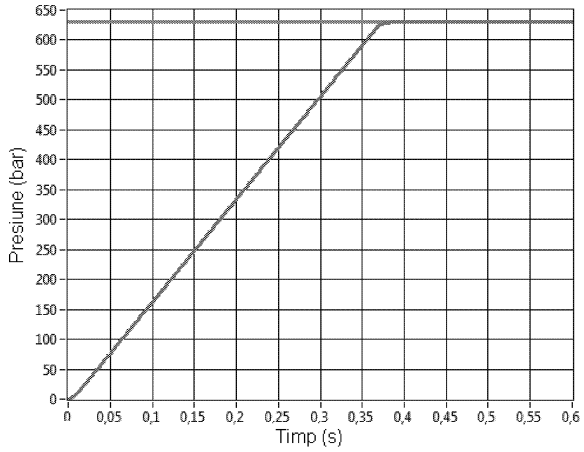

Figure 7: Valve behavior simulation to a step signal: P=630 bar; Q=4.2 l / min

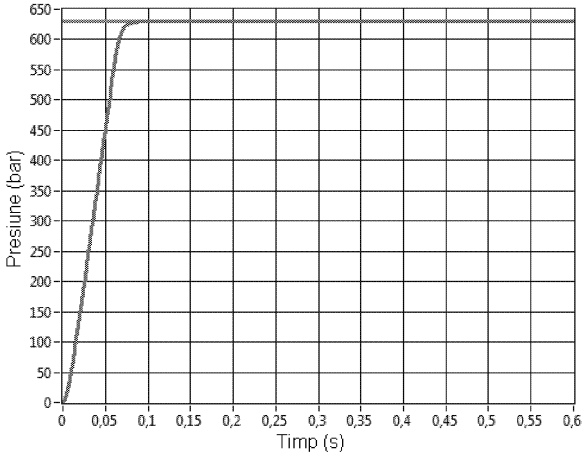

Figure 8: Simulation of the valve behavior for an input signal of 20 l/min and an opening pressure of 630 bar

DYNAMIC TEST OF THE VALVE

Various tests with step signal for different level of the opening pressures were performed for the relief valve of the stand, aiming previously monitored parameters. The tests were performed at set pressure of the valve 100, 200, 300, 400, 500, 600 and 630 bar, but in the article only the tests carried out at the pressure of 630 bar, at 4.2 l and 20 l / min are graphically shows.

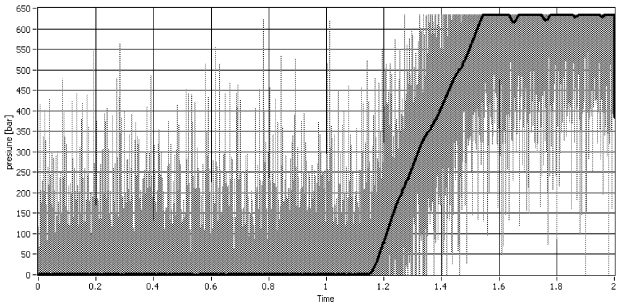

Figure 9: Response to step input signal at a pressure of 630 bar and a flow of 4.2 l/min

Calculating the above parameters, we obtain:

$t_d = 0.170$ s, $t_r = 0.318$ s, $t_s = 0.388$ s

The tests of 20 l/min gave the following results:

$t_d = 0.042$ s, $t_r = 0.046$ s, $t_s = 0.072$ s

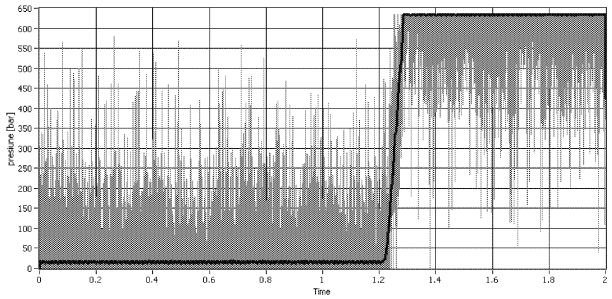

Figure 10: Response of the valve to a step input signal at the pressure of 630 bar and a flow of 20.0 l/min

CONCLUSIONS

Comparing the values from simulation and real tests, we obtained close values; the values obtained from simulation for the delay times, rise times and stabilization times is usually lower.

Table 1. The comparison of experimental results with the simulation, pressure 630 bar

Parameter		Flow (l/min)			
		4,2		20	
		Value	Diff. (%)	Value	Diff. (%)
t_d(s)	**Experimental**	**0,170**	4,7	**0,042**	-7,1
	Simulated	0,178		0,039	
t_r(s)	**Experimental**	**0,318**	- 6,4	**0,046**	-4,4
	Simulate	0,297		0,044	
t_s(s)	**Experimental**	**0,388**	- 1,8	**0,072**	0
	Simulated	0,381		0,072	

This is explained by some differences in real behavior compared to standard conditions considered in the simulation (oil temperature, viscosity, compressibility oil). However, these results validate the mathematical model, and also demonstrates that the stand can be used effectively in tests for high pressure hydraulic apparatus, both in research and in industrial environmental benefit.

REFERENCES

1. Vasiliu N., Vasiliu G. C., Vasiliu D., Irimia P.C. 2012. "Modern developments of the hydraulic transmissions in automotive technology", Zilele Academice ale Academiei de Ştiinţe Tehnice din România, Bucureşti, Buletinul Agir, Ediţ ia A VII-A, 11-12 Octombrie, Editura Agir, ISSN 2066-6586, COPERNICUS indexed.
2. Avram, M., Acţionări hidraulice şi pneumatice – Echipamente şi sisteme clasice şi mecatronice, Editura Universitară, Bucureş ti, ISBN 973-7787-40-4, 2005.
3. Radoi R., Dutu I., Blejan M. 2011. "Stand and equipment's for determining the dynamic performances of electrohydraulic proportional directional control valves" - Proceedings – HERVEX, pp. 365-372, ISSN 1454-8003 http://www.hervex.eu/.
4. Popescu, T.C., Blejan, M., Lepădatu, I. 2013. „Electrohydraulic Servomechanism for Driving the Reels of Coil Winding Machines specific to Wire Rolling Mills". "HIDRAULICA" (No. 3/2013) - *Magazine of Hydraulics, Pneumatics, Tribology, Ecology, Sensorics, Mechatronics,* ISSN 1453 – 7303.

*** AMESIM R13. User Manual. Leuven, 2013.

WEB REFERENCES

www.boschrexroth.com
www.hawe.com
www.parker.com
www.sauer-danfoss.com
www.eaton.com

BIOGRAPHIES

DUMITRESCU CĂTĂLIN graduated from the Faculty of Mechanical Engineering, within the Polytechnic Institute of Bucharest, class of 1997 and in 2011 he was granted a PhD in fluid power, high pressure systems. From 1997 until now he has been working in the Hydraulics and Pneumatics Research Institute of Bucharest (INOE 2000-IHP), in the field of control and adjustment hydraulic actuation systems.

TEODOR COSTINEL POPESCU graduated from the Faculty of Installations' Engineering, within the Institute of Civil Engineering in Bucharest, class of 1978, and he also graduated from the Faculty of Mechanical Engineering, within the Polytechnic Institute of Bucharest, class of 1989. In 2008 he was granted a PhD in fluid power systems, at the Faculty of Power Engineering within "POLITEHNICA" University of Bucharest, with the distinction "CUM LAUDE". From 1983 until now he has been working in the Hydraulics and Pneumatics Research Institute of Bucharest, in the field of control and adjustment hydraulic actuation systems.

DANIELA VASILIU graduated in mechanical engineering in 1981 and prepared the Ph.D. thesis in the field of the numerical simulation of the hydrostatic transmissions. She is currently professor in the Department of Hydraulics, Hydraulic Machines and Environmental Engineering, head of Fluid Power Laboratory of the University POLITEHNICA of Bucharest with works in the field of modeling, simulation, and experimental identification of the electro hydraulic control systems.

ENGINE TUNING SIMULATION

ELECTRIC MOTOR NOISE ANALYSIS BASED ON MULTIBODY SIMULATION

Claudia Martis
Technical University of Cluj-Napoca
Faculty of Electrical Engineering
Str. G. Bariţiu nr. 26-28
Cluj-Napoca Romania
E-mail: claudia.martis@emd.utcluj.ro

Cristi Irimia
Calin Husar
Mihail Grovu
Raluca Dora Ionescu
Luca Zanne
Siemens Industry Software SRL
Bd. Garii 13A et. VII Brasov Romania
E-mail: cristi.irimia@siemens.com

KEYWORDS
Sound Pressure, Electromagnetic Analysis, Multibody Simulation, Acoustic Model

ABSTRACT

The acoustic analysis and noise contribution of the electric motors is a topic of many companies in the (H)EV industry. It is important to predict the acoustic properties of the PMSM in the design phase. The goal of this paper is to investigate a vibro-acoustic behavior of a permanent synchronous motor (PMSM) by coupled electromagnetic-vibro-acoustic approach. A multi-physics simulation environment is developed and used for electromagnetic forces and sound pressure evaluation of a PMSM for vehicle applications. The radial forces obtained by the electromagnetic analysis are exported to an integrated suite of 3D FE and multibody simulation software. The complex analysis performs optimized characteristics for noise and vibration of the PMSM.

INTRODUCTION

The acoustic analysis and noise contribution of the electric motors on electric/hybrid vehicles (EV/HEV) is a topic of high interest in the automotive industry. For this reason, it is very important to predict the acoustic properties of the vehicle as early as possible in the design phase.

While the combustion engine has a higher sound power level, with typically a low-frequency signature, the noise from an electric motor and from accompanying subsystems, like the converter, consists mainly of tonal components. Many component noises, becoming audible as annoying sounds due to the missing masking effect of the electric motor and the high tonal characteristics, are only detected after the first vehicle prototypes. Therefore, a closer analysis, assessment and optimization of the electrical drivetrains from noise-vibration-harshness (NVH) point of view in early development phase are essential.

PMSMs are widely accepted as the best candidate for the considered applications. They are adopted, due to their advantages (Zeraoulia et al. 2006; Finken et al. 2008; Laskaris and Kladas 2010; Aimeng, Yihua and Soong 2011) by a large part of the well-known automakers (from Europe, USA and Asia) for both propulsion (EV, HEV) and small power automotive applications (as steering, assisted or powered, and electromechanical brake) systems. Its major disadvantages are the high cost of rare-earth magnets, as these materials are expected to become less available in the future.

The present work aims to present a vibro-acoustic behavior analysis of a PMSM electric mobility scooter by coupled electromagnetic, multi-body and vibro-acoustic approach.

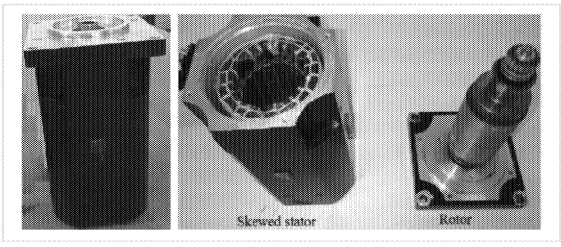

Figure 1: The prototype of studied PMSM motor

WORKFLOW AND SIMULATION ENVIRONMENTS

The multi-physics simulation environment, presented in Figure 2, provides the tool for integrating electromagnetic, multi-body, structural and vibro-acoustic analysis.

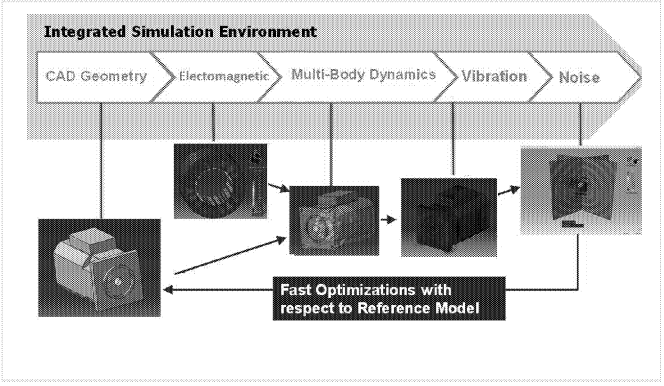

Figure 2: Simulation Environments

The noise prediction can be divided in four parts:

- calculation of stator electromagnetic forces;
- multibody simulation using flexible bodies and electromagnetic forces;
- housing vibration calculation by using MPFs from multibody simulation;
- noise generation.

Three interlinked software packages are used in this analysis. The electromagnetic analysis is performed using the JMAG software for determining the electromagnetic forces exerted on the stator and rotor surfaces. The structural analysis using the NastranNX permits the determination of the natural vibration frequencies, the coupled modal shapes and the modal participation factors. of the machine group. Virtual.Lab is used to create the multi-body and vibro-acoustic study.

Moreover, the LMS Virtual.Lab Acoustics is the integrated solution to minimize noise and optimize sound quality in new electric motor designs.

The whole process of the acoustic prediction methodology is shown on Figure 3. Each input steps can be modified, to check for improvements in the final results.

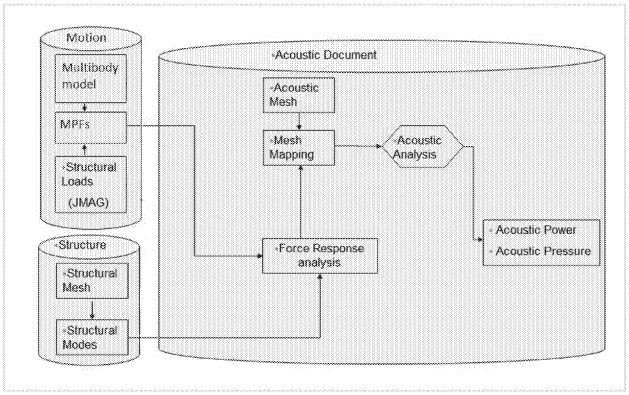

Figure 3: Vibro-acoustic process overview

ELECTROMAGNETIC ANALYSIS OF PMSM

The electromagnetic forces assuming to play an important role in acoustic noise radiation are the Maxwell forces which depend on the airgap radial flux density. The entire electromagnetic field is determined by solving Maxwell's equations within a finite region of space with user-defined initial conditions and appropriate boundary conditions
The FEA-based tool allows the design and optimization of components with static, harmonic, or transient solvers and under consideration of moving parts, and the connection to the external driver circuit, providing valuable information for the overall performances and specific behavior assessment of the machine.
The radial force density or pressure can be written as:

$$p_{rmp}(\alpha,t)=\frac{1}{2\mu_0}\left[B_{\delta n}^2(\alpha,t)-B_{\delta t}^2(\alpha,t)\right] \quad (1)$$

where $B_{\delta n}$ and $B_{\delta t}$ are the normal and tangential components of the airgap magnetic field density. As the tangential component is much smaller than the normal component of the airgap magnetic field density, the magnetic pressure results as:

$$p_{rmp}(\alpha,t)\approx\frac{B_{\delta n}^2(\alpha,t)}{2\mu_0} \quad (2)$$

The airgap magnetic flux density can be written as:

$$B_{\delta n}(\alpha,t)=\left[B_s(\alpha,t)+B_r(\alpha,t)\right]\cdot\Lambda_\delta(\alpha) \quad (3)$$

with $B_s(\alpha,t)/B_r(\alpha,t)$ the stator/rotor magnetic field density for uniform airgap, as function of angle and time, and $\Lambda_\delta(\alpha)$ the relative permeance of the airgap.

The machine under study is a PMSM with 18 stator slots and 6 rotor poles, excited with rear earth permanent magnets (of Ne-Fe-B type, with 1.15T of remanent flux density and 907kA/m coercivity), iron on both armatures being of M335 type. The motor is running at 3400 RPM with a generated power of 1.2kW. One-layer winding configuration is analyzed for 1mm airgap length, Figure 4.

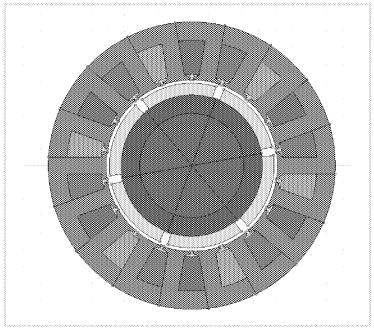

Figure 4: Cross-section of the one-layer winding

The main geometrical data of the machine are given in Table I.

TABLE I
MAIN GEOMETRICAL DATA OF THE STUDIED MACHINES

Parameters	Notation	Value [u.m.]	
Stator outer diameter	D_{so}	0.08539 [m]	
Stator inner diameter	D_{si}	0.051 [m]	
Air gap	δ	0.001 [m]	0.0005 [m]
Stack length	L_s	0.08 [m]	

The radial force distribution along the inner surface of the stator is presented in Figure 5 for both no load and full load operation. The harmonic components of these forces are given in Figure. 6.

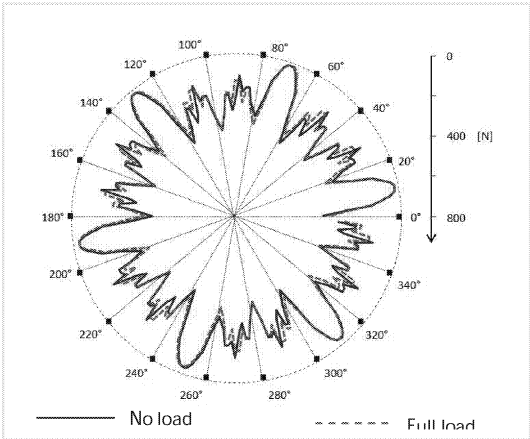

Figure 5: Radial force distribution along the inner surface of the stator for no load and full load

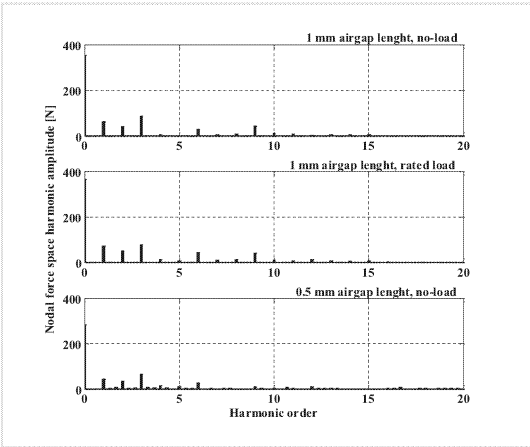

Figure 6: Harmonic content of the radial forces.

After performing the electromagnetic calculation the stator teeth surface and the Maxwell forces are exported to Universal File.

Figure 7 show the Maxwell forces mapped onto the stator surface nodes of a structural 3D mesh at a given moment in time after importing the results from Universal file in LMS Virtual. Lab.

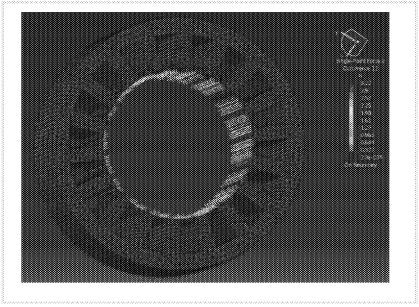

Figure 7: Stator mesh and Jmag forces imported in LMS Virtual.Lab

MULTIBODY ANALYSIS

The LMS Virtual.Lab Motion analysis allows to model and simulate the mechanical systems, to predict component and system loads for use in structural analysis, noise and vibration simulation.
The multibody model start with solid geometry to describe each body, where every part bodies are connected to the others by kinematic joints or force elements to make an assembly. The time-dependent driving constraints and external electromagnetic forces act on the assembly of bodies to make them move. The solution process assembles the bodies, joints, and forces and solves a system of differential-algebraic equations using a variable step numerical integration process. The time-domain results are used to animate the position of all bodies and are also available for plotting.
The motion equations of a generic structural system, in the time-domain, are described in Equation 4:

$$[M]\{\ddot{x}(t)\} + [K]\{\dot{x}(t) + [C]\{x(t)\} = \{F(t)\} \quad (4)$$

where [M], [K] and [C] are the global mass, stiffness and damping matrices, *{x(t)}* is the displacement vector corresponding to the degrees of freedom of the structure, and *{F(t)}* is the vector of excitation forces.

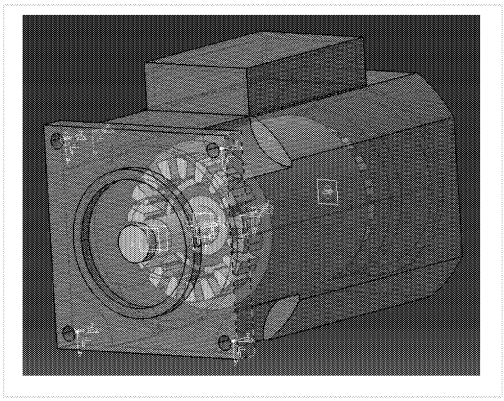

Figure 8: Multibody model

The flexible mode displacement time-histories, also known as modal participation factors, from the Motion results are used as input to the NVH calculations.
In order to evaluate the radiated sound power, the deformation field of the flexible housing must be exported from the multibody analysis in order to be used into a forced response simulation.

This process has the added benefit of capturing the most accurate representation of the body deformation throughout time. To make use of the time-history data in the NVH, it is converted to the frequency domain using the Digital Signal Processing (DSP) feature within LMS Virtual.Lab.
Through FE simulations the deformation field for each node of the model is obtained. Using flexible multibody, the MPFs are used to calculate the displacements at all the nodes. In this manner, the radiated noise can be directly evaluated.

VIBRO-ACOUSTIC ANALYSIS

Forced response is the next step in the dynamic evaluation process. After calculating the normal modes of the electrical motor, the MPF's are mapped to the structural model to compute the vibrations on the housing outer surface.

In Figure 9 the first vibration modes values of the electrical motors are presented.

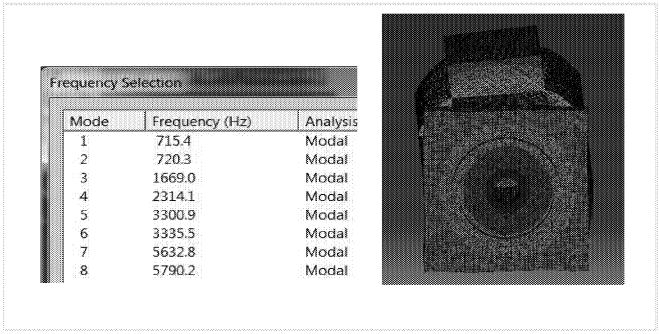

Figure 9: First vibration modes and mode shape at 2314 Hz

To predict noise and vibration behavior under operating conditions a Modal-Based Forced Response analysis was performed. This allows to compute the response of the system for given modal data and given load data. The basic methodology uses modal superposition, which multiplies the mode shape values with the modal participation factors.

In this way the forced response of the system can be written as a superposition of the modes (modal contribution analysis).

When the *Nk* (number of) modes are computed, the FRF's can be written like this:

$$\{H_{syn}(j\omega)\} = \sum_{r=1}^{N_k} \frac{1}{a_r} \frac{\{\psi_r\}\{\psi_r\}^T}{j\omega + \lambda_r} + \frac{1}{a_r^*} \frac{\{\psi_r\}^*\{\psi_r\}^{*T}}{j\omega + \lambda_r^*} \quad (5)$$

...and multiplied with the applied forces

$$\{X(j\omega)\} = [H_{syn}]\{F(j\omega)\} \quad (6)$$

where: {Ψr} is the value of the mode shapes on the output point DOF, $F(j\omega)$ represent the load, a_r represents the modal *a* scale factor of the *r*-th mode.

The modal response functions can then be calculated (7):

$$P_{r,1}(j\omega) = \frac{1}{a_r}\left(\frac{\{\psi_r\}^T}{j\omega - \lambda_r}\right)\{F(j\omega)\}, \quad P_{r,2}(j\omega) = \frac{1}{a_r^*}\left(\frac{\{\psi_r\}^{T*}}{j\omega - \lambda_r^*}\right)\{F(j\omega)\}$$

The forced response of the system can then be written as a superposition of the modes:

$$\{X(j\omega) = \sum_{r=1}^{N_k}\{\psi_r\}P_{r,1}(j\omega) + \sum_{r=1}^{N_k}\{\psi_r\}^* P_{r,2}(j\omega) \quad (8)$$

where $P_r(j\omega)$ indicates how much a particular mode is excited by the particular force.
The physical response $X(j\omega)$ is obtained by combining the modal response with the modal amplitude of the output DOF (and adding this modal contributions for all modes)

$$X(j\omega) = \sum_{i=1}^{N_k} C_r(j\omega) \quad (9)$$

where $C_r(j\omega)$ is the modal contribution function.

For the acoustic calculation the forced response data calculated on structural mesh is transferred on a coarser acoustical mesh to serve as vibration boundary conditions.
The mapping of the vibration data consists of two separate steps:
a). Setting-up the Vibro-Acoustic Mesh Mapping which characterizes the mapping of the data from the Source Mesh to the Target Mesh.
b). Executing the Data Transfer Analysis which actually maps the data.

Figure 7 sketches the FEM acoustic model used for the permanent synchronous motor. As can be seen in the picture, only a couple of FEM elements are needed to cover the distance between the motor surface and a special boundary condition which is applied at the outer surface of the acoustic FEM domain. This special boundary condition represents an Automatically Matched Layer (AML) condition, which is a cutting-edge FEM acoustics technique, a special type of non-reflective boundary condition implemented in LMS Virtual. Lab Acoustics.

The sound prediction method described before is based on the finite element method using AML for exterior radiation (Figure 10).

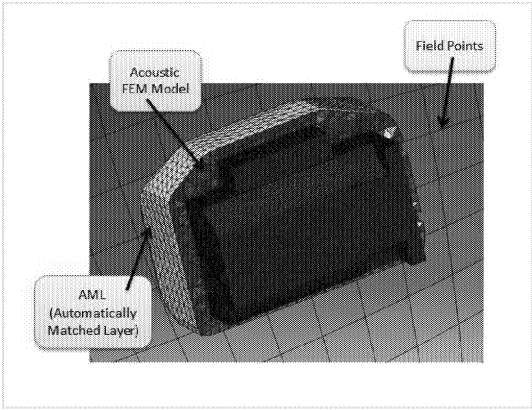

Figure 10: AML model

This method allows the usage of field point meshes which permits the system's response to be visualized at that specific location.

The acoustic radiation can be computed in a fast and efficient way by, equation (10):

$$\nabla^2 p(x, y, z) + k^2 p(x, y, z) = -j\rho_0 \omega q(x, y, z) \quad (10)$$

where p is the acoustic pressure at a point (*x, y, z*) due to a time-harmonic source distribution q at frequency ω, with the wavenumber $k = \omega/c$, c being the speed of sound in the fluid of ρ_0 density.

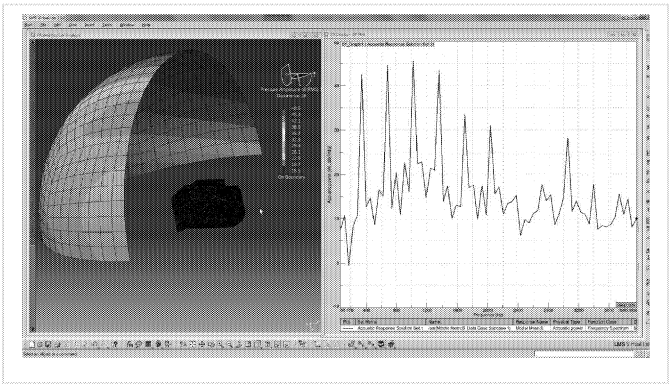

Figure 11: Sound pressure and acoustic power

The amount of noise emitted from a source depends on the acoustic power of that source.

On Figure 11, left side, the acoustic pressure of the simulation case is shown for a spherical field point mesh with 1 m radius. The acoustic power response displayed using a 2D display on the right side is computed with the equation (11).

$$W_t = \sum_{i=1}^{N_{LC}} \sigma_i * W_i \quad (11)$$

where W_t is the total acoustic power, N_{LC} is the number of pseudo load-cases, σ_i are the singular values (Virtual Autopowers) and W_i is the acoustic power for load case *i*.

CONCLUSIONS

The paper presents a multi-physics approach for the noise and vibration analysis of a permanent magnet synchronous rotor machine.

As is illustrates, the vibro-acoustic performance of electric motors are possible to predict, using an electromagnetic and multibody approach. This is possible due to the close connection between Jmag, LMS Virtual.Lab Motion and the NVH analysis solutions, an advanced multi-attribute CAE simulation capability.

For our electrical motor the overall sound power level is 38.14 dB (RMS) and the maximum pressure amplitude 48.5 dB witch belong to the limit values predicted by the IEC 34-9 International Standard, for electrical machines with powers less than 5kW.

ACKNOWLEDGEMENTS

This work was supported by the Romanian Executive Agency for Higher Education, Research, Development and Innovation Funding (UEFISCDI) under the AUTOMOTIVE LOW-NOISE ELECTRICAL MACHINES AND DRIVES OPTIMAL DESIGN AND DEVELOPMENT (ALNEMAD) Joint Applied Research Project (PCCA) in the frame of "Partnerships" projects (PN II – National Plan for Research, Development and Innovation).

REFERENCES

Abaitancei, H.; S. Radu, C. Irimia; C. Husar and M. Grovu. 2015: "Multibody analysis and acoustic simulation for a hydraulic motor", *EAEC-ESFA Bucuresti, European Automotive Congress.*

Aimeng, W.; J. Yihua and W.L. Soong. 2011: "Comparison of Five Topologies for an Interior Permanent-Magnet Machine for a Hybrid Electric Vehicle", *IEEE Trans. on Magnetics, Vol. 47.*

Finken, T. et al. 2008. "Comparison and design of different electrical machine types regarding their applicability in hybrid electrical vehicles", Proc. ICEM.

Langhe, K.D.; J. Anthonis; F. Santos and H. V. Auweraer. 2011: "Multiscale Noise and Vibration models for a Switched Reluctance-based drivetrain for EV and HEV", *JMAG Users Conference in Tokyo.*

Laskaris K. I. and A.G. Kladas. 2010: "Internal Permanent Magnet Motor Design for Electric Vehicle Drive", *IEEE Trans. on Industrial Electronics, Vol. 57.*

Martis, S.M.; D. Fodorean; P.C. Irimia and C.I. Husar. 2014. " Vibroacoustic Behaviour Analysis of a Permanent Magnet *Synchronous Machine for Automotive Applications", International Universities' Power Engineering Conference, UPEC 2014, Cluj.*

Meek, B.; K. D. Langhe and K. Vansant. 2013: "Optimizing the Acoustic Performance of a Switched Reluctance Motor using a combined multi-physics & FEA simulation approach", *JMAG Users Conference in Germany.*

Miyakawa, T.; T. Enomoto, H. Tadayuki and T. Tanimoto. 2011: "Vibration and Noise Analysis of the Motor for an Electric Vehicle", *JMAG Users Conference in Tokyo.*

Vansant K. 2014: "From Tesla to Pascal, a magneto-vibroacoustic analysis linking Flux to LMS Virtual. Lab", Cedrat News, No. 66, June

Zeraoulia, M. et al. 2006. "Electric Motor Drive Selection Issues for HEV Propulsion Systems: A Comparative Study", *IEEE Trans. on Vehicular Technology*, vol. 55, no. 6.

TUNING THE SERVO SYSTEM OF A COIL WIRE ROLLER BY AMESIM

Teodor Costinel Popescu, Cătălin Dumitrescu
Hydraulics and Pneumatics Research Institute
INOE 2000-IHP
40558, Bucharest, Romania
popescu.ihp@fluidas.ro ; dumitrescu.ihp@fluidas.ro

Constantin Călinoiu, Daniela Vasiliu
University POLITEHNICA of Bucharest
POWER ENGINEERING FACULTY
060042, Bucharest, Romania, 6th County
calinoiu@fluid-power.pub.ro ; vasiliu1958@gmail.com

KEYWORDS

Electro hydraulic servo system, numerical simulation, digital controller tuning, coil wire, aluminum wire rolling mill

ABSTRACT

The paper presents a practical engineering problem solved by numerical simulation with AMESIM language. An aluminum wire rolling mill has at the exit a coil wire roller, actuated by an electrohydraulic linear servo system. The speed of the aluminum wire, exiting from the final stage of the mill, has to be correlated both with the roller angular speed, and with the roller axial advancement. Many parameters have to be adjusted in real time: the wire reel speed, the wire diameter, and the number of layers already siting on the roller. Any mistake produced during the wiring process increases the production cost, because the wrong mass coils are melted again. The use of a well-tuned controller allows the eliminating of the different type of mistakes occurring in the process of wiring. The controller delivers the input of the electrohydraulic servo system which axially move the roller according to the other process parameters.

INTRODUCTION

The drive systems of wire reels inside rolling mills have to simultaneously generate rotational movement of the reel that the wire is wrapped around, and a linear movement of the wire reeling device. The dynamic performances of these systems determine, to a large extent, the quality of wire coils delivered to beneficiaries, the reducing of losses caused by melting again the wire which was first improperly reeled, and finally - the efficiency of the rolling mill.
These equipment's are electromechanical systems, based on adjustable speed electric motors and ball screws or hybrid mechanical-electrohydraulic screws, without a speed control loop. They are based on adjustable speed electric motors and speed reducers, but with on-off hydraulic drive systems only. Usually, the reel that the wire is wrapped around has an electromechanical actuation, in both of the above systems. In the first type of system, the reeling device, which moves the wire coming out of the rolling mill linearly along the roller, is actuated by a ball screw. In the second case, a hydraulic drive without control loop is used.
Experience shows that the systems which actuate the reels rise no problem; they provide both sufficient uniformity of the rotational movement, for each layer of reeled wire, and appropriate reduction of rotational speed, when starting each new layer of wire which is to be reeled. The two known types of systems for actuation of the reel head have certain shortcomings relating to correlation with the reel speed, in the first type, or relating to reliability, in the second type.

A wire reel is the terminal point of an aluminum wire production line, Figure 1. It comprises two rollers actuated by turns, by means of a variable speed electric motor and a double output shaft reducer. The wire coming out of the rolling mill is directed through a groove to the roller which is rotating evenly. The constant angular speed value is a function of the diameter of wire which is to be wrapped around the roller, namely: 9.5; 12; 15; 19.3 mm.

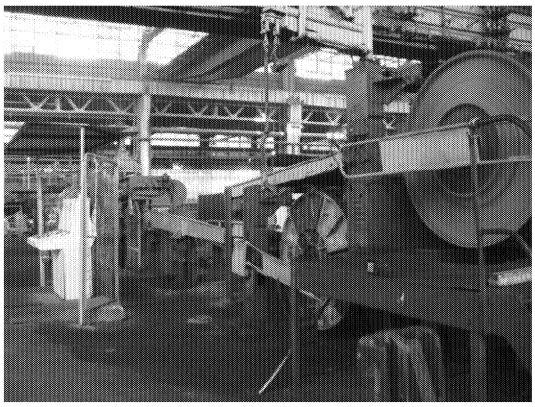

Figure 1: Wire Production Line
(Rear to Front View): Furnace, Rolling Mill, Two-Roller (Top and Bottom) and Two-Reeling Device Reel

The authors of this paper have developed and commissioned an original system for actuation of the reel head, Figure 2, (Popescu et al. 2014; Popescu et al. 2013; Drumea and Blejan 2013) allowing position and speed control by means of electro-hydraulic control loop. Thanks to this system, the quality of wire coils, Figure 3, has increased significantly.

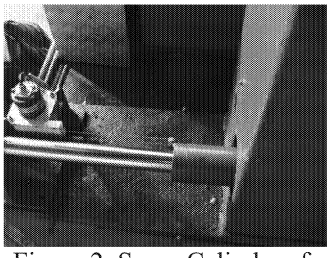

Figure 2: Servo Cylinder of the Reel Head

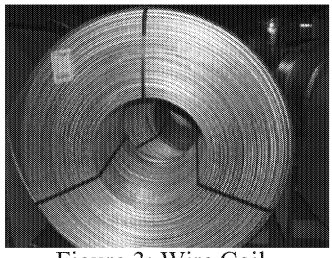

Figure 3: Wire Coil Pulled from the Roller of the Reel and Bundled for Delivery

MATHEMATICAL MODEL OF THE REELING DEVICE

Mathematical model of the rolling mill-wire reel-reel head system

Tangential speed of the wire string:

$$v = \omega \cdot R \qquad (1)$$

Where,
v – Speed of the wire string coming out of the rolling mill [m/s];
ω – Roller angular speed [rad/s];
R – Radius of wire winding around the first line of spires [m].
The tangential speed of the wire string has constant value equal to its speed when coming out of the rolling mill.

Length of the coil spire:

$$l_s = 2 \cdot \pi \cdot R \quad (2)$$

Time required for winding a spire:

$$t_s = \frac{l_s}{v} = \frac{2 \cdot \pi \cdot R}{v} \quad (3)$$

Number of spires in a line:

$$n_{sr} = \frac{L_b}{d} \quad (4)$$

where,
n_{sr} – number of spires in a line;
L_b – coil length [m];
d – wire diameter [m].

Advancement speed of the reeling device:

In order to achieve uniform and compact (one coil spire beside the next) winding the spooler must travel by a distance equal to the wire diameter d in a time t_S.

$$v_d = \frac{d}{t_s} = \frac{d \cdot V}{2 \cdot \pi \cdot R} \quad (5)$$

where,
v_d – spooler speed [m/s].

Diameter of the wire string winding:

If the radius of wire winding around the first line of spires is R, the next line will have the winding radius

$$R_2 = R_1 + d \quad (6)$$

where,
R_1 – radius of wire winding around the first line of spires [m];
R_2 – radius of wire winding around the second line of spires [m].
Since the tangential speed of the wire string should be constant and equal to the speed at which the wire comes out of the rolling mill, it follows that the advancement speed of the spooler is a function depending on the radius R of wire winding and the wire diameter d, according to the relation (5). Each line of coil spires will be achieved at different linear and angular speeds.

Time required for achieving a spire line:

If the coil length is L_b, then the time required for achieving the first line of coil spires is:

$$t_r = \frac{L_b}{v_d} = \frac{L_b \cdot 2 \cdot \pi \cdot R}{d \cdot V} = \frac{n_{sr} \cdot d \cdot 2 \cdot \pi \cdot R}{d \cdot V} = \frac{2 \cdot \pi \cdot R \cdot n_{sr}}{V} \quad (7)$$

Speed of the reeling device required for achieving the "i" spire line:

$$v_{di} = \frac{d}{t_s} = \frac{d \cdot V}{2 \cdot \pi \cdot R_i} \quad (8)$$

where,
R_i – radius of winding the i spire layer [m].

Mathematical model of the hydraulic cylinder

The reel head is actuated by a double-acting bilateral rod hydraulic cylinder. Schematic diagram of the unit directional control valve-hydraulic cylinder is shown in Figure 4.
The fluid flow Q_1 intaken by the cylinder through the directional control valve is calculated by the relation:

$$Q_1 = K \cdot x \cdot \sqrt{(p_s - p_1)} \quad (9)$$

The fluid flow discharged off the cylinder through the directional control valve, Q_2, is calculated by the relation:

$$Q_2 = K \cdot x \cdot \sqrt{(p_2 - p_r)} \quad (10)$$

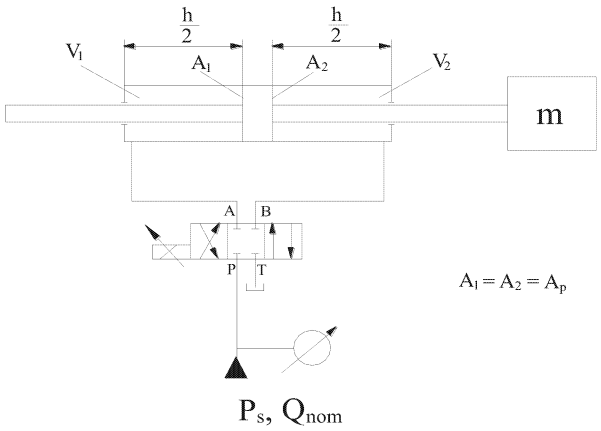

Figure 4: Schematic Diagram of the Unit Hydraulic Directional Control Valve - Hydraulic Cylinder

The continuity equation for the hydraulic cylinder

For the hydraulic drive system shown in Figure 4, when there are established the connections P-A and B-T of the hydraulic directional control valve, we have a cylinder input flow Q_1 and a cylinder output flow Q_2.
The fluid flow entering the hydraulic cylinder chamber, which is connected to the pressure coupling, ensures the flow required for moving the piston, the internal leakage flow, the external leakage flow and also the compressibility flow. Since the fluid pressure in this chamber increases, there occurs compression of the fluid volume, and therefore the flow of compressibility is a flow "consumed" by this chamber. The continuity equation for this chamber takes the form:

$$Q_1 = A_p \cdot \frac{dz}{dt} + c_{ip} \cdot (p_1 - p_2) + c_{ep} \cdot p_1 + \frac{\vartheta_1}{E} \cdot \frac{dp_1}{dt} \quad (11)$$

For the hydraulic cylinder chamber which is connected to the tank the fluid flow generated by the movement of the piston, the fluid flow due to internal leakage and the compressibility flow ensure the external leakage flow and the flow discharged from the cylinder chamber. Regarding the compressibility flow, two observations have to be made:
a. Since the pressure in the cylinder chamber decreases, there occurs fluid expansion, and therefore the flow of compressibility is a flow "generated" by this chamber.
b. In the continuity equation this flow must be entered with the sign (-) because the pressure variation, which is negative, also has the sign (-).
The continuity equation for this chamber takes the form:

$$A_p \cdot \frac{dz}{dt} + c_{ip} \cdot (p_1 - p_2) - \frac{\vartheta_2}{E} \cdot \frac{dp_2}{dt} = Q_2 + c_{ep} \cdot p_2 \quad (12)$$

The piston motion equation

$$A \cdot (p_1 - p_2) = m \cdot \ddot{z} + K_{fv} \cdot \dot{z} + K_e \cdot z + F_0 \quad (13)$$

If we denote:
- Pressure drop across the hydraulic cylinder:

$$P = p_1 - p_2 \quad (14)$$

- Average flow consumed by the motor:

$$Q = \frac{Q_1 + Q_2}{2} \quad (15)$$

- Overall leakage coefficient:

$$K_s = c_{pi} + 0{,}5c_{pe} \qquad (16)$$

- Total volume of the cylinder:

$$V_1 = V_2 = \frac{V_t}{2} \qquad (17)$$

Then, from the relations (11) and (12), it follows:

$$Q = A_p \cdot \frac{dz}{dt} + K_s \cdot P + \frac{V_t}{4E} \cdot \frac{dP}{dt} \qquad (18)$$

and the relation (13) turns into:

$$A_p \cdot P = m \cdot \ddot{z} + K_{fv} \cdot \dot{z} + K_e \cdot z + F_0 \qquad (19)$$

By applying the Laplace transform to the relations (18) and (19), we get:

$$Q = A_p \cdot Z \cdot s + K_s \cdot P + \frac{V_t}{4E} \cdot P \cdot s \qquad (20)$$

$$A_p P = m \cdot Z \cdot s^2 + K_{fv} \cdot Z \cdot s + K_e \cdot Z + F_0 \qquad (21)$$

From the relations (20) and (21), by eliminating the variable "P", we obtain the relations:

$$Q = A_p \cdot Z \cdot s + \left(K_s + \frac{V_t}{4E} \cdot s\right)\left(\frac{F_0}{A_p} + \frac{m \cdot s^2 + K_{fv} \cdot s + K_e}{A_p} Z\right) \qquad (22)$$

$$Q - \frac{F_0}{A_p}\left(K_s + \frac{V_t}{4E} s\right) = Z\left[A_p s + \frac{1}{A_p}\left(K_s + \frac{V_t}{4E} s\right)\left(ms^2 + K_{fv} \cdot s + K_e\right)\right] \qquad (23)$$

In terms of stability of the hydraulic cylinder, the worst situation occurs when the disruptive force "F_0" and the resistant force, elastic nature, "K_e·Z" have zero values. In this case the transfer function of the hydraulic motor has the form:

$$H(s) = \frac{Z(s)}{Q(s)} = \frac{K_m}{s\left(\frac{s^2}{\omega_m^2} + \frac{2 \cdot \zeta}{\omega_m} \cdot s + 1\right)} \qquad (24)$$

where,

$$K_m = \frac{A_p}{A_p^2 + K_s \cdot K_{fv}} \qquad (25)$$

is the amplification factor,

$$\omega_m = \sqrt{\frac{4 \cdot E \cdot (A_p^2 + K_s \cdot K_{fv})}{m \cdot V_t}} \qquad (26)$$

is the natural pulsation, and

$$\zeta_m = \frac{K_s \cdot m + \frac{K_{fv} \cdot V_t}{4 \cdot E}}{\sqrt{\frac{m \cdot V_t}{E} \cdot (A_p^2 + K_s \cdot K_{fv})}} \qquad (27)$$

is the damping factor.

Mathematical model of linear speed servo system of the reel head

A linear speed servo system, Figure 5, is an automated system which has as the input parameter an electrical signal, and as the output parameter – a linear speed. It is used in drive systems which require constant speed regardless of load variations, within certain limits, from the hydraulic cylinder rod.

A linear speed servo system has the following component parts: hydraulic cylinder; electro hydraulic amplifier (servo valve or proportional directional control valve); servo controller (comparator + electronic compensator); linear speed transducer.

We present further the equations describing the stationary behavior of the speed servo system components.

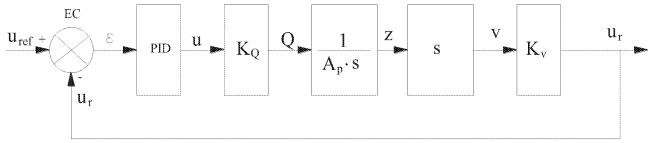

Figure 5: Schematic Diagram of the Linear Speed Servo System

The comparator equation

$$\varepsilon = U_{ref} - u_r \qquad (28)$$

where : ε = error; U_{ref} = input signal (the reference); u_r = output signal (the response).

The electronic compensator equation

The electronic compensator (the controller) is a PI type compensator whose tuning law is shown by the relation:

$$u = K_p \cdot \left(\varepsilon(t) + \frac{1}{T_i}\int \varepsilon(t)dt\right) \qquad (29)$$

where: u = control signal (voltage); K_p - proportional amplification factor; T_i = integration time (constant).

The compensator transfer function is:

$$H_{PI}(s) = \frac{U(s)}{\varepsilon(s)} = K_p\left(1 + \frac{1}{T_i \cdot s}\right) \qquad (30)$$

Static characteristic of the proportional directional control valve

The static characteristic of the proportional directional control valve is the variation of flow passing through the device according to the control signal, namely:

$$Q = K_Q \cdot u \qquad (31)$$

Where K_Q is the flow amplification factor of the proportional directional control valve.

The continuity equation characteristic of the hydraulic cylinder

The flow supplied by the proportional directional control valve is fully consumed by the hydraulic cylinder, and the continuity equation is in the form:

$$Q = A_p \frac{dz}{dt} \qquad (31)$$

Where A_p = piston area; z = piston movement.

The transfer function of the hydraulic cylinder is in the form:

$$H_{CH}(s) = \frac{Z(s)}{Q(s)} = \frac{1}{A_p \cdot s} \qquad (32)$$

The transfer function of the speed transducer

The speed transducer has as the input parameter the movement of cylinder rod, and as the output parameter a speed.

$$V = \frac{dz}{dt} \qquad (32)$$

Or, by applying the Laplace transform

$$V(s) = Z(s) \cdot s \qquad (33)$$

we obtain the transfer function

$$H_{TV}(s) = \frac{V(s)}{Z(s)} = s \qquad (34)$$

Static characteristic of the speed transducer

$$u_r = K_V \cdot V \qquad (35)$$

To obtain the transfer function of the servo system there is determined the transfer function by the forward path and the closed-loop transfer function.

SIMULATION OF THE REEL HEAD DYNAMICS

Diagram of the simulation model developed in AMESim (www.plm.automation.siemens.; AMESIM R13. User Manual) is shown in Figure 6.

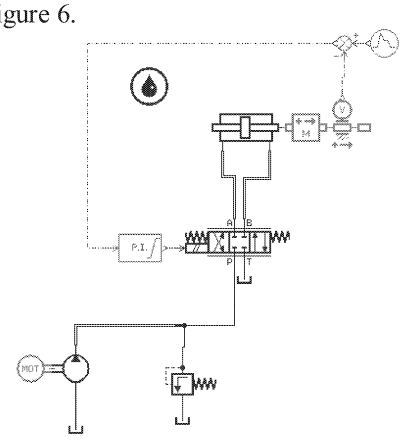

Figure 6: AMESim Simulation Model for the Reel Head

The parameters of the simulation model are: opening pressure of the safety valve = 60 bar; pump capacity = 3.65 cm^3/rev; pump drive rotational speed = 1400 rev/min; cylinder piston diameter = 65 mm; piston rod diameter = 48 mm; piston stroke = 1000 mm; length of pipes between the cylinder and directional control valve = 2x20m; equivalent mobile mass to the cylinder rod (body) = 10kg; speed transducer sensitivity = 10 V/m/s; type of controller = PI (proportional integrative); the amplification factor of the proportional component = 1; the amplification factor of the integral component = 20; rated control voltage of the proportional directional control valve = 10V; characteristic of the proportional directional control valve = strictly proportional.
The simulation results are shown in Figures 7 to 17.

When exciting the servo system with the step type reference signal shown in Figure 7, the variation over time of piston stroke and speed, for two successive wire layers wrapped around the roller of the reel are shown in Figure 8 and Figure 9.

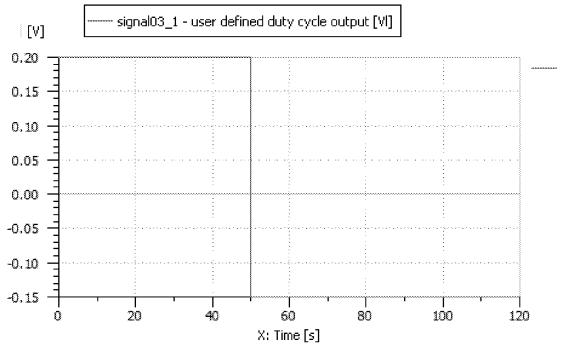

Figure 7: Shape of the Reference Step Signal

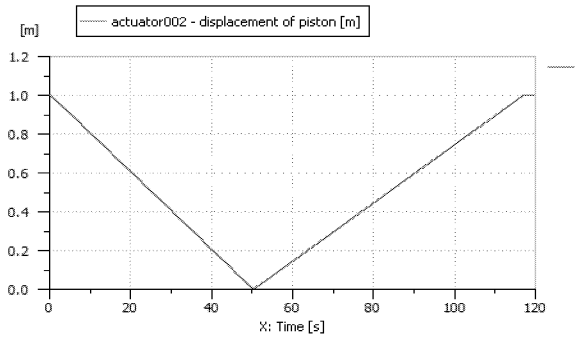

Figure 8: Dynamics of the Piston Forward and Reverse Stroke

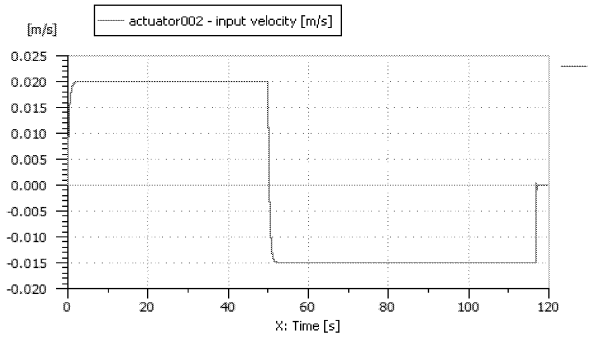

Figure 9: Variation of the Piston Speed along the Forward and Reverse Stroke

The error of piston speed compared to the prescribed value occurs when changing its movement direction that is at the beginning at each new wire layer wrapped around the roller, Figure 10.

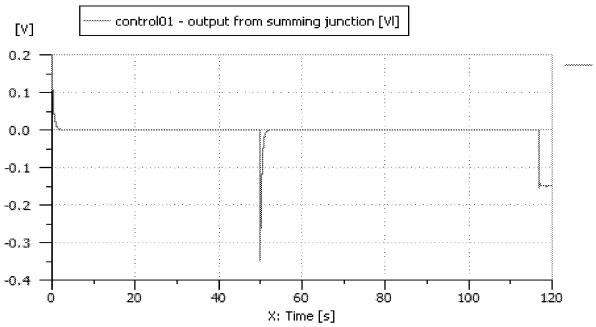

Figure 10: Shape of the Speed Error Signal

The output signal of the PI controller, namely the command of the proportional directional control valve, has the shape in Figure 11.

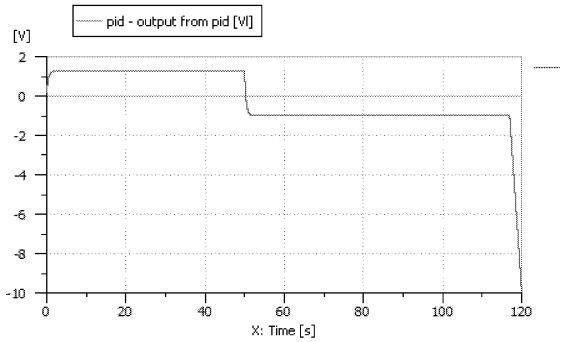

Figure 11: Shape of the Control Signal

The variation over time of the flow rate consumed by the hydraulic cylinder, measured at P port of the directional control valve, is shown in Figure 12.

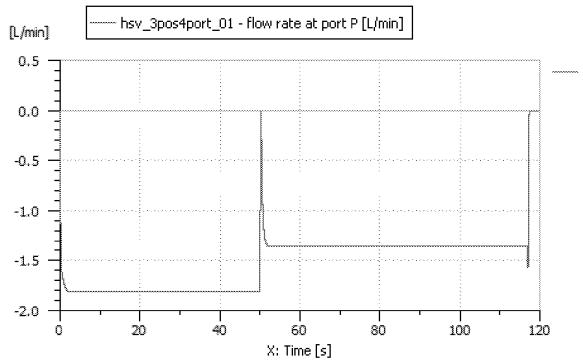

Figure 12: Fluid Flow Consumed by the Hydraulic Cylinder

To simulate wrapping around the roller of four successive wire layers the servo system is excited with a speed step signal, with decreasing amplitude, in the shape of the one in Figure13.

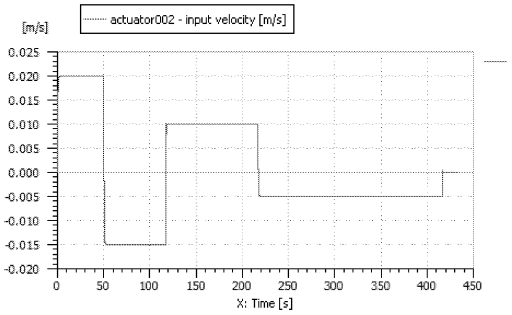

Figure 13: Reference Signal for Wrapping Four Wire Layers

The variation over time of the piston stroke in the cylinder which actuates the reel head, when wrapping four successive wire layers, is shown in Figure 14.

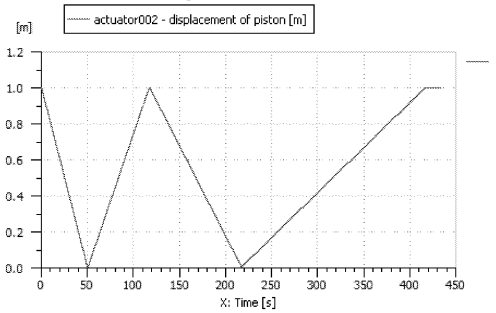

Figure 14: Variation of the Piston Stroke while Wrapping Four Successive Wire Layers

The influence of the integral component amplification factor, *Ki,* on the system dynamics has been exemplified by running the model simultaneously for three different values *Ki*=10, *Ki*=20, *Ki*=30.

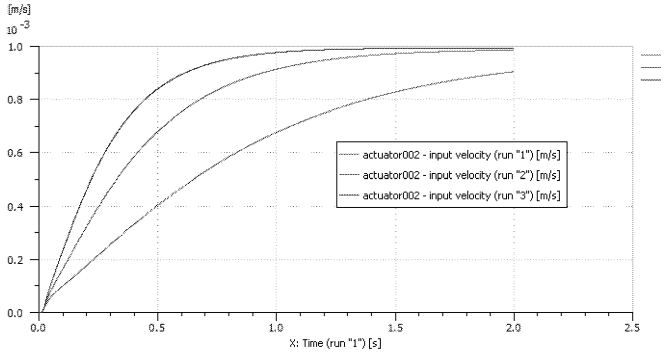

Figure 15: The Response to a Step Signal of 10^{-3}m/s

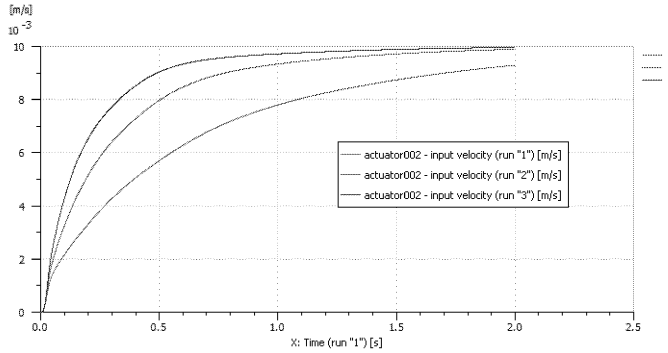

Figure 16: The Response to a Step Signal of 10^{-2}m/s

By analyzing the response of the servo system to a step signal with an amplitude of 10^{-3} m/s, Figure 15, a step signal with an amplitude of 10^{-2} m/s, Figure 16 and a sine wave signal, Figure 17, it is found that the optimum value is *Ki*=20 (median curve).

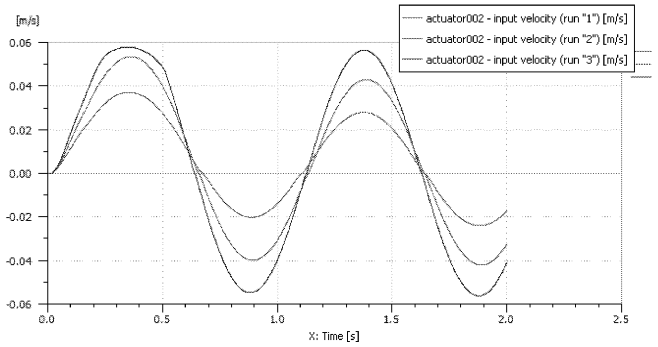

Figure 17: The Response to a Sine Wave Signal

THE DRIVE DIAGRAM OF THE REELING DEVICE

The schematic drive diagram of the reel head, shown in Figure 18, has been developed based on the AMESim numerical simulation model. This schematic diagram was at the basis of developing the actuation, control and adjustment system of the reel head.

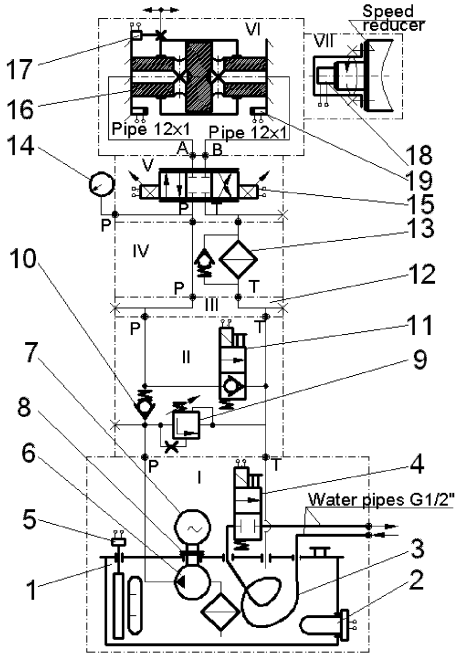

Figure 18: Schematic Drive Diagram of the Reel Head

The schematic diagram in Figure 18 only refers to drive of a single reel head. Nevertheless, it can be extended to two reel heads, keeping the same hydraulic unit to power both hydraulic cylinders, as they work almost continuously in sequence, except for a short sequence of time (at the end of wrapping around one roller and start of wrapping around the other roller).

For the practical case considered by the authors, the structure of the diagram, developed on seven levels (**I**...**VII**), is as follows: **1**- oil tank, fitted with tight cover, level indicator, filling and ventilation opening, drain plug, with $V_{max.}$= 30 l and $V_{effective}$=22 l; **2** - oil heating resistor, with N=1330 W; **3**- winding tube for cooling the water inside the copper 14x1 pipe; **4**- normally closed electro valve, G1/2", Δp_{max}= 6 bar, supply voltage 24 V dc; **5**- temperature sensor Pt 100; **6**- gear pump, capacity 3.65 cm^3/rev, maximum pressure 250 bar, inlet filter; **7**- electric motor, 220 V, single phase, 0.55 kW, 1400 rev/min; **8**- grip mechanical coupling; **9**- pressure control valve 0...60 bar; **10**- check valve, opening pressure 1 bar; **11**- 2/2 hydraulic directional control valve, normally closed, operated electrically and manually, which protects the pump at starting. **12**- intermediate plate with role in fastening and mounting the pumping unit; **13**- return filter, filtration fineness 10µm, equipped with bypass valve; **14** - glycerin filled pressure gauge, measurement range 0...100 bar; **15**- hydraulic proportional directional control valve, 4/3, Dn6, closed center; **16**- hydraulic cylinder, bilateral fixed rod and mobile liner, $Ø_{piston}$ = 65 mm; $Ø_{rod}$ = 48 mm; Stroke = 870 mm; **17**- cable position transducer, for monitoring and control of hydraulic cylinder speed; **18**- rotational speed transducer of winding machine roller; **19**- end of stroke signaling devices, controlling the change in direction of hydraulic cylinder movement.

CONCLUSIONS

Mathematical modelling and numerical simulation (Akers et al.2006; Jelali and Kroll) have cut down the time required to develop the prototype of a drive, control and adjustment system of the reel head of a wire reel.

When commissioning such a control and adjustment system the time required to correlate the speed of the reel head with the reel rotational speed, the speed of the wire leaving the rolling mill and the wire diameter is at least 15 days, 8 hours per day. During this time the rolling mill is off the current production cycle, which is 3 shifts of 8 hours per day. By adjusting the parameters of the system to the values obtained at the simulation model, the commissioning time has been reduced to 8 hours.

The system has been tested under real operating conditions in an aluminum wire rolling mill existing at ALRO Slatina, Romania. The mill has been set into operation and there have been produced six coils of wire: three of them having a diameter of 9.5 mm and other three coils having a diameter of 12 mm. After each coil produced the mill has been stopped and the settings of the system controlling the reel head have been adjusted.

The system working parameters, monitored and measured on the prototype, Figure 19, prove good estimation of the results obtained by running the simulation model, Figure 20. To this end, there have been required only three consecutive adjustments of the over-settings of the system controlling the reel head, at each diameter of wire wrapped on the reel.

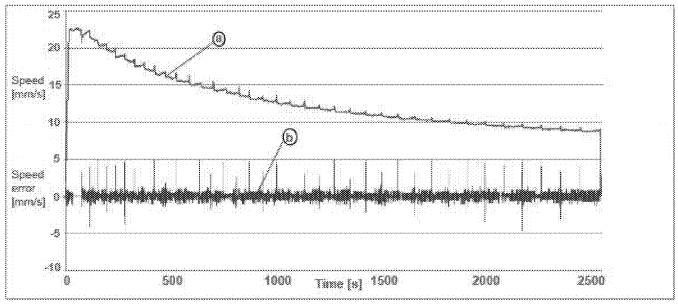

Figure 19: Variation of Prescribed Speed (a) and Variation of Real Speed Error (b) of the Reel Head during the Winding of One Spool

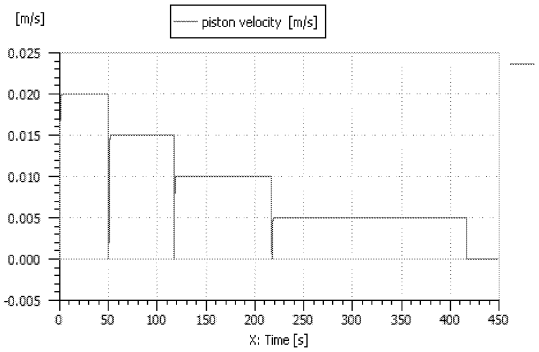

Figure 20: Variation of the Reeling Device Velocity while Wrapping Four Successive Wire Layers

ACKNOWLEDGEMENTS

The authors are grateful for all the technical support received from the LMS COMPANY (now - a member of SIEMENS Group of Companies) in different manners: free licenses, free technical training for the research team members, and many other facilities.

REFERENCES

Popescu, T.C.; Blejan, M.; Vasiliu, D. 2014. „Innovative Solution of Energy Efficiency and Management for the Production of Aluminum Wires". DOI:10.5593/SGEM2014/B41/S17.041. 14th International Multidisciplinary Scientific GeoConference SGEM 2014, *Conference Proceedings*, ISBN 978-619-7105-15-5 / ISSN 1314-2704, June 19-25, 2014, Book 4, Vol. 1, 315-322 pp.

Popescu, T.C.; Blejan, M; Lepădatu, I. 2013. „Electrohydraulic Servomechanism for Driving the Reels of Coil Winding Machines specific to Wire Rolling Mills". "HIDRAULICA" (No. 3/2013) - *Magazine of Hydraulics, Pneumatics, Tribology, Ecology, Sensorics, Mechatronics,* ISSN 1453 – 7303.

Drumea, A.; Blejan, M. 2013. "Design, implementation and testing of an electrohydraulic system for automated winding machine for aluminum wire rods", International Conference on Electronics, Computers and Artificial Intelligence (ECAI), 2013, D.O.I.:10.1109/ECAI.2013.6636184, 1-4 pp.

*** AMESIM R13. User Manual. Leuven, 2013.

Akers, A.; Gassman, M.; Smith, R. 2006. „Hydraulic Power System Analysis (Fluid Power and Control)". ISBN 9780824799564 - CAT# DK2324. Series: Fluid Power and Control

Jelali, M.; Kroll, A. 2003. „Hydraulic Servo-systems. Modelling, Identification and Control". Advances in Industrial Control. ISSN: 1430-9491.

WEB REFERENCES

http://www.plm.automation.siemens.com/en_us/products/lms/imagine-lab/index.shtml

BIOGRAPHY

TEODOR COSTINEL POPESCU graduated from the Faculty of Installations' Engineering, within the Institute of Civil Engineering in Bucharest, class of 1978, and he also graduated from the Faculty of Mechanical Engineering, within the Polytechnic Institute of Bucharest, class of 1989. In 2008 he was granted a PhD in fluid power systems, at the Faculty of Power Engineering within "POLITEHNICA" University of Bucharest, with the distinction "CUM LAUDE". From 1983 until now he has been working in the Hydraulics and Pneumatics Research Institute of Bucharest, in the field of control and adjustment hydraulic actuation systems.

HEATER SIMULATION

NUMERICAL SIMULATION AND EXPERIMENTAL VALIDATION OF AN AUTOMOTIVE ADDITIONAL HEATER

Rădoi Florin, Sorohan Ştefan, Vasiliu Nicolae, Călinoiu Constantin, Cojocaru-Greblea Toma
University POLITEHNICA of Bucharest
313, Splaiul Independentei, Sector 6
RO 060042 Bucharest, Romania
E-mail: vasiliu1946@gmail.com

KEYWORDS
Mathematical modeling, thermal and structural analysis, infrared thermography, auxiliary automotive heating system

ABSTRACT

An automotive auxiliary heater is a complex thermal system used in vehicles to improve engine startup and ensure a warm environment in passenger compartment when the car is operating in extreme cold conditions.
This paper presents our team's efforts to develop a reliable steady state thermal and thermo-elastic simulation model for a heater. For this purpose a detailed finite elements model was developed and calibrated based on laboratory experimental results, and available information about the power balance of the device. The simulation model was created using CAE software Catia v5 r18, and ANSYS Workbench v15. The FE model consists of the main parts of the assembly, including a description of thermal and mechanical loads, and contact interaction between its parts and external boundary conditions. The experimental part of the research was conducted in the laboratory on a special designed test stand. The test stand can operate the heater completely autonomous, while making data logging with the aid of National Instruments PXI system. Infrared thermography was done using FLIR ThermaCam PM350 camera. The test stand can be very useful for the future development of another types of heater suited to middle class passengers cars.

INTRODUCTION

This paper presents an important part of the research team's efforts to develop a functional automotive auxiliary heater prototype designed to work in extreme cold areas of the world. The research is focused on developing a reliable thermal and thermo-elastic simulation model for a heater. For this purpose, a detailed 3D model was developed using Catia v5. The model was further analyzed using finite elements model with ANSYS and the results compared to the experimental data obtained in the laboratory.
For experimental purposes, we have developed an integrated test stand, which is able to operate the heater autonomous, while measuring and logging all the functional parameters.

A work cycle of the heater starts with the user command from an on-board or remote controller. The heater fan (blower) "washes" the burner with fresh air. Than the fuel is aspirated by a solenoid volumetric pump from the petrol tank and sent to the combustion chamber of the heater. The fuel-air mixture is ignited by a glow plug and the combustion chamber starts to warm up. A centrifugal circulating pump moves the cooling agent along a closed loop: from the auxiliary heater to the car heater's heat exchanger, then into the engine and back to the auxiliary heater. The car heater's heat exchanger send the heat into the cabin via the car's fan. The cooling agent is also introduced in the car engine and warms it up as well.

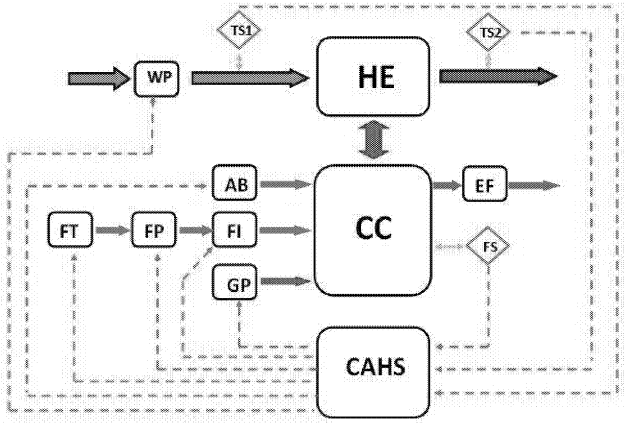

Figure 1: General diagram of an Automotive Auxiliary Heater

The main components of a heater are: WP – water pump, HE – heat exchanger, CC – combustion chamber, AB – air blower, EF – exhaust gases filter, FT – fuel tank, FP – fuel pump, FI – fuel injector, GP – glow plug, CAHS – controller for automotive heating systems.
The system is actively monitored by minimum 3 sensors: TS1 – temperature sensor 1 (cold water sensor), TS2 – temperature sensor 2 (hot water sensor), FS – flame sensor.

The biggest part of the thermal energy produced by the combustion process is transported with the exhaust gases and transferred to the heat exchanger boundaries of the combustion chamber by different heat transfer mechanisms: radiation, forced convection and conduction.

The initial hypothesis of the simulation is centered on the theoretical power balance of the heater.Net heating value of light oil (or diesel) is around of 36 MJ/l. If the fuel consumption in the water heating system is around of 0.65 l/h, results an average net generation power from fuel burning around of 6.5 kW. The desired heat exchanger power is 4.3 kW, so the effective power of the heat exchanger is estimated to be around of 66 %.

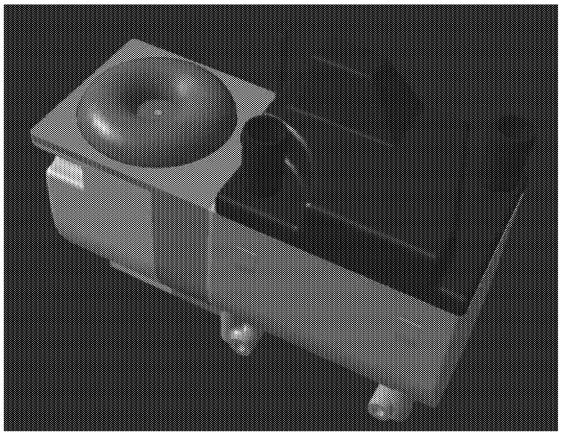

Figure 2: CAD model of typical auxiliary water heater system

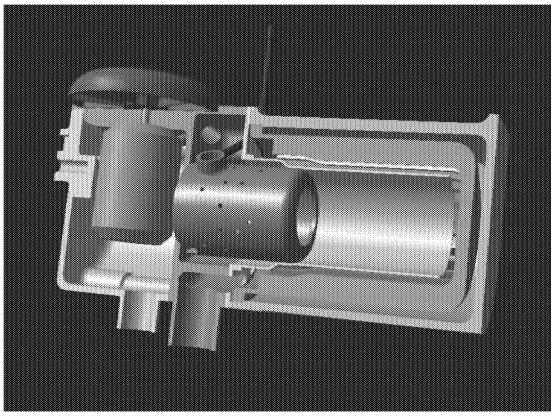

Figure 3: Cut-away view of typical auxiliary water heater

FINITE ELEMENTS MODELLING

The target of the finite element analysis was to get the temperature distribution and maximum stresses generated in the components of the water heater system. Because the measuring of the temperatures is a very complex task and the CFD analysis is not yet available for the first phase of the design a simplified analysis was done. The complete temperature distribution in structural components can be obtained using an adequate finite element model in thermal analysis and neglecting the structural effects. Then, using the obtained temperature distribution as loads (Fig. 4) a sequentially multi-physics coupled analysis may be developed (Ansys 2004).

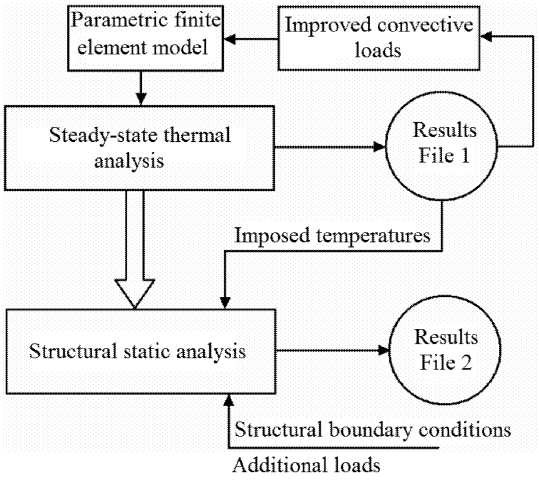

Figure 4: Sequential coupling of thermal and structural problem

Due to some unknowns concerning the real boundary conditions in the thermal analysis, the steady state thermal analysis has a supplementary loop for convective load improvement to fit the imposed thermal boundary condition for partial validate the thermic balance.

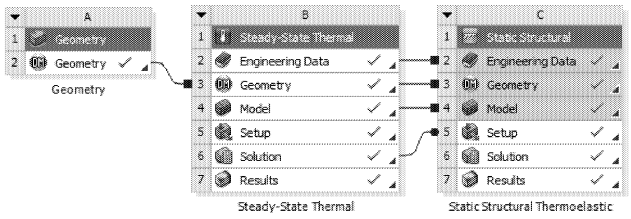

Figure 5: Workflow of the sequentially coupled physics analysis

Except the thermal conductivity and Young's modulus which were considered as temperature functions, the remaining properties were considered constant. For Poisson it were considered a value of 0.28 for steel and 0.33 for aluminum alloy; also, for thermal expansion coefficient it were considered a value of $17*10^{-6}$ 1/K for refractory steel and $23*10^{-6}$ 1/K for aluminum alloy.

MESH DESCRIPTION

Due to irregular shape of the parts, we have adopted for meshing a tetrahedral finite element type, Solid87 for thermal analysis and Solid187 for structural analysis. A total of 205491 of nodes and 112178 finite elements result after the automatic mesh using maximum relevance of the mesh algorithm (Fig. 6). Some parts were further refined using a 2 mm element size criterion. The same mesh was used for thermal and for structural analysis.

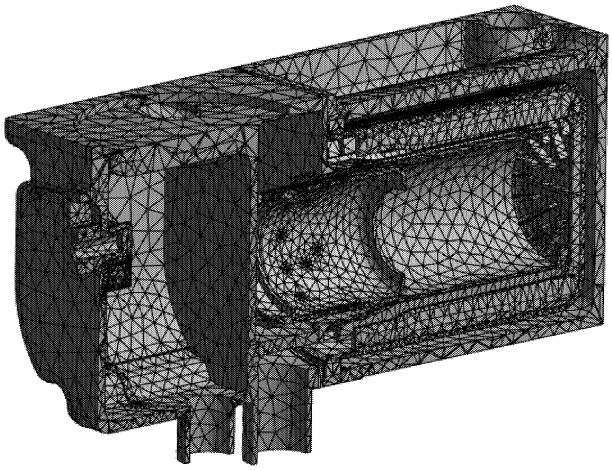

Figure 6: Mesh of the finite element model using ten nodes tetrahedral elements

Thermal interactions between parts were modeled by perfect non thermal resistence contact elements, whereas the structural contact elements were considered according to real interactions, i.e. bonded or no separation linear contacts were introduced between involved surfaces.

THERMAL BOUNDARY CONDITIONS

The thermal loads were applied iteratively on surfaces, with the updated values mentioned in Table 1. The model was iterated until the desired result was obtained - the heat exchange power for heat exchanger around of 4 kW.

Table 1. Convective boundary conditions

Part	Location	h $\left[\frac{W}{m^2 °C}\right]$	T_B [°C]
1-Blower cover	Interior	45	0
	Exterior	25	0
2-Ports housing	Interior near motor	45	0
	Exterior	25	0
	To burner	50	0
	To outlet	100	400
3-Heat exchange housing	Exterior to air	25	0
	Interior to water	1500	100
4-Heat exchange body	Exterior to water	1500	100
	Interior to combustion gases	150	700
5-Flame guide	Exterior to admission air	50	0
	Interior to flame	200	720
6-Burner tube	Interior to admission air	50	0
	Interior to combustion gases	150	700
	Exterior to combustion gases	150	700
	Flange to outlet	100	500

THERMAL RESULTS

For the boundary conditions from Table 1 it was obtained a power of 4.53 kW for convective heat transfer between combustion gases and heat exchanger body and 4.16 kW for convective heat transfer between heat transfer medium (water) and heat exchanger body. The temperature distribution in structural parts varies between 77 ºC and 700 ºC (Fig. 7).

STATIC STRUCTURAL RESULTS

The reaction forces were very small (max 32 N) due to adequate fixing the model. The total displacement distribution for thermo-elastic analysis for all components is presented in figure 9 where the legend is not uniform because the maximum displacement is inside of the heater. One can see where one fixed point on three direction was chosen (dark blue area).

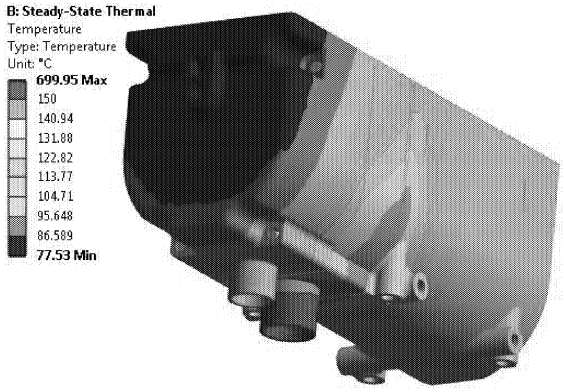

Figure 7: Temperature distribution on all model. (Maximum temperature is inside; here the top legend is not uniform, it was modified for improving clarity)

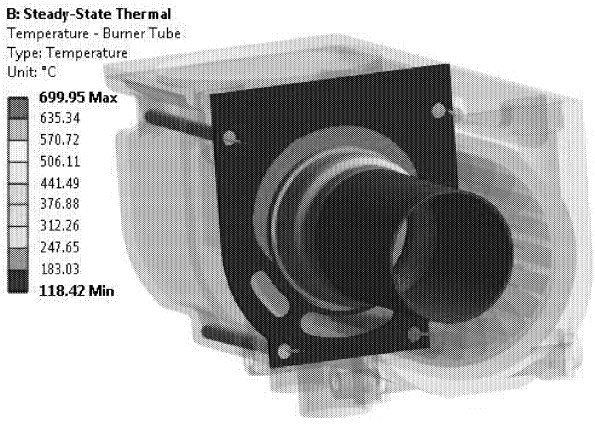

Figure 8: Temperature distribution on the burning tube

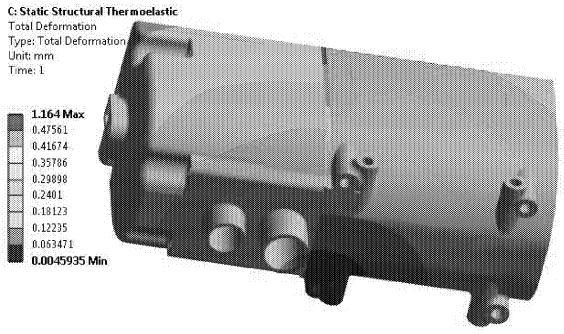

Figure 9: Total displacement distribution for thermo-elastic analysis

The axial deformation of the burner tube is around of 1 mm (Fig. 10) because the maximum temperature in the cylindrical tube is high.

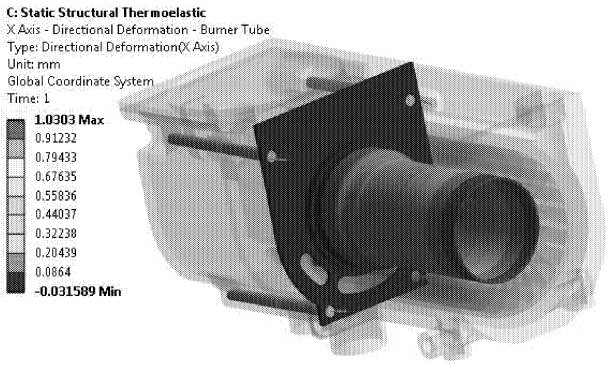

Figure 10: Axial displacements for burner tube

The maximum von Mises stress in the heat exchanger body is not very large, only some picks of 103 MPa can be observed, whereas in the burning tube, due to the high gradient of the temperature, the maximum von Mises stress is around of 306 MPa (Fig. 11).

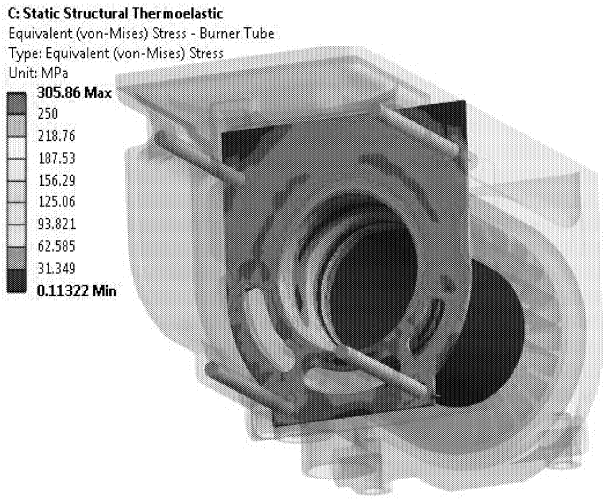

Figure 11: Von Mises stress distribution for burner's tube

TEST STAND AND EXPERIMENTAL PROCEDURES

The test stand was designed to operate the heater and continuous monitor and log all the functional parameters: electrical power consumption, fuel consumption, water and air temperatures, fan speed, exhaust gas composition, surface temperature, etc. The block diagram of the test stand is presented in figure 12, where the main components are: SIS – heater; DE – electric pannel; SAD – NI data aquisition sistem; R- power converter; B- 12 V car battery; CEP –electronic precision scale; RC – fuel reservoir; PC – fuel pump; MEcc – DC electric motor; RAT – cooling water tank; PA- water pump; FGA – exhaust gases filter; AG – exhaust gases analyser (TESTO); SG – gas probe. The following sensors are used in the test bench: Tcc – DC sensor; Tpa – air pressure sensor; Tda – air flow sensor; Tpc – fuel pressure sensor; Ttg – exhaust gases temperature sensor; Tp – pressure sensor; Td – flow sensor; Ttr – water inlet temperature sensor; Ttc – water outlet temperature sensor.

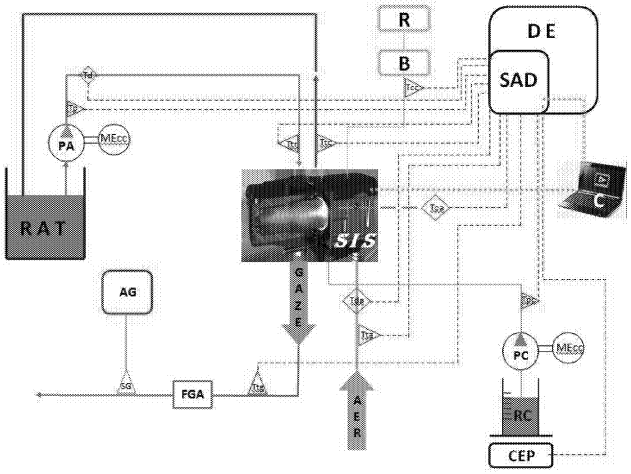

Figure 12: Test stand block diagram

One of the heating system analyzed is Hydronic II DS4 produced by Eberspacher Germany. The following image presents another type of heater mounted on the bench.

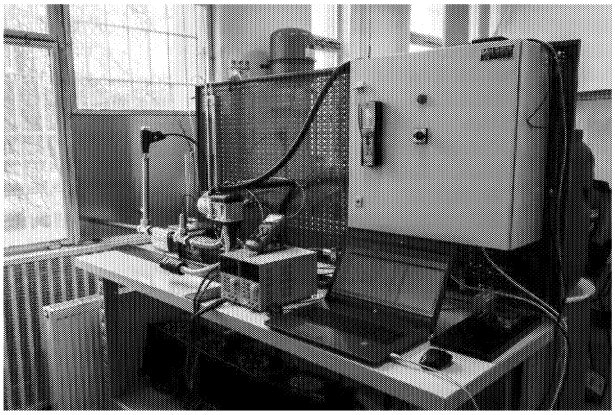

Figure 13: Automotive auxiliary heater test stand

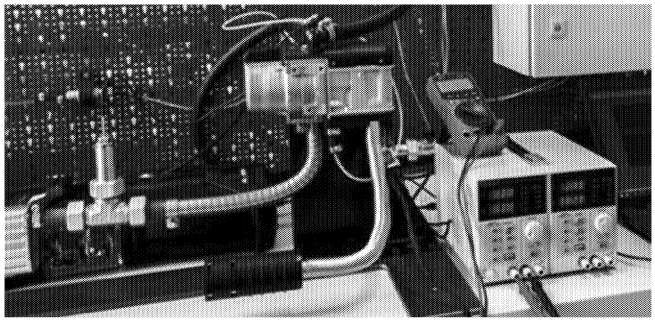

Figure 14: Typical heater mounted on the test stand (Webasto type)

The infrared analysis was done using a FLIR - ThermaCAM PM350 camera that was operated from the computer by a specialized person. The first step of the testing procedure is to identify several key points of interest for measurement. Afterwards the heater is turned on, and operated until it reach nominal working regime (usually, around 2 to 3 minutes). For each measurement point are taken six recordings, and the most conclusive results have been presented below.

EXPERIMENTAL RESULTS

A selection of infrared images are presented below.

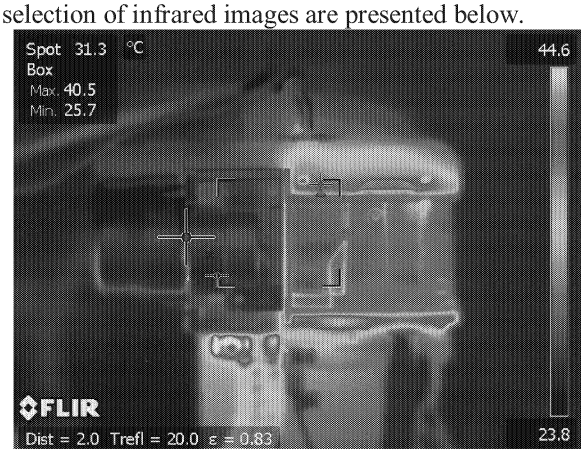

Figure 15: General temperature distribution on the heater

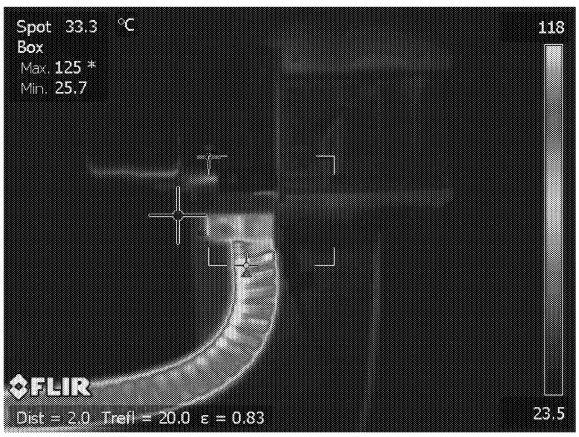

Figure 16: Temperature distribution on the exhaust of the heater

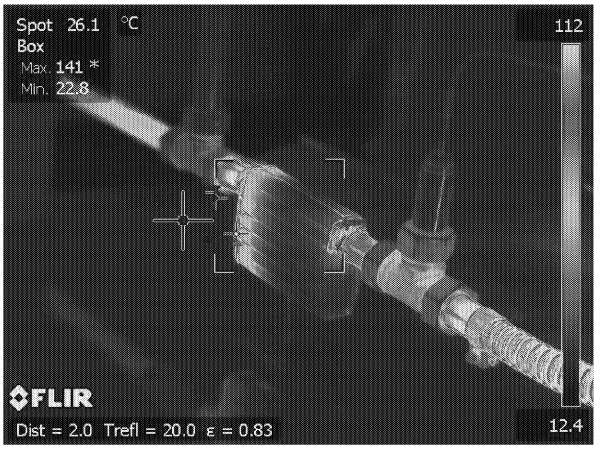

Figure 17: Temperature distribution on the muffler, exhaust gases temperature and TESTO© exhaust gases composition sensor

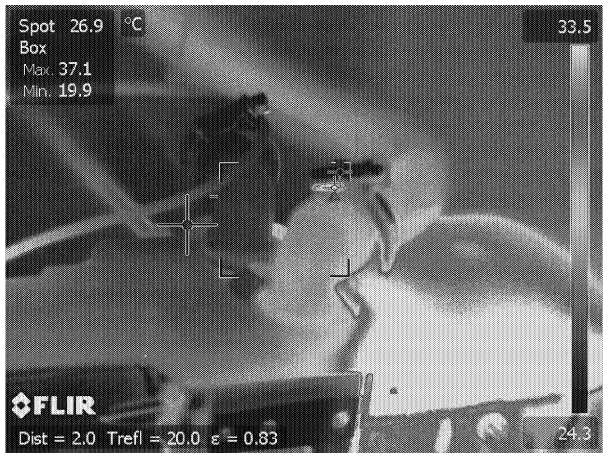

Figure 18: Temperature distribution on the water connection ports

CONCLUSIONS

The experiments validate our simulation results, which now can be used as a base for mechanical and thermal design of a new original and improved automotive auxiliary heater.

Based on this temperature distribution, the stress distribution in the model is effortless to obtain. In the future a more detailed experimental thermal analysis of the interior components of the heater will be necessary, in order to further optimize heat transfer quoeficients. At this stage, important results were obtained only by careful trials of different thermal boundary condition from the literature until the desired power output was reached (Jonathan et al. 2007).

Finite element modeling and simulation is a very simple and effective procedure for determining temperature distribution in a water heating system and the obtained results are in accordance with the current literature and experimental results.

REFERENCES

***ANSYS Coupled-Field Analysis Guide. 2004. ANSYS, Inc., Canonsburg.

Ashby, M. 2005. *Material Selection in Mechanical Design.* Butterworth-Heinemann.

Baukal, C. E. jr. 2000. *Heat Transfer in Industrial Combustion.* CRC, pp 65-117.

Cook, R. D., Malkus, D. S., Plesha, M. E. 1989. Concepts and Applications of Finite Element Analysis, 3rd ed., John Wiley & Sons, University of Wisconsin-Madison.

Gülder, O. L. 1986. Flame temperature estimation of conventional and future jet fuels. *J. Eng. Gas Turbine Power*, *108*, 376–380.

Heywood, J. B. 1988. "Internal combustion engine fundamentals", New York: McGraw-Hill.

Illán, F., Alarcón, M., 2010. "Numerical analysis of combustion and transient heat transfer processes in a two-stroke SI engine", Applied Thermal Engineering vol. 30, 2469-2475.

Incropera, F. P., DeWitt, D. P. 2002. *Introduction to Heat Transfer*, Fourth Edition, Wiley.

Jafari, A., Hannani, S. K. 2006. "Effect of fuel and engine operational characteristics on the heat loss from combustion chamber surfaces of SI engines", Int. Communications in Heat and Mass Transfer vol. 33, pp. 122– 134.

Kays, W. M., Crawford. M. E. 2005. *Convective heat and Mass Transfer* McGraw-Hill.

Lefbvre, A. H., Ballal, D. R. 2010. *Gas Turbine Combustion - Alternative Fuels and Emissions*, 3rd ed. CRC Press: Boca Raton, FL, USA.

Matarazzo, S. and Laget, H. 2011. *Modelling of the Heat Transfer in a Gas Turbine Liner Combustor*, MCS 7, Chia Laguna, Cagliari, Sardinia, Italy, September 11-15.

Serth, R.W. 2007. "Process Heat Transfer Principles and Applications", Elsevier, Amsterdam.

Strakey, P. A., Eggnspieler, G. 2010. Development and validation of a thickened flame modeling approach for large eddy simulation of premixed combustion. *J. Eng. Gas Turbine Power*, *132*, 1–9.

Tuediger, G. Heat exchanger of an auxiliary heater. 2005. US Patent 6 932 151 B2.

Jonathan, Y., Douglas, Th., Faccone, P.A. 2007. Vehicle heater and controls here for. US Patent 7 270 098 B2.

WEB REFERENCES

www.webasto.com
www.parkingheater.com
www.eberspaecher.com
www.ansys.com

BIOGRAPHIES

FLORIN RADOI received a Bachelor degree in Automotive Engineering (2011), and a M.Sc. in Advanced Hydraulics and Pneumatics Systems, both from University POLITEHNICA of Bucharest. He started to work at Parker Hannifin since early college, and now is serving as application engineer in the field of complex hydraulics and pneumatics automation systems. He is also Ph.D. candidate within UPB, where he is developing R&D activity in the field of automotive auxiliary heating systems.

ŞTEFAN SOROHAN received the M.Sc. degree in Mechanical Engineering, in the Transportation Faculty, Railway Systems from the University POLITEHNICA of Bucharest in 1989. He became a Ph.D. in Finite Element Model Reduction in 2001, and now he is full professor at Strength of Materials Department within the same university. His main activity consist in finite element modeling of structural, thermal and multiphysics problems.

NICOLAE VASILIU graduated in Hydropower Engineering from University POLITEHNICA of Bucharest in 1969. He became a Ph.D. in Fluid Mechanics after a research stages in Ghent State University and Von Karman Institute from Bruxelles. He became state professor in 1994 and a member of the Romanian Technical Science Academy in 2008. He was always involved in solving complex concurrent engineering problems in fluid power systems.

CONSTANTIN CALINOIU graduated in Hydropower Engineering from University POLITEHNICA of Bucharest in 1975. In 1980, he became a member of the Hydraulic Laboratory from the Romanian Aerospace Institute. In 1998, he became Ph.D. and associated professor in the Fluid Power Laboratory from U.P.B. He is working mainly in modeling, simulation, and identification of the hydraulic and electro hydraulic control systems.

TOMA COJOCARU - GREBLEA graduated in Automotive Engineering (1988) and a M.Sc. in Expertise of Materials (2013), both from University POLITEHNICA of Bucharest. He has a rich experience in the automotive engineering field, working for car dealers and motor insurance activity in Romania. He developed good computer skills during a long stage in IT companies. Now he is Ph.D. student within U.P.B., developing different hydraulic steering systems models.

A NEW GENERATION OF CONTROLLERS FOR AUTOMOTIVE WATER HEATING APPLICATIONS

Vasiliu Nicolae, Călinoiu Constantin, Daniela Vasiliu, Rădoi Florin, Cojocaru Greblea Toma
University POLITEHNICA of Bucharest
313 Splaiul Independentei, Sector 6
RO 060042 Bucharest, Romania
E-mail: vasiliu1946@gmail.com

KEYWORDS
Automotive auxiliary parking heater, microcontroller, low price

ABSTRACT

A "**C**ontroller for **A**utomotive **H**eating **S**ystems" (CAHS) is an essential element for any auxiliary heating system. The controller has to provide enough computing power to control and monitor all the active components of the heater, while being able to communicate with other car systems via on-board CAN bus. In addition, the CAHS must receive user commands through on-board control panel or wireless (via Wi-Fi, GSM, and Bluetooth).

INTRODUCTION

This paper presents the activities developed in order to design, build and test a prototype controller for automotive auxiliary heating system having a low price. Based on an extensive study over existing heating systems, the authors developed the following general functional diagram of the heater (Figure1).

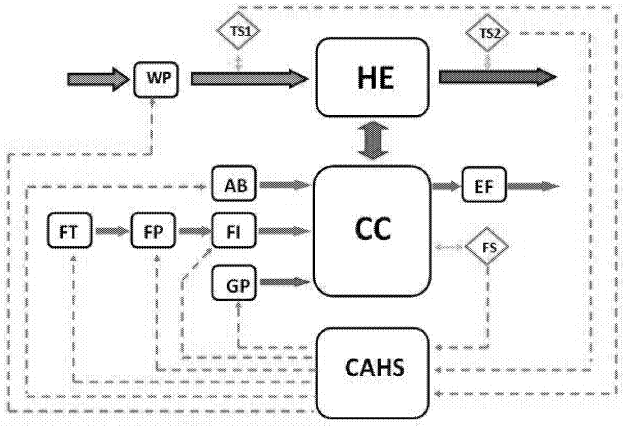

Figure 1. Structural diagram of an Automotive Auxiliary Heater

The main components of a heater are: WP – water (cooling) pump, HE – heat exchanger, CC – combustion chamber, AB – air blower (fan/compressor), EF – exhaust gases muffler, FT – fuel tank, FP – fuel pump, FI – fuel injector, GP – glow pin, CAHS – controller. The system is continuously monitored by minimum 3 sensors: TS1 – temperature sensor 1 (cold water sensor), TS2 – temperature sensor 2 (hot water sensor), FS – flame sensor. Optional, the heater can be monitored by mass airflow sensor, water flow sensor, knocking sensor, and exhaust gases composition sensor (not represented on the diagram).

The critical task of the CAHS is to read the information from all this sensors and control the operational components of the heater in order to obtain maximum heating power, with highest fuel efficiency, safety and low emissions. In order to reach this task, the heater has three different operational phases for start-up, stable operation and shut down, each of them with different control algorithms and procedures.

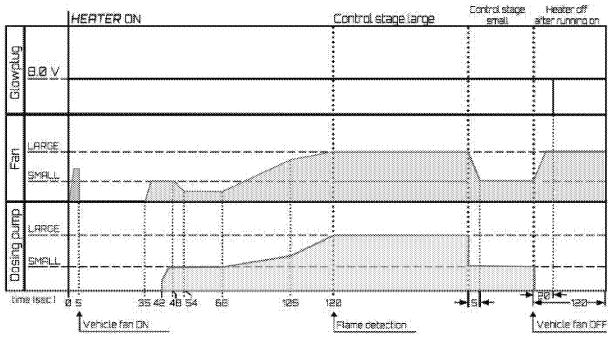

Figure 2. Standard work cycle of a commercial heater

GENERAL ARCHITECTURE OF CAHS

The control board is built around a **dsPIC33FJ128GP804** 16-bit digital signal controller produced by Microchip Technology (Figures 3 and 4). This is a 44 pin, 40MHz microcontroller, with 128 Kb program flash memory, and 16 Kb RAM. The CAHS was designed to control the AHS in wide and extreme variety of situations. The key aspects taken into account in its design are reliability and efficiency. The digital signal controller (DSC) represents the main system component. It is designed around a powerful arithmetic logic unit (ALU) necessary to perform the algorithm for control and self-diagnose of the CAHS. The DSC taken into account has a series of key peripherals to permit to interface it with the exterior environment: Analog to digital controller (ADC), digital to analog controller (DAC), pulse width modulators (PWM), asynchronous serial communication module (UART), CAN bus module, general inputs and outputs (GPIO). The elements around the DSC are reduced to a minimum,

keeping only essential ones: N-MOS power transistors, anti-aliasing filters between sensors and the ADC, CAN and USB transceiver, voltage regulators and p-MOS decoupling transistor for dynamic power consumption.

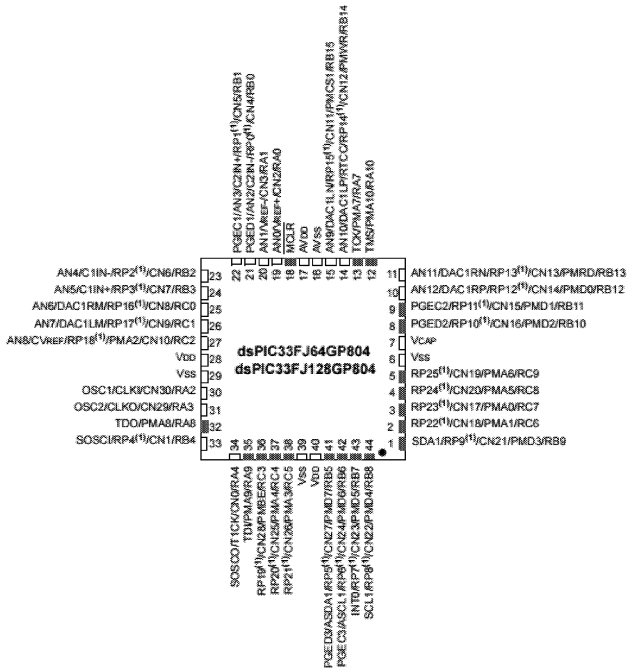

Figure 3. Pin diagram of dsPIC33FJ128GP804 microcontroller

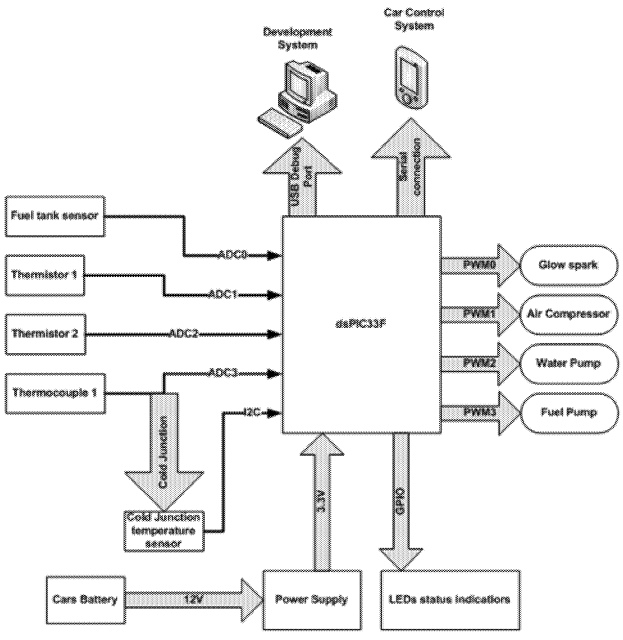

Figure 4. General block diagram of CAHS

Inputs available on the prototype controller are the following (Figure 5, 6):
-Analogue control of the cooling liquid temperature (potentiometer);
-Serial asynchronous bus (UART) to allow control from a digital interface;
-CAN interface, to allow connectivity to the cars electronic control system;
-Low temperature sensors;
-High temperature sensor, to measure the temperature inside the burning chamber and to detect combustion;
-Fuel sensor in tank;
-Self-diagnose inputs, used to determine is different systems block or sensors are working properly.
Outputs:
-High current PWM for: water pump, air blower, fuel pump, glow plug (pin) etc;
-USB connection to diagnose or set internal parameters;
-Auxiliary outputs for self-diagnose purpose.

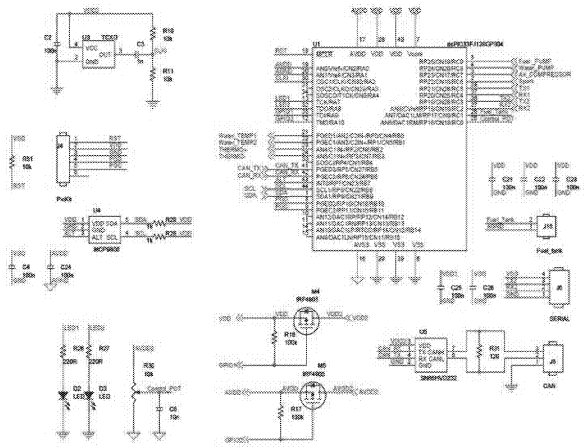

Figure 5: Main DSC diagram

.

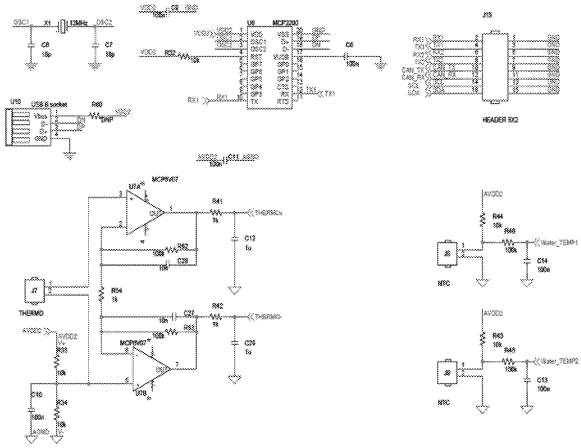

Figure 6: Inputs and USB connection diagram

.

Hardware structure enables dynamic control of power consumption in various situations. The controller has three sections: two digital and one analog. To minimize energy consumption, one digital and one analog section are alternatively powered from the power supply, while only power section and the digital surveillance mode are activated. Once the system is ready to run, the cooling agent temperature is maintained within the specified limits

according to the engine specifications, and the electric control module will begin to monitor the system until at least one condition to stop the fuel supply is fulfilled.

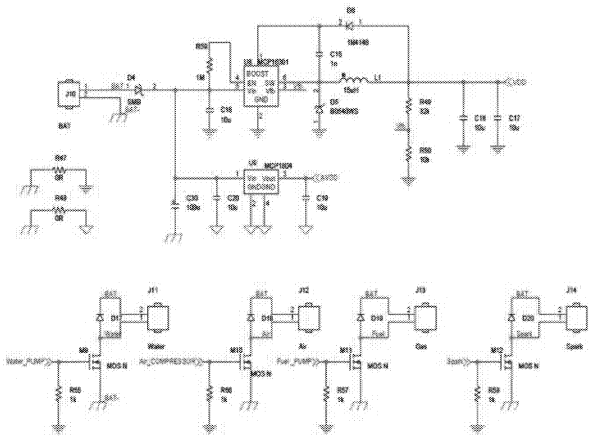

Figure 7: Outputs wiring diagram

INTEGRATION OF THE PROTOTYPE CONTROLLER ON EXPERIMENTAL STAND

For experimental researches and validation, a prototype controller was developed (Figure 8). The module was extensively tested in the laboratory on existing heaters. For experimental purposes a specialized test stand was developed. The stand is able to operate the heater completely autonomous while monitoring and data log all the functional parameters. On experimental mode, the prototype controller is able to control the heater manually, according to live commands received from a laboratory operator. This facility was very useful for experimental identification of various components of the heater (for example - blower characteristics). The commands are sent from a PC through a serial USB connection to the controller. For this purpose, a graphical interface was developed using LabVIEW programming environment.

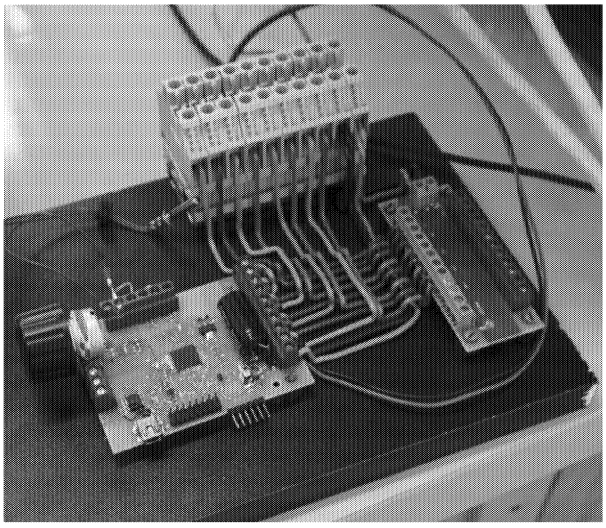

Figure 8: Prototype controller integrated on existing heater platform of a test bench

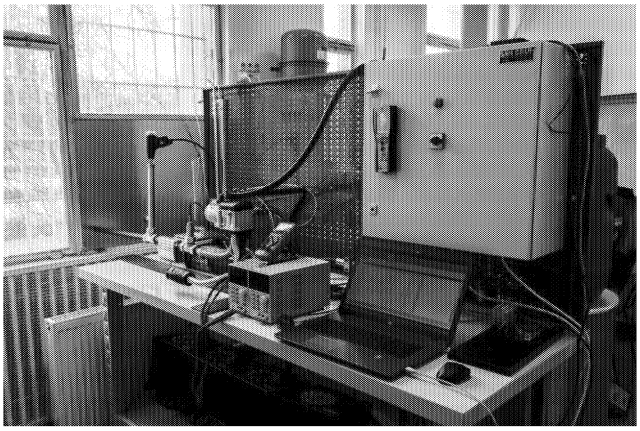

Figure 9: Experimental test bench for auxiliary heaters

.

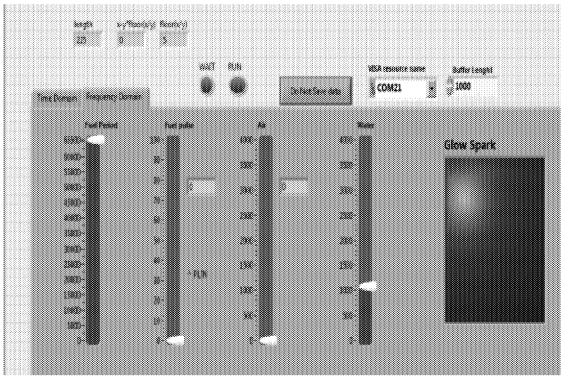

Figure 10. LabVIEW measurement controller interface

.

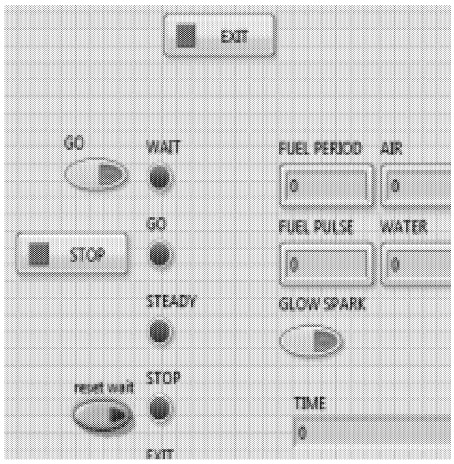

Figure 11. LabVIEW controller interface

EXPERIMENTAL RESULTS

The variations of the main operational parameters of the heater, controlled with the new CAHS are presented in the following graphics. These were obtained with the controller integrated on a commercial standard heater. The start and the stop operating periods (Fig. 12 and 13) are dominated by special variation of the main operational parameters: glow plug current [A] fuel pump current [A] air blower current [A] water pump current [A], and airflow [m^3/h].

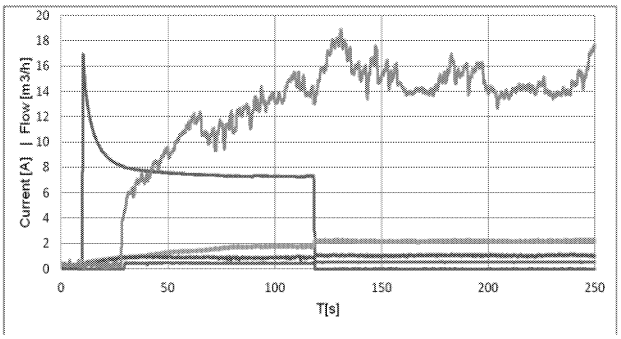

Figure 12: Main operational parameters during start-up and nominal working regime

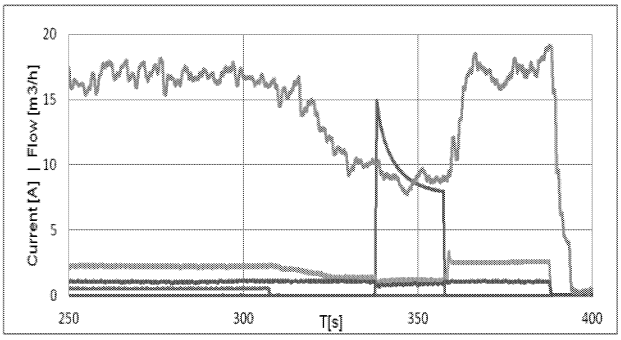

Figure 13. Operational parameters during end of nominal regime and stop

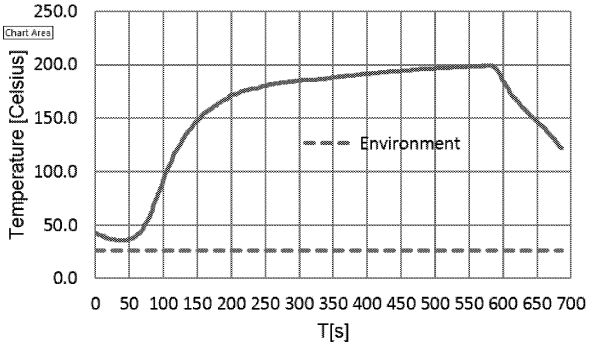

Figure 14: Exhaust gases temperature during a cycle

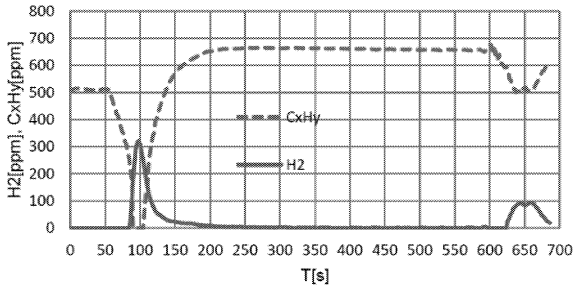

Figure 15: Hydrocarbons and Hydrogen emissions during a cycle

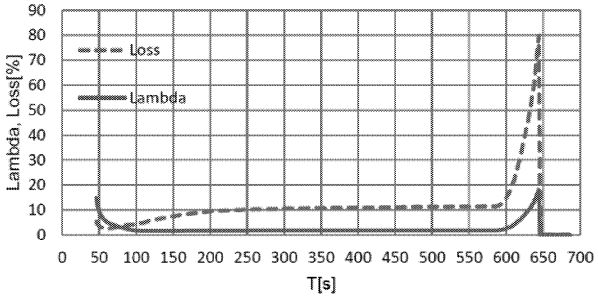

Figure 16: Evolutions of λ and loss during a cycle

The following diagrams present the behavior of a commercial water heater driven by the new microcontroller.

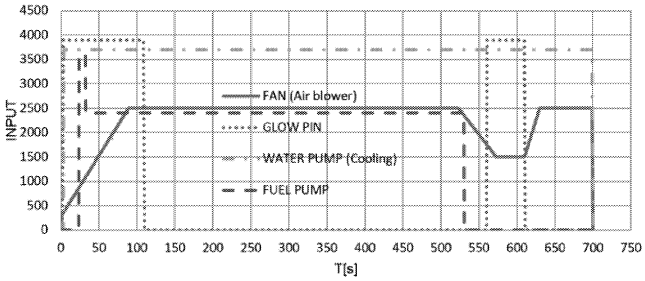

Figure 17: Control inputs for an operating cycles

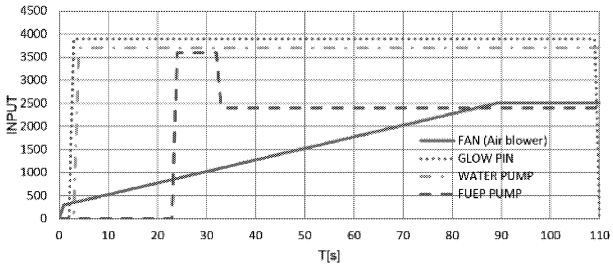

Figure 18: Control inputs for the starting phase

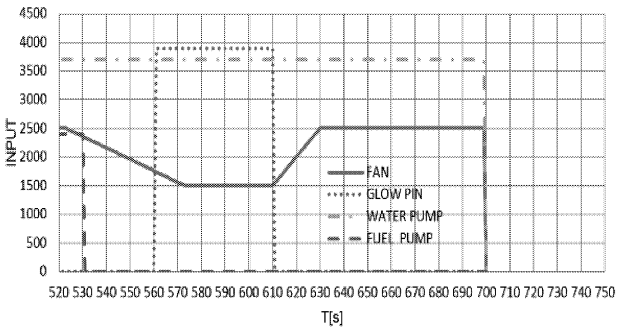

Figure 19: Control inputs for the final phase

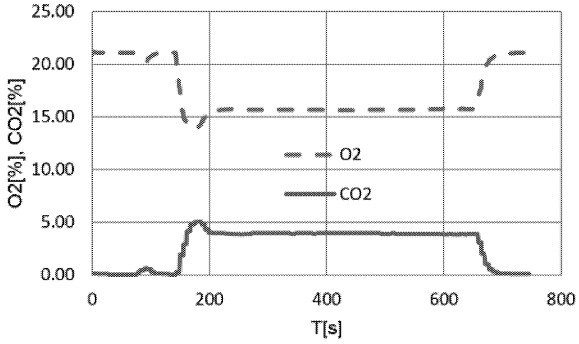

Figure 20: Oxygen and carbon dioxide variation in a typical operating cycle

.

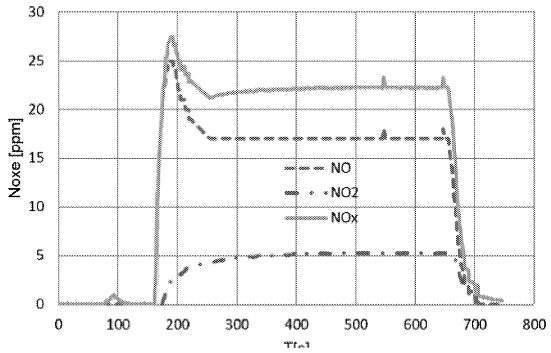

Figure 21: NO, NO_2 and NOx produced by the heater in a typical operating cycle

CONCLUSIONS

The research efforts of the team led to a new high performance prototype controller validated through rigorous experimental research. Intensive thermal numerical simulations were performed with ANSYS based on the examples of (Sorohan 2014). The new controller is more flexible, offers multiple communication options and can easily be integrated through CAN bus on any car on the road today. On the economical side, an estimated serial production cost for 100.000 pcs/year is around 3 Euro, much lower than any other existing alternatives on the market.

REFERENCES

Sorohan, St., *Applications of Finite Element Analysis*, POLITECHNICA PRESS HOUSE, Bucharest, 2014.
ANSYS 14, Thermal Analysis Guide, 2011 SAS IP, Inc.

WEB REFERENCES

www.webasto.com
www.parkingheater.com
www.eberspaecher.com
www.ansys.com
http://www.engineeringtoolbox.com/
http://www.engineeringtoolbox.com/
http://www.buehlermotor.com/
http://www.robotshop.com/
http://www.ereplacementparts.com/
http://1025880.en.makepolo.com/products/
http://leisonmotor.en.alibaba.com/product/
http://kmclh70.motors-biz.com/
http://www.conrad.de/ce/de/product/
http://www.lihaomotor.com/
http://news.directindustry.com/

ACKNOWLEDGEMENTS

The work was partially funded by the Sectorial Operational Program Human Resources Development 2007-2013 of the Ministry of European Funds through the Financial Agreement POSDRU/159/1.5/S/134398.
The whole research was funded through the POSCCE project, Code SMIS 50069, financing national contract P05003/204271/2014-2015.

BIOGRAPHIES

CONSTANTIN CALINOIU graduated in Hydropower Engineering from University POLITEHNICA of Bucharest in 1975. In 1980, he became a member of the Hydraulic Laboratory from the Romanian Aerospace Institute. In 1998, he became Ph.D. and associated professor in the Fluid Power Laboratory from U.P.B. He is working mainly in modeling, simulation, and identification of the hydraulic and electro hydraulic control systems.

DANIELA VASILIU graduated in mechanical engineering in 1981 and prepared the Ph.D. thesis in the field of the numerical simulation of the hydrostatic transmissions. She is currently professor in the Department of Hydraulics, Hydraulic Machines and Environmental Engineering, head of Fluid Power Laboratory of the University POLITEHNICA of Bucharest with works in the field of modeling, simulation, and experimental identification of the electro hydraulic control systems.

FLORIN RADOI received a Bachelor degree in Automotive Engineering (2011), and a M.Sc. in Advanced Hydraulics and Pneumatics Systems, both from University POLITEHNICA of Bucharest. He started to work at Parker Hannifin since early college, and now is serving as application engineer in the field of complex hydraulics and pneumatics automation systems. He is also Ph.D. candidate within UPB, where he is developing R&D activity in the field of automotive auxiliary heating systems.

TOMA COJOCARU - GREBLEA graduated in Automotive Engineering (1988) and a M.Sc. in Expertise of Materials (2013), both from University POLITEHNICA of Bucharest. Has a rich experience in the automotive engineering field, working for car dealers and motor insurance activity in Romania. He developed good computer skills during a long stage in IT companies. He is working as Ph.D. candidate within U.P.B., developing different hydraulic steering systems for mobile equipment.

SOLAR ENERGY SIMULATION

A DIRECT METHOD FOR SIMULATION AND DESIGN OF A FLAT-PLATE TYPE SOLAR COLLECTOR FOR WATER HEATING

Robert R.M. Neacsu
Adrian Ciocanea
Department of Hydraulics, Hydraulic Machines and Environmental Engineering,
Power Engineering Faculty, University Politehnica of Bucharest,
313 Spl. Independentei, 060042, Bucharest, Romania
Email:adrian.ciocanea@upb.ro

KEYWORDS
Energy, solar flat-collector, thermodynamics, numerical solution simulation, design.

ABSTRACT

An operative simulation algorithm for design and efficiency assessment of a flat-plate solar collector for water heating is proposed. In order to ensure the reliability of the theoretical model, testing was accomplished and the thermal yields have been compared. Good agreement was obtained for a case study where a basic geometry for the absorber plate was considered. A simple and accurate method was used for numerically solving the time dependent heat transfer equation. Thermal behavior of the absorber plate, and water temperature variation were obtained. Simulation by using the proposed operative method, performed at a large amount of data for various materials and dimensions for absorber, solar radiation and water inlet temperature, provides appropriate dimensions for the collectors, the thermal efficiency, and reducing the cost in prototype construction and testing.

INTRODUCTION

For the solar water heating systems described in literature (Ramlow and Nutz 2010; Thirugnanasambandam et al. 2010; James and James 2010), a large amount of studies are available concerning various specific issues. Basically reports on the collectors behavior are available for: natural circulation of the liquid (passive systems) (Jaisankar 2009; Ntsaluba et al. 1997; Mertol 1981), forced flow, driven by a pump (active system) (Razika et al. 2014; Yan et al. 2013; Afif 1997), structures with or without tank/heat exchanger and storage (Singh et al 2016; Buonomano et al. 2013; Bădescu 2008). An effective design for solar water heating systems, provide maximum efficiency and low cost to the end user, especially for large systems. Designing the solar collectors for water heating requires the appropriate sizing of different components, based on the predicted solar radiation and hot water demand.
As concerning certain studied issues as the tube arrangement, the collector position, pressure losses, flow distribution in the pipe, influence of buoyancy etc. a relevant number of reports have provided conclusions on the collector's design and efficiency. Studies revealed that the efficiency of flat-solar collectors with riser and header arrangements is dependent of the flow distribution throughout the absorber tubes (Duffie and Beckman 2006) and could decrease by more than 20% in unfavorable cases (Chiou 1982). Therefore, turbulent models were extended to laminar flow models (Maharudrayya et al. 2005) and validated for 3D calculations for various Reynolds numbers and tube configurations. The flow distribution was estimated by measuring the temperature of the absorber tubes, in order to highlight the buoyancy effect over the forced conversion (Fan and Furbo 2008). Some numerical models for simulation of flow distribution inside the flat plate collector tubes use the correlation for pressure losses (Facão 2015; Klein 2012). Difficulties in taking into account all the transfer mechanisms inside solar collectors were highlighted (Tian and Zao 2013).
Under such conditions some attempts to solve both energy and flow equations are known, providing information about fluid flow pattern, the absorber temperature field and the distribution of the heat flux (Ceron et al. 2015; Wang et al. 2015; Tagliafico et al. 2014).
In this work it is proposed the model of a basic geometry for a collector - flow tubes imbedded in the metallic absorber plate. Time dependent energy equation for the plate is solved for a constant solar irradiation and steady-state water flux. A numerical simple solving algorithm is proposed, containing material characteristics and plate geometry, providing appropriate data for designing the solar collector.

SOLAR COLLECTOR MODEL AND SIMULATION

In order to derive the 3D time dependent mathematical model for the absorber plate with tube imbedded – figure 1 – the heat flux is considered where the pipe and metallic sheet are placed in an insulated box covered by a transparent cover - figure 2a.
where: $\lambda_{m,a}$ - thermal conductivity for the metallic sheet/tube and water respectively; T - temperature.

$$q_{x,y,z} = \lambda_{x.y.z} \frac{\partial T}{\partial (x, y, z)} \tag{1}$$

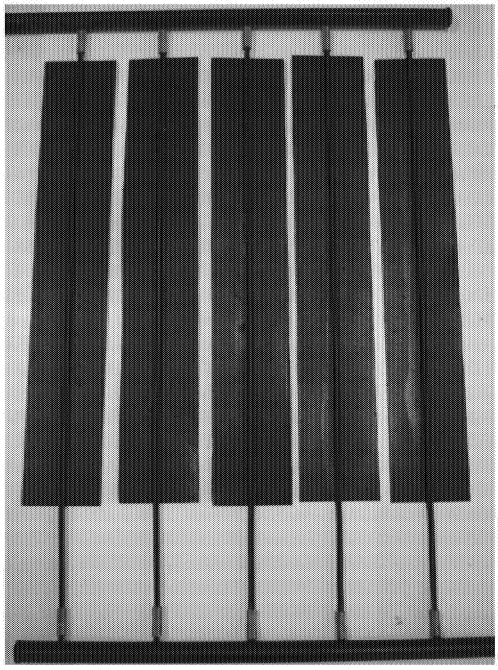

Figure 1: Absorber modules of the flat-plate solar collector

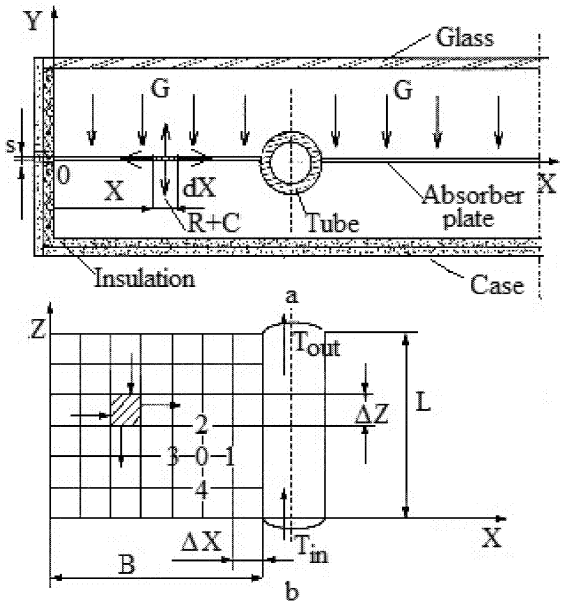

Figure 2: Schematic representation of one module of the flat-plate solar collector.
a. Schematic representation of radiation distribution (G - solar radiation; R - radiation heat losses in the environment; C - conduction heat losses through the collector insulation);
b. Numerical solar model scheme;

According to figure 2 a, energy balance under solar radiation G for an elementary volume of the absorber and tube is considered – figure 3:

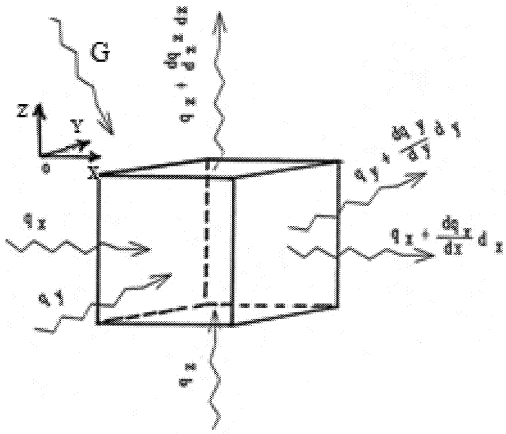

Figure 3: Energy balance for an elementary volume of the absorber plate and tube

Therefore the energy balance is:

$$dXdYdZ\,\rho_m\,c_m\,\frac{\partial T}{\partial t}=\left[q_X-\left(q_x+\frac{\partial q_X}{\partial X}dX\right)dYdZ\right]+\left[q_Y-\left(q_Y+\frac{\partial q_Y}{\partial Y}dY\right)dXdZ\right]+\left[q_Z-\left(q_Z+\frac{\partial q_Z}{\partial Z}dZ\right)dXdY\right]-GdXdZ-C\left(T^4-T_a^4\right)dXdZ \quad (2)$$

where: T_a – outdoor temperature; $\rho_{m,a}$ – metal and water density respectively; c_m – metal specific heat; t; t_0 – time and initial time considered for working regime.

In the energy balance equation, the second right term represents the conduction heat losses through the case insulation, and were neglected for the case study. Also it is neglected the last term representing the radiation losses, in outdoor environment. Finally considering that elementary volume is $dv = dxdydz$ and $dy = s$ is the thickness of the plate one obtain:

$$\frac{\partial T}{\partial t}=\frac{\lambda_m}{\rho_m c_m}\left(\frac{\partial^2 T}{\partial X^2}+\frac{\partial^2 T}{\partial Z^2}\right)+\frac{G}{s\rho_m c_m} \quad (3)$$

A finite difference integration method is used in order to obtain the solution for the time dependent model. First, the non-dimensional equation is written considering the uniform heat flux $q=G/s$:

$$\frac{\partial\theta}{\partial\tau}=\frac{\lambda_m}{\rho_m c_m}\frac{t_0}{L^2}\left(\frac{\partial^2\theta}{\partial x^2}+\frac{\partial^2\theta}{\partial z^2}\right)+\frac{q}{\rho_m c_m}\frac{t_0}{T_i} \quad (4)$$

where:

$$x=\frac{X}{L};\ z=\frac{Z}{L};\ \theta=\frac{T}{T_i};\ \tau=\frac{t}{t_0};\ h=\frac{G}{G_0} \quad (5)$$

(x, z, θ, τ, h, – non-dimensional values for X and Z coordinates, time, temperature, radiation; G_0 – the reference solar radiation (ex. 1000 W/m^2); t_0 – initial time considered for the current iteration; T_i initial temperature of the absorber plate; L – tube length;)

or:

$$\frac{\partial\theta}{\partial\tau}=\frac{1}{F_o}\cdot\left(\frac{\partial^2\theta}{\partial x^2}+\frac{\partial^2\theta}{\partial z^2}\right)+R_a\cdot h \qquad (6)$$

where:

$$F_o=\frac{\rho_m\cdot c_m\cdot L^2}{\lambda_m\cdot t_0};R_a=\frac{t_0 G_0}{\rho_m\cdot c_m\cdot T_i\cdot s} \qquad (7)$$

F_o – Fourier number and R_a – radiation number.

A network is defined for the integration domain – figure 2 b – and Taylor series expansion is used:

$$\begin{aligned}\frac{\partial^2\theta}{\partial x^2}&=\frac{\theta_1-2\theta_0+\theta_3}{x^2};\\ \frac{\partial^2\theta}{\partial z^2}&=\frac{\theta_2-2\theta_0+\theta_4}{\zeta^2};\\ \frac{\partial\theta}{\partial\tau}&=\frac{\theta_0-\bar{\theta_0}}{\Im}\end{aligned} \qquad (8)$$

where:

$$\chi=\frac{\Delta X}{L};\zeta=\frac{\Delta Z}{L};\Im=\frac{\Delta t}{t_0} \qquad (9)$$

(χ, ζ= non-dimensional network steps; $\Im$ - non-dimensional time step;)

Finally the algebraic equation related to (6) is derived:

$$\theta_0=\frac{1}{F_0\left(\frac{1}{\Im}+\frac{2}{\chi^2}+\frac{2}{\zeta^2}\right)}x\left(\frac{\theta_1+\theta_3}{\chi^2}+\frac{\theta_2+\theta_4}{\zeta^2}+\frac{F_0\bar{\theta_0}}{\Im}+F_0 Rah(\tau)\right) \qquad (10)$$

where $\bar{\theta}$ is non-dimensional value of the temperature at previous time step iteration. . For the steady state case the non-dimensional temperature value is:

$$\theta_0=\frac{1}{2\left(\chi^2+\zeta^2\right)}x\left[\zeta^2\left(\theta_1+\theta_3\right)+\chi^2\left(\theta_2+\theta_4\right)+F_0 Rah\chi^2\zeta^2\right] \qquad (11)$$

The boundary conditions for the numerical integration are:

a. Perfect insulation of the collector box :

$$\begin{aligned}\frac{\partial\theta}{\partial x}&=\frac{\theta_1-\theta_3}{2\chi}=0\Rightarrow\theta_1=\theta_3=\theta_0;\\ \frac{\partial\theta}{\partial y}&=\frac{\theta_2-\theta_4}{2\zeta}=0\Rightarrow\theta_2=\theta_4=\theta_0\end{aligned} \qquad (12)$$

b. On the tube surface one write the heat flux from both metal sheets:

$$2\lambda\cdot 2\Delta Zs\cdot\frac{T_3-T_0}{\Delta X}=c_w\cdot\rho_w\cdot V_w\cdot\left(T_2-T_4\right) \qquad (13)$$

(c_w – water specific heat; ρ_w -water density; V_w – water velocity in the tube)

and the tube temperature is:

$$\theta_0=\theta_3-\frac{c_w\cdot\rho_w\cdot V_w\cdot\left(\theta_2-\theta_4\right)\cdot\chi}{4\cdot\lambda\cdot s\cdot\zeta} \qquad (14)$$

c. At the water tube output section the overall heat flux transferred to the water is :

$$2\cdot G\cdot B\cdot L=c_w\cdot\rho_w\cdot V_w\cdot\left(T_{out}-T_{in}\right) \qquad (15)$$

(B - absorber width;)

and finally:

$$T_{out}=T_{in}+\frac{2\cdot G\cdot B\cdot L}{\rho_w\cdot c_w\cdot V_w} \qquad (16)$$

RESULTS AND DISCUSSION

In order to simulate the proposed method, special software for flat-plate solar collector type was created. By using the proposed algorithm, various materials and geometries for absorber plate and tubes, diverse flow rates and solar irradiation can be considered. Therefore the absorber plate temperature, the distribution of the heat flux, and water temperature variation are available for an optimum design. Due to space reasons only one geometry for the absorber plate is presented, as case study. In figure 4a is presented one of the five absorber plate modules made of copper. The size of one sheet is (570 x 86 x 1.5) mm. The central tube is also of copper with d_t = 4 mm internal diameter and 1mm wall thick.

In figure 4 b,c,d are presented the results of simulation in the case study where only the flux variation is considered for ±15% and constant values for the other parameters (solar radiation G = 900 W/m^2; T_{in} = 20 ^{0}C; horizontal position for the collector).

In figure 4.c one considers the reference working regime for a fluid flow of $Q_{100\%}$ = 0.6 cm^3/s. In figure 4.b and 4.d, where fluid flow variation is presented, one observe the change in temperature lines - more clear at the bottom and at the top of the absorber plate. If the mean water velocity value is increasing inside the tube, the temperature lines become more vertical oriented, near the tube. If the water velocity is decreasing, the temperature lines are more horizontal near the tube.

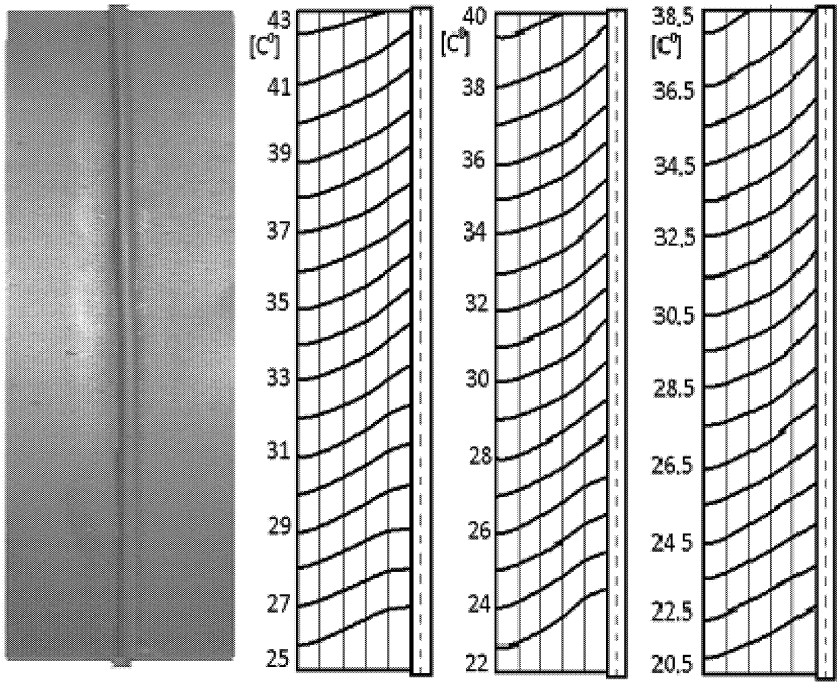

Figure 4: The module of the absorber plate and numerical solutions foe the case study
a. Module of the absorber plate; b. Temperature field for $Q_{85\%}$ = 0.51cm^3/s; c. Temperature field for $Q_{100\%}$ = 0.6cm^3/s; d. Temperature field for $Q_{115\%}$ =0.69 cm^3/s

Also, for each case, one observes that temperature lines at the basis of the domain, near the input water section, are more horizontal oriented, and more inclined at the top near the output water section. This is because the heat transfer is more effective at the bottom side of the absorber plate and less efficient at the top side.
In order to validate the theoretical model and hence to settling down of a simulation strategy - the iterative calibration of the software and building the data library - efficiency of the solar module collector was computed and compared with the experimental tests. Thermal efficiency for one module of the flat-plate solar collector was expressed as a function of the incident radiation, absorber surface A_m and useful power $\dot{Q}_m$:

$$\eta = \frac{\dot{Q}_m}{G \cdot A_m} \tag{17}$$

where:

$$\dot{Q}_m = \dot{m} c_w (T_{out} - T_{in}) \tag{18}$$

($\dot{m}$ - mass flow rate per tube; c_w specific heat for water). Theoretical and experimental results are presented in table 1. Experiment was performed for the same geometry, solar radiation and inlet water temperature as for the simulation case study.

Table:1 Simulation and experimental results

	T_{in} ^0C	T_{out} ^0C	Q $x10^{-6}$ m^3/s	Re -	η -
Simulation	20	36	0.6	289	0.783
Experiment	20	37.5	0.53	255	0.755

The thermal efficiency obtained by simulation was successfully validated against experimental data, at low Reynolds numbers ($Re = V_w/d_t$) – an error of 3.6% was computed. Moreover the results are in good agreement with other papers (Karanth et al. 2015; Ceron at al. 2015) where the results obtained showed that the absorber plate temperature decreases with an increase in the mass flow rate.

CONCLUSIONS

The proposed direct method provides accurate results in a more rapid manner comparing with the models available in the analyzed literature. The main conclusions are as follows:

- it was analyzed in detail the heat transfer mechanism under specific boundary conditions;
- a simple finite-difference numerical method was used for rapid solving the energy equation and a simulation software has been accomplished in order to obtain data for the collector's design in various working conditions;
- absorber plate temperature, distribution of the heat flux, and water temperature variation were

obtained, available for an optimum design of the absorber plate;

- the numerical model reproduced with good agreement the behavior of the absorber plate module comparing the computed thermal efficiency with experimental data.

Using the proposed operative method, large amount of data can be processed by simulation obtaining efficient solar water collectors, reducing cost in prototype construction and testing.

REFERENCES

Afif, H., 1997. "Thermosyphon solar water heaters: effect of storage tank volume and configuration on efficiency". *Energy Conversion and Management* 38 (1997) 847-854.

Badescu, V., 2008. "Optimal control of flow in solar collector systems with fully mixed water storage tanks". *Energy Conversion and Management*; 49 (2008) 169–184.

Buonomano A; Galise F; Ferruzzi G; Vanoli, L, 2014."Variable-volume storage systems for solar heating and cooling system: a case study for different Italian climates". *Energy Procedia*; 48 (2014) 290-299.

Buonomano A.; Calise F; Ferruzzi G, 2013. "Thermoeconomic analysis of storage systems for solar heating and cooling systems: A comparison between variable-volume and fixed-volume tanks". *Energy*; 59 (2013) 600-616.

Ceron J.F; Perez-Garcia J; Solano J.P; Garcia A; Herrero-Martin, 2015. "A coupled numerical model for tube-on-sheet flat-plate solar liquid collectors. Analysis and validation of the heat transfer mechanisms". *Applied Energy* 140 (2015) 275–287.

Chiou, J.P., 1982. "The effect of non-uniform fluid flow distribution on the thermal performance of solar collectors". *Sol. Energy* 29 (6), 487–502.

Duffie, J.A.; Beckman, W.A., 2006. "Solar Engineering of Thermal Processes", third ed. John Wiley & Sons, Inc.

Facão J, 2015. "Optimization of flow distribution in flat plate solar thermal collectors with riser and header arrangements". *Solar Energy* 120 (2015) 104–112.

Fan, J. and Furbo, S., 2008. "Buoyancy effects on thermal behavior of a flat-plate solar collector", J. Solar Energy Eng. *Trans. ASME* 130 (2),0210101–02101012.

Jaisankar S; Radhakrishnan T. K; Sheeba K. N, 2009. "Experimental studies on heat transfer and friction factor characteristics of thermosyphon solar water heater system fitted with spacer at the trailing edge of twisted tapes". *Applied Thermal Engineering;* 29 (2009) 1224-1231.

James and James, 2010. „Planning and Installing Solar Thermal Systems". *Deutsche Gesellshaft für Sonnenenergie.*

Karanth K; Manjunath M; Sharma N, 2011. "Numerical simulation of a solar flat plate collector using Discrete Transfer Radiation Model (DTRM) – a CFD approach". *Proceedings of the world congress of engineering.* London (UK); 2011.

Klein, S.A., 2012. "Engineering Equation Solver. F-Chart Software". Middleton, USA.

Maharudrayya, S., Jayanti, S., Deshpande, A.P., 2005. "Flow distribution and pressure drop in parallel-channel configurations of planar fuel cells", *J. Power Sources* 144 (1), 94–106.

Mertol A; Place W; Webster T; Greif R, 1981. "Detailed Loop Model (DLM) analysis of liquid solar thermosiphons with heat exchangers". *Solar Energy*; 27 (1981) 367–386 Elsevier.

Ntsaluba S; Zhu, B; Xia X, 2016. "Optimal flow control of a forced circulation solar water heating system with energy storage units and connecting pipes". *Renewable Energy* 89 (2016) 108-124.

Ramlow B. and Nusz B., 2010."Gabriola Island, British Columbia". Canada: New Society Publishers, 2010, ch. 3-5.

Razika I; Nabila I; Madani B; Fatima Z, 2014. "The effects of volumetric flow rate and inclination angle on the performance of a solar thermal collector". *Energy Conversion and Management*; 78 (2014) 931-937.

Singh R; Lazarus I.J; Souliotis M, 2016. "Recent developments in integrated collector storage (ICS) solar water heaters: A review". *Renewable and Sustainable Energy Reviews* 54 (2016) 270–298.

Tagliafico L.A; Scarpa F; De Rosa M; 2014. "Dynamic thermal models and CFD analysis for flat-plate thermal solar collectors – A review". *Renewable and Sustainable Energy Reviews* 30 (2014) 526–537.

Thirugnanasambandam M; Iniyan S; Goic R, 2010. "A review of solar thermal technologies". *Renewable and Sustainable Energy Reviews*; 14 (2010) 312–322.

Tian, Y. and Zhao, C.Y, 2013. "A review of solar collectors and thermal energy storage in solar thermal applications". *Appl Energy* 2013;104:538–53.

Wang N; Zeng S; Mi Z; Wang S, 2015. "Numerical study of flat plate solar collector with novel heat collecting components". *International Communications in Heat and Mass Transfer* 69 (2015) 18–22.

Yan G; Qunli Z; Rui F; Xinxing L; Yong Y, 2013. "Effects of thermal mass and flow rate on forced-circulation solar hot-water system: Comparison of water-in-glass and U-pipe evacuated-tube solar collectors". *Solar Energy*; 98 (2013) 290–301.

BIOGRAPHIES

ROBERT R. M. NEACSU is a mechanical engineer working at AIRBUS – Germany. He attended the University Politehnica of Bucharest where he studied mechanical engineering, obtaining his bachelor degree in 1985 and the PhD in 1997 in the field of applied fluid mechanics (turbomachinery).

ADRIAN CIOCĂNEA is a professor at University Politehnica of Bucharest. He attended the University POLITEHNICA of Bucharest where he studied mechanical engineering, obtaining his bachelor degree in 1985. He obtained his PhD in 1998 in the field of applied fluid mechanics (fluid-structure interaction). His main fields of interest are related to numerical integration of Navier-Stokes equations, turbomachinery, hydro-aerodynamics, and renewable sources of energy.

COMPARATIVE MODELING AND SIMULATION OF CONTROL METHODS FOR SOLAR TRACKING SYSTEMS

A. RĂDULESCU
S.C. ICPE ACTEL S.A.
Splaiul Unirii Blvd., ICPE Complex
RO 030138 Bucharest, Romania
E-mail : adi_radulescu@yahoo.com

M. GHEAMALINGA
S.C. ICPE ACTEL S.A.
Splaiul Unirii Blvd., ICPE Complex
RO 030138 Bucharest, Romania
E-mail : mina.gheamalinga@icpe-actel.ro

KEYWORDS
Modeling and simulation, solar power, tracking systems, energy management.

ABSTRACT

As the renewable energy market is continuing its growth at a steady pace, photovoltaic systems still represent a high cost initial investment with solar panels holding the biggest proportion of that initial cost while energy conversion efficiencies are around 20% for the mainstream offer. That is the reason why it is important to make the best of the energy provided by the solar panels through careful panels positioning and high quality and efficiency elements used throughout the photovoltaic system. The current paper contains an assessment of the simulation models available for the main types of control systems used for solar tracking applications while also highlighting the experimental work done to test these simulations. Computational methods, control algorithms, on the field problems, and experimental validation are presented.

INTRODUCTION

The main factors that influence a solar panel's efficiency are light intensity, light incidence angle and panel temperature. All of these factors have a natural variance in the field, light intensity varies according to day and year cycles of the sun, light incidence angle varies according to the panel's mounting orientation and solar day cycle while temperature varies with the ambient temperature and because of solar heating of the panel.
In the following figure, we can observe an arbitrary tilted panel towards the sun and the relevant measurements that describe the incident radiation.

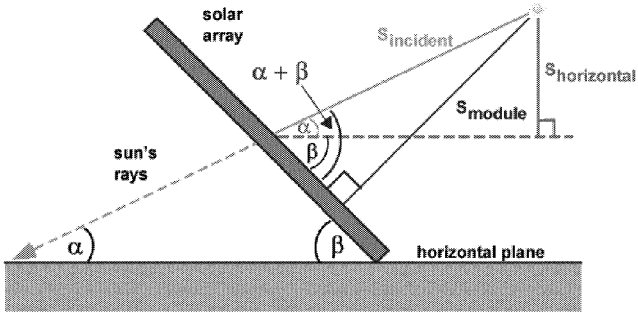

Fig. 1 Diagram of solar radiation on a tilted panel

Considering that:

- α is the elevation angle of the sun for the given position
- β is the tilt angle of the solar module
- $S_{incident}$ is the solar radiation measured perpendicular to the sun
- S_{module} is the solar radiation measured perpendicular to the panel

Then we can notice that:

$$S_{module} = S_{incident} \cdot \sin(\alpha + \beta)$$

Where the elevation angle is:

$\alpha = 90 - \varphi + \delta$ and $\delta = 23.45° \cdot \sin\left[\frac{360}{365} \cdot (284 + d)\right]$

- φ is the latitude
- δ is the declination as a function of d, the day of the year

FIXED AND MANUAL POSITIONED SYSTEMS

For any given photovoltaic system, the simplest solution is a fixed mounting position relative to earth, where the mounting plane can vary from 0° – being parallel to the ground for locations on the equator to ±90° – being perpendicular to the ground and oriented towards south for the northern hemisphere and north for the southern one.

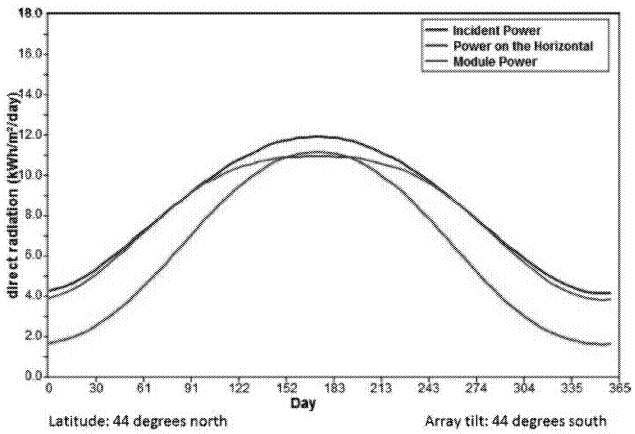

Fig. 2 Comparison of Incident, Horizontal and Module power

In Fig. 2 a test case for 44° North latitude comparison can be seen between the incident power (maximum power available in a plane always perpendicular to the solar

rays), horizontal power (power available in a plane parallel to the ground) and a module's power tilted to the same degree as the local position's latitude which gives the optimum yearly energy yield.
Even though this is a simplification that doesn't take into account any other factors that influence the energy output like cloud coverage, temperature and so on, it can easily be seen that a fixed location isn't an optimal solution as it loses available power both in days of minimum and maximum illumination.
Fixed mounting at a given angle can be considered as a reference from which all the other variable mounting systems grow in efficiency.
The next step for improving this efficiency while keeping both costs and complexity low is with systems that can be manually set usually in two positions: summer and winter tilting. This is only feasible though only for small panels, small systems, and only recovers energy from yearly variations of sun's position while daily variations are still unaccounted for.

LOCATION & TIME TRACKING

First tracking method is based on an open loop system where the solar array can track the sun on one or two axes based on the mounting location on the globe and the current date and time using algorithms, that can give accuracy to within about 1 degree.
Such values are feasible for flat plate solar modules given that other factors contribute to the final power output.
Sun's elevation and azimuth angles are given by the following equations:

$$Elevation = \sin^{-1}[\sin\delta \sin\varphi + \cos\delta \cos\varphi \cos(HRA)]$$

$$Azimuth = \cos^{-1}\left[\frac{\sin\delta \cos\phi - \cos\delta \sin\phi \cos(HRA)}{\cos\alpha}\right]$$

Where: α – elevation angle, δ – declination angle which depends on the day of the year, φ - latitude of the location of interest, HRA – hour angle.
Getting higher accuracy is a required demand for application involving solar concentrators that need tracking within 0.06° for 1000:1 systems.
Obtaining this performance through computational algorithms, increases the computational power needed while still not taking into account environmental factors like cloud coverage.

FEEDBACK TRACKING - PID

By feedback tracking, we are referring to a closed loop control system composed of a MCU/DSP based controller, electromechanical actuators for solar array positioning and light sensors for determining maximum intensity direction.
The diagram for a general control system is presented in Fig. 3.

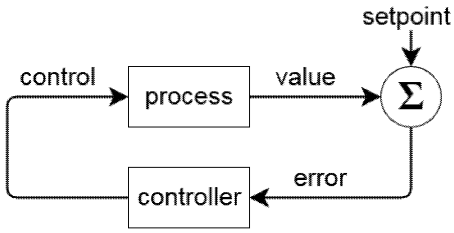

Fig. 3 Block diagram for general feedback control system

For solar tracking applications, the process is represented by the solar tracker made of: a mechanical steerable support, electric actuators for 1 or 2 axes, a solar array, light sensors. For each control axis there must be 2 light sensors mounted at 90° between themselves and 45° between the axis so as to be able to tell when sensors for the given axis receive the same amount of light and thus the axis is perpendicular to the light rays.

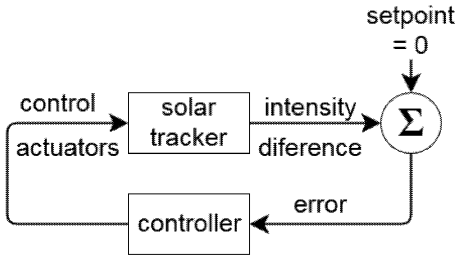

Fig. 4 Block diagram for solar tracker control system

A PID controller is the usual choice for an industrial application, but not always the best. Its implementation is based on the measurement of a process variable with no knowledge of the underlying process, which does not guarantee optimal control or stability.
The equivalent transfer function in the Laplace Domain is:
$L(s) = K_p + K_i/s + K_d s$
Where K_p, K_i, K_d are tuning parameters for proportional, integral and derivative gains, since where the name for the control method. Zeroing any parameter simplifies the controller into a PI, PD, P or I controller. In case of solar tracking, the process is slow changing so there is no need for the P and D terms that are best suited for fast changing systems.

FEEDBACK TRACKING – FUZZY LOGIC

Fuzzy logic together with genetic algorithms and neural networks are gaining importance in control systems as alternatives to PID for more complex systems, being able to deal with multiple input values that are translated to logical variables with continuous values between 0 and 1.
A fuzzy control system is conceptually made of a fuzzification unit, a rule evaluation unit and a defuzzification unit. The fuzzification unit maps input data to the appropriate membership functions and truth-values. The rule evaluation unit is a processing stage that invokes each appropriate rule and generates a result for each, then combines the results of the rules. The defuzzification unit converts the combined result back into a control output value. The advantage of fuzzy logic over PID control is

that there is no need to know intimately the mathematical model by which the controlled system works while also being able to implement the controller on cheap, low performance hardware thus keeping costs and complexity low.

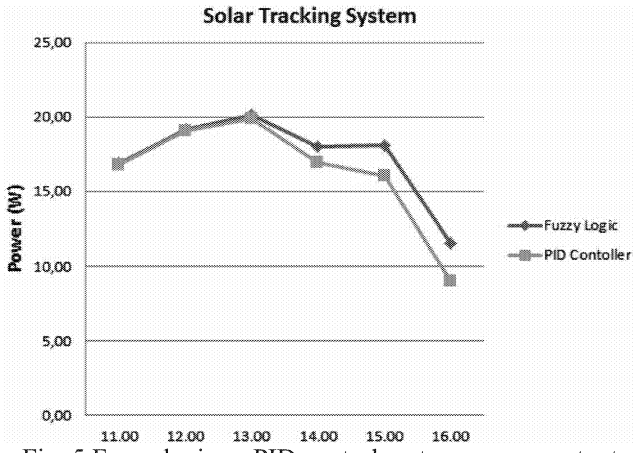

Fig. 5 Fuzzy logic vs PID control systems power output

As presented by Kiyak and Gol, a fuzzy logic based controller can outperform a PID implementation by up to 2.39%. Such a small difference can count if applied to large enough systems where the value translated in energy is big enough, especially since the fuzzy variant is easier to implement and run.

HIL TEST STAND

In order to test the modeling and simulation of the methods presented above, a Hardware in the Loop (HIL) test bench was constructed. The simplified schematic of a complete HIL test bench (Rădulescu A. 2015) is presented in Appendix A and below, in fig. 6 and 7 show the stand itself.

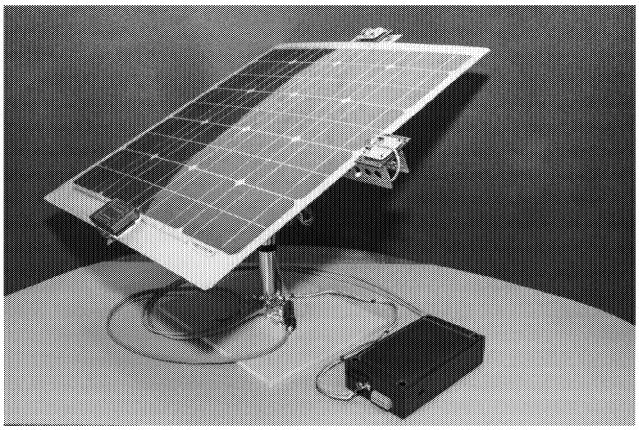
Fig. 6 View of the experimental solar tracker

The stand is made up of a solar tracker capable of implementing all of the methods described, both in real life situations working with sunlight or by using test scenarios through a sun simulator capable of imitating both solar paths and illumination variance.

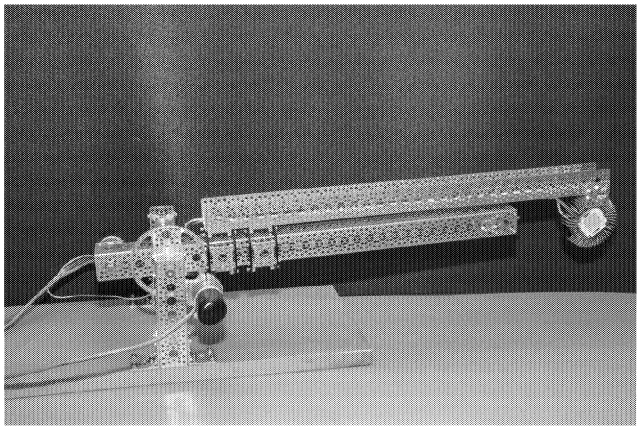
Fig. 7 View of the experimental solar simulator

The solar tracker can function both as a static system or a single or dual axis electric motor actuated tracker. It has a modular construction made of readily available parts that can easily be changed or reconfigured obtaining a degree of freedom in researching and testing various tracking topologies. As presented in fig. 6, the tracker is equipped with geared DC motors for 2-axis actuation, a 40W solar panel, four light sensors for two axis positioning and MCU based controller.
The solar simulator consists of an extendable arm that pivots on a fixed axis of rotation. In the tip of the arm a power light source mimics sunlight with variable output intensity. Thus, any sun path can be simulated to scale. As presented in fig. 7, the simulator is equipped with geared DC motors for 2-axis actuation, a LED module capable of up to 13.000 lumens and the same MCU based controller that oversees the operation of the whole test stand.

CONCLUSIONS

Because theoretical comparisons of different tracking methods are based on starting conditions assumptions, the results obtained cannot be used in real life situations without a close examination of particularities from case to case. In such way, even though in most cases solar installations and especially photovoltaic ones benefit from the presence of a tracking system, it is implementing cost is not always justified or covered by the return cost. For small size applications, only special scenarios can make a tracking installation feasible while on large-scale power plants the power benefits tend to amortize the implementing cost.
Starting from the models and simulations presented, further practical experimental work will be carried out with the test bench to validate the theory and optimize solutions from a manufacturing standpoint.

ACKNOWLEDGEMENTS

Authors are grateful to Professor Nicolae Vasiliu, member of the Romanian Technical Science Academy, for the modern engineering vision and full support in developing challenging researches in the field of modeling and simulation for renewable energies.

REFERENCES

Golovanov N. 2015. "New Renewable Power Sources integrated in the Power System". AGIR Press House, Bucharest (in Romanian).

Di Piazza M. C. 2013. "Photovoltaic Sources. Modeling and simulation". Springer, London.

Julian Chen C. 2011. "Physics of Solar Energy". John Wiley & Sons, New Jersey.

Rădulescu A. 2016. "Energy management of low power photovoltaic plants". Preliminary Ph.D. Thesis, University POLITEHNICA of Bucharest.

Parikhit Sinha1, Matthew Schneider. 2013. "Eco-Efficiency of CdTe Photovoltaics with Tracking Systems". 39th IEEE Photovoltaic Specialists Conference.

Emre Kiyak, Gokhan Gol. 2016. "A comparison of fuzzy logic and PID controller for a single-axis solar tracking system". Springer Open Journal.

Liping Guo, Jingbo Han, Andrew W Otieno. 2013. "Design and Simulation of a Sun Tracking Solar Power System". American Society for Engineering Education.

Ciobanu D., Visa I., Diaconescu D.. 2009. "Virtual Prototyping of a New Tracking System". International Conference on Environmental and Geological Science and Engineering

WEB REFERENCES

http://www.mathworks.com/products/simulink/
http://www.powerfromthesun.net/
http://www.satellite-calculations.com/
http://www.pveducation.org/

BIOGRAPHIES

RĂDULESCU ADRIAN graduated in applied informatics in electrical engineering in 2007 in the frame of the Electrical Engineering Faculty of the University POLITEHNICA of Bucharest, and prepared a M.Sc. at the same university. He elaborated a Ph.D. thesis in the field of power management for renewable energies. He is currently a development engineer in the Department of Electric Drives and Automation Engineering from ICPE ACTEL Company.

GHEAMALINGA MINA graduated in material science in 2004, and prepared a M.Sc. at I.N.P. Toulouse in 2006. He elaborated a Ph.D. thesis in the field of the electric vehicle batteries management in the frame of the Power Engineering Faculty of the University POLITEHNICA of Bucharest. He is currently a scientific researcher in the Department of Electric Drives and Automation Engineering from ICPE ACTEL Company, with works in the field of modeling, simulation, and experimental identification of the electromechanical control systems.

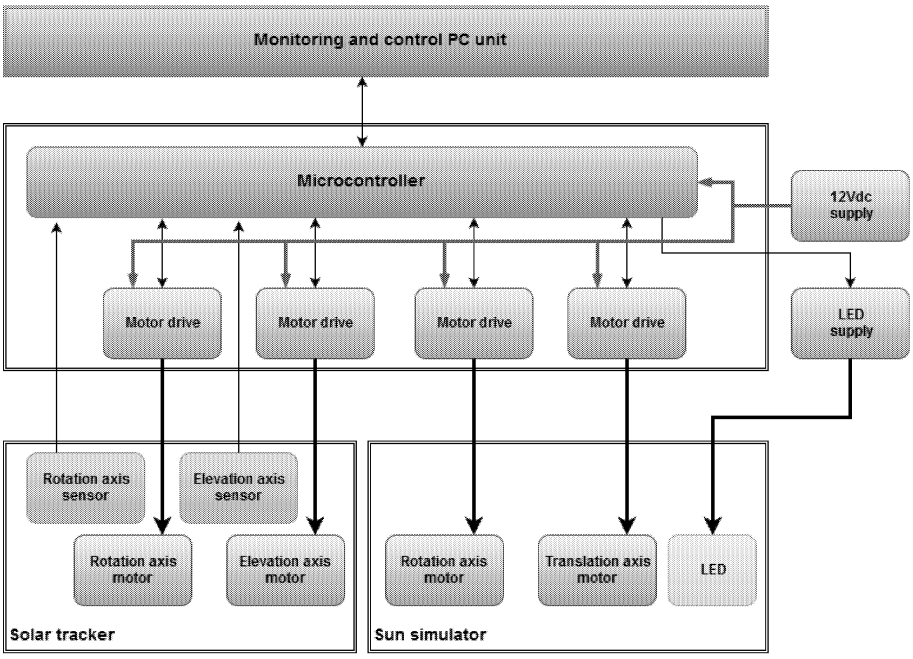

APPENDIX A. Test bench diagram for Hardware-in-the Loop simulation of a solar tracker (Rădulescu A. 2016)

HYDROPOWER SIMULATION

SIMULATION TOOLS FOR LARGE HYDRO POWER PLANT MAINTENANCE

Vlad Florin Pîrăianu, Nicolae Vasiliu, Constantin Dragoi
University Politehnica of Bucharest
313, Splaiul Independentei
RO 060042 Bucharest, Romania
E-mail: vlad.piraianu@upb.ro

Constantin Pîrăianu
Hydropower Senior Expert
225 Priporu Street
RO 247743 Rm. Vâlcea, Romania
E-mail: ctin_piraianu@yahoo.com

KEYWORDS

simulation, stress analysis, modelling, industrial equipment

ABSTRACT

This paper aims to present the main results of researches done in the field of simulation for the industrial equipment existing in large hydroelectric power plants. Starting from the existing tools used in the data acquisition and diagnostics, studies were done to determine, based on actual measurements, modelling and simulation with FEM the remaining lifetime of equipment in order to plan the maintenance and limit its operation of it within acceptable limits until entering into maintenance procedures

INTRODUCTION

Large hydroelectric power plants in Romania have a total installed capacity of more than 6300 MW in operational plants. The installed power is achieved through all sort of power plant schemes and layouts from run-of-river power plants, pumped storage schemes and hydropower plants with large reservoirs. The technological equipment existing within these power plants are mostly old and in the need of refurbishment and more often also modernization. The selection of the units that enters into refurbishment can be done preliminary by the analysis of hours of operation and number of start-ups and shut-downs per day in order to calculate overall operational hours and compare them to the normal lifetime expectancy. Then, each component is going through the phase of dismounting, refurbishment and/or modernization and then mounted again in a complex mechanism called the hydropower unit. This is the most simple case to be dealt with by engineers. The most difficult task is to estimate the remaining lifetime of equipment in which some incidents have occur e.g. cracks in the turbine chamber, cracks on turbine shafts, on axial bearings, etc. When a small accident occurs like the one mentioned before, a complete analysis should be done in order to identify the cause and to establish proper measures to repair correctly the defect and to modify the solution and construction of equipment itself if needed.

HYDROPOWER UNITS MONITORING

Over the last few years, in Romania, important attention was given to actively monitoring operational parameters of each unit, with an implementation program established for every unit of the large hydro, with the final purpose to have enough data and knowledge to elaborate a complete analysis of equipment behavior. For this purpose some actions were taken: vibrations monitoring, partial unload of generators monitoring, thermal monitoring of all equipment, levels and pressures monitoring, anticorrosive protection monitoring of the hydro mechanical equipment used in water in order to establish the actual state of the metallic structures, generator airgap monitoring in functioning, transformer monitoring and auxiliary equipment monitoring (trash racks, valves, spillway structures etc.) (Pîrăianu C, 2011). Vibrations monitoring first started to be used at the beginning only when hydropower units were having unusual noises during operation in order to assure the balancing of the rotating parts, but the next steps were not completed: analysis of the raw data and measurement interpretation to elaborate a complete dynamic analysis. (Pîrăianu C. et all, 2000, Teodorescu M., et al 2000)

REMAINING LIFETIME ANALYSIS OF CRITICAL COMPONENTS

Evaluation of the remaining lifetime of critical components of a hydraulic machine (e.g. hydraulic turbine) has multiple and important uses, as it is generating valuable information and proper knowledge necessary in operation management, maintenance and repair but more importantly, for the modernization of equipment and replacement of the main machine if case (Anghern, Pîrăianu C., 2011). For a complete analysis of the remaining lifetime proper methods are used in the finite element method analysis correlated with data from the history of operation, complete set of vibrations measurements, technical expertise of the current state and modal analysis. For the refurbishment and/or maintenance of the hydropower unit, the evaluation of the mechanical safety of the components that should remain within the unit is critical and the main task of the remaining lifetime analysis that has the main objective to identify, analyze and follow the evolution of a crack, in order to assure the safety in operation of the unit. For a hydraulic machine, it is known that for the main mechanical parts the water influences the fatigue behavior by the acceleration of crack evolution. Therefore, a complete remaining lifetime analysis should take into consideration the following: material quality and structure integrity, fatigue behavior of material, material wear tolerances, geometric integrity, operation history, environmental influences, and construction equipment interface.

ANALYSIS METHODS IN HYDROPOWER

Finite Element Methods (FEM) has become an important instrument in industrial simulation, where the need to solve technical problems and to overcome challenges is imperative for the scope of development. In hydropower, FEM is a common analysis tool used in various phases of design and operation. FEM is a numerical method with the main purpose to solve problems described by differential equation cu partial derivations with knows boundary conditions. (Pîrăianu C. 2011)

The dynamic analysis of the hydropower units is another tool used to determine the operation conditions in different regimes. This is applied to the main rotating part (turbine, shaft and generator rotor) which during operation is stressed under vibrations, bending and torsion. The behavior of the rotating part of a hydropower unit is strongly influenced by its geometry and mounting tolerances accepted, bearing type and restrictions as well as stress forces, axial loads on concrete foundation. An important aspect in the dynamic response of rotating machines is the major influences of the friction bearings and a more accurate modelling on the bearings will allow high precision and prediction of phenomenon (Părăuș anu I. 1996). The main parameter of the operation state of each hydropower unit is the amplitude of vibration. The limits in vibrations are difficult to establish from one machine to another and each type of defect which is causing increase in vibrations has its own evolution pattern. In the modern literature and standards a multitude of consideration are presented regarding vibrations. (ISO, IEC, STAS Standards).

For each hydropower unit, the values of the vibration amplitude could be classified on four levels which indicates the operation state of the unit: good, acceptable, inadequate or unacceptable as shown in Figure 1. (Pîrăianu C., 2001).

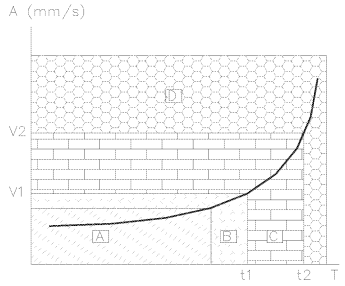

Figure 1: Amplitude classification for hydro units

STUDY CASE: DYNAMICAL ANALYSIS ON A KAPLAN TURBINE OPERATION

The targeted element of the research was a Kaplan hydraulic turbine (Roș u C. et al 2000). The hydro unit has an output power of approx. 35 MW and an installed discharge of 165 m^3/s. The analysis was completed due to high level of noise while operating in the entire range of power and flows, and also because of the problems occurred in operation: high level of vibrations, many operation hours, a large number of start-ups and shut-downs and cracks in the concrete foundation of the axial bearing. The possible defects than can occur have been analyzed to elaborate a first probable cause of the vibrations: mass unbalanced, shaft misalignment and radial load of the rotor, rotor and stator contact, weakening of the bearing fixing elements, shaft cracks, bearing gap tolerances. In order to assure a complete set of vibrations measurements for the hydropower unit operation, an entire set of 11 (eleven) transducers and one acquisition data system was used. The transducers were used to acquire the position of shaft within the radial bearings of the generator and turbine, the position of axial bearing and skate, the position of the axial bearing support related to the bearing, the angular position of the shaft.

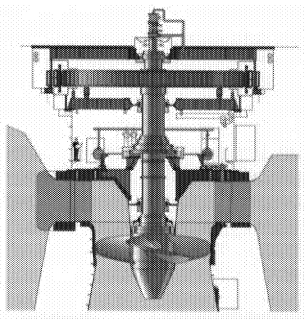

Figure 2: Kaplan Turbine section (*Source: VOITH*)

The measurements were done for different operation regimes of the hydropower on the variation of head and flow. The recorder data obtained were used to formulate preliminary conclusions regarding the dynamic behavior of the hydropower unit. The evolution of the shaft center within the radial bearing of the generator and the radial bearing of the turbine was determined and the results are presented in Figure 3 and Figure 4. Also, the variations in the axial bearing were obtained.

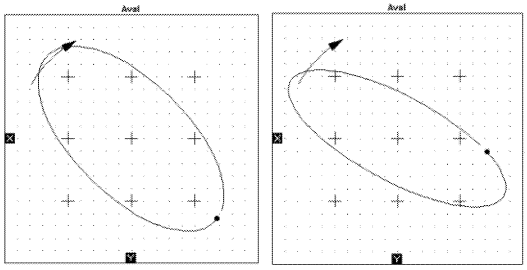

Figure 3: Evolution of the shaft center within radial bearing of turbine (left) and generator (right)

STRUCTURAL ANALYSIS OF THE AXIAL BEARING SUPPORT MECHANISM

A complete structural analysis of the axial bearing support (a star-shaped element fixed with embedded elements in construction) was completed in order to establish the effects of the vibrations. The load on the axial bearing support generated mainly by the rotating part is considerably higher for this type of turbines, reaching more than 300 tones. An additional axial load is given by the pressure of the water transformed into axial and radial forces on the runner blades and the additional stress caused by the electric forces of the generator while connected to the grid. Both hydraulic forces and electrical forces are having significant variation due to the hydrological conditions but also grid condition caused especially by power and frequency regulating or grid system services on a larger scale. These dynamic variation of the loads are creating a series of stress in material, which must be determined in order to determine the remaining lifetime of the equipment for the structure. In order to simulate the dynamic regime of operation and to determine the loads and stress effect of the axial bearing support and advanced geometric model of the equipment was created and is presented in Figure 5.

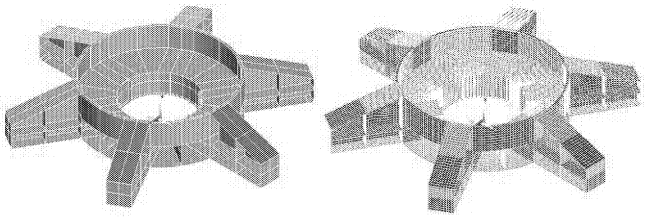

Figure 5: Geometrical model

A simulation was carried out in order to determine the von Misses diagram and the results are presented in Figure 6.

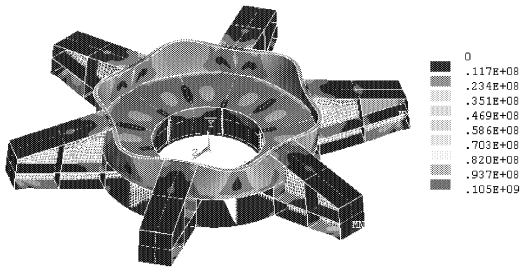

Figure 6: Von Misses Diagram (N/m^2)

The results of the simulation established the maximum points of the stress analysis and the decision of the careful supervision of the state of welding was taken. Another important parameter which is influencing the behavior of the rotating part and therefore the stress on the support and construction is the vertical misalignment of the rotating part. This misalignment can influence the functional deviations of the rotating part. Modelling loads and misalignment of the shaft were taken into consideration when completing the simulation of the behavior of the support mechanism and the results are presented in Figure 7.

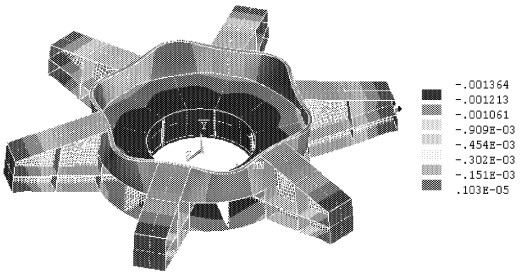

Figure 7: Simulation of axial displacement

The results obtained showed the importance of the rotating part mounting while achieving the recommended deviation imposed by the supplier in order to increase the lifetime, safety in operation and reduce the cost of maintenance.

CONCLUSIONS

Simulation tools are powerful instruments to use in the design but more important in the operation and maintenance of hydro mechanical equipment. Simulation can be used to determine the causes of any defect, any misalignment or deviation higher than recommended. Also, simulation can be used successfully to determine the remaining lifetime of a machine, to limit its operation within safety condition until maintenance is schedule or to improve the knowledge in design of the equipment during rehabilitation and modernization of power plant units.

REFERENCES

***Annual Reports on Olt – Lotru Hydroelectric Power Plants. 2000.

Anghern, R., Sultzer Escher-Wyss Ltd. Lifetime evaluation for critical components of hydraulic machines, International Water Power / Dam Construction, 2000.

Blumenfeld, M. Finite Element method introduction, Technical Press, Bucharest, 1995

Dragoi, C., Piraianu, V.F., Piraianu, C. 2012. "Evaluating the Lifetime of Hydro-Mechanical Equipment for Low Head Hydropower Plants", U.P.B. Scientific Bulletin, Series D, Vol. 74, Iss.1, ISSN 1451-2358, Bucharest.

Pîrăianu, C. 2001. "Researches upon transitory phenomena on low head power plant units". Ph.D. Thesis, University POLITEHNICA of Bucharest.

Pîrăianu, C., Sorohan, Şt., Roşu, C.A., Vasiliu, N. 2000. Analysis of the Bulb Type Turbine Shafts by the Finite Elements Method. Fifth International Conference on Hydraulic Machinery and Hydrodynamics, Timiş oara.

Pîrăianu, C., Dorobanţu C., Antonescu I., Vasiliu N. 2000. Experimental Researches of the vibrations from Frunzaru Hydropower Plant. International Power Conference, U.P.B.

Pîrăianu, C., Evolution of maximum admissible deviation from manufacturing, mounting or repairing technical passports and their influence on River Olt hydropower plant units operation, Refurbishment of hydropower plant equipment symposium, 28-30 October 1998, Reş ita, Romania.

Pîrăianu, C., Călinoiu, C., Antonescu, I., Vasiliu, N., Vibrations monitoring system for Turnu Hydropower Plant, Scientific Session, Energetica-50, 10-11 November 2000, Bucharest, Romania

Părăuş anu, I., Rotative machine dynamics, Cavallioti Press, Buchrest, 1996.

Radeş , M. Dynamic methods for mechanical system identification. Academic Press, Bucharest, 1979.

Roş u, C., Pîrăianu, C., Călinoiu, C., Vasiliu, N., Numerical analysis and simulation of resistance structure of Turnu Hydropower Plant, Scientific Session, Energetica-50, 10-11 November 2000, Bucharest, Romania.

Teodorescu, M., Pîrăianu, C., Vasiliu, N. Fatigue – corrosion behavior of bulb turbine shafts, Scientific Session, Energetica-50, 10-11 November 2000, Bucharest, Romania.

ISO standards no. 2372, 3719/1994, 10816-5/2000

STAS standard 6910/87

IEC Standard 60994

SIMULATION TOOLS FOR HYDRO POWER PLANT OPERATION

Vlad Florin Pîrăianu, Marius Daniel Bontoş , Daniela Vasiliu, Constantin Dragoi
University Politehnica of Bucharest
313, Splaiul Independentei
RO 060042 Bucharest, Romania
E-mail: vlad.piraianu@upb.ro, vasiliu1958@gmail.com, constantin.dragoi@upb.ro

KEYWORDS
simulation, hydroelectric power plant, water management

ABSTRACT

The paper identifies some major challenges for research and practice needed to improve by simulation the common understanding of the transition from the current water management regimes to adaptive water management especially in the hydropower sector. The authors developed a web platform in which new scientific methods, practical tools and simulation tools are promoted for the participatory assessment and implementation of adaptive water management at local, and basin scale. This paper presents some of the results obtained by numeric simulation study cases done for the purpose of the IT platform developed.

INTRODUCTION

Adaptive management is a general expression for adaptive resource management. It is a structured and iterative process for making optimal decision in the face of uncertainty that insists on system monitoring in order to reduce the uncertainty over long periods of time. Therefore the decision making simultaneously maximizes one or more resource objectives and, either passively or actively, accrues information needed to improve future management. Adaptive management is often characterized as a "learning by doing" process. (Pîrăianu VF et al. 2009) The operation of a large hydroelectric power plant (HPP) is a challenging task especially when the hydropower plant has a large dam and reservoir with multiple uses. Also, the task becomes challenging when a cascade of hydroelectric power plants are considered.

SIMULATION IN ADAPTIVE MANAGEMENT AND HYDROPOWER SECTOR

Adaptive management is a general expression for adaptive resource management. It is a structured and iterative process for making optimal decisions in the face of uncertainty that insists on system monitoring in order to reduce the uncertainty over long periods of time. Therefore the decision making simultaneously maximizes one or more resource objectives and, either passively or actively, accrues information needed to improve future management. Adaptive management is often characterized as a "learning by doing" process. Adaptive management can be considered either passive or active. Passive adaptive management begins by using predictive modeling based on present knowledge to inform management decisions. As new knowledge is gained, the models are updated and the management decisions are accordingly adapted. Because adaptive management is used to make decisions regarding the management of valuable natural resources, it directly affects (and is affected by) public policy and politics.
Monitoring is a critical component of adaptive management because it involves deliberate and systematic observation, detection, and recording of conditions, resources, and environmental effects of human and management programs and actions.

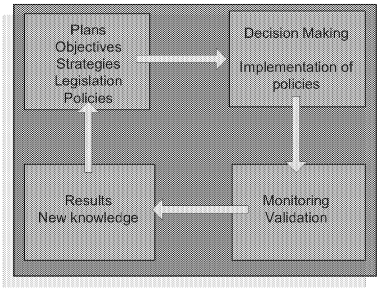

Figure 1: The principle of adaptive management

Monitoring is currently performed by agencies and other entities, but it is typically not well coordinated and integrated among parties involved. Examples of common obstacles include inadequate communication and coordination, conflicting or non-complementary agency interests or mandates, underlying technical issues, inconsistent data integration and sharing, and inadequate funding. Developing and implementing a decision-making system that is guided by the best available science and that uses new information generated from the monitoring of conservation actions remains a general goal in many countries. Within the adaptive water management concept one of the most significant domains is related to the operation of hydroelectric power plant dams and lakes. Usually, the lake of a HPP has multiple scopes and uses: power generation, flood protection, population and industrial water supply systems, agricultural purposes (irrigation), recreation and water sports; a significant issue is related to keeping the highest responsibility for the environmental protection. A particular field in hydropower sector is represented by the small hydroelectric power plant which is considered by many of the modern states in the world and by all European Union member states to be a renewable source of energy. Simulation tools used in hydro power plant operation may relate to the main aspects: design, operation and maintenance.
For the design of any hydropower plant simulation the following tools are available for the: river simulation

(InfoWorks RS®, HEC-RAS, DHI Mike, etc), CFD simulation software, geotechnical simulation (GeoStudio), dam simulation, penstocks and other etc. While the river simulation is used to determine flooded areas in natural or modified river bed conditions, CFD software is used to design and optimize hydraulic machines (turbines, pumps, etc) and finite element methods (FEM) which can be used to design and validate hydrotechnical constructions. For the operation of large hydroelectric power plant reservoir, multiple researches have been done in order to optimize reservoir operation (Banos et al. 2011, Cheng et al. 2008, Ferreira and Teegavarapu 2012). The optimization of reservoir operation by simulation was also used to maximize the income generated by a cascade of power plants in the context of any competitive energy market (Pîrăianu et al. 2014).

Simulation is also mostly used in the diagnosis of the equipment especially of the rotating part. Simulation using FEM software can be used in order to determine the actual state and the remaining lifetime of any equipment of the dams (valves, by-pass, etc) and of the power generation unit (Drăgoi et al. 2012).

SIMULATION TOOLS FOR THE STRUCTURE DESIGN OF SMALL HYDROELECTRIC POWER PLANTS

Simulation software for river simulation is currently being used widely in different stages of the development of any hydropower plant, any water supply system or any water storage system. Infoworks RS was used for the design of a derivation small hydroelectric power plant (SHPP). The water intake of the SHPP was designed according to the technical and ecological conditions imposed by the current legislation. Therefore, the water intake is able to collect the installed discharge, to clean the sediments according to the requirement of a Pelton hydraulic turbine and then redirect the entire volume through the pipe while assuring the ecological flow of servitude on the river with the use of a fishway. The digital model of the water intake is presented in Figure 2.

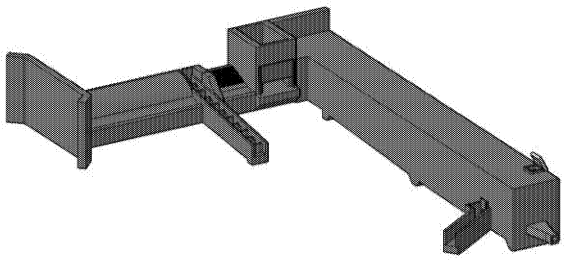

Figure 2: 3D water intake simulation model

Once the digital geometrical model of the water intake equipped with necessary elements (bar screen, inlet valve, etc) was finished then modelling proceeded to the next phase of developing the simulation mode (using InfoWorks RS). The configuration of the river was inserted into the simulation software based on the topographic measurements and cross sections. Also, the hydrological study obtained from the national administration was considered while dimensioning the water intake spillway into the simulation model.

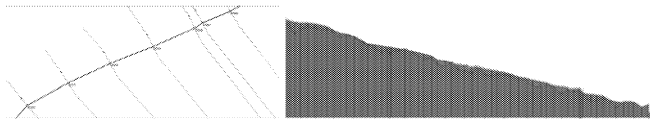

Figure 3: Simulation network and longitudinal profile

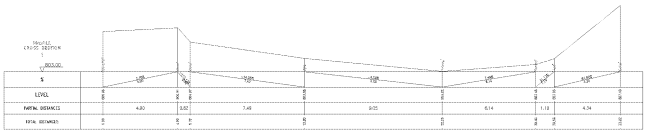

Figure 4: Cross section of river used in simulation model

In order to simulate the operation of the water intake in terms of water collect and water transit with priority through the fishway in order to meet the requirements of the continuity of the water stream and ecological flow downstream, cross sections of the water intake were transferred into the simulation model by modifying the natural river bed cross section with the cross section of the water intake.

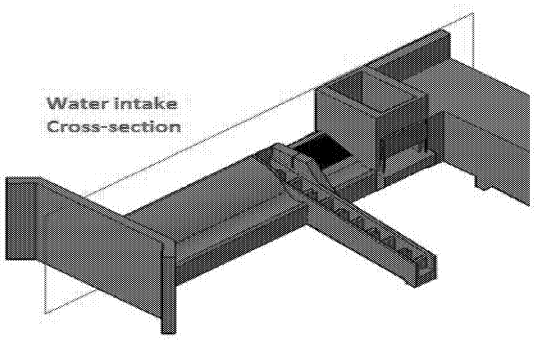

a) water intake cross section

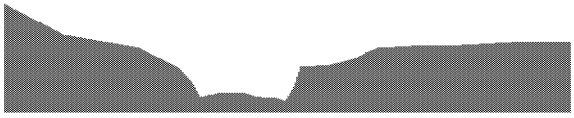

b) natural cross section

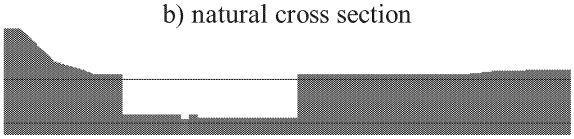

c) cross section after water intake construction

Figure 5: Water intake cross section and river cross sections

A simulation hydrograph was used to simulate the behavior of the water intake. The installed discharge of the SHPP is 3.50 m^3/s and refers to the maximum flow taken by the water intake for energy purposes. The ecological flow transited through the fishway is 0.45 m^3/s and a flood scenario (due to a raining episode) with a duration of 45 hours, starting from 0.42 m^3/s and a peak flow value of 47 m^3/s was used. The results of the simulation showed that the

water intake is able to capture the installed discharge, to accomplish the connectivity of upstream and downstream to achieve continuity of the flow without disturbance even when the flow has very low values. Then, the extra volumes of water not being used for power generation are transiting downstream through the spillway which was design according to the technical norms to the flow with 5% probability of appearance.

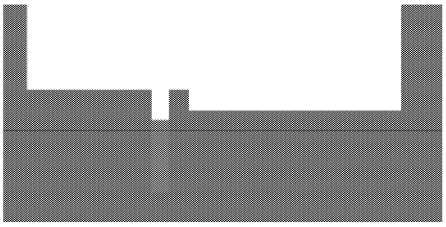

Figure 6: Cross section of the water intake (Q < 0.45 m^3/s)

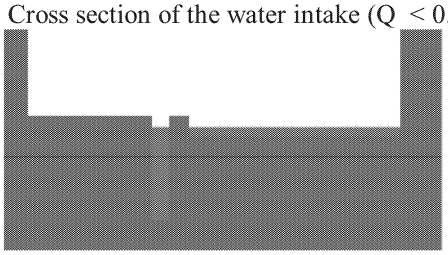

Figure 7: Cross section of the water intake (Q ≈ 4 m^3/s)

SIMULATION TOOLS FOR THE OPERATION OF HYDROPOWER PLANT RESERVOIRS

The same simulation tools can be also used to evaluate and to plan the operation of a large hydropower plant (HPP). It is well known that large HPP usually have large water reservoirs often used both for power generation and non-power purposes (e.g. irrigation, industrial usage, water supply). For the purpose of the prediction of the water level evolution in a large lake, a study case on a HPP was completed. The model of the lake was developed in InfoWorks RS, a certain rainfall event was established and a simulation was carried out in order to determine the variations in levels.

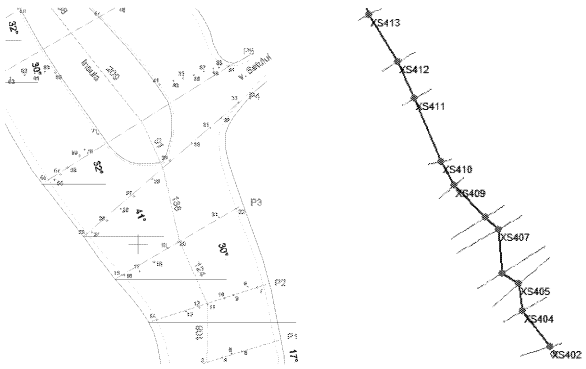

Figure 8: Simulation model of the lake

The results obtained by simulation were used to determine the variations in levels within the lake. A cross section view of the lake near the dam is presented in Figure 9.

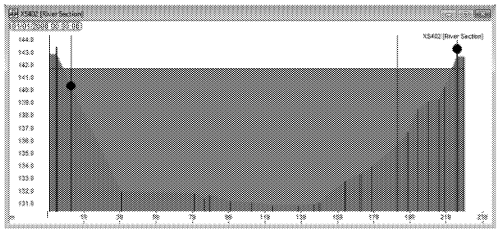

Figure 9: Cross section upstream of dam

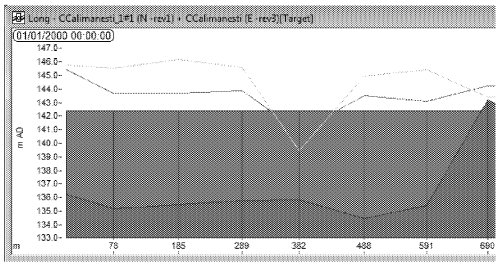

Figure 10: Cross section 5 km upstream of dam

CONCLUSIONS

Simulation tools are powerful instruments to use in the design of HPP elements as well as in the operation simulation. This use of simulation is critical also in the prevention of floods, the optimization of the exploitation of large reservoirs, runoff estimation and commercial planning of the energy produced. In this paper a short presentation was given in order to emphasize the importance of mathematical models and simulation in water management.

REFERENCES

Banos, R.; Manzano-Agugliaro, F.; Montoya, F.G.; Gil, C.; Alcayde, A.; Gomez, J. (2011). "Optimization methods applied to renewable and sustainable energy: A review" *Renew. Sustain. Energy Rev.*, 15, 1753–1766.

Cheng, C.T; Wang, W.C; Xu, D.M; Chau, K.W; (2008). "Optimizing Hydropower Reservoir Operation Using Hybrid Genetic Algorithm and Chaos", *Water Resource Management*

Drăgoi, C., Pîrăianu V.F., Pîrăianu, C., *Evaluating the lifetime of hydro-mechanical equipment for low head hydropower plants*, UPB Scientific Bulletin, Series D: Mechanical Engineering 74, 2012, 1454-2358, pag. 73-82

Ferreira, A.R.; Teegavarapu, R.S.V. (2012). "Optimal and adaptive operation of a hydropower system with unit commitment and water quality constraints". *Water Resources Management*, 26, 707–732.

Mallipeddi, R.; Suganthan, P.N. (2010) "Ensemble of constraint handling techniques. IEEE Trans". *Evol. Comput.*, 14,

Pîrăianu, V.F., Marius Daniel Bontoş , Daniela Vasiliu, Constantin Drăgoi, "PMA – IT Tool for adaptive water management", *International Conference on Energy and Environment*, 2009, Politehnica University of Bucharest

Pîrăianu, V.F., Vasiliu N., Iana, Gh., "Modelling, simulation and optimization of hydropower plants cascade by genetic algorithms", Middle Eastern Simulation and Modelling Multiconference, 2014

CHEMICAL ENGINEERING SIMULATION

POLLUTANT DISPERSION OF S-SHAPED OPEN CHANNEL FLOW WITH A SIDE DISCHARGE USING COMPUTATIONAL FLUID DYNAMICS

Alhassan H. Ismail
Diana Robescu
Faculty of Power Engineering,
Department of Hydraulics and
Environmental Engineering,
University POLITEHNICA of Bucharest
E-mail: hassan19851988@yahoo.com

KEYWORDS
Computational fluid dynamics (CFD), Pollutant dispersion, Open channel flow, BOD.

ABSTRACT

Pollutant dispersion of S-shaped open channel flow with a side discharge has been investigated using two-dimensional numerical model. Numerical computations were carried out using Fluent 6.2.16, which is based on the finite volume approach. Both the volume of fluid (VOF) and user defined scalar (UDS) methods were used in this study. VOF method was used to allow the free-surface to deform freely with the underlying turbulence. Moreover, the pollutant (BOD) is assumed to be mixed throughout the system as a passive scalar. The study comprised the effect of flow rate on the dispersion behavior for five different scenarios. The numerical simulation results show a good fit with observed data in the literature. The findings of this study may provide a proper basis for water quality management in rivers.

INTRODUCTION

Open channel flow such as rivers and streams are the major sources of water for many human activities such as farming, water supply and industry. However, they are playing a major role in carrying off the municipal and industrial wastewater and run-off from agricultural land. The deterioration in water quality of rivers and stream has increased due to the growth of population, urbanization, industrialization, and agriculture activities which forcing developing countries into remediation options of river water quality (Ismail et al. 2014). Although the river system is complex, different studies have been conducted to assess, evaluate and simulate the water quality in rivers (Antanasijevi et al. 2014; Vieira et al. 2013)
Moreover, the fate and transport of pollutants in rivers is relatively important for reliable water quality management. Numerical model has been widely used as an effective tool to simulate and predict pollutant transport in rivers and stream. Numerous studies have been carried out to understand and simulate the transport phenomena and the change in the pollutants concentration in order to gain insight into the impact of these pollutants, and to provide a basis for water quality management (Deng and Jung 2009; Duarte and Boaventura 2008).
Various commercial and public domain models have been developed in literature to consider the changes in contaminated concentration based upon physical, chemical, and biological principles such as QUAL2Kw, QUASAR, MIKE11, SIMCAT and WASP (Sharma and Kansal 2013). Furthermore, computational fluid dynamics (CFD) tools have also been used for certain researches to provide valuable information relating the description of the water flow hydrodynamics and the pollutant behavior along the river and stream (Khaldi et al. 2014; Khaldi et al. 2015; Elghanduri 2015).
The main aim of this study is to predict the pollutant dispersion in an S-shaped open channel flow with a side discharge with different flow rate using volume of fluid (VOF) method and scalar transport. This study may serve as a basis for understanding the effect of the flow rate on the concentration of pollutant from the polluted tributary on the river.

MATERIALS AND METHODS

Assumptions

A CFD code (FLUENT), has been used in the present study for analysis of 2D S-shape open channel flow with a side discharge. FLUENT uses a finite-volume discretization of the Reynolds Averaged Navier-Stokes (RANS) equations to compute the flow dynamics within a given computational domain.
A real open channel flow was considered for modeling the dispersion of pollutant. The geometry used in this study is shown in Fig. 1, and Gambit was used for mesh generation. It was assumed that the main open channel flow is representing the Danube River at the lower course and the side discharge is represented as a tributary of the Danube (Arges River). S-shape open channel flow was considered to provide valuable information on the pollutant dispersion behavior.

Different set of flow rate were adopted to explore the dispersion of pollutant behavior during different flow condition along the river. Table 1 show the values of flow rate in the Danube and Arges Rivers alongside with BOD values in the rivers. Biochemical oxygen demand (BOD) was considered as a pollutant and the aim is to produce different scenarios of the BOD dispersion along the river on the basis of the discharges.

Table 1 water quality and quantity data used in this study.

Variables / River name	BOD (mg/L)	Flow rate (m^3/sec)
Danube River	5	5000 - 10000
Arges River	40	50 - 90

Both Multiphase free surface flow (volume of fluid) and user defined scalar (UDS) was used in this study. For volume of fluid (VOF), Euler-Euler multiphase models were used. It is a surface-tracking approach and designed for two or more immiscible fluids where the position of the interface between the fluids is of interest (Khazaee and Mohammadiun 2012). Furthermore, this study assumed that the BOD is mixed throughout the system as a passive scalar. A passive scalar is any species that can be transported but is non-reactive. Moreover, it was assumed that the BOD is in a liquid form and there are no sources or sinks of the pollutant in the channel.

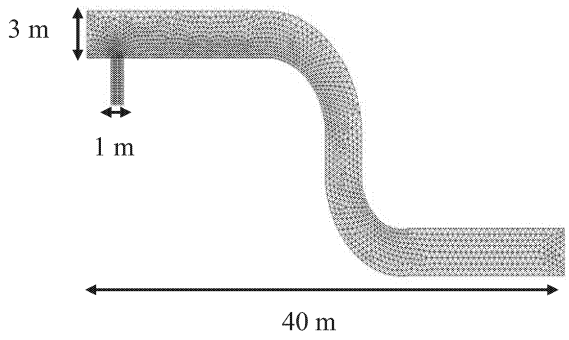

Fig. 1 Geometry and mesh of the study

Governing equations

The VOF model can model two or more immiscible fluids by solving a single set of momentum equations and tracking the volume fraction of each of the fluids throughout the domain (Khaldi et al. 2014). The VOF formulation relies on the fact that two or more fluids are not interpenetrating. This is the case with dispersion process in open channel flow (Rivers). The governing differential equations of mass and momentum balance for unsteady free surface flow can be expressed as:

$$\frac{\partial \rho}{\partial t} + \frac{\partial (\rho U_i)}{\partial x_i} = 0 \qquad (1)$$

$$\frac{\partial (\rho U_i)}{\partial t} + Ui \frac{\partial (\rho U_i)}{\partial xi} = \frac{\partial \tau_{ij}}{\partial x_j} + \frac{\partial P}{\partial x_i} + \rho g_i + S_{i,s} \qquad (2)$$

where u is the velocity vector in the three directions; p is the pressure; v is the molecular viscosity; g is the gravitational acceleration in the three directions, and ρ is the density of flow. In the momentum Equation (2) the interaction between the phases is modeled by the surface tension Si, s .

In the present study air is set as primary phase and water is set as the secondary phase. The tracking of the interface between the phases is done with the solution of the continuity Equation (1) for the secondary phase (the water). This interface is so calculated with the following equation (Khaldi et al. 2014):

$$\frac{\partial (\alpha_2 \rho_2)}{\partial t} + \frac{\partial (\alpha_2 \rho_2 U_i)}{\partial x_i} = s_2 \qquad (3)$$

where s_2 is the source of the phase 2 (s_2 is equal to zero in this work), ρ_2 is the density of the secondary phase and α_2 is the volume fraction of the secondary phase ($\alpha_2 = V2/V$). V is the total volume of fluids ($V = V1 + V2$); $V1$ is the volume of phase 1 and $V2$ is the volume of phase 2. The volume fraction of the primary phase ($\alpha_1 = V1/V$) is calculated by the constrain

$$\sum_{i=1}^{2} \alpha_{i=1} \qquad (4)$$

The standard κ-ε model has been used in the present case. It is a semi-empirical model based on model transport equations for the turbulent-kinetic energy 'κ' and its dissipation rate 'ε', and is expressed by the following equations:

$$\frac{\partial k}{\partial t} + u_j \frac{\partial k}{\partial x_j} = \frac{\partial}{\partial x_j}\left[\frac{v_T}{\sigma_k}\frac{\partial k}{\partial x_j}\right] + v_T \frac{\partial u_j}{\partial x_j}\left[\frac{\partial u_j}{\partial x_i} + \frac{\partial u_i}{\partial x_j}\right] - \varepsilon \qquad (5)$$

$$v_T = c_\mu \frac{k}{\varepsilon^2} \qquad (6)$$

The dissipation of k is denoted ε, and modeled as:

$$\frac{\partial \varepsilon}{\partial t} + u_j \frac{\partial \varepsilon}{\partial x_j} = \frac{\partial}{\partial x_j}\left[\frac{v_T}{\sigma_\varepsilon}\frac{\partial \varepsilon}{\partial x_j}\right] + c_{\varepsilon 1} \frac{\varepsilon}{k} v_T \frac{\partial u_j}{\partial x_j}\left[\frac{\partial u_j}{\partial x_i} + \frac{\partial u_i}{\partial x_j}\right] + c_{\varepsilon 2} \frac{\varepsilon^2}{k} \qquad (7)$$

The values of the model constants are as follows: $\sigma_k = 1.0$, $\sigma_\varepsilon = 1.3$, $C_1\varepsilon = 1.44$, $C_2\varepsilon = 1.92$, $C\mu = 0.09$.

The transport equation for an arbitrary, user-defined scalar (UDS) is solved similarly to the transport equation for a scalar such as species mass fraction. For multiphase flow, the generic transport equation for the scalar is given by

$$\frac{\partial \rho_m \varphi}{\partial t} + \nabla . (\rho_m \varphi_m - \Gamma_m \nabla \varphi) = S \qquad (8)$$

where φ is the local mean age of the fluid, ρ_m is the mixture density, mixture velocity, Γ_m is the mixture diffusion coefficient for the scalar, S is the source term of the scalar and ρ_m, and Γ_m are calculated according to

$$\rho_m = \sum_l \alpha_l \rho_l \qquad (9)$$

$$\rho_{m\,m} = \sum_l \alpha_l \rho_{ll} \qquad (10)$$

$$\Gamma_m = \sum_l \alpha_l \Gamma_l \qquad (11)$$

where α is the volume fraction. The term S in Equation (8) is taken as equal to 1 and for the diffusion term in turbulence flows.

$$\Gamma = \frac{\mu_{eff}}{\varphi_{sc}} \qquad (12)$$

A CFD code, Fluent 6.2.16 was used to solve the Equations (1-12).

Boundary condition

Different boundary condition was set until appropriate condition at domain boundaries have been specified. In the present study, mass flow inlet boundary condition for the inlet 1 and inlet 2 of the channel and pressure outlet boundary condition for the outlet of the channel is specified (see Fig. 2). The no-slip boundary condition is specified to set the velocity to be zero at the solid boundaries and walls and bed assumed to be rough. A mesh with 1770 nodes was found to provide required spatial resolution for studied channel geometry. The solution is considered to be converged when the difference between successive iterations is less than 10^{-7} for all variables.

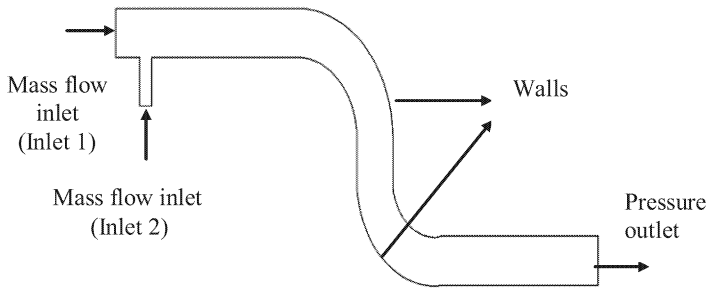

Fig. 2 Boundary condition adopted in the study

Numerical methods

Numerical computations were carried out using Fluent 6.2.16 which is based on the finite volume approach. It provides flexibility in choosing discretization schemes for each governing equation. The discretized equations, along with the initial and boundary conditions, were solved using the segregated solution method in which the governing equations were solved sequentially (segregated from one another) (Khaldi et al. 2014). The first order upwind scheme was used. The PISO method was used to calculate the pressure–velocity coupling.

RESULTS AND DISCUSSIONS

Five different scenarios were considered to represent the pollutant dispersion in the channel by setting different flow rate values, in which the values adopted in this study is demonstrate the actual values in the Danube river and its tributary (Arges river). The BOD concentrations were set as fixed values in all cases and it was assumed 5 mg/L in the inlet 1 (main channel) and 40 mg/L in the inlet 2 (tributary) as these values stated in the previous technical reports and studies (Pfeiffer et al. 2008; Apele Romane 2007).

In case 1, the Q inlet1 was set as 10000 m^3/s and Q inlet2 = 50 m^3/sec and the result shown in Fig 3a whereas, in case 2, the Q inlet1 = 10000 m^3/s and Q inlet2 = 90 m^3/sec and the result shown in Fig 3b. The Q inlet1 in case 3 was set as 7000 m^3/s and Q inlet2 = 50 m^3/sec and shown in Fig 3c. In case 4 and 5, the Q inlet1 = 7000 m^3/s and Q inlet2 = 90 m^3/sec and Q inlet1 = 5000 m^3/s and Q inlet2 = 90 m^3/sec respectively, and the results are shown in Figs. 3d and 3e. The five scenarios are considered to be conceptual cases which related to actual situation of the Danube River to understand the conception of scalar transport through multiphase flow (air-water).

According to high flow rate in the main channel, the dilution process of BOD concentration is quite clear in which the concentration of BOD is reduced downstream the channel. Moreover, BOD concentration is dispersed more closely along the bank of the channel when the flow rate in the main channel is high, i.e. the highest the flow rate in the main channel (inlet 1), the dispersion behavior tend to be along the bank of the channel as depicted in the Figs. 3a-3e. Comparison and agreement between the numerical simulation results and experimental data of BOD along the river which have been observed in the literature show some error between the results. However, the agreement between the prediction and the field observation is acceptable and the present model is reliable for the predictions the impact of Arges River as tributary on the Danube River, i.e. the computational fluid dynamics (CFD) can be used as an effective tools for predicting the pollutant transport phenomena in open channel flow with a side discharge flow.

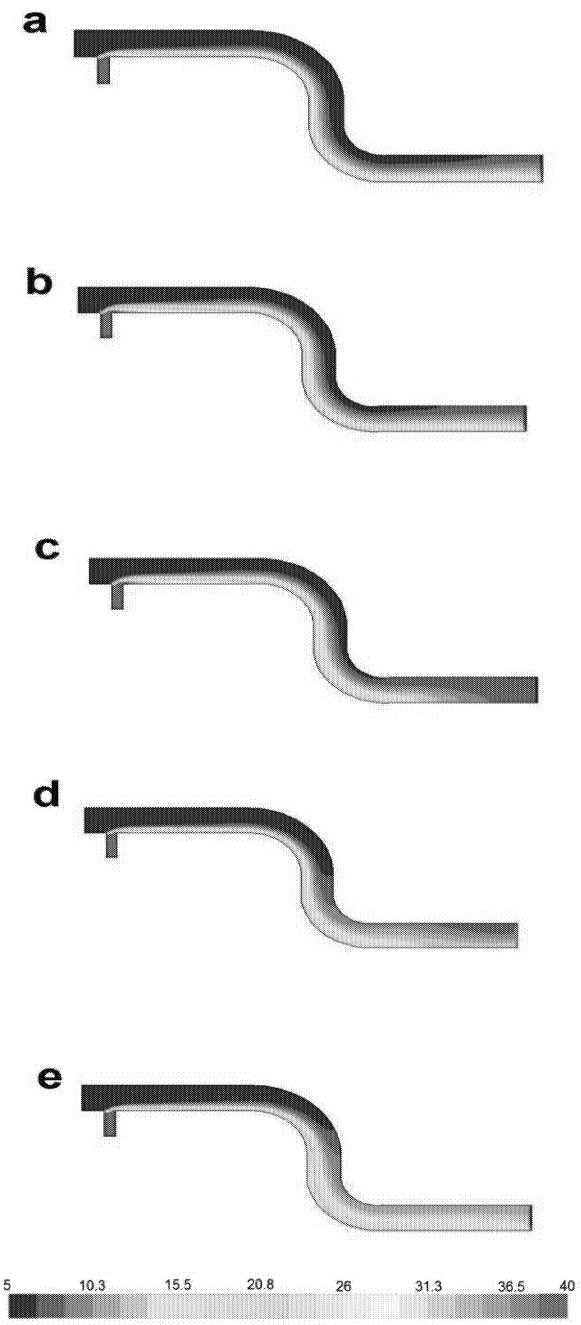

Fig. 3 The dispersion of BOD along the channel: a Q_{inlet1} = 10000 m^3/s and Q_{inlet2} = 50 m^3/s, b Q_{inlet1} = 10000 m^3/s and Q_{inlet2} = 90 m^3/s, c Q_{inlet1} = 7000 m^3/s and Q_{inlet2} = 50 m^3/s, d Q_{inlet1} = 7000 m^3/s and Q_{inlet2} = 90 m^3/s and e Q_{inlet1} = 5000 m^3/s and Q_{inlet2} = 90 m^3/s, the scale is in mg/L.

CONCLUSIONS

The pollutants dispersion along S-shaped open channel flow with an effluent discharging are conducted in this paper. A complete two-dimensional and two phase (VOF) coupled with passive scalar CFD model with finite volume method (FVM) have been investigated. In spite of some error between simulated dispersion of BOD along the channel and observed water quality data, the numerical simulation results show a good agreement with observed data in the literature. The results of different flow rate scenarios revealed that the BOD concentrations are highly reduced downstream the channel due to the high flow rate in the main channel. Furthermore, BOD concentration is dispersed more closely along the bank of the for same reason.

REFERENCES

Antanasijevic, D.; V. Pocajt; A.P. Grujic; M. Ristic. 2014. "Modelling of dissolved oxygen in the Danube River using artificial neural networks and Monte Carlo Simulation uncertainty analysis " *Journal of Hydrology*, 519, 1895–1907.

Deng Z. and H. Jung 2009. "Scaling dispersion model for pollutant transport in rivers" *Environmental Modelling and Software*, 24,627–631, doi:10.1016/j.envsoft.2008.10.007.

Duarte, A.A.L.S. and R.A.R. Boaventura 2008. "Pollutant dispersion modelling for Portuguese river water uses protection linked to tracer dye experimental data" *Wseas Transactions on Environment and Development*, 12, 4, 1047-1056.

Elghanduri, N.E. 2015. "CFD Tracer Tracking within and over a Permeable Bed I: Detail Analysis" *American Journal of Environmental Engineering*, 5(3): 58-71.

Ismail A.H.; B.S. Abed. and S. Abdul-Qader 2014. "Application of Multivariate Statistical Techniques in the surface water quality Assessment of Tigris River at Baghdad stretch" *Journal of Babylon University*, 22, 450-462.

Sharma D. and A. Kansal 2013. "Assessment of river quality models: a review" *Rev Environ Sci Biotechnol*, 12: 285–311.

Khaldi, N.; S. Marzouk; H. Mhiri; and P. Bournot 2015. "Distribution characteristics of pollutant transport in a turbulent two-phase flow" *Environ Sci Pollut Res*, 22, 6349-6358.

Khaldi, N.; H. Mhiri and P. Bournot 2014. "Prediction of pollutant dispersion in turbulent two-phase flows" *Environ Fluid Mech*, 14, 647–662.

Khazaee, I. and M. Mohammadiun 2012. "Effect of flow field on open channel flow properties using numerical investigation and experimental comparison" *International Journal of Energy and Environment*, 3 (4), 617-628.

Apele Romane (National Administration) 2007. Ministry of Environment and Sustainable Development, Water Directorate Arges, Technical reports.

Pfeiffer, E.; G. Pavelescu; A. Baker; C. Roman; C. Ioja; and D. Savastru 2008. "Pollution analysis on the Arges River using fluorescence spectroscopy" *Journal of Optoelectronics and Advanced Materials*, 10 (6), 1489 – 1494.

Vieira, J.; A. Fonseca; V.J.P Vilar; R.A.R. Boaventura and C.M.S Botelho 2013. "Water quality modelling of Lis River Portugal" *Environ Sci Pollut Res*, 20, 508–524.

STATISTICAL OPTIMIZATION APPLIED TO CHEMICAL YIELD EQUATIONS

William Conley
Austin E. Cofrin School of Business
480B Wood Hall
University of Wisconsin at Green Bay
Green Bay, Wisconsin 54311-7001
U.S.A.
Conleyw@uwgb.edu

KEYWORDS
Chemical equation systems, nonlinear multivariate optimization, complex problems, statistics

ABSTRACT

Computers are so powerful now (from a computational speed perspective), that it is possible to use the classical statistical survey sampling techniques (along with some geometry) to "randomly" search the feasible solutions space of any multivariate nonlinear optimization problem, to locate and find the optimal solution region, and close in on a useful solution. Hence, this statistical optimization approach will be used on selected chemical yield equations in this presentation. The solution techniques also will be illustrated and explained. This technique is also called multi stage Monte Carlo optimization. It is an approach that constantly improves the answer as the simulation proceeds.

INTRODUCTION

Market researchers and professionals who conduct polls know that because of the central limit theorem and the laws of large numbers (that govern so much of scientific survey sampling), it is not necessary to draw a large percentage sample of the population in question to find out their opinions on some new product or important topic. It is only necessary to draw a reasonable size sample (usually 500 to 5000 is cost effective) regardless of the size of the overall population.

These same principles apply to survey sampling of the feasible solution space of the optimization problem in question as long as consistently decreasing in size geometric shapes govern and control the constantly "funneling in" of the statistical optimization algorithm to the optimal solution or a useful approximation. Please see Figure 1 for a partial illustration of this phenomenon. Another name for this approach is multi stage Monte Carlo Optimization. The regular Monte Carlo approach of drawing a random sample of 5,000 or 50,000 or 500,000 feasible solutions and storing and printing this approximate answer is just considered as stage one. This is followed by many more stages as the geometric shapes get smaller and smaller at each subsequent stage as they cross the sampling distribution of the feasible solutions (Please see Figure 1) in pursuit of the true optimal or a useful approximation. Let us look at some chemistry examples.

A SIX VARIABLE CHEMICAL YIELD EQUATION

We seek to maximize the chemical yield equation (which governs the output amount of the company's compound it produces).

$$PF = 1{,}915{,}633 - x_1^2 + 78x_1$$
$$+x_2 x_5 - x_2^4 + 24x_2^3 - 216x_1^2 + 864x_1$$
$$-x_3^2 + 116x_3 - x_4^2 + 550x_4$$
$$- x_5^2 + 62x_5 - x_6^2 + 80x_6$$

in units of output subject to
$x_4 + 5x_6 \leq 425$

and
$0 \leq x_1 \leq 50$ pounds of chemical 1
$0 \leq x_2 \leq 15$ pounds of chemical 2
$0 \leq x_3 \leq 100$ pounds of chemical 3
$0 \leq x_4 \leq 500$ degrees temperature
$0 \leq x_5 \leq 1000$ pressure in pounds per square inch
$0 \leq x_6 \leq 60$ minutes length of reaction time
and all x_i's are whole numbers with a ten stage multi stage Monte Carlo optimization program drawing 500,000 sample answers at each stage. (Note that the engineers want the $x_4 + 5x_6 \leq 425$ constraint adhered to so as to guarantee that there is no explosion in the process (Hayter 2002)).

Two runs of this statistical optimization solution program produced the answer (in seconds of run time) of $x_1=39$, $x_2=8$, $x_3=58$, $x_4=275$, $x_5=35$, $x_6=30$ with an output value of 3,000,148 units.

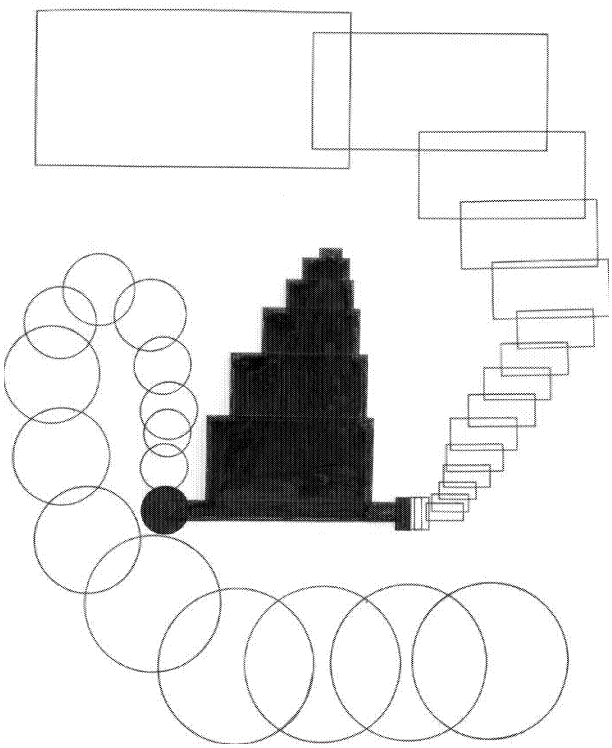

Figure 1: N Dimensional Rectangles Pursuing the Maximum and N Dimensional Spheres Looking for the Minimum Solutions

A LARGE CHEMICAL YIELD EQUATION

The chemical engineers have developed the following yield equation for their company's massive chemical process (Anderson, 2003). It is

$$PF = 38{,}784{,}974 + x_1x_{15} - x_1^2 + 156x_1 - x_2^2 + 126x_2 - x_3^2 + 118x_3 - x_4^2 + 250x_4 - x_5^2 + 286x_5 - x_6^2 + 160x_6 - x_7^2 + 126x_7 - x_8^2 + 34x_8 - x_9^2 + 82x_9 - x_{10}^2 + 70x_{10} - x_{11}^2 + 152x_{11} - x_{12}^2 + 190x_{12} - x_{13}^2 + 42x_{13} - x_{14}^2 + 32x_{14} - x_{15}^2 + 94x_{15} - x_{16}^2 + 60x_{16} - x_{17}^2 + 36x_{17} - x_{18}^2 + 216x_{18} - x_{19}^2 + 704x_{19} - x_{20}^2 + 494x_{20} - x_{21}^2 + 790x_{21} - x_{22}^2 + 1628x_{22} - x_{23}^2 + 624x_{23} - x_{24}^2 + 1502x_{24} - x_{25}^2 + 1082x_{25} - x_{26}^2 + 1198x_{26} - x_{27}^2 + 506x_{27} - x_{28}^2 + 1834x_{28} = 3x_8x_{15}$$

in units of output.

The engineer's goal is to maximize this equation subject to

$50\% \leq x_i \leq 150\%$ of standard catalyst amounts used in the past production runs for i = 1, 2, 3, 4, 5

and $1 \leq x_i \leq 100$ for the 100 control settings for each one of the twelve machines controlling this production run for i = 6, 7, 8, 9, 10, . . . 17

and $0 \leq x_i$ 1000 input units for i = 18, 19, . . .28 for the 11 input compounds in units and

$\sum_{i=1}^{5} x_i \leq 450$ to preserve the chemical integrity of the process as the engineers worry about too much of the five catalysts being added to the production run.

A twenty stage ever focusing statistical optimization search was carried out drawing one million feasible solutions at each of the twenty stages. This computer simulation (for the maximum chemical output) was run three times producing three nearly optimal solutions. They are:

41,999,048 is maximum produced by

x_1=101	x_2=59	x_3=50	x_4=102
x_5=131	x_6=57	x_7=38	x_8=38
x_9=20	x_{10}=2	x_{11}=39	x_{12}=61
x_{13}=6	x_{14}=1	x_{15}=51	x_{16}=4
x_{17}=7	x_{18}=104	x_{19}=338	x_{20}=239
x_{21}=381	x_{22}=798	x_{23}=303	x_{24}=737
x_{25}=530	x_{26}=583	x_{27}=241	x_{28}=913

The second program run yielded

x_1=87	x_2=52	x_3=48	x_4=113
x_5=123	x_6=60	x_7=37	x_8=52
x_9=11	x_{10}=2	x_{11}=44	x_{12}=61
x_{13}=4	x_{14}=8	x_{15}=50	x_{16}=11
x_{17}=1	x_{18}=96	x_{19}=345	x_{20}=239
x_{21}=377	x_{22}=800	x_{23}=305	x_{24}=742
x_{25}=525	x_{26}=582	x_{27}=240	x_{28}=899

with a maximum of 41,999,200 units

The third maximum function value of 41,998,576 was produced with

x_1=104	x_2=55	x_3=50	x_4=116
x_5=125	x_6=47	x_7=34	x_8=41
x_9=5	x_{10}=6	x_{11}=53	x_{12}=64
x_{13}=1	x_{14}=0	x_{15}=49	x_{16}=11
x_{17}=3	x_{18}=94	x_{19}=329	x_{20}=235
x_{21}=379	x_{22}=806	x_{23}=300	x_{24}=741

x_{25}=530 x_{26}=588 x_{27}=238 x_{28}=911

These three approximate solutions should help the engineers to run this chemical yield process for the maximum number of output units of production. Please note that the eleven input compounds had a range of 0 to 1000. Therefore, the square root of 2 is about 1.42 and 1.42 raised to the twenty power is a little more than 1000. So it was decided to divide the search region dimensions for the variables 18 through 28 by 1.42 at each subsequent stage so that in the last stage of this statistical optimization simulation run the "width" of the search region in dimensions 18 through 28 would be a reasonable value of a little less than one.

However, for dimensions 1 through 17 (representing variables 1 through 17), the variables there have only a range of 100. Therefore, at each subsequent stage their search region was reduced by a factor of 1.27 so that there would be some reasonable width left in those dimensions in the later stages of the "random" search for the optimal.

A problem whose variables all have ranges of the same width needs only one focusing factor. However, this 28 variable problem required two focusing factors (of 1.27 and 1.42) to prevent some ranges in the search from "disappearing," so to speak.

A CHEMICAL BLENDING SYSTEM

A company has one weekly run of its chemical blending problem where seven input chemicals (in units of tons) are run in a process that produces ten output compounds (in numbers of output units). Please see the yield chart 1.

Chart 1: Yield of output compound (in units) per input tons of Chemical 1 through 7

	Compound One	Compound Two	Compound Three	Compound Four	Compound Five	Compound Six	Compound Seven	Compound Eight	Compound Nine	Compound Ten
x_1	x_2x_5			x_3x_5		x_6^2		x_2x_7	x_1x_4	
x_2		x_1x_5	x_4^2		x_4x_6		$5x_4x_5$			$4x_3^2$
x_3	x_1x_4	$3x_2x_6$		$2x_2x_7$		x_3x_6			$3x_2x_5$	
x_4		x_3^2	$4x_2x_5$		x_2x_5			x_3x_4		$6x_1x_4$
x_5	x_3^2		x_6^2	x_1x_6			x_7^2		$4x_4x_6$	
x_6	x_6x_7	x_4x_6		$2x_3x_4$		x_5^2		x_1x_6		$3x_5x_7$
x_7	x_1x_7	$2x_3x_7$	x_1x_3		x_1x_5		x_2x_6		$3x_3^2$	
	Required output amounts in units									

Therefore, use a statistical optimization computer simulation to solve this nonlinear yield system of equations.

$$x_1x_2x_5 + x_1x_3x_4 + x_3^2x_5 + x_6^2x_7 + x_1x_7^2 = 5{,}848{,}688 \quad (1)$$

$$x_1x_2x_5 + 3x_2x_3x_6 + x_3^2x_4 + x_4x_6^2 + 2x_3x_7^2 = 3{,}597{,}574 \quad (2)$$

$$x_2x_4^2 + 4x_2x_4x_5 + x_5x_6^2 + x_1x_3x_7 + = 6{,}448{,}655 \quad (3)$$

$$x_1x_3x_5 + 2x_2x_3x_7 + x_1x_5x_6 + 2x_3x_4x_6 = 2{,}412{,}380 \quad (4)$$

$$x_2x_4x_6 + x_2x_4x_5 + x_1x_5x_7 = 3{,}695{,}724 \quad (5)$$

$$x_1x_6^2 + x_3^2x_6 + x_5^2x_6 = 1{,}111{,}737 \quad (6)$$

$$5x_2x_4x_5 + x_5x_7^2 + x_2x_6x_7 = 8{,}494{,}630 \quad (7)$$

$$x_1x_2x_7 + x_3x_4^2 + x_1x_6^2 = 2{,}790{,}183 \quad (8)$$

$$x_1^2x_4 + 3x_2x_3x_5 + 4x_4x_5x_6 + 3x_3^2x_7 = 6{,}554{,}832 \quad (9)$$

$$4x_2x_3^2 + 6x_1x_4^2 + 3x_5x_6x_7 = 16{,}323{,}476 \quad (10)$$

subject to

$0 \leq x_i = \leq 200$ and whole numbers for i = 1,2 , 3, …. 7
after transforming it to minimize

$$PF = \sum_{j=1}^{10} \left| L_j - R_j \right| \text{ subject to } 0 \text{ X } x_i \leq 200 \text{ where the } L_j$$

and R_j are the left and right hand sides of the 10 equations for j = 1, 2, 3,…. 10.

The company will use a 17 stage multi stage Monte Carlo optimization (statistical optimization) simulation drawing 1,000,000 feasible solutions at each stage over an ever narrowing and refocusing "random" search which will funnel into and find the solution.

The answer is:
$x_1 = 39$ $x_2 = 83$ $x_3 = 29$ $x_4 = 126$
$x_5 = 99$ $x_6 = 59$ $x_7 = 160$ with PF = 0 error indicating an exact solution.

Therefore, these seven x values are the input amounts in tons that should be put into the weekly yield process run to satisfy the last time period customer demands. (The right hand sides of the equation are the demands.)

Therefore, in each future week when new customer demands come along, the right hand side of these equations should be updated to reflect the new amounts ordered. Then the program is to be rerun for the new weekly inputs and solution.

Also note that with the number of equations outnumbering the number of variables, in some weeks there may be no exact solution to the system. However, this approach will give a new "solution" with a hopefully manageable minimum total error value (which the computer program will print out, giving the seven x values and the total equation errors and individual equation errors too).

CONCLUSION

Three examples were presented here. A six variable chemical yield equation to be maximized was presented. Additionally, a 28 variable yield equation to be maximized and a seven variable by ten equation blending system to be solved were presented. All three problems were nonlinear multivariate and very difficult to solve theoretically. Therefore, a simulation technique like statistical optimization (please see Figure 1) (also called multi stage Monte Carlo optimization) was used on all three to obtain good results in a timely cost effective manner (Anderson, Sweeney and Williams 1999) and (Black 2014).

Statistical optimization is a general purpose nonlinear multivariate solution technique for our computer age. Additional examples of its versatility can be found in (Conley 2012), (Conley 2014) and (Wong 1996), among others.

REFERENCES

Anderson, T. W. 2003. Multivariate Statistical Analysis, 3rd edition, Wiley and Sons, New York.

Anderson, D. R., Sweeney, D. J., Williams, T. A. 1999. Statistics for Business and Economics, 7th edition. South-Western College Publishing, Cincinnati, Ohio.

Black, K. 2014. Business Statistics for Contemporary Decision Making, 8th edition. John Wiley & Sons, New York.

Conley, W. C. 2012. "A million variable nonlinear transportation problem." In *Proceedings of 2012 Industrial Simulation Conference*. ISC2012 EUROSIS, Ghent, Belgium, pp. 113-121.

Conley, W. C. 2014. "The business of outer space Croquet." In *Proceedings of 2014 Industrial Simulation Conference*, ISC2014 EUROSIS, Ghent, Belgium, pp. 45-52.

Hayter, A. J. 2002. Probability and Statistics for Engineers and Scientists, 2nd Edition, Duxbury Press, Pacific Grove, California.

Wong, J. Y. 1996. Á note of optimization in integers. *International Journal of Mathematics Education in Science and Technology*, Vol. 27, pp. 865-874.

BIOGRAPHY

WILLIAM CONLEY received a B.A. in mathematics (with honors) from Albion College in 1970, an M.A. in mathematics from Western Michigan University in 1971, an M.Sc. in statistics in 1973 and a Ph.D. in mathematics-computer statistics from the University of Windsor in 1976. He has taught mathematics, statistics, and computer programming in universities for over 30 years. He is currently a professor emeritus of Business Administration and Statistics at the University of Wisconsin at Green Bay. The developer of multi stage Monte Carlo optimization and the CTSP multivariate correlation statistics, he is the author five books and more than 200 publications world-wide. He is a member of the American Chemical Society, a fellow in the Institution of Electronic and Telecommunication Engineers and a senior member of the Society for Computer Simulation.

DATA ANALYSIS

ANALYSING PICTURES BY BIOLOGICAL INSPIRED SIGNAL PROCESSING METHODS TO OPTIMIZE THE DETECTION OR IDENTIFICATION OF OBJECTS

Sabine Bohlmann[1], Matthias Reuter[2]
Technical University of Clausthal
Julius-Albert-Str. 4
D-38678 Clausthal-Zellerfeld, Germany
E-mail: [1] sabine.bohlmann@tu-clausthal.de,
[2]matthias.reuter@tu-clausthal.de

KEYWORDS
Bionic Neural Structures, Genetic Based Preprocessing Methods, Visual Analysis, Contour Detection, Potential Oriented Pattern Analysis.

ABSTRACT

Even so modern adaptive methods like deep learning, random forest and other methods enable robots to navigate via visual recognition systems in a more or less autonomous way, praxis shows that in complex situation, under flickering light conditions or under rapid changing situations these systems more or less fail. It's the unsolved problem to define prototypes to be learned or used by the methods mentioned above, which choose these problems as same as it seems to be impossible to find of special structures like hyperbola structures out of noisy pictures or if several hyperbolas are overlapped. Even in medical oriented pattern recognition systems often it seems to be impossible to mark and/or extract special cell structures in histological samples or x-ray pictures by expert software tools. Otherwise the human eye seems to have no problem to concentrate on special structures of a picture. Rule by our focus of attention we can change our biological filter routines in that way, that we analyze now small and very small structures and in the next moment the global structure of the picture. In the last recent years the authors – working especially on the problem of anti-mine resp. IED detection on land via ground penetrating radar and on the detection and categorization of dumped ammunition in the Baltic and Northern Sea – developed new biological inspired filter chains by modeling the retinal structures and the special methods of the retinal signal processing. In this paper some of those methods are discussed and examples of these powerful filter technics are shown

BIOLOGICAL BACKGROUND OF THE RETINAL PATTERN ANALYSIS

It is one of the most surprising findings that the signal processing in the retina of the mammals is done on a more or less none numerical structure, means, is based on the temporary activity of different kinds of neurons, their potential differences, topological characteristic, so called ON-OFF path ways and non-learning methods. So at least those retinal structures act as special kind of pre-processing, whereby this structure can change its structure immediately, rule by the momentary focus of interest by changing the combination of the so called receptive fields; means the number of neurons which are analyzing a section of an optical scene.

From those facts follows, that common models of artificial neurons and/or neural nets, neither methods to condition those structures like back-propagation, deep learning or self-organizing cannot meet these processing structures, whereby mainly the common structure of the inter-neuronal connections and the weighting of those information paths doesn't met the biological reality at all. Furthermore the pre-processing is surely done by no-conditionable neuronal (clusters), so at least we are talking about a kind of genetic based pre-processing structure with variable dimension of simultaneous acting neuron clusters.

Do to these facts, we start to model retinal structures and show some time ago, that changing the basic structure of the synapses (and so the inter-neuronal information processing) by neglecting the restrictive condition that an axon has one and only one effector, the leads to a totally new behavior of simulated neuron structures if a synapsis at least have one or more than one excitatory and one or more than one inhibitory input path-wax. A simple structure of this architecture is as shown in Figure 1.

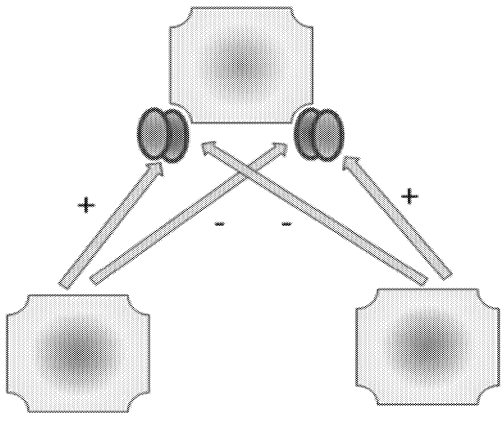

Figure 1: Scheme of a BN-Structure

With the special synaptic structure, whereby the red colored contribution is the inhibitory part and the green colored contribution is the excitatory part of the synaptic structure. Next the question, how the different contribution interact is to solve. In our experiments we used a linear transfer-function, whereby the transfer function is limited in an interval [-100, 100] and the contributions are combined by an additive way. In modification to the classic theory – taking into account that in biological systems no negative activation occurs – the result of this combination will be in the interval [0, 100] only. So at least our model is a purely potential oriented one. The features of the shown non-conditinable three-neuron structures are more or less surprising, as for example this simple structures solves along the way the 80 years old XOR-paradigm of the neural nets which say, that only by a three layer net structure a XOR-structure can be realized [3], as now only one sensor-data input layer and one information processing neuron is necessary to realize this structure.

Looking a little bit deeper in theory our improvements ends immediately to the knowledge that in simulated neural structures too, not a single neuron will act "as a standalone system" but "basic neuronal structures" (BN-Structures), involving a minimum size of three neurons seems to form the smallest processing units in an visual pre-processing, whereby – once again- the two basic neurons on the lower side on a BN-Structure act a as more or less input layer, innervating at least two synaptic structures of the upper neuron synchronically and – as a kind of supersymmetry – one of the synaptic structures acts in an excitatory and the other in an inhibitory way. (Remark: In nature this structure is more complicated, as only so called interneurons can change a neurons output from excitatory to inhibitory. These neurons are not visualized in Figure 1. But it is important to mention, that these neurons not from a new layer of the BN-Structure.)

Based on these BN-Structures we modeled in the next step larger and flexible in their dimension retinal structures, means receptive fields of different dimensions, lateral inhibitions done by interneurons, ON/OFF-pathways and the integration of these passes.

APPLICATIONS USING BN-STRUCTURES

Military Applications

It follows out of theory that the dimension of the receptive field size defines whether the contour of an object is accentuated or its overall shape. Form this fact follows, that especially under out-door situations and so far unknown scenes the dimension of the receptive fields has to be changed in that way that objects of interest are "high-lighted". This search in the space of receptive rating can be done either in an automatically or via a user action.

The sensitivity of the pattern recognition/pattern pro-processing by choosing the dimension of the receptive fields is visualized in Figure 2.

The original Figure 2a shows a scene with three cars. If the receptive field dimension is chosen 3x3 the contours of the object are accentuated, this is shown in figure 2b. In Figure 2c and 2d the receptive field is enlarged by factor 3 and 4.

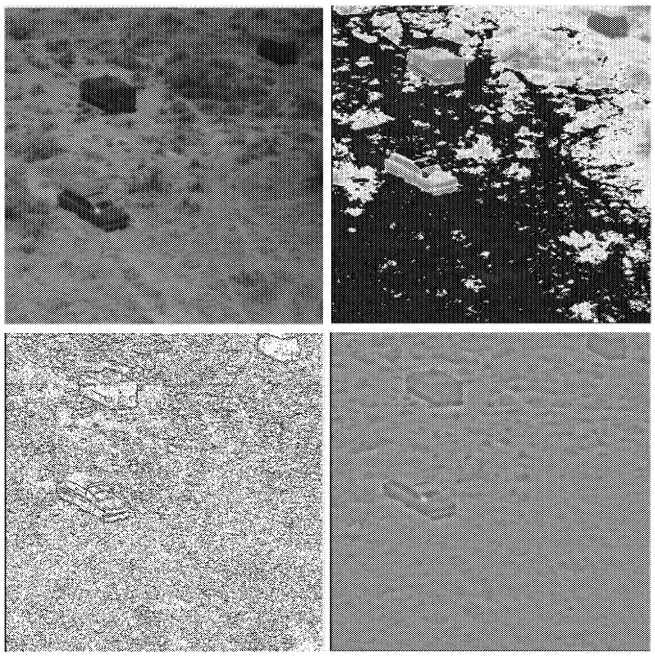

Figure 2a-2d: Shape or object accentuation influenced by receptive field size

Next we used the same modules to identify hyperbola structures in an on-line object-detection-tool. Figure 3 shows such a detection process, at which the signatures of three mines (two in the middle of the picture, one at the right margin – with half signature present only) are detected and their position are marked by a white triangle. As the system detect suspicious objects the left hand panel is coloured red and an acoustical signal occurs. Lower sides the A-scan of the radar gram is shown.

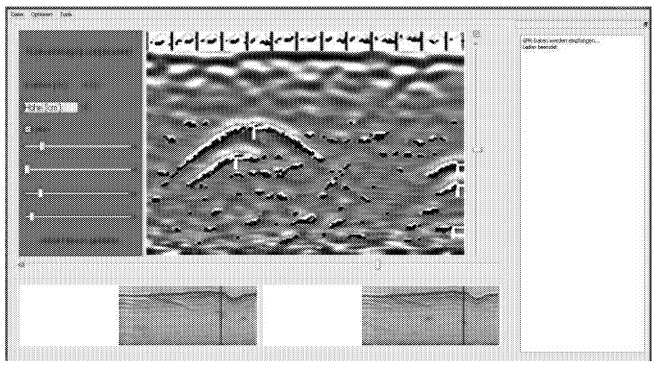

Figure 3: Landmine detection by potential oriented, non numerical signal processing routines

Medical Applications

The high sensitivity of the new methods opens also a wide range for the analysis of biologic tissues and here especially the detection of different structure in biological slices. The following picture series 4a- give an overview how by changing the parameters of the potential oriented sensitivity calculation of the BN-structure different cell types structures can be highlighted in a histological slice a an snake nervous system part.

While Figure 4a shows the original slice, by changing the sensitivity of the potential oriented sensitivity of the synaptic structures, different tissues can be high-lighted and

therefore specified/identified regarding their density, internal structure and interconnection.

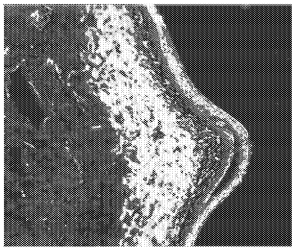

Figure 4a:
Original slice

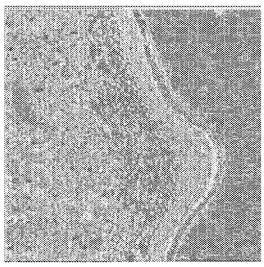

Figure 4b:
Connective tissue

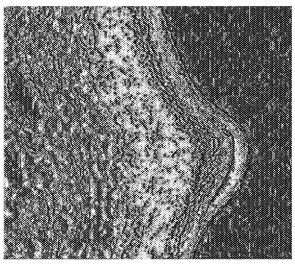

Figure 4c:
Nerve tissue

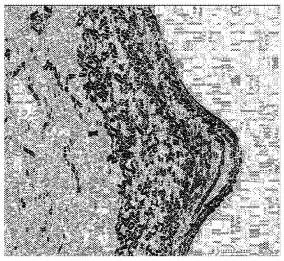

Figure 4d:
Second cellular Layer

Technical Applications

The last example show that the new method is extremely robust even if the contours to be detected are more or less near by zero. Shown is a glass with water in front of a white sheet of paper – for normal edge-detectors a more or less insoluble task. As this contour fealty holds even under flickering light, the described method is used in robotics and technical detection systems for structure change equipment.

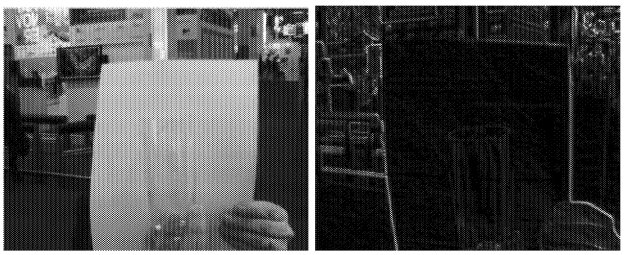

Figure 5: Couture Discrimination by BN-Structures

CONCLUSIONS

We showed in our investigations that BN-Structure based signal processing routines will model the biological optical and (here not shown) acoustical pattern recognition in ear and eye by a more or less non-numerical and very quick and simple way and that high adaption to background noise, intensity and mixed information structures can be done by changing the range of the underlying receptive field dimensions of the BN-Structures. Paired with an extreme sensitivity for edged structures these new methods enable to detect and visualize also equipotential lines of magnetic surveys and hyperbolic structures in deeper (up to 7 m) ground areas, highlight different tissue structures and even almost hidden edges.

REFERENCES

Reuter, M. (2001). Analysing the Structure of Poly-Crystalline Materials by 2-dimensional DLS-Spectra and Neural Nets. Computational Intelligence, LNCS 2206, pp. 420-427

Kim, J. Green, M.J. et al., (2014). Space-Time Wiring Specificity Supports Direction Selectivity in the Retina. Nature 509, pp. 331–336

Reuter, M. (2014). Biological Inspired Synapses and the XOR-Problem. https://www.researchgate.net/publication/270283328_Biological_Inspired_Synapses_and_the_XOR-_Problem

Jol, H. (2015). Ground Penetrating Radar Theory and Applications. Elsevier Science

Israelowitz, M, Weyand, B, Leiterer, C et al. (2014). Biomimetic-Inspired Infrared Sensors from Zn3P2, Microwires: Study of Their Photoconductivity and Infrared Spectrum Propertie, Hindawi Publishing Corporation, New Journal of Science, Volume 2014, Article ID 524042

Integrating Discrete Event Simulation Packages: A Case Study of Arena and Simul8 Data Integration

Jamiu Yusuf, Seng Chong, Parminder Kang and Alistair Duffy
Faculty of Technology
De Montfort University
The Gateway, Leicester, LE1 9BH,
United Kingdom
Email: jamiu.yusuf@email.dmu.ac.uk

KEYWORDS
DESP–discrete event simulation packages, simulation, interpretability, heterogeneity, Global Schema, data sharing, Arena and Simul8.

ABSTRACT

This paper discusses a framework for data integration and contributes towards solving of heterogeneity between discrete-event simulation packages (DESP). Arena and Simul8 DESP have been used as an example in this paper. We analysed how their data is structured in terms of modelling elements (ME) and their associated attributes.
It has also been shown that creating custom-assembled exclusive interfaces are too exorbitant and make utilising re-enactment innovation restrictive for most clients using the DESP. The outcome of this paper can be seen as an important step in addressing heterogeneity in DESP types of simulation software. Therefore, this paper contributes to the integration needs of the DESP.

I. Introduction

Data integration is an important and critical aspect of simulation process.
Discrete event simulation is a tool based on computer techniques used to investigate complex dynamic systems and behaviours. The discrete event referred to in this paper, is a type of simulation used to model variables in a given system that change with time and events (Law & Kelton, 2000).

Discrete event simulation packages (DESP) are majorly used for supporting research, system analysis, acquisition, education, organisational change, planning and facilitation of the diverse range of area and disciplines such as manufacturing, defence, healthcare, commerce, transportation and supply chain (Pawan, 1998, Kang,2012, Kang et al..2013 and Robinson, 2004).

DESP are also the available commercial software packages (e.g. Arena, Simul8 and Simio) developed to facilitate the process of discrete event simulations. The discrete event simulation system is almost equivalent as building a production company itself, but this simulation process has yet to achieve its full potential due to lack of a standard format for data exchange and sharing among these tools.

One of the unresolved arguments in this field is the choice of common data format (Mike, Martin, and Peter, 2009).

The majority of experts favour an object-oriented approach, with the evidence being that it has a semantic of other models. For example, the automated generation model for reuse of existing of simulation data (Mike, Martin, and Peter, 2009). However, the issues still remain that the simulation tools producer will continue to use a different construct database based on the tools they choose to develop these DES tools.
However, this creates number of issues when the integration is required between the DES packages

- Firstly, both the time and the cost of analysing, developing, implementing, and using simulation technology is extremely high.
- Secondly, the costs of integrating simulation data are even higher.

Previous works have been attempted in the area of heterogeneous DESP integration. However, researchers such as Yücesan, et al. (2002), Mertins, et al. (2000) and Taylor, et al. (2003) concluded that the approaches were elusive, and that there were strong arguments that no standard method exists in the field.

II. Arena/Simul8

The Arena (www.arenasimulation.com) and Simul8 (www.simul8.com) are currently two of the most popular DESP in the market. Both Arena and Simul8 models have their distinct modelling elements and associated attributes.
Investigation shows that separate data structures and format are being used separately by the two DESP as seen in Figure 1 for modelling elements and Figure 2 for their associate attributes.

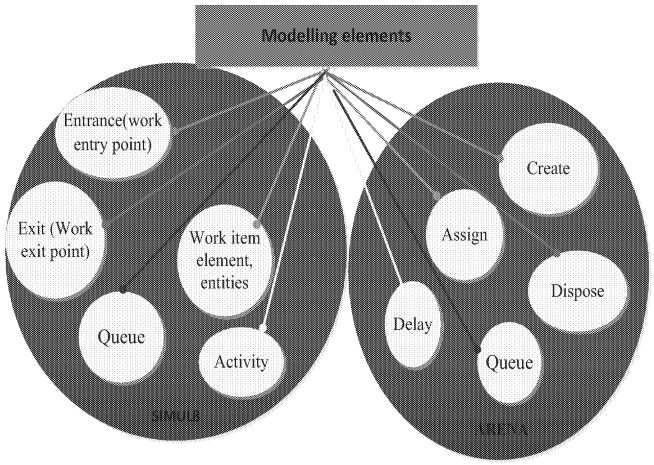

Figure 1: Modelling Elements' interaction diagram

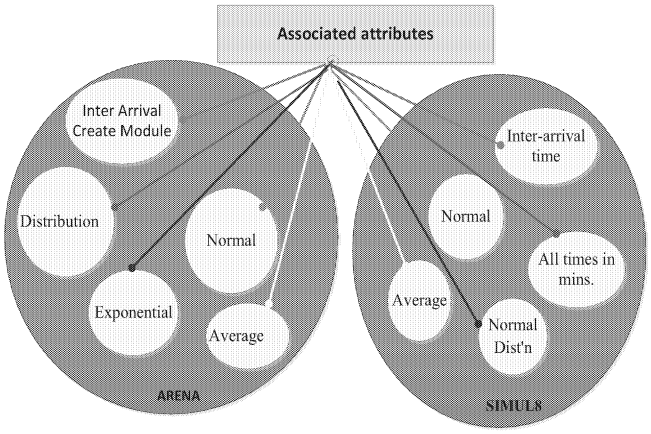

Figure 2: Associates attribute interaction diagram

III. DESP Heterogeneity

Many of the discrete event simulation packages used today have different representation, terminology and behaviour, for example, elements in one DESP may have an attribute as 'name' and call 'entity type' in another DESP.
Likewise, another observation is their interrelationship that makes it even more complicated. Example is the modelling elements in various DESP, such as Entrance (Work entry point), Work item (element, entity) resources, Queue (Storage bin, stack), Activity (Work Centre, action) and Exit (Work exit point) which in Simul8 are differently represented when compared to Arena's modelling element such as Create, Assign, Size, Delay, and Dispose.
Two simulation packages (Simul8 and Arena) are adopted to build a simple process with each model consisting of modelling elements, parameters, associate attributes and entities. The degree of incompatibility and heterogeneity as seen in Figure 1 and 2 above presents an argument that there are a substantial challenge and lack of governing standard that exists in this area and is the primary motivation for this paper.

Another concern is how data are stored in different DESP, (e.g. xml in Simul8 and access in Arena), this means the interactions between the different ME and their attributes are not represented in the same manner.

IV. Critical Review of Existing Integration Techniques

The problems of data sharing make it impossible for DESP to interlink seamlessly as a result of conflict and economic issues (Chen, et al., 2002). The existing methods lack neutral interface to allow one type of DESP to import data from another DESP without the need to develop a new process from the scratch. The literature also highlights that the current solutions for data sharing among DESP has not really shown an in-depth solution on how to streamline data transfer (Simon, et al., 2006).

We now present various techniques previously attempted to integrate heterogeneity DESP and systems.

- **Data distribution**

In manufacturing system and beyond, data and information extraction uses simulation technologies such as Computer Aided Engineering (CAE) and Product Data Management (PDM) model software to predict the manufacturing processes.
One drawback of this is that it does not use the same data format as input and for analysis. Therefore, it offers limited interfaces between the simulation software (Chen, et al., 2002).

Drath (2010) identified the need for seamless and coherent approaches that has the capability to import the data of one model to another.

Researchers have only succeeded in the development of product information with the only capacity of introducing some form of data (Peters, et al., 2001).

The current standard data exchange, between different simulation tools has not been established as most of the data format is usually tools specific, without supporting standard (Miriam & Rainer, 2008).

- **Incompatible terminology**

Modelling elements and associated attributes in terms of model information are the keys to any system integration and exchange, but most of the available models often use different names or terms for describing their input and output data, therefore, leading to customised models (Skoogh & Johansson, 2007).
The difference in terminology has created a lot of interpretation and misunderstanding in the knowledge sharing and exchanges in simulation software (Waktersdorfer & Zoitl, 2010).
In this regards, Lee & Yan (2005), used a shared database to describe a data exchange for machine shops for simulation software by using an XML file and generic database to extract the raw data.
Skoogh and Johansson (2007) also presented an Excel interface for standard terminology to support information exchange and a dynamic simulation model.

However, the practical and readily applicable method that shows these tools can share relationship and data is still missing (McLean & Leong, 2012).

- **Scenarios Navigator-based data transfer**

Scenarios Navigator-based data transfer is another method with a centralised navigating database system (Arnim & Scholz, 2006 and Kagioglou, 2007).

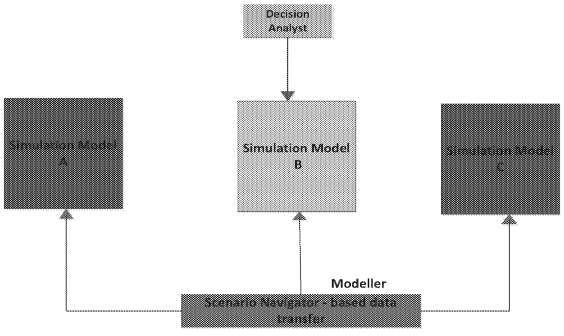

Figure 3: Scenario navigator-based data transfer

Figure 3 shows an example of scenario navigator-based data transfer.

The advantage of this method is its ability to read files from separate simulation tools (Arnim & Scholz, 2006).

The scenarios manager enables the model to have a standard access to data through interface without the need to have an interface for individual software and also provide a centralised data storage system for the models (Kagioglou, et al., 2007).

However, one of the limitations in Scenarios Navigator-based data and File-base data conversion approaches was its inability to detect conflicts of interest among the available data (Waltersdorfer, et al., 2010).

In addition, Woolf and Hope (2011) highlighted other limitations in Scenarios Navigator-based data transfer. These include the use of a large database that requires a large data structure, making it lacking the flexibility to accommodate changes to the simulation models.

- **Data translation**

As pointed out by Miriam & Rainer (2008), data automated translation is necessary to eliminate or reduce the time taken by human to interpret different data. To achieve data sharing and among the customised simulation tools, there is also a need to identify and share a common relationship and concepts between the simulation models.

As highlighted by Kahng & McLeod (1998) and Viviana, et al. (2008), the use of ontology approach allows the semi-automated transfer of data between different simulation models.
Ontology according to Dejing, et al. (2004) is a formal specification of concepts of vocabulary (source) and axioms relating to them, which describe the semantics of data.

Notwithstanding, the many ontologies developed and researched upon, a clear and robust solution for data integration are still missing. Therefore, a more novel approach is needed (Euzenat & Shvaiko, 2008).

Data transfer

Data transfer refers to a typical classification system among different simulation software based on the principle of a central database, file exchange, and message exchange according to individual applications (Kagioglou, 2007). A universal principle related to data transfer between different tools is demonstrated in Figure 4 below.

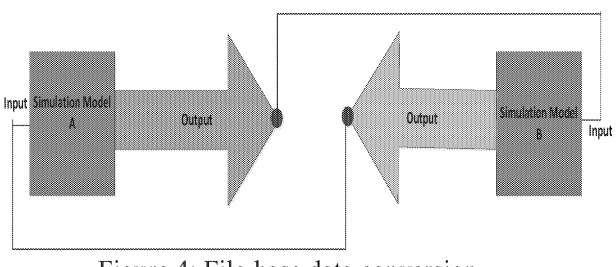

Figure 4: File-base data conversion

Notably, Miriam and Rainer (2008) used a CAEX (Computer Aided Engineering Exchange) format to transform hierarchical information between different simulation tools. The same approach was also adopted by Barnes & Arnaud (2006) to convert data from kinematics and 3D CAD models.

Due to the fact that both used XML format based file method, it has a major contribution to data sharing due to their inbuilt support for XML which is compatible with most simulation tools.

Despite this, Woolf & Hohpe (2011) highlighted the limitations in Miriam & Rainer (2008) and Barnes & Arnaud (2006) as their integrated approach requires a protocol to read files before it can be transformed to another. As a result, it needed a translator to create a separate location for each file, which tends to be problematic and time consuming. Therefore, Woolf & Hohpe (2011) suggested the need for more research towards data sharing among the software tools.

- **Summary**

In brief, literature have shown that some of problems that limited data exchange are issues of incompatibility and interdisciplinary, such as (i) data distribution, (ii) description level (the problem of supporting standard), (iii) independent variable and attributes, (iv) format representation (fundamental incompatibility: Access file against Xml files), and (v) expressiveness (e.g. Separate entity composition against single objects are the main problems).

However, the simulation software developers have been focusing on improving their own tools with little considerations for the integration needs of end users.

It is unlikely that these software developers will make their process more user-friendly and aligning with other tools in the foreseeable future, therefore researchers need to focus on developing strategies for improving data sharing and integration.

The literature has also shown that the existing software tools are considered to be device specific, and others are deemed to be proprietor particular (Simon, 2006). Therefore, it is clear that there is a need to develop a new method that could address the limitations highlighted in the literature.

V. The Approach

The goal of this paper is not to present yet another schema integration algorithm or a data model. It aims to critically investigate the data structures in different DESP and propose a framework for the integration process.
This will be carried out by identifying how entities and their associates' attributes are structured in various models and how this can enhance data integration.

Table 1. Model information and specification table

	ARENA	SIMUL8	MAPPING
Modelling elements	Assign Create Decide Dispose Process (includes Delay)	Work entry points Work centers Resources Storage bins Resources	Simul8: (Entity (Type, Inter-arrival time distribution, Name, Resource, Variable, Timing (distribution, average), (Entity) Attribute)
Attributes	Entity (Type) Queue Resource Variable (Entity) Attribute	Inter-arrival time distribution, (average) Name Timing (distribution, average) Pool resources Shift dependant, Capacity.	ARENA (Assign, Create, Decide, Dispose, Process includes: Delay, Work entry points, Work centers, Resources, Storage bins Resources.
File type	Access	Xml	

The semantic relationship applicable to the two models with their elements and associated attributes were presented in Table 1.

This was identified and specified according to their equivalence, uniqueness, incompatibility, identical and equal.
For example, some elements possess the same name and same attributes that they are referred to as being identical.

Each associated attributes and elements are unique, therefore, modelling elements with the same name and same attributes are grouped as the same component.

Likewise, elements that have different associated attributes, but with different modelling elements with the same representation, are categorised as being equal.

Furthermore, elements that have the same name and definition are considered relevant.

On the other hand, an element with a different name but the same associate attributes, with the condition of having a direct meaning with other attributes, do satisfy that the semantic relationship are equal.

Yet elements with different names, different attributes that are not related to any identical definition across the models are referred to as unique.

Lastly, any elements with different characteristics and same name and definition but that have not satisfied the semantic relationship are considered to be incompatible.

VI. Integration Model

The high level integration model in Figure 5 below demonstrates the intention on how data from different homogenous discrete event simulation packages can be processed (e.g. extraction, integration and transformation) into a proper understandable structure.

After this process the data is processed to the final target, which is the database. A template is then provided for the shared database.

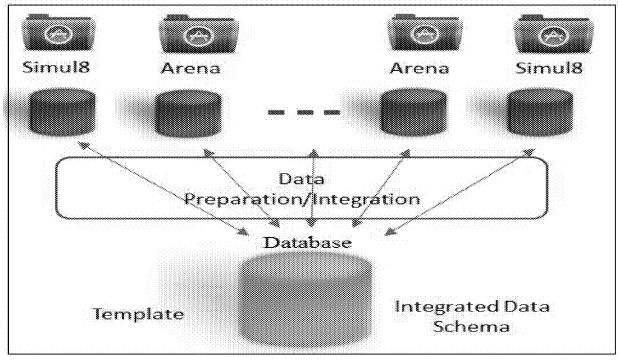

Figure 5: High level integration model

The proposed overall architect of the approach is shown in Figure 6 below. In this paper, we intend to use a combination of different DESP, referring to the discrete event simulation packages, the GS (Global Schema) as the connected view of heterogeneous database in Figure 6 below.

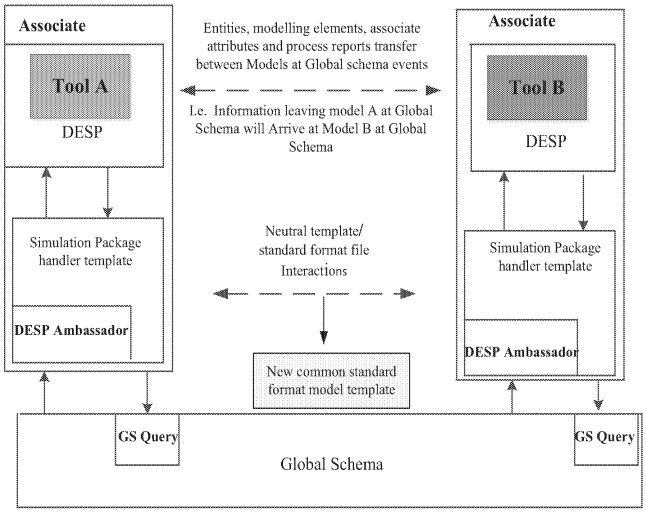

Figure 6: The Proposed Integration Architecture

The DESP are mapped into the global schema. The GS Query allows the users to pose queries against what appears to be homogenous.

The model template provides a common format for the DESP representation, where each package defines its model and the information to be shared with other DESP and the information it needed from the other DESP.

The model template combines the data from the each DESP into a single representation and defines the overall unified output data that can be used and shared by the DESP.

VII. Conclusions

In this paper, a data integration amongst two or more DESP has been proposed.

A solution has also been proposed to address the issue of heterogeneity, allowing file sharing between different simulation software without the need to build another model from the scratch.

The process of data integration between different discrete event simulation packages have also been discussed and analysed extensively; this has contributed to the solution of how to resolve the structural, semantic, naming, modelling, and attribute differences among the different DESP.
Data sharing has also contributed to the development of methods for determining the heterogeneous among different the discrete event simulation.

As such, the time and cost necessary to build a new model from the scratch will be reduced.

The following is the summary of the main contribution of this paper. One contribution is the identification of how data are structured in different DESP models. Another contribution is the presentation of the overall overview of data integration methods of discrete event simulation packages. Finally, the data integration scheme proposed presents a comprehensive and standardised method to fill the gap in previous studies.

The proposed method is currently limited to the commercial discrete event simulation packages, where Arena and Simul8 models were used as a case study due to their popularity. It is planned that in the future work, other simulation software tools will be accommodated.

REFERENCES

Arnim, W. & Scholz, W., 2006. Functions of scenarios in transition processes. *Futures,* 38(7), pp. 740–766

Barnes, M. & Arnaud, R., 2006. COLLADA, Mass: Peters Wellesley

Chen, J. L., Yücesan, E. & Snowdon, L., 2002. *Simulation: Software and Model Reuse: A Polemic.* New York, Association for Computing Machinery Press

Dejing, D, Drew, M. & Peishen, Q., 2004. Ontology Translation on the Semantic Web. *Journal on Data Semantics II,* pp. 35-57

Euzenat, J. & Shvaiko, P., 2008. Ten Challenges for ontology matching: On the move to meaningful internet systems. Pp. 1164-1182.

Kagioglou, M., Aouad, G. & Bakis, N., 2007. Distributed product data sharing environments. *Automation in construction,* 16(5), pp. 586-595.

Kang, P., 2012, Improving Manufacturing Systems Using Integrated Discrete Event Simulation and Evolutionary Algorithms, Phd Thesis, De Montfort University, Leicester, UK.

Kang, P., Khalil, R. and Stockton, J., 2013, Job Sequence. Optimisation Using Combinatorial Evolutionary Approach in High Variety/Low Volume Manufacturing Environment, International Journal of Scientific Research, Vol. 4, No. 6, pp. 2145 – 2150

Kahng, J. & McLeod, D., 1998. Dynamic Classification Ontologies: Mediation of Information Sharing on Cooperative Federated Database Systems. *Cooperative Information Systems Trends and Directions,*2(5),pp.179-203.

Law, A. M. & Kelton, W. D., 2000. *Simulation Modelling and Analysis.* 3rd ed. New York: McGraw-Hill.

Lee, Y. T. & Yan, L., 2005. *Data Exchange for Machine Shop Simulation.* New Jersey, Institute of Electrical and Electronics Engineers, Inc.

McLean, C. & Leong., L., 2001. *The expanding role of simulation in future manufacturing.* New Jersey, Institute of Electrical and Electronics Engineers, Inc.

Mertins, K., Rabe, M. & Jäke, F. W., 2000. *Neutral template libraries for efficient distributed simulation within a Manufacturing system engineering platform.* Orlando, FL, In Proc. Winter Simulation Conference.

Mike B, Martin S, Alexander F, Peter W, 2009. *Object-oriented engineering data exchange as a base for automatic generation of simulation models*, IEEE.

Miriam, S. & Rainer, D., 2008. *The system independent data exchange format CAEX for supporting an automatic configuration of a production monitoring and control system.*. s.l., IEEE.

Pawan, P.,1998. *Handbook of Simulation Principles,Methodology, Advances, Applications.* New York: Wiley.

Peters, J. S., Smith, D. J. & Medeiros, M. W., 2001. *The Expanding Role Of Simulation In Future Manufacturing.* Gaithersburg.

Robinson, S., 2004. *Simulation: The Practice of Model Development and Use.* Chichester, UK: Wiley.

Simon, J. E., Taylor, X. W., Stephen , J. & Malcolm,L.,2006. Integrating Heterogeneous Distributed Cots Discrete Event Simulation Packages: An Emerging Standards-Based Approach. *Ieee Transactions On Systems, Man, And Cybernetics,* 36(1).

Skoogh, A. & Johansson, B., 2007. *Time consumption analysis of input data activities in discrete event simulation projects.* Gothenburg, Swedish Production Symposium.

Taylor, J. E., Gan, B. P., Strassburger, S. & Verbraeck, A., 2003. "HLA-CSPIF technical panel on distributed simulation. *Winter Simulation Conference,* pp. 881–887.

Viviana, M., Angela, L. & Paolo, R., 2008. *Automatic Ontology Matching via Upper Ontologies: A Systematic Evaluation.* Genova, IEEE Computer Society.

Waktersdorfer, F. & Zoitl, A., 2010. *Version Management And Conflict Detection Across Heterogenous Enginering Data Models In Industrial Infomatics.* London, Ieee.

Waltersdorfer, F., Moser, T. & Zoitl, A., 2010. Version management and conflict detection across heterogenous

engineering data models. *8th International conference on IEEE,* pp. 928-935.

Woolf, B. & Hope, G., 2011. *Enterprise intergration patterns, Designing, building and deploying solution,* Readings: Admission-Wesley.

Yücesan, E., Chen, C., Snowdon, J. L. & Charnes, J. M., 2002. *The possible role of backbone architecture in real-time control.* San Diego, CA, Winter Simulation Conference, pp.1675–1682.

HARDWARE SIMULATION

USING LABVIEW FOR MODELING A 3 PHASE TRANSMISSION LINE WITH FAULTS

V. ZILERIU, M. STREMTAN and N. VASILIU
University POLITEHNICA of Bucharest
313, Splaiul Independentei, Sector 6
RO 060042 Bucharest, Romania
E-mail: vlad.zileriu@ni.com

KEYWORDS
Modeling and simulation, Design, Prototype, Deploy, Digital Protective Relays, Real-Time Simulation

ABSTRACT

In the current paper, we will present how to design the model of a 3-phase transmission line with all the possible faults that we can generate. This is a software model that will run on a Real Time Machine in order to emulate the real time behavior of a transmission line. Using Off-the-shelf Hardware platforms and a Graphical System Environment, we will transfer from a Software model to electrical signals

INTRODUCTION

We are using a Design, Prototype and Deploy approach to develop an Intelligent Digital Protective Relay (DPR). Our first step is the emulation of a 3-phase transmission line and all the possible faults that we may encounter in the real life.
The necessity of building such a software model that will run on a Real Time Hardware platform and will generate real time electrical signals as inputs for our DPR is driven by a number of different factors as follows:

1) Project design approach: the world around us is more and more software design. Everything that surrounds us has a piece of software that is running on an ASIC. More and more studies are showing that it is more convenient and cheaper to do software testing compared to hardware testing. We plan to build a SW model, test it, make sure it has the needed behavior and only after that adapt it to run on a hardware platform. This will minimize the overall development time, detect very early bugs of our model with no direct cost associated with it
2) Limited resources: we want to have the possibility to test our DPR more than just a software model. The access to a 3-phase transmission line is problematic. The possibility of generating desired faults on a 3-pahse transmission line is almost impossible to achieve, so our current approach can provide us the same experience and all the flexibility that we require
3) Cost: a generic Off-the-Shelf platform provides generic Inputs/Outputs module that normally have a ± 10 V. The voltage divider circuits and the current clamps that are required to adapt the V/I levels of a 3-phase system are expensive. The suggested approach is avoiding this extra cost.

The current paper is proposing an open, flexible and manageable approach of a 3-phase transmission line simulation in which we will have the flexibility of generating generic or particular faults.

BACKGROUND

The world evolution is requesting a higher demand of energy. The integration of traditional energy generation sources (fossil, atomic ,hydro) with the new green energy (wind, solar) plus the expansion of rural areas are adding extra pressure in the grid, creating more imbalance and more possible factors that can generate faults in the system.
The need to act quickly to protect circuits and equipment as well as the public often requires protective relays to react and trip a breaker within a few thousandths of a second. In these cases, it is critical that we have the possibility to test this behavior during the development phase.
Transmission lines have the highest probability of fault incidence from all the components of the power system because they are interconnecting all the energy producers, the consumers and they are the most exposed to the environment. Majority of the faults are generated by nature: lightning, storms, earthquakes, vegetation fall or different climatic variations are beyond our real-time control.
There faults that we encounter in a 3-phase transmission line are divided in two categories:

1) Unbalance faults:
    a. Single line to ground
    b. Line to line
    c. Double line to ground
2) Balance faults:
    a. Three phase to ground

(Zhuokang Jia 2012)

Our model will integrate all this possible faults and appropriate Voltage and Current signals are generated from our Real Time Hardware platform that will serve as inputs to our DPR.

3-Phase transmission lines and Faults

Transmission line faults occur more frequently among the faults of any power system. About two thirds of the faults in the power systems occur in the transmission line network (Sanaye –Pasand & Malik, 2001). As mentioned previously the types of faults that can be found in a transmission line are:

Single Line to Ground Fault

This type of fault occurs when a single phase (A,B or C) is connected to the Ground of the power system. As a direct result, the current for that particular phase is increasing a lot and the voltage level is decreasing. The other 2 phases will experience a slight increase in Voltage levels as you can see in Fig.1.
To simulate this fault we are changing the Voltage and Current amplitude level for the corresponding error phase.

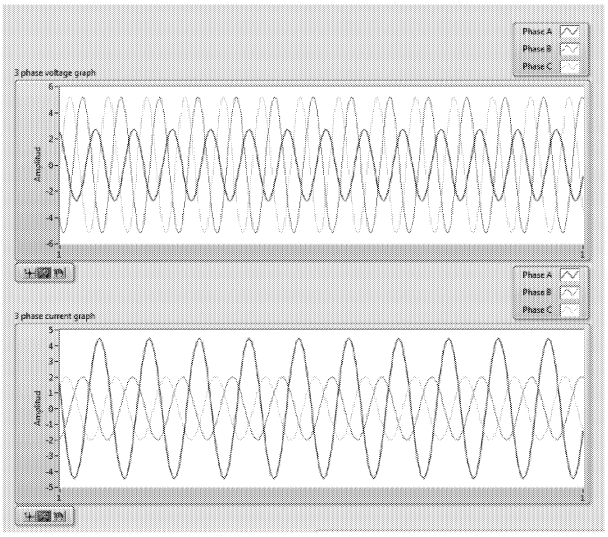

Fig 1 Phase A to Ground simulation

Line to Line Fault

This type of Fault occurs when any two phases are connected together, with the exception of the third phase or the ground. Similar to single line to ground fault in the case of Line to Line fault the voltages of the 2 phases connected together are dropping and the corresponding current is increasing as we can see in Fig.2. From the phase (angle) perspective the voltages are close to each other while the currents are at 180º. The 3rd phase remains unchanged.
(Ron Alexander 2009)

Double Line to Ground Fault

This type of fault occurs between any two phases and the ground of the power system. The third phase is not affected. In this situation, we have a very similar behavior like in the situation of Single line to ground fault. As a direct result, the current for the two particular phases is increasing while the voltage level is decreasing. The third phase will experience a slight increase in Voltage levels as you can see in Fig.3.
To simulate this fault we are changing the Voltage and Current amplitude level for the corresponding error phase.

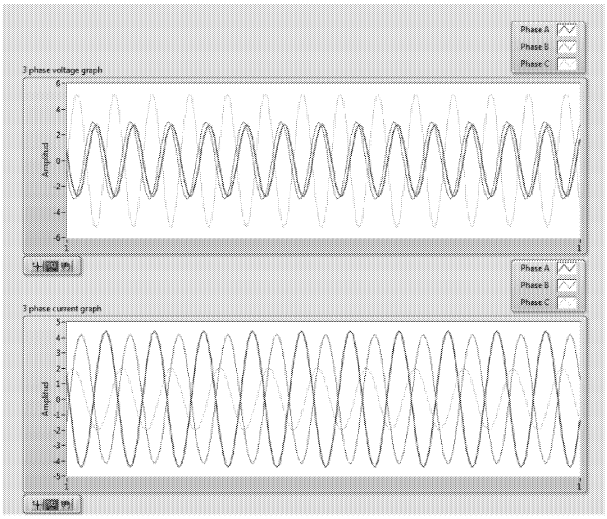

Fig 2 Phase A to Phase B simulation

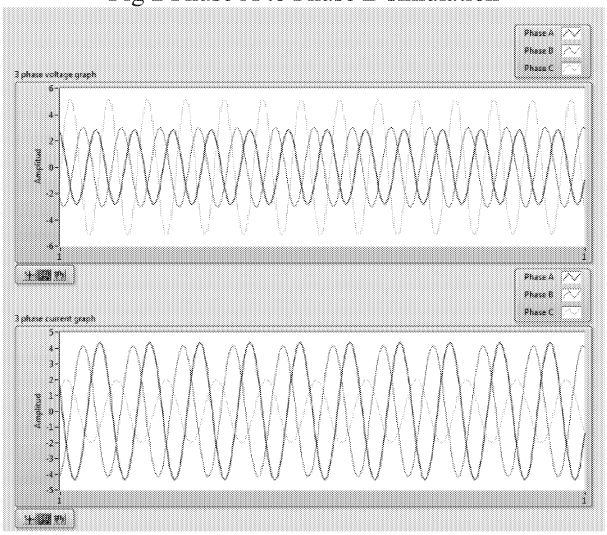

Fig 3 Phase AB to Ground

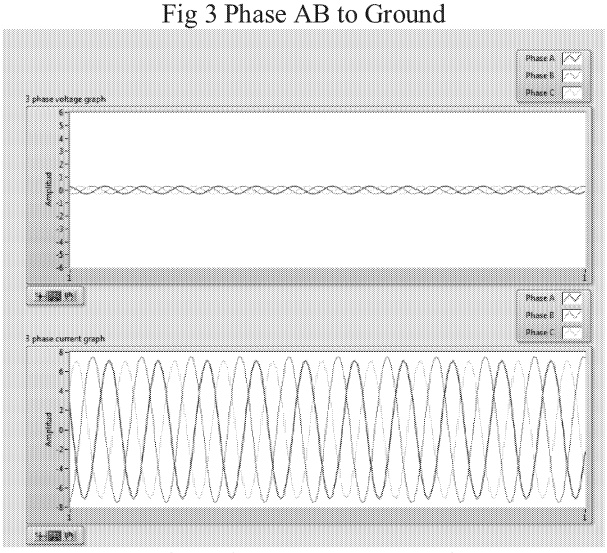

Fig 4 Phase ABC to Ground

Three Phases to Ground

A 3 phase to ground Fault is a type of fault that occurs when all 3 phases are connected to the ground of the power system. This type of faults are very rare, less than 5% of total number of errors. The voltages of all 3 phases is dropping close to 0 and the currents are increasing on all 3 phases as you can see in Fig 4.

LabVIEW simulations

All the presented graphs are a result of the simulation algorithms developed in LabVIEW. LabVIEW is a Graphical System Design Platform that is a providing a set of pre-build functions perfect for simulation algorithms. We used the Waveform palette functions to generate sine wave signals. The parameters that we used to generate the signals in No error mode are:

a) Frequency : 50 Hz
b) Voltage Amplitude: 5 V
c) Current Amplitude : 2 V
d) Phase: Line A=0,Line B=120,Line C=240

After generation all the 3 phases voltages were merged to a Waveform graph for display. We did the same with the currents.

In order to have the ability to generate the appropriate signals each time depending on the fault time we build a state machine architecture that is driven, by the user. On the front panel there is a control that has defined all the possible combinations of faults. The user is choosing one of them and the application will run the appropriate state from the state machine application generating the signals for voltages and currents.

The faults that are pre-defined are:

- No Faults – Default Balance system
- Phase A to Ground
- Phase B to Ground
- Phase C to Ground
- Phase A to Phase B
- Phase B to Phase C
- Phase C to Phase A
- Phase AB to Ground
- Phase BC to Ground
- Phase CA to ground
- Phase ABC to Ground

In LabVIEW we can load a Matlab or Simulink model in the same code to compare results. The openness of the platform allows easy integration with other software environments.

From Model to Electric Signals

In the last 40 years, Digital Relays evolved in parallel with the evolution of technology. Faster processors, faster ADC's allow algorithms that are more complex and we can provide more sampling point with a higher accuracy. In the 1960', the first generations of Digital Relay were deploy in the grid. They were develop as fault location algorithms where the engineers could control the reach characteristic of a distance relay (Gilcrest et al, 1972). This type of digital faults locators calculates the reactance of a faulty line taking in consideration voltages and currents phasors.

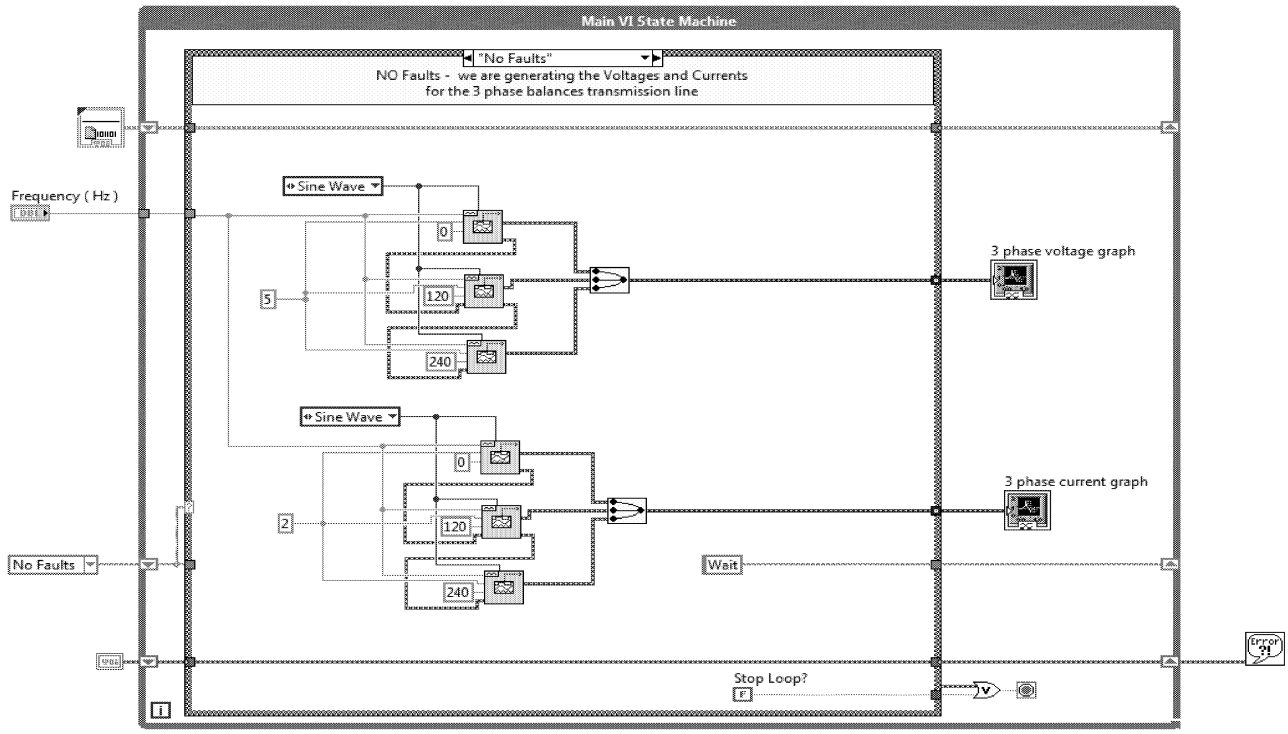

Fig 5 LabVIEW Application State Machine

In the late 70's the research was focus on travelling waves. The fault was detected in the first two-three cycles after the error occurred which represented a high frequency transient waveform front. In the last 30 years, different algorithms for implementation of traveling wave distance protection can be find (Shehab-Eldin et al., 1988, Ancell et al., 1994).
In the late 80's with the help of the Global Positioning System (GPS), the possibility of taking synchronized measurements at big distances open new opportunities. The Phasor Measurements Units (PMU) are the most commonly used in the grid, with the help of GPS they are providing a very accurate location of the fault. The measurements are base on the impedance measurement and algorithms for fault location are presented. (J. Izikovski et al, 2006).

modification at the functionality; all we need to add is the IO integration. We are using a ±10V analog output module that has four simultaneous sampling channels each one at a rate of 100 KS/s. We used isolated channels to assure signal integrity. The first module is generating the Voltages and the second module is generating the Currents.
In the application, we implemented a triggering mechanism that is starting the generation of Voltages for each line at the same time. The same triggering mechanism applies to the currents. This way we are assuring that the phase alignment equals the values that we define in the application.
As we are showing in the Fig 6 with the help of the I/O Variables we are passing the information from the Real Time Controller to a stand-alone computer were the operator is defining what stage we should generate in the same way as previously defined through Ethernet

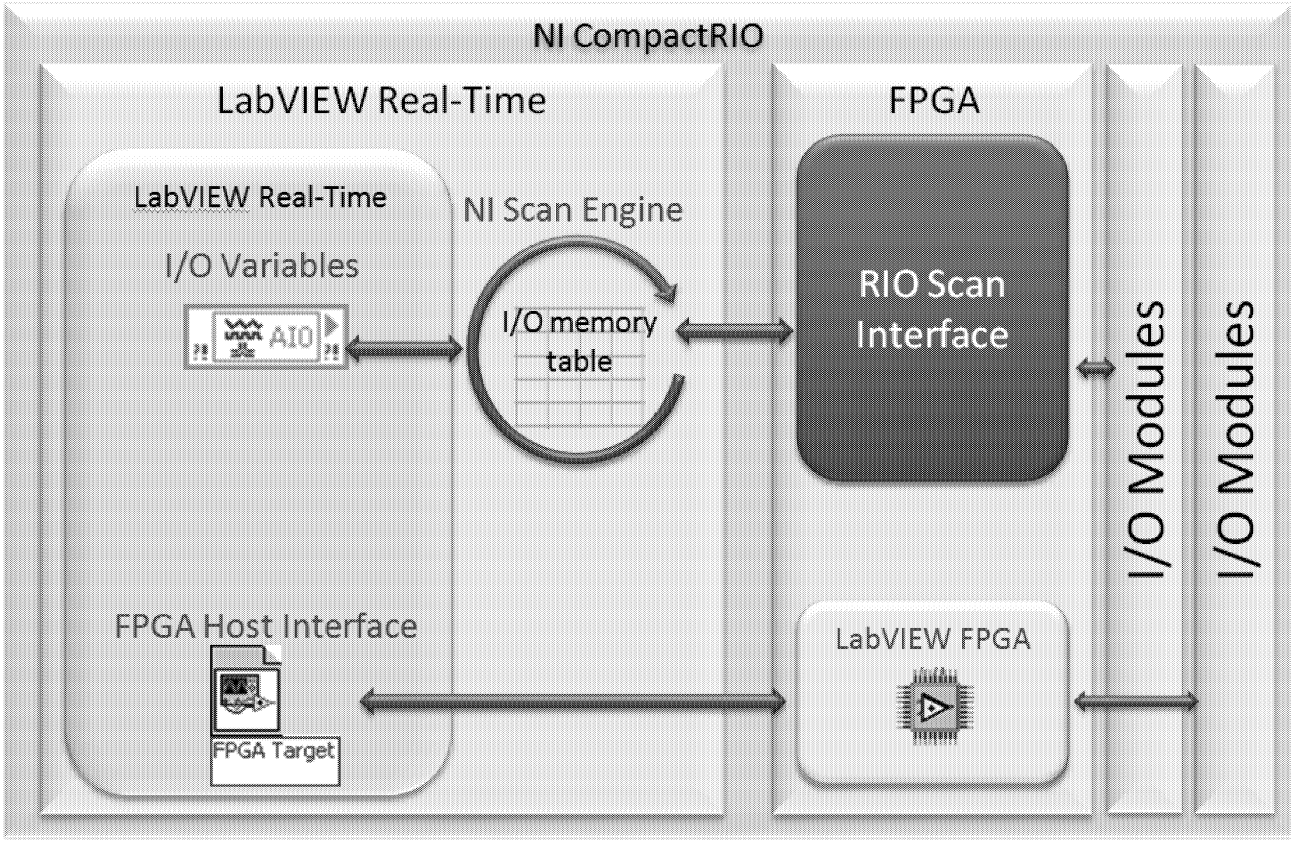

Fig 6. The CompactRIO architecture

All the above research is in the need
of a flexible software hardware platform that will have the capability of integrating software algorithms developed in different simulations environment. With LabVIEW, we have the possibility of loading simulations developed in Simulink or Matlab. In this way, we have the capability of testing other models using the same architecture.
At this stage, we have a software simulation model. The flexibility that LabVIEW provides is the integration with the Hardware platforms. For this reason, we choose the CompactRIO platform as a deployment platform. The code build previously does not need any

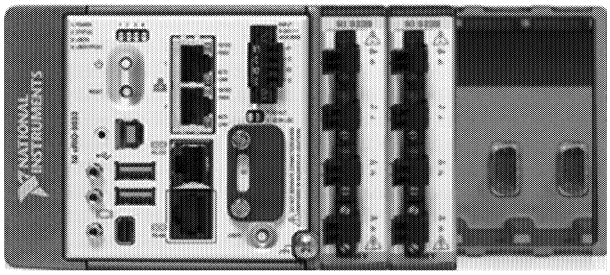
Fig 7 The CompactRIO Hardware platform

After loading the simulation code and linking it to the Analog Output modules, we generated all the possible error and measure the electrical signals that we generated using a four channels oscilloscope. The result is identical with the simulation profiles that we already presented.
There are a many reasons why we choose CompactRIO platform from National Instruments. One of the most important aspects is a collaboration project between National Instruments and Siemens in the field of Smart Grid, monitoring and protection. The second is the flexibility that it provides to switch from Software simulation to real signals using off the shelf components. Last but not least, the graphical system design approach allows any engineer to develop algorithms without spending time on learning syntax.
More than this the open platform concept allows any researcher to collaborate and share their models while using the same Hardware platform and modules so now we can validate algorithms not only as software simulation response but also as real signals simulators.

CONCLUSIONS

With the use of LabVIEW and National Instruments hardware platform CompactRIO we had the capability of building a 3-phase transmission line fault emulator that we can use to test the functionality of our DPR
Using the V-Diagram principle we generated a simulation software. We have the flexibility of adding extra errors or to simulate situations that are hard to replicate in real scenarios like rapid voltage changes or phase imbalances or any theoretical or practical error situation as a way to test how DPR's are reacting.
We managed to identify a flexible, affordable way to simulate a 3 phase transmission line with faults.

REFERENCES

Sanaye-Pasand, M., & Malik, O. (2001).
"Neural Network-Based Fault Direction Discrimination for High-Speed Transmission Line Protection. *Electric Power Components and Systems, 29* (8)."
Zhuokang Jia (2012)
"Power Transmission Line Fault Classification Using Support Vector Machines"
Ron Alexander (2009)
"Phasor Diagram Fault Analysis "
G.B. Gilcrest ,G.D. Rockefeller ,E.A. Udren (Jun 1972)
"High-Speed Distance Relaying Using a Digital Computer I - System Description"
E. H. Shehab-Eldin , P. G. McLaren (Jul 1988)
"Travelling wave distance protection-problem areas and solutions"
G.B. Ancell, N.C. Pahalawaththa (Apr. 1994)
"Maximum likelihood estimation of fault location on transmission lines using travelling waves "
J. Izykovski, R. Molag, M. Bozek (2006)
„Fault location on three-terminal overhead lines with using two-terminal synchronized voltage and current phasors)

WEB REFERENCES

http://www.ni.com
http://www.mathworks.com
http://www.intechopen.com

BIOGRAPHIES

ZILERIU VLAD graduated Applied Electronics and Telecommunication from the Technical University of Cluj Napoca with Major in Electronics in 2005, currently working on a Ph.D. thesis in the field of advanced Digital Protective Relays at Fluid Power Laboratory from the University POLITEHNICA of Bucharest. He is currently Technical Sales Manager at National Instruments Romania, working in the field of Data Acquisition, Industrial Automation, Simulation and Control.

STREMTAN MIRCEA graduated Electronics and Telecommunication from University "POLITEHNICA" of Timisoara in 2008, and a Major in Telecommunication. He is currently working on a PhD research thesis on Real-Time Simulation of wind power stations with LabVIEW at the Fluid Power Laboratory of the University POLITEHNICA of Bucharest.

NICOLAE VASILIU graduated in Hydropower Engineering from University POLITEHNICA of Bucharest in 1969. He became a PhD in Fluid Mechanics after a research stage in Ghent State University and Von Karman Institute from Bruxelles. He became state professor in 1994, leading the Fluid Control Laboratory from the Power Engineering Faculty of the above university. He worked always for the industry, as project manager or scientific advisor. He was also leading five years the Romanian Innovation Financing Agency.

LATE PAPERS

Analysis and Performance of Handover in UMTS Network Using OPNET Modeller

Wafa BENAATOU
Cadi Ayyad University
ENSA Marrakech
Morroco
Wafaa.benaatou@gmail.com

Adnane LATIF
Cadi Ayyad University
ENSA Marrakech
Morocco
a.latif@uca.ma

Vicent PLA
Universitat Politècnica de
València
Spain
vpla@upv.es

KEYWORDS
handover, UMTS, Mobility, Simulation, OPNET modeler.

ABSTRACT

Handover is of great significance to achieve seamless connectivity in wireless networks. This paper gives an impression of the main factors which are being affected by the soft and the hard handovers techniques. To know and understand about the handover process in UMTS network different statistics are calculated. This paper focuses on the quality of service (QoS) of soft and hard handover in UMTS network, which includes the analysis of received power, signal to noise radio, throughput, delay Traffic, traffic received, delay, total transmit load, end to end delay and upload response time using OPNET simulator.

INTRODUCTION

The overlapping of different wireless networks and their hierarchical and asymmetric relationship is called vertical, when a mobile user switch from one network to another is called handover. Handover is the essential component for dealing with the mobility of end users. It guarantees the continuity of the wireless services when the mobile user moves across cellular boundaries. In a heterogeneous network, handover process is classified into two categories: horizontal handover and vertical handover.Horizontal handover takes place when a mobile user moves from one network to another within the same network technology. Vertical handover happens when a mobile user moves from one network to another with different technology meanwhile horizontal handover happens within the same type of network. In our work we focus in the horizontal handover.

OBJECTIVES OF HANDOVER

Handover can be initiated in three different ways: mobile initiated, network initiated and mobile assisted .

Mobile Initiated

The Mobile makes quality measurements, picks the best BS, and switches, with the network's cooperation.This type of handover is generally triggered by the poor link quality measured by the mobile.

Network Initiated

The BS makes the measurements and reports to the RNC, which makes the decision whether to handover or not. Network initiated handover is executed for reasons other than radio link control, e.g. to control traffic distribution between cells. An example of this is the BS-controlled Traffic Reason Handover (TRHO). TRHO is a load-based algorithm that changes the handover threshold for one or more outgoing adjacencies for a given source cell depending on its load. If the load of the source cell exceeds a given level, and the load in a neighboring cell is below another given level, then the source cell will shrink its coverage, handing over some traffic to the neighboring cell. Therefore, the overall blocking rate can be reduced, leading to a greater utilization of the cell resource.

Mobile Assisted

Here the network and the mobile both make measurements. The mobile reports the measurement results from nearby BSs and the network makes the decision of handing over or not.
The objectives of handover can be summarized as follows :

- Guaranteeing the continuity of wireless services when the mobile user moves across the cellular boundaries
- Keep required QoS
- Minimizing interference level of the whole system by keeping the mobile linked to the strongest BS or BSs.
- Roaming between different networks
- Distributing load from hot spot areas (load balancing)

The triggers that can be used for the initiation of a handover process could be the link quality (UL or DL), the changing of service, the changing of speed, traffic reasons or O&M (Operation & Maintenance) intervention

SIMULATION OF SOFT AND HARD HANDOVER IN OPNET

For the implementation of our different scenarios we have used the OPNET Modeler 14.5. Figure 5 shows the scenario of UMTS network, the first operating system with a hard handover and the second with the soft handover. The network also includes two mobile users whose movements were defined by us. Then each piece of equipment has been configured in a more or less optimally to meet our needs for comparison.

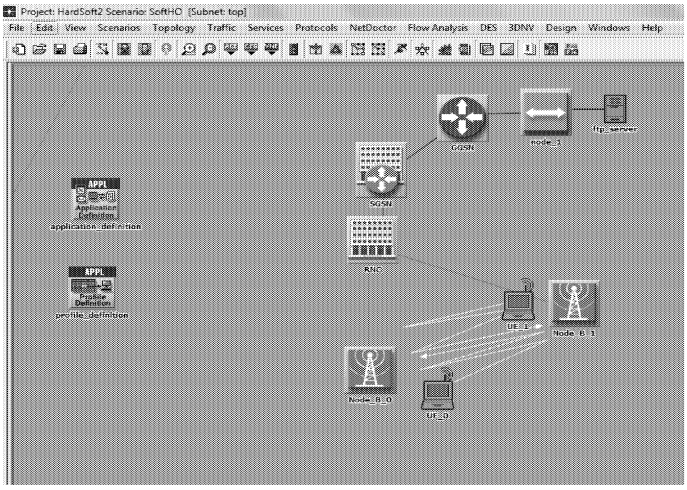

Figure. 1 UMTS OPNET Simulation Model Overview

When all configurations are done correctly, the simulation runs smoothly; what we see in the following screenshots:

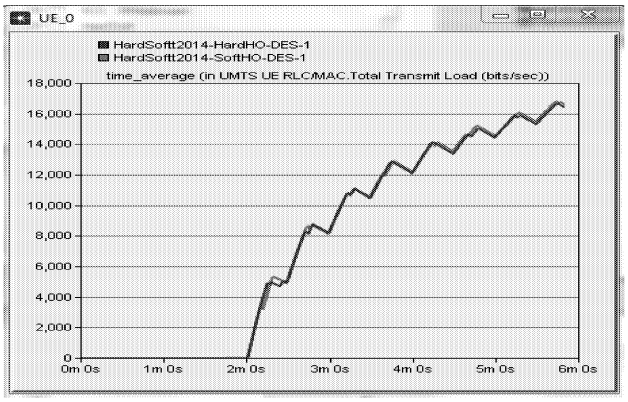

Figure. 2 Total Transmit load

Figure 2 shows the total transmit load, Blue color graph shows the Total Transmit load for hard handover and red color graph shows the Total Transmit load for soft handover it is clear from the results that for the soft and the hard handover there is almost no difference between the total transmit load.

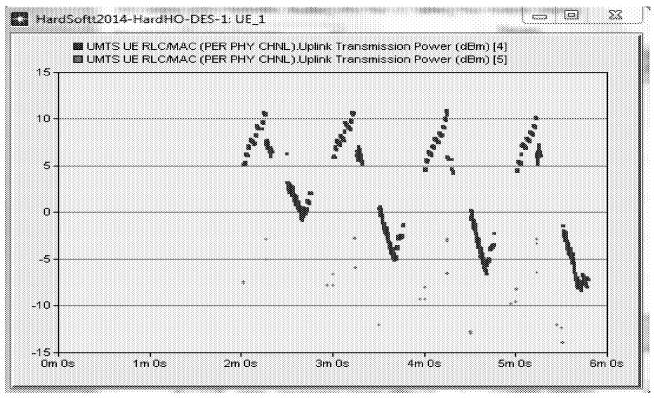

Figure. 3 Uplink Transmission Power

It is cleared from the Fig. 3 that the blue dots are higher and red dots are lower which means that the hard handover has higher uplink transmission power than the soft handover.

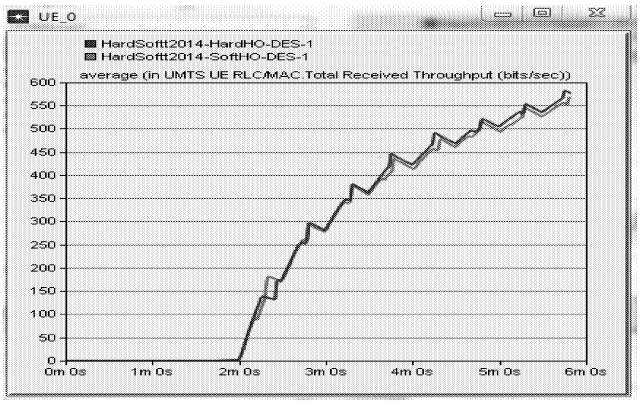

Figure. 4 Total Received Throughput

Figure 4 shows the total received through put, Blue color graph shows total received through put for hard handover and red color graph shows total received through put for soft handover as we move left to right the total received through put for hard and soft handover increase and we have a peak average of 390 bits/sec.

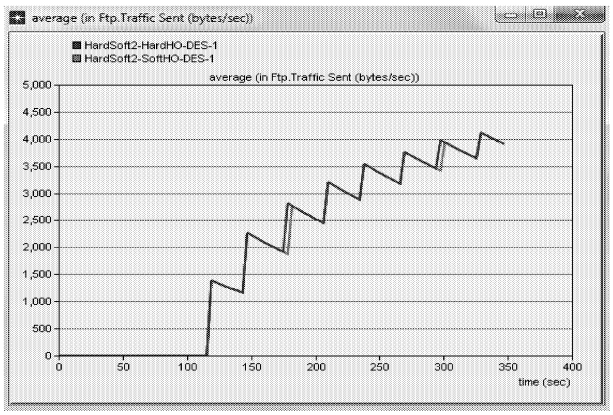

Figure. 5 Traffic Sent

Figure 5 represents the traffic received according the time, it's clear from the results that the traffic sent of hard handover is slightly better than the soft handover .

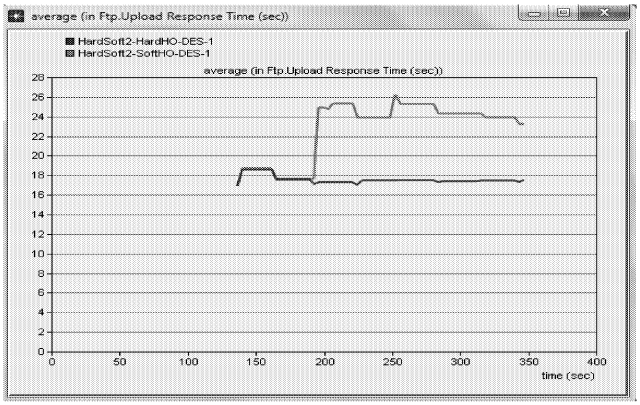

Figure. 6 Upload Response Time

The Figure 6 shows that the upload response time according the time, we can see that the upload response time of soft handover is higher than the upload response time of hard handover.

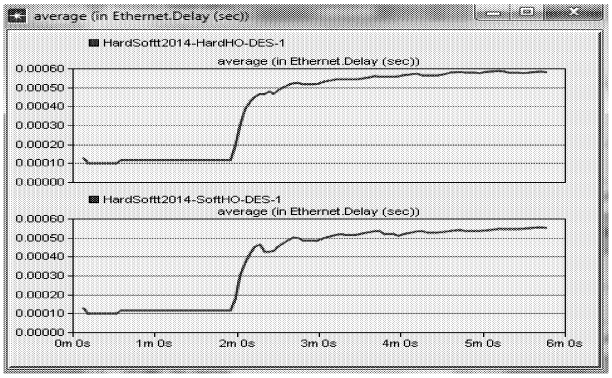

Figure. 7 Delay

First graph shows the delay for hard handover and the second graph shows delay for soft handover.

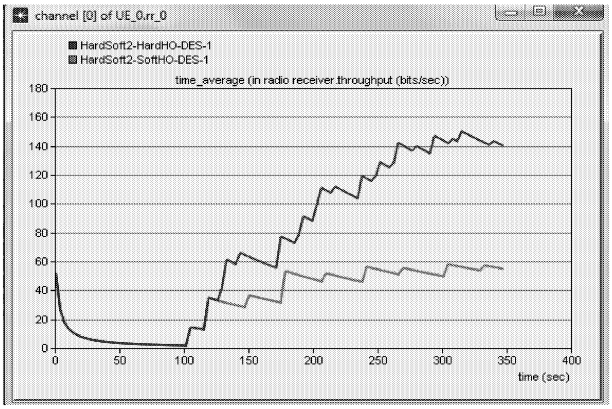

Figure. 8 Throughput

Based on the maximum throughput value in Figure 8, the maximum throughput of the hard and soft handover are 142 bits/sec and 39 bits/sec, respectively. It is obvious that the throughput of hard handover is higher than soft handover.

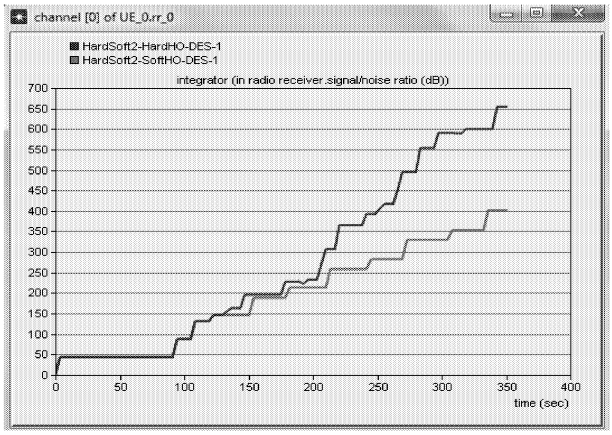

Figure. 9 Signal to Noise Radio

Figure 9 represents the signal to noise ratio according the time. It was found that the signal to noise ratio of hard handover is higher than soft handover.

CONCLUSION

In this paper, performance analysis of UMTS network is done for voice conferencing using OPNET Modeller.The simulation results show that the uplink transmission power, traffic sent, throughput, received power and signal to noise ratio of network with hard handover are good as compared to the network with the soft handover. But the upload response time in soft handover is higher than the hard handover. The total transmit load, total received throughput, traffic received, delay and end to end delay are some of two types of handover in UMTS network. For future work number of networks in this structure can be increased and simulated with different applications.

REFERENCES

S.Busanelli, M.Martal`o, G.Ferrari, and G. Spigoni "Vertical Handover between WiFi and UMTS Networks: Experimental Performance Analysis", International Journal of Energy, Information and Communications Vol. 2, Issue 1, February 2011

Cheema, R.A. and M.Jehanzeb Irshad. 2008. "Issues and Optimization of UMTS Handover".

Chen , Y. 2003. "Soft Handover Issues in Radio Resource Management for 3G WCDMA Networks".

Sandrasegaran, Mo Li. and K. Huang, X. 2005. "Identity Management in Vertical Handovers for UMTS-WLAN Networks" .

Ahmed Abdulhadi Ahmed, Hawraa H. Abbas Al-Rubiae and Haider Galil Al-Qurabi "Evaluation and Comparison of Soft and Hard Handovers in Universal Mobile Telecommunication (UMTS) Networks", Journal of Kerbala University , Vol. 8 No.1 Scientific . 2010

Ferrus, R., Glonch, A., Sallent, O., Pérez-Romero, J. "Vertical Handover Support in Coordinated Heterogeneous Radio Access Networks".

S.Busanelli, M.Martal`o, G.Ferrari, and G. Spigoni. 2001 "Vertical Handover between WiFi and UMTS Networks: Experimental Performance Analysis", International Journal of Energy, Information and Communications Vol. 2, Issue 1.(Feb)

Lee, S., K. Sriram, K. Kim, Y. H. Kim and N. Golmie, 2009. "Vertical Handoff Decision Algorithms for Providing Optimized Performance in Heterogeneous Wireless Networks," IEEE Transactions on Vehicular Technology, vol. 58, no. 2, pp. 865-881, (Feb).

BENMIMOUNE, A . 2010. "HANDOFF VERTICAL ENTRE RÉSEAU UMTS ET WLAN" ,QUÉBEC,Canada.

Ferrus, R. , A. Glonch, O.Sallent and J. Pérez-Romero, " Vertical Handover Support in Coordinated Heterogeneous Radio Access Networks".

Rukhsar A.C and M. Jehanzeb Irshad . 2008 "Issues and Optimization of UMTS Handover", Blekinge Institute of Technology (Feb).

LARGE VIRTUAL MANUFACTURING SYSTEMS
MODELLING AND SIMULATION BETWEEN GO TO AND THE OBJECT ORIENTED APPROACH

Florin IONESCU
Blarerstr. 56
D – 78462 Konstanz, Germany
E-mail: florin.ionescu@stw.de

KEYWORDS
Modelling & Simulation, Hybrid Drives and Control, Large Manufacturing Systems, Cutting and Cutting Tools, Machine Tools, Robots, Sensors, Logistics.

ABSTRACT

The paper presents achievements leading towards attaining complex and easy to handle tools, for research, technical development and innovation and, last but not least, for education. It covers the Object Oriented Modelling and Simulation (OOM&S) of Large Virtual Manufacturing Systems (LVMS). Some evaluatori moments along with the evolution of "easy" modelling of any large device, installation, machines or systems of machines are presented. An important part of the paper refers to the OO modelling of hybrid drives and control systems – using the HYPAS Technology. It shows how scientists succeed to appropriately organize mathematical models, to approach differential equations, and static and dynamic (non)linear properties, to accomplish and facilitate easy approaches for M & S. New notions were used to define the structures: simple properties, modules, groups, chains, braches, installation and so on, towards large systems, by associating working machines tools, (mobile) robots, sensors, human operators and logistics, all envisaged with both, hybrid direct drives (HDD) and control of solid bodies, making use of a 3D-M&S for design, FEM (inclusively fluid) technologies. In this way it is appropriate and easy to understand, how to further change, develop and handle models of any large systems that can be obtained, simulated and virtualized.

COMPONENTS OF A LARGE VIRTUAL MANUFACTURING SYSTEM

In the framework of the Project Large Scale Manufacturing Systems (Figures 1, … 7) the following subsystems were developed: 1. Cutting and Cutting Tools; 2. Machine Tools; 3. Industrial Robots & Manipulators with both, Inverse and Direct Dynamics; 4. Personalized Logistic Environment; 6. Fault Detection & Prediction; 7. Sensors & Networking; 8. Human operators. The paper will try to show, while focusing on Hydraulic Drives the spectacular evolution of the last 30 years from FORTRAN`s GO TO, to the actual technological achievements. The figures employed present achievements refering to Solid Body Modelling & Simulation of Machines Tools and Robots, by using the SDS/Motion Inventor Platform, with both inverse and direct dynamics and a Multi Level Modelling, Simulation and Control of hybrid Drive Systems with the HYPAS-Platform.

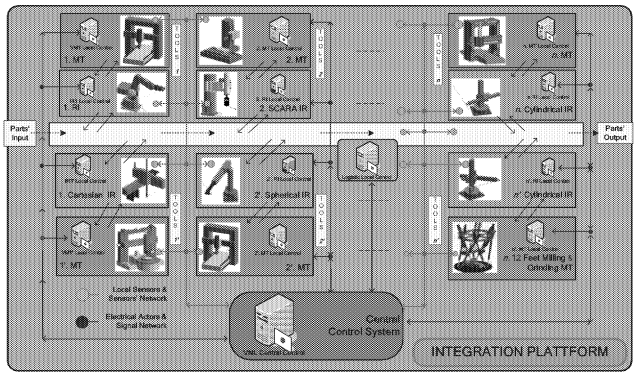

Figure 1: Space Distribution of a Large Scale Virtual Manugacturing System (LSMS).

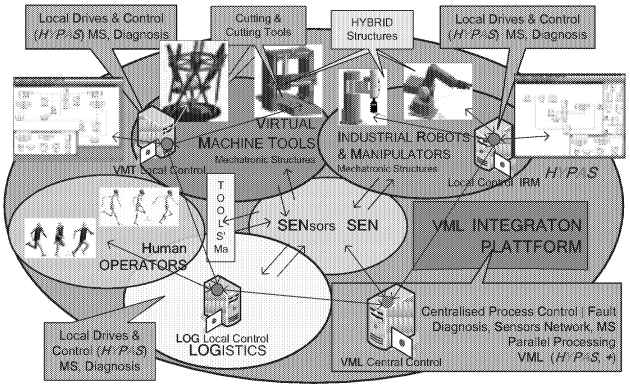

Figure 2: Proposal for Integration of LSMS`s Components

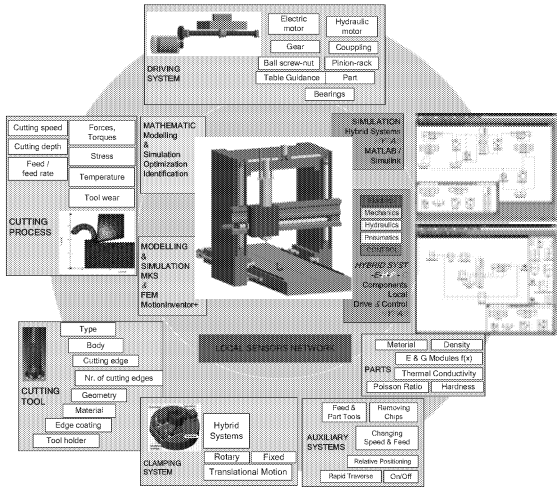

Figure 3: Subsystem Machine Tool in LSMS: Cutting; Cutting Tools; Devices; Parts; Driving & Control

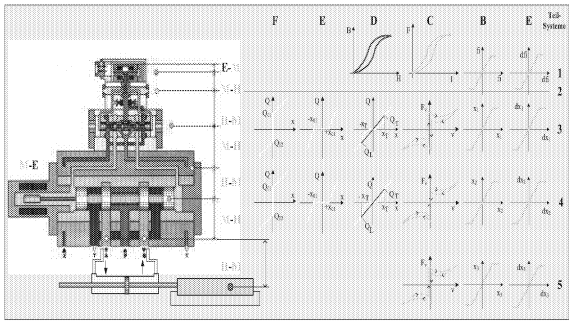

Figure 4: Non-Linearities of a Hybrid Drive System (BOSCH© & Ionescu© et all)

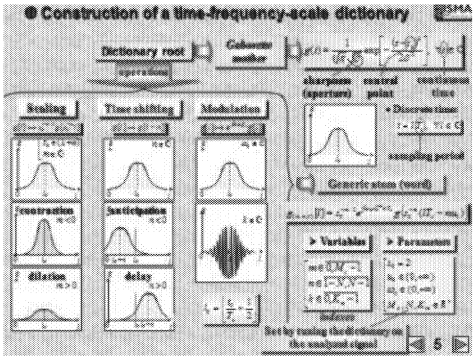

Figure 5: Fault Diagnosis & Prediction by Bearings (Stefanoiu & Ionescu)

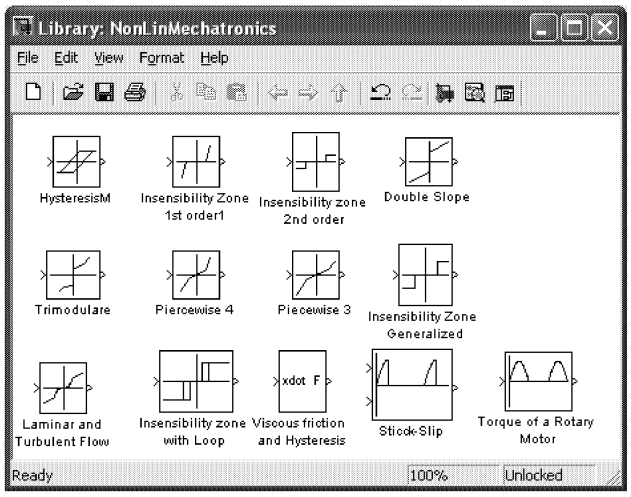

Figure 6 Nonlinearities in *HYPAS* (Ionescu© et all)

A SHORT HISTORY OF MATHEMATICAL MODELLING AND CONTROL OF DRIVE SYSTEMS

To obtain more and high performant devices, machines and installation, for individual, social and global needs scientists and engineers were continuously concerned with increasing the quality, reducing involved materials, using less energy and costs both for production, utilisation, development, production and maintenance. The humanity was continuously concerned with finding explanations to the phenomenon and to extend theoretical approaches. Thus the door towards extention of the knowledge and means for rapid approach and extrapolation to the mastering of complex functioning was open.

This has amplified the natural desire of humanity to develop and use new methods, means and, by increased expec-tations, to search for explanations and more intimate descriptions of the physical reality. This was also the case of electro-hydro-pneumo-mechano actuated devices, of installations and machines. New technologies were born and developed in harmonie and with the support of the evolutions and implicitly of computing devices and machines and their programming. These, starting with FORTRAN, via PASCAL and the latter on C and C+ to support the gigantic needs towards optimization, by available mathematical background were.

A special approach for MM were the programs aimed to "simulate" and "visualize" the achieved results. General purpose programs were developed rather for the IBM Large Computers, than for the Mini Computers and then, step by step for PCs, according to their computing speed, memory.

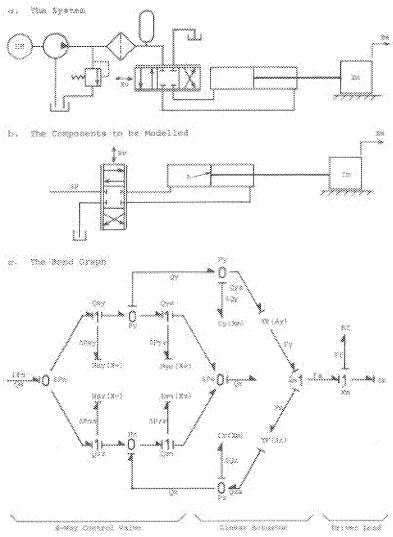

Figure 7: Bond Graph (Dransfield©)

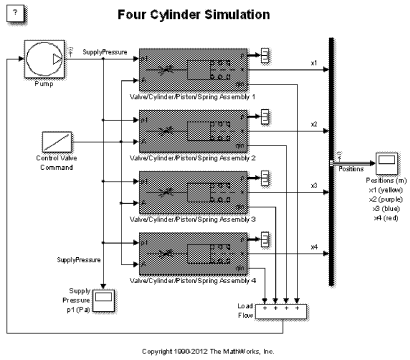

Figure 8: *MATLAB*©/*Simulink*–Plattform

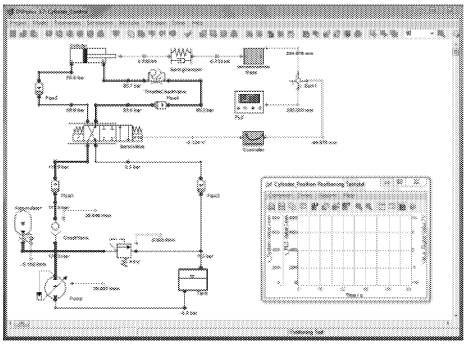

Figure 9: *DSHPlus* (Source: DSH)

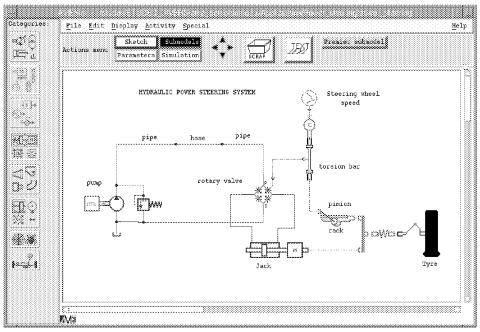

Figure 10: *AMESim* (Source: AMESIM©)

HOW TO MANAGE THE GROWING NUMBER OF VARIABLES AND DIFFERENTIAL EQUATIONS. THE *HYPAS*'s SOLUTION

By considering a hydraulic drive (Figure 12) and the attached equations one could transpose, into the ABD, and may accept that, it could be possible with the same old methods to solve it and to manage the obtained results.

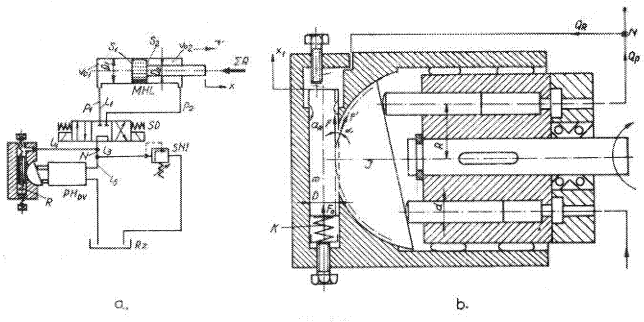

Figure 11: Functional BD (a) of a variable displacement axial pistons pump (b) with automatic flow Q control.

Ecuația lui Kirckhoff în nodul N

$$Q_P = Q_R + Q_M \tag{3.22}$$

Ecuația de mișcare la nivelul motorului hidraulic liniar

$$Q_M = \frac{\pi D_1^2}{4}\frac{\mathrm{d}x}{\mathrm{d}t} + \left[\frac{\pi d_0^2}{4}(l_1 + l_3 + l_8) + V_{01} + \frac{\pi D_1^2}{4}x\right]\frac{1}{E}\frac{\mathrm{d}p}{\mathrm{d}t} + a_M(p_1 - p_2) \tag{3.23}$$

Ecuația de echilibru dinamic al motorului și sarcinii legate rigid

$$M\frac{\mathrm{d}^2x}{\mathrm{d}t^2} + c\frac{\mathrm{d}x}{\mathrm{d}t} + \Sigma R = p_1\frac{\pi D_1^2}{4} - p_2\frac{\pi(D_1^2 - D_2^2)}{4} \tag{3.24}$$

Ecuația de mișcare la nivelul motorului de comandă a pompei

$$Q_R = \frac{\pi D^2}{4}\frac{\mathrm{d}x_1}{\mathrm{d}t} + \left(\frac{V_{03}}{E} + \frac{\pi D^2}{4}\frac{x_1}{E}\right)\frac{\mathrm{d}p}{\mathrm{d}t} + a_R \cdot p \tag{3.25}$$

Ecuația de echilibru dinamic al motorului de comandă

$$m\frac{\mathrm{d}^2x_1}{\mathrm{d}t^2} + c_1\frac{\mathrm{d}x_1}{\mathrm{d}t} + F_0 + kx_1 + F = \frac{\pi d^2}{4}p \tag{3.26}$$

Ecuația de mișcare la nivelul pompei

$$Q_P = \left(\frac{\pi d^2}{2}zR\sin\alpha\right)\cdot\omega_p - \frac{\frac{\pi d^2}{4}z\cdot R\cdot\sin\alpha + V_P'}{E}\frac{\mathrm{d}p}{\mathrm{d}t} - a_p\cdot p \tag{3.27}$$

Ecuația de echilibru dinamic al discului pompei

$$J\frac{\mathrm{d}^2\alpha}{\mathrm{d}t^2} + c_2R_1\frac{\mathrm{d}\alpha}{\mathrm{d}t} + (\Sigma F_i)\cdot R = F'(R_1 - \overline{m})^{*)}. \tag{3.28}$$

Ecuația de echilibru dinamic al pompei și motorului electric legate rigid

$$J_{EP}\frac{\mathrm{d}\omega_P}{\mathrm{d}t} + b_P\cdot\omega_P + (1 + c_{fp})\frac{\pi d^2}{4}(zR\sin\alpha)\cdot p = k_E(\omega_s - \omega_P) \tag{3.29}$$

Ecuația pierderilor de presiune între pompă și motor

$$p_1 = p - k_0(Q_M)^2 \tag{3.30}$$

Ecuația de legătură dintre x_1 și α

$$x_1 = (R_1 - \overline{m} + D/2)\sin\alpha \tag{3.31}$$

Proiecția forței F' pe direcția x_1

$$F = F'\cos\alpha \tag{3.32}$$

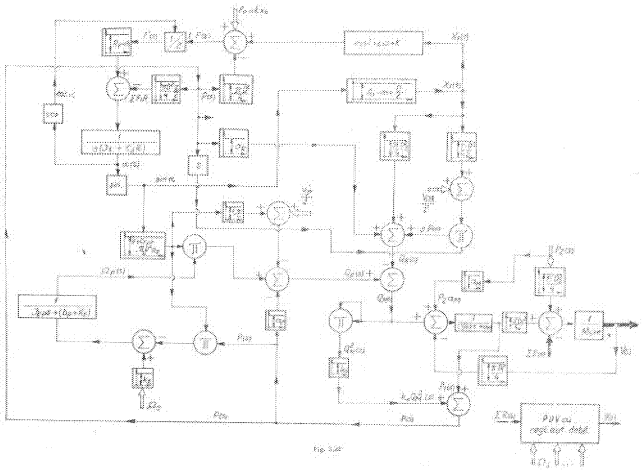

Figure 12: Non structured Analogue Block Diagram of the mathematical model presented above

The adopted solution by *HYPAS*, uses a (de)composition of mathematical properties – (variable) coefficients, algebraical or differential operations (linear or nonlinear), (differential) equations to build: groups, half modules, modules, half chains, double chains, (complete/incomplete) installations, etc. They may be, functionally, associated –theoretically unlimited–, or deleted as not interesting/insensitive) allowing the "user to complete or simplify, to change modules to any extend desired ones, including automatically self adapted ones.

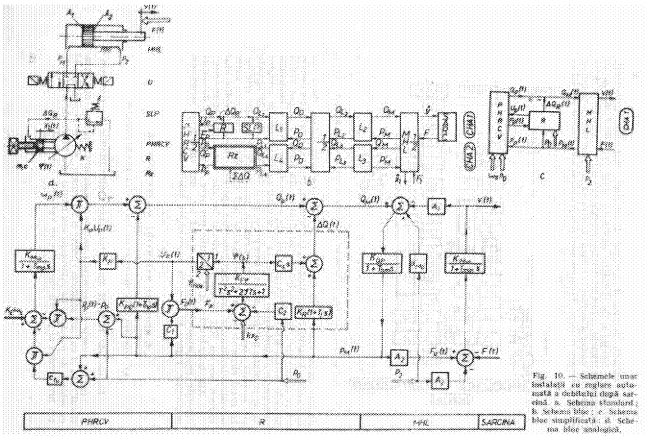

Figure 13: *HYPAS*-like transformed ABD of the above MM.

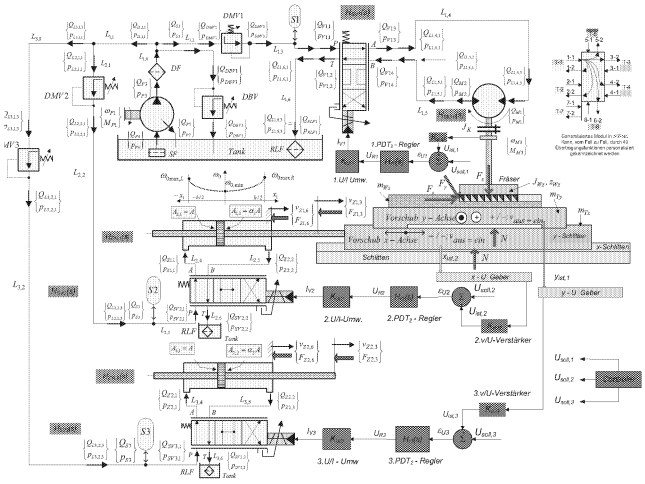

Figure 14: Hydraulic Drive Installation of a Milling Machine with Plane Milling Rotation

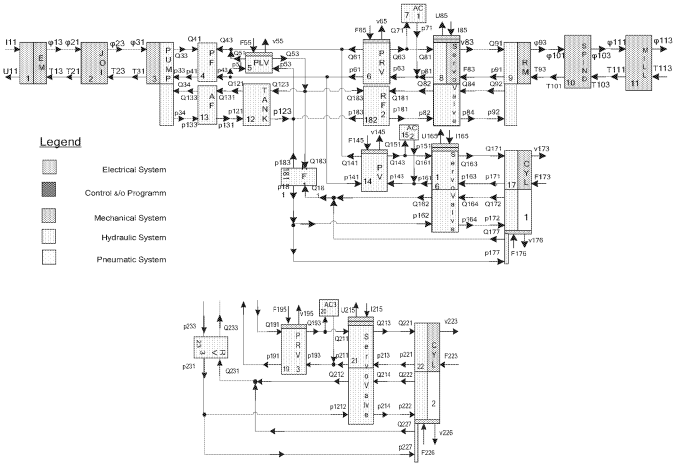

Figure 15: Block Diagrams with appropriately associated multipolar Elements (Ionescu©).

The components in the diagrams are pointing out –even suggesting– the high dimension of the mathematical model, attached to the real physical elements (1-ElMotor; 2-Spindel; 1-Pump; 2-Cylinder; 1-Hydro Motor; 3-Servo Valves, 3-Pressure Reducing Valves; 1-Pressure Limiting Valve; 4-Filters; 20- Lines (short/longue); 3-Accumulators, 1-Milling Tool) and its Interfaces with the Machine.

There are approximately 150 (nonlinear) Diferential Equations, and thus, approximately 300 Transfer Functions –for a linear(ised) MM–. These data are facilities and an important support for the RTDI, for training and education. Approximately 300 Transfer Functions – for a linear(ised) MM –. These data are facilities and an important support for the RTDI, for training and education. Approximately 300 Transfer Functions – for a linear(ised) MM –. These data are facilities and an important support for the RTDI, for training and education. The logical connections between variables, were automatically achieved by *HYPAS*, as all connections are achieved.

A numerical data set is proposed and can be, interactively appropriately changed. Dependent on the reasoning of the engineer, elements of installation and thus the associated MM, are created as a study-case, on the construction screen using a drag-and-drop action.

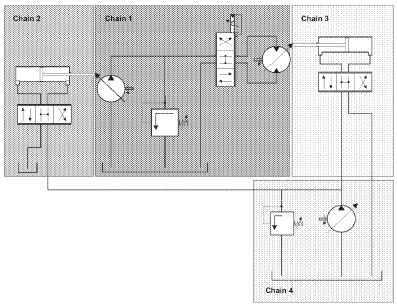

Figure 16: Manually designed ISO – Block Diagram of a Volumetric Speed Drive Installation–Chain 1. (Ionescu©)

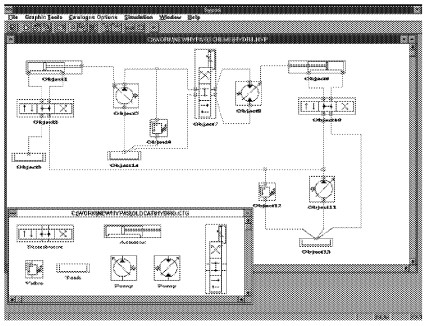

Figure 17: Simplified ISO–Analogue–Block–Diagram of the Installation generated like in Fig. 17. It was created with HYPAS by using a drag-and-drop function.

The Analogue Block Diagram and the MM (49 VAR, 98 TransFunc, by 25 Dif Eq), are equally created in parallel, and are available at any moment – with a basic data set - and can be appropriately appealed (Ionescu©).

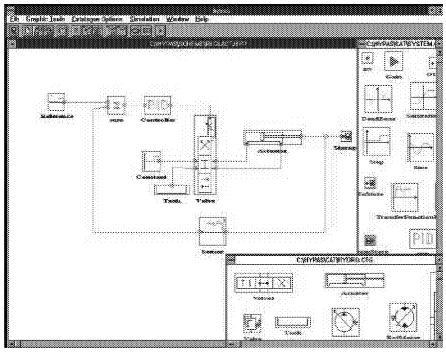

Figure 18: The ISO Analogue-Bloc-Diagram of a PID Controlled EH Drive with Position and Speed Control.

The functional connection of the MM of modules will be placed, as performed on the ISO-Block Diagram, through the connection of each input and output of the modules. After setting the individual data of the modules, the simulation can be started. Appropriate diagrams in the time and frequency domains are available. An interface data communication with other programs, including Motion-INVENTOR, MATLAB®/ Simulink, representations could be. Hybrid Drive Installations have several particularities; 1. They consist of hydraulic, pneumatic, mechanic and electric components which are statically and dynamically multiple non-linear while in association of modules which are placed, in correspondance to the appropriate control functions; 2.They have internal different properties; 3. The Elements 4. They work also with the phenomena and variables of different physical natures, which require high/fine matching of numerical approach and dimensions;

ACKNOWLEDGEMENTS

The author is deeply grateful to following German organizations: AvH, BMBF, DFG, DAAD, BWMFK, KDAW, AiF, RWTH-AC, TU-DA, UAS-KN, STW, SHB and UPB, for their support, having facilitated the achievement of solutions leading to the actual State of Art of Large Scale *Virtual Manufacturing Systems of the Future*. Cordial thanks for their contributions are due to the following colleagues: D. Andreescu, S. Arghir, D. Arotaritei, T. Borangiu, A. Ciomaga, F. Choynovski, G. Constantin, C. Constantin, R. Dobrescu, K. Harabadjinskii, F. Haszler, R. Hradynarski, R. Al-Kasahsbeh, K. Kostadinov, D.D. Popescu, J.R. Raol, H. Riehle, D. Stefanoiu, M. Al-Shamasin, C.I. Vlad. Best thanks for the friendly support along the years are due to: SDS GmbH, MATLAB©/Simulink, AutoDESK AG.

REFERENCES

Backé, W. 1979. Servohydraulik, Ed. of RWTH-Aachen, D.

Viersma, T.J.1980. Analysis, Synthesis and Design of Hydraulic Servosystems and Pipelines. Elsevier.

Dransfield, P. 1981. Hydraulic Control-Systems-Design, and Analysis of their Dynamics, Springer-Verlag.

Borangiu, T., Ionescu, F. and R. Dobrescu.1982. Modern Structures for Automatic Control of Machine-Tools. Technical Ed., Bucharest, RO.

Sprinceana, N., Dobrescu, R., Borangiu, Th. and F. Ionescu. 1976. Algorithm for Simulation of Adaptiv Control of Vertical. Milling Machines. (Original in RO). Review "Automatization, Management and Computers", Technical Ed., Bucharest, RO, Vol. 24, pp. 378 – 394.

Oprean, A., Ionescu, Fl. and A. Dorin.1982. Hydraulic Drive Systems. Elements & Systems. Technical Ed, Bucharest.

Ispas, C., Ionescu, F., Simion, F. and D. Boboc. 1985. Vibrations of Machine-Tools, Ed. UPB, Bucharest, RO.

Ionescu, F. 1987. Computer Aided Design of Hydraulic and Electro-Hydraulic Drive Installations. Multi Chapter Authors Book*: "Computer Assisted Research & Design in Machine Construction, Electrotechnics and Electronics"* (Eds. V. Baltac & A. Davidoviciu). Ed. of RO Academy, Bucharest, RO, pp. 149 - 180.

Dumitrache, I. and M. Dragoicea. 2013. *Fuzzy Reactive Behaviour in Autonomous Mobile Robotics*. ARA-Journal, Vol 2000–2002, Nr. 25-27, ISBN: 3-00-011583-8, Montreal/KN, CND/D, pp. 114–120.

Stefanoiu, D. and F. Ionescu. 2004. Fractal Data Compaction through Matching Pursuit and Genetic Algorithm, Multi-Author Chapter Book: *"Interdisciplinar Application of Fractal and Chaos Theory"*, (Eds.: R. Dobrescu & C. Vasilescu), Ed. of RO Acad, Bucharest, pp. 99 – 118.

Stefanoiu, D., Borangiu, Th. and F. Ionescu. 2004. Robots Modelling and Simulation. Solutions of Problems. Ed. of RO Academy, Bucharest, RO.

Borangiu, Th. and Ionescu, F. 2005. Visual Conveyor Tracking, Chap. 4 in Multi Authors-Chapter Book: *"Intelligent and Allied Approaches to Hybrid Systems Modelling"*, (Eds. F. Ionescu, & D. Stefanoiu) Steinbeis Ed. Berlin/Stuttgart, D, ISBN: 3-938062-31-2 & "M. Drinov" Acad Publ House, BG, ISBN: 954-322-107-3, Sofia, pp. 4-1–4-61.

Stefanoiu, D. and F. Ionescu. 2006. Fuzzy–Statistical Reasoning in Fault Diagnosis, Contribution in Multi Authors-Chapter Book: "*Computational Intelligence in Fault Diagnosis"* (Eds.: V. Palade, B.D. Bocaniala & L. Jain), Springer-Verlag, pp. 125–177.

Ionescu, F., Vlad, C.I. and D. Arotaritei. 2007. Advanced Control of an Electro-Hydraulic Axis, Multi Author-hapter Book: "*The Handbook of Mechatronics"*, CRC Press, 2nd Edition, (Ed.: R. Bishop, Austin, FL, USA),

Stratulat, F. and F. Ionescu. 2009. Linear Control Systems. *Analysis and Synthesis. Theory and Applications*, Steinbeis-Ed, Stuttgart, D.

Ionescu, F., Arotaritei, D., Arghir S., Constantin G., Stefanoiu, D. and F. Stratulat. 2011. A Library of Nonlinearities for Modelling and Simulation of Hybrid Systems, Proc of 15th KES Int Conf, Springer, Vol. I, Sept 12-14, Kaiserslautern, 2011, pp. 7 –81.

Andreescu, D., Riehle, H., Ionescu, F. and S. Arghir. 2011. Human Body as Mechatronic System. Complex Modelling, Simulation and Control. Proc of SIMULTECH Intern Conf, July 29-31, Noordwijkerhout,

NL (Eds: J. Kacprzyk, N. Pina and J. Filipe), ISBN: 978-989-8425-78-2, pp. 339-342.

Talpasanu, I., Ionescu, F. and K. Kostadinov. 2015. Inverse Dynamics and Design for a 6,5 DOF Manipulator with Micro and Nano Precision for Biomedical Applications. Multi Author-Chapter Book*: Inverse Problems and Computational Mechanics* (Eds.: L. Marin, L. Munteanu and V. Chiroiu), Edition of RO Academy, Bucharest, RO.

Ionescu, F., Constantin, C., Nicolae, M. and V. Kotev. 2014. Object Oriented Virtual Manufacturing Lines. Proc of 5th ICMEN Intern Conf on Manuf Eng, Oct 1–3, Thessaloniki, GR. (Ed. K. Bouzakis), ISBN: 978-960-98780-9-8, pp. 119 - 132.

*** Solid Dynamics, Manual of Operation, Roanne, FR, (2000-2005).

*** AutoDesk.Motion Inventor, Manual of Operation, USA.

*** AMESim, Manual of Operation, Roanne, FR.

*** DSH+, Manual of Operation, Aachen, D.

*** MATLAB©/Simulink, Manual of Operation, CA, USA.

AUTHOR LISTING

AUTHOR LISTING